
THE UNIVERSITY
*of* EDINBURGH

# Macrophage-Derived WNTs *in* Normal Cardiac Growth *and* Regeneration Following Injury


**Raphaël, Fabrice, Paul CASTELLAN**

Thesis for the Degree of Doctor of Philosophy (PhD)

The University of Edinburgh, 2017

# Declaration

I hereby declare that all work carried out during this PhD was performed by myself, unless otherwise stated, under the supervision of Dr. Gillian Gray and Prof. Jeffrey Pollard. This thesis has not previously been submitted for any other degree or qualification.

Raphaël, Fabrice, Paul CASTELLAN

# Acknowledgments

I would like to thank my primary supervisor Gillian Gray for her patient support, encouragements, and optimism when I needed it. Her guidance and feedbacks have been essential. Many thanks also to my second supervisor Jeff Pollard who always provided help and guidance throughout my PhD giving me the opportunity to travel to New York to carry out work essential to this thesis. I would also like to thank Rick Kitsis for hosting me in his lab in New York, making sure that everything was set in place for me to get the most out of my short stay, and also for making me feel so welcomed! I have greatly enjoyed our scientific discussions together with Nick Frangogiannis.

Thank you to Paul Riley and his group, especially Megan Masters, who allowed me to look over her shoulder to learn the neonatal cardiac injury model.

Many thanks to the members of the Gray lab throughout the years who I have pestered with questions: Katie, Barry, Xiaofeng, Iqbal, Jill, and Kieran. You have been great support and provided the pints when required! The members of the Pollard lab in Edinburg: Matina, Luca, Agi, Gael, Ezra, Daniel who have helped me along the way. Agi and Ezra, thanks for taking care of me when I was attacked by an angry microtome. Luca, thanks for answering the longest list of questions! Daniel, thank you for putting so much effort into making the impossible possible! The Pollard lab in New York: Mark, Juifeng, and Liyin! Thank you for helping me when I was there and collecting all those hearts for me!

Thank you to everyone in the animal unit in Edinburgh (Sharon, Keith, Duncan, Jon, Will, Larraine) but especially to Sandra! Thank you to the histology staff for bringing good fun and chats in the last months of my PhD, thank you Mel and Laura! Thank you Will and Shonna for putting up with my flow questions! A massive thank you to Adrian with whom I spent a lot of time around the ultrasound machine, you've been a great teacher! Also, thank you Carmel Moran for reading over my ultrasound methods!

My friends at the Einstein College of Medicine, Carolina and Patricio, thank you! Thank you for taking me into your group and making my stay in New York so enjoyable! Thanks for the Pisco Sour, now that's a true discovery.

Thank you to all my CVS friends: Emma, Kate, Callam, Amelia, Matt, Chris. It would not have been the same without you!

Thank you to the ones who have left the centres but without whose friendship and support this thesis could not be. Thank you Sam for being you and being there every step of the way and for providing highly needed Sam time into my life. Thank you Gianna for putting up with me on our various trips and for being one of the most understanding person I know. Thank you Tracy for your positivity and your enthusiasm, it is a real inspiration.

Thank you to my flatmates throughout the years. Mélissa and Nicholas, merci d'avoir mangé autant de pizza avec moi. Avoir trainé sur le canapé avec vous fut un honneur ! Thank you to my friends and flatmates Clare and Marlène. Clare your friendship from the first days of this PhD has been essential to keeping me to an adequate level of sanity and cynicism! Our chats, provided copious amounts of red wine, have helped me get through this and many other things. Marlène, thank you for the fun we've had and the fun we'll have. As long as we stay away from the swimming pool we should be safe.

Thank you Steven, you have truly been incredible in those last months. I simply couldn't have done this without your support, understanding, and your lemon tarts. You are truly the bestest. Looking forward to what awaits!

Thank you to my aunt and uncle, Paul and Anne-Marie. Seeing your passion for what you do is a true inspiration!

Thank you to my mum, Josiane, and my dad, Fabrice. Merci de m'avoir toujours permis et encouragé de faire ce que je désirais. Vos conseils, votre support, et votre compréhension m'ont permis d'en arriver là ! Vos serez toujours une inspiration d'intelligence et de persévérance. Merci aussi à la plus forte de toutes les sœurs du monde entier, Stéphanie, et au plus fort de tous les frères du monde entier, Jérémie. Vous êtes les meilleurs et je suis tellement fière d'être votre petit frère !

# Abstract

Unlike other regenerative organs such as the liver, the adult mammalian heart does not regenerate tissue lost following injury such as myocardial infarction (MI). Instead a non-contractile fibrous scar develops that in the longer term leads to the development of heart failure (HF). In contrast to the adult, neonatal mammals, including mice and man, retain potent cardiac regenerative capacities and can replace myocardium lost following injury. Understanding the mechanisms underlying scar free repair in the neonate may help in development of new approaches to reduce the impact of myocardial injury in adults. In this thesis MI was induced by coronary artery ligation in mice at post-natal day 1 (P1). Novel electrocardiogram gated high resolution cardiac ultrasound was developed to permit non-invasive confirmation of injury 1 day later and regeneration 21 days later by loss, then restoration, of contractile function.

Macrophages (MΦ) play important roles in organ growth and homeostasis, and are required for scar-free regeneration of the neonatal mouse heart following MI. WNTs are secreted lipophilic proteins with multiple roles in development. MΦ-derived WNTs are essential for scar free tissue regeneration following injury in the kidney, liver, and gut, but their role in the heart is unknown. The primary aim of this thesis was to investigate the role of MΦ, and in particular MΦ-derived WNTs in determining normal growth of the myocardium from neonate to adult and also in regeneration of the neonatal heart following injury.

In wild-type neonatal mouse hearts, *Csf1r*-expressing cells density (mostly macrophages) was consistent across all time points studied. Three populations of resident cardiac mononuclear phagocytes were identified by flow cytometry: F4/80$^{hi}$, CD11b$^{lo}$, Ly6C$^{-ve}$ - F4/80$^{lo}$, CD11b$^{hi}$, Ly6C$^{-ve}$ - F4/80$^{lo}$, CD11b$^{hi}$, Ly6C$^{+ve}$. F4/80$^{hi}$, CD11b$^{lo}$, Ly6C$^{-ve}$ cells were hypothesised to correspond to yolk-sac derived mononuclear phagocytes and F4/80$^{lo}$, CD11b$^{hi}$, Ly6C$^{-ve}$ - F4/80$^{lo}$, CD11b$^{hi}$, Ly6C$^{+ve}$ to foetal liver/bone marrow derived mononuclear phagocytes. Three phases of myocardial growth were identified by ultrasound and histological techniques: hyperplastic (P2-P8, with increased Ki67 and cardiac troponin immunopositive cells), hypertrophic/reorganisation (P8-P21, with increasing cardiomyocyte size and no change in left ventricle wall thickness), and finally hypertrophic solely (P21-P42, with

increasing cardiomyocyte size and left ventricle wall thickness). Average coronary vessel size was shown to decrease between P2 and P8 whilst vessel density was increased. The number of α-smooth muscle actin (αSMA) coated vessels greatly increased between P8 and P42, indicating vessel maturation. Throughout all phases cardiac systolic function was maintained at steady state. Diastolic function was however shown to mature from a foetal to an adult pattern between P2 and P8, with reversal of the E:A wave ratio on Doppler ultrasound.

In mice globally deficient in MΦ due to a germline knock-out of the *Csf1r* gene (*Csf1r*-null mice), both body and heart weights were decreased from P7 onwards. The number of proliferating ($Ki67^{+ve}$) cardiomyocytes at P1 and P7 was unchanged in *Csf1r*-null mice but there was a trend towards decreased cardiomyocyte size at P7, suggesting an influence on hypertrophic rather than hyperplastic growth of the myocardium. There was also a trend for slowed vascular network maturation, with a delay in the shift from large to smaller vessels in hearts from *Csf1r*-null mice. In mice with MΦ-directed (*Csf1r-icre* mediated) depletion of Porcupine (*Porcn*), a gene encoding an enzyme required for WNT acylation and secretion cardiac growth, vascularisation, fibrosis and function were all similar in $Cre^{-ve}$ and $Cre^{+ve}$ animals until P41, when cardiomyocyte size and cardiac systolic function were both significantly increased in $Cre^{+ve}$ animals. However, the underlying mechanism is unknown.

In the neonatal mice, *Csf1r* expressing cells, mostly MΦ, were identified in association with regenerating myocardium after induction of MI at P1. Flow cytometry data showed that by P7 the putative resident yolk-sac derived population had mostly disappeared from the heart and was replaced by $F4/80^{lo}$ cells, similar to the pattern reported in the adult. In the regenerating myocardium, *Axin2* expression was increased consistent with activation of canonical Wnt signalling. Expression of *Wnt5b* and *Fzd2* receptor, both associated with fibrosis, was significantly increased relative to age matched uninjured hearts. MΦ-directed depletion of *Porcn* did not influence either the functional decrease at day 1 or recovery at day 21 following induction of MI at P1. Coronary re-vascularisation was also unaffected by the genotype. However, retention of intra-myocardial fibrosis (picrosirius red staining) was significantly increased in hearts at day 21 post-MI from mice with MΦ-directed depletion of *Porcn*. MΦ-derived

WNTs are therefore required for scar-free wound healing in the heart, as they are in the liver and the kidney where they regulate matrix metalloproteinase activity.

In summary, novel ECG-gated high-resolution in vivo ultrasound developed in this project has allowed characterisation of cardiac structure and function during early post-natal growth and following injury and regeneration in neonatal mice. The resident MΦ population of the heart is established pre-natally, and may play a role in determining maturation of the developing vascular network, although this does not involve MΦ-derived Wnt signalling. Following MI, the MΦ population may expand from bone marrow cells and MΦ accumulate around the regenerating tissue. MΦ derived WNTs are not required for regeneration of the neonatal myocardium but do have a role in ensuring scar free wound healing and this merits further investigation.

# Lay summary

A heart attack is caused by a blood clot forming in one of the vessels supplying the heart muscle with oxygen. Because of the lack of oxygen, the heart muscle dies. Unlike other organs such as the liver, the adult human and mouse heart does not repair itself optimally. The dead muscle is replaced by a stiff scar. This forces the remaining of the heart muscle to adapt and work harder. Depending on how severe the heart attack is, the heart can then become tired of the extra work. This can lead to heart failure.

Unlike the adult, new-born humans and mice are good at repairing their hearts with no scar after a heart attack. This is known to be dependent on white blood cells called macrophages. Those macrophages are also known to help repair other organs without a scar by producing a type of molecule called WNTs. This is true in the kidney, the gut, and the liver.

In this PhD thesis we have aimed to understand whether WNTs produced by macrophages help repairing new-borns heart without scarring. Understanding this would help us identify potential drugs to favour scar-free repair of the adult heart after a heart attack.

First we needed to understand if anything different in the way the new-borns' heart work and are built could help scar-free repair. In order to achieve this goal we adapted a set-up of echocardiography made for adult mice to new-born mice. This and other techniques has allowed us to confirm what other researchers had found. The heart muscle cells are better at multiplying than those in an adult heart.

We then identified the types of macrophages present in the new-born mouse heart. Removing them did not change the ability of heart muscle cells to multiply. Our results and others' suggest that they may have very specific importance at certain times as the heart grows after birth. This is especially true for blood vessel formation within the heart which is essential to deliver nutrients and oxygen. Other methods to remove macrophages should be looked into to understand their role in heart growth better.

In order to understand how the new-born heart repairs scar-free, we used a method that induces a heart injury very similar to the one observed after a heart attack. This was done in new-born mice. We saw that macrophages gathered at the site of injury. We also saw that the heart contains more molecules important in the activity of WNTs when compared to a normal heart.

We were then able to prevent production of WNTs from macrophages and to see whether it affected the way new-born mice are able to repair their hearts scar-free. Three weeks after injury the hearts of mice able to produce WNTs from macrophages were normal with normal function. On the other hand, the hearts of mice unable to produce WNTs from macrophages contained a scar although heart function was normal.

Our results have showed that macrophages produce WNTs that in turn are able to promote scar-free repair of the new-born heart. If we can identify which WNT is the best at promoting scar-free repair and how it acts, we can then try and favour this in adult.

# Abstract from thesis

**Castellan RF**, Thompson M, Soong DYH, Mylonas KJ, Thomson A, Moran CM, Kitsis RN, Pollard JW, Gray GA. Macrophage-derived WNTs are required for scar-free regeneration of the neonatal mouse myocardium. Scottish Cardiovascular Forum (SCF) annual conference, February 2017, Glasgow, UK. *Poster presentation, New England Biolabs special poster prize.*

**Castellan RF**, Thompson A, Moran C, Pollard JW & Gray GA. Characterisation of neonatal cardiac growth and regeneration using high-resolution in vivo ultrasound. BMUS annual conference – Translational Ultrasound Day, December 2016, York, UK. *Oral presentation.*

**Castellan RF**, Thompson A, Moran C, Pollard JW & Gray GA. Can macrophage-secreted WNTs promote neonatal cardiac regeneration? Centre for Cardiovascular Science Annual Symposium, June 2016, Edinburgh, UK. *Poster presentation.*

**Castellan RF**, Thompson A, Moran C, Pollard JW & Gray GA. Characterisation of neonatal cardiac regeneration using high-resolution in vivo ultrasound. Edinburgh Preclinical Imaging Symposium, June 2016, Edinburgh, UK. *Oral presentation*.

**Castellan RF**, Thompson A, Moran C, Pollard JW & Gray GA. Cardiac macrophages and the structural/functional maturation of the murine neonatal heart. Keystone symposium – Heart disease and regeneration: Insights from development, March 2015, Copper Mountain, Colorado, USA. *Poster presentation*.

**Castellan RF**, Thomson A, Moran C, Pollard JW & Gray GA. Ultrasound characterisation of the murine myocardium reveals dynamic modification during the early post-natal period. British Society for Cardiovascular Research – New frontiers in cardiovascular science, June 2014, Manchester, UK. *Poster presentation*.

**Castellan RF**, Thompson A, Moran C, Pollard JW & Gray GA. Ultrasound characterisation of post-natal murine myocardial structure and function by B and M mode ultrasound. 5th Preclinical Ultrasound Imaging day, November 2013, Edinburgh, UK. *Oral presentation*.

# Publication from thesis

**Castellan RF**, Thomson A, Moran CM, Pollard JW, Gray GA 'The use of electrocardiogram-gated high-resolution in-vivo ultrasound to study neonatal cardiac growth and regeneration following injury' (in preparation for submission to Journal of Physiology)

**Castellan RF**, Thompson M, Soong DYH, Mylonas KJ, Thomson A, Moran CM, Kitsis RN, Pollard JW, Gray GA 'Macrophage-derived WNTs are required for scar-free cardiac regeneration of the neonatal mouse' (in preparation)

**Castellan RF**, Thompson M, Soong DYH, Mylonas KJ, Thomson A, Moran CM, Kitsis RN, Pollard JW, Gray GA 'Macrophage-derived WNTs are required for scar-free regeneration of the neonatal mouse myocardium' (Scottish Cardiovascular Forum abstract, Heart Journal 2017, Heart 2017;103:A4-A5)

# Abbreviations

| | |
|---|---|
| % | Percentage |
| $^{o}$C | Degrees Celsius |
| ALPACA | Anomalous left artery arising from pulmonary artery |
| APC | Adenomatous polyposis coli |
| AKT | Protein kinase B |
| ANP | Atrial natriuretic peptide |
| αSMA | α smooth muscle actin |
| BMMNCs | Bone marrow mononuclear cells |
| BMMΦ | Bone marrow derived macrophages |
| BNP | Brain natriuretic peptide |
| CAL | Coronary artery ligation |
| CCL2 | C-C motif chemokine ligand 2 |
| CCR2 | C-C chemokine receptor type 2 |
| CDE | Choline deficient, ethionine deficient diet |
| CF | Cardiac fibroblasts |
| CK1 | Casein kinase 1 |
| cm | Cardiomyocyte |
| CMCSA | Cardiomyocyte cross sectional area |
| CSF-1 | Colony stimulating factor - 1 |
| CSF1R | Colony stimulating factor - 1 receptor |
| Ct | Threshold cycle |
| cTnI | Cardiac troponin I |
| cTnT | Cardiac troponin T |
| CX3CR1 | C-X3-C chemokine receptor type 1 |
| D | Dimensional |
| DAG | Diacylglycerol |
| DAPI | 4,6-Diaminido-2-phenylindole |
| DNA | Deoxyribonucleic acid |
| Dsh | Dishevelled |

| | |
|---|---|
| ECG | Electrocardiogram |
| ECM | Extracellular matrix |
| EDD | End diastolic distance |
| EDV | End diastolic volume |
| EF | Ejection Fraction |
| EGFP | Enhanced green fluorescent protein |
| EKV | Electrocardiogram gated kilohertz visualisation |
| ELISA | Enzyme linked immunosorbent assay |
| EMT | Epithelial to mesenchymal transition |
| ER | Endoplasmic reticulum |
| ESD | End systolic distance |
| ESV | End systolic volume |
| ET | Ejection time |
| FAC | Fractional area change |
| FACS | Fluorescent assisted cell sorting |
| FGF | Fibroblast growth factor |
| FHF | First heart field |
| Flp | Flippase |
| FRT | Flippase recognition target |
| FS | Fractional shortening |
| FSC-A | Forward scatter - area |
| FSC-H | Forward scatter -height |
| FZD | Frizzled |
| GOI | Gene of interest |
| GSK3β | Glycogen synthase kinase 3 β |
| H&E | Haematoxylin & Eosin |
| HBSS | Hank's balanced salt solution |
| HF | Heart failure |
| HKG | Housekeeping gene |
| HRP | Horseradish peroxidase |
| IACUC | Institutional Animal Care and Use Committee |

| | |
|---|---|
| IB4 | Isolectin B4 |
| IL | Interleukin |
| IP3 | Inositol triphosphate |
| IVCT | Isovolumetric contraction time |
| IVRT | Isovolumetric relaxation time |
| JNK | c-Jun N-terminal kinases |
| KO | Knock-out |
| LAD | Left anterior descending |
| LA | Left atrium |
| LPS | Lipopolysaccharide |
| LRP5/6 | Low-density lipoprotein receptor-related protein 5/6 |
| LV | Left ventricle |
| LVEDA | Left ventricular end diastolic area |
| LVESA | Left ventricular end systolic area |
| MBOAT | Membrane bound O-acyltransferase |
| MI | Myocardial infarction |
| M-mode | Motion-mode |
| MMP | Matrix metalloproteinase |
| MMTV | Mouse mammary tumour virus |
| MPI | Myocardial performance index |
| MPS | Mononuclear phagocytes system |
| MRI | Magnetic resonance imaging |
| MSCs | Mesenchymal stem cells |
| МΦ | Macrophage(s) |
| NFAT | Nuclear factor of activated T-cells |
| NIH | National Institute of Health |
| NK | Natural killer |
| NS | Not significant |
| OCT | Optical cutting temperature |
| OD | Optical density |
| OFT | Outflow tract |

| | |
|---|---|
| OLAW | Office of laboratory animal welfare |
| PBS | Phosphate buffered saline |
| PCP | Planar cell-polarity |
| PCR | Polymerase chain reaction |
| PEO | Pro-epicardial organ |
| PET | Positron emission tomography |
| PFA | Paraformaldehyde |
| PKC | Protein kinase C |
| PLAX | Parasternal long axis |
| PORCN | Porcupine |
| PS | Primitive streak |
| PSR | Picrosirius red |
| RA | Right atrium |
| RNA | Ribonucleic acid |
| RT | Room temperature |
| RT-qPCR | Real time quantitative polymerase chain reaction |
| RV | Right ventricle |
| SEM | Standard error to the mean |
| SFRP | Secreted frizzled-related protein |
| SHF | Second heart field |
| SMC | Smooth muscle cell |
| SSC-A | Side scatter - area |
| SSC-H | Side scatter - height |
| TBE | Tris/Borate/EDTA |
| TBS | Tris buffered saline |
| TCF/LEF | T-cell factor/lymphoid enhancer-binding factor |
| TGFβ1 | Transforming growth factor β1 |
| TIMP | Tissue inhibitor of metalloproteinases |
| TNFα | Tumor necrosis factor α |
| UV | Ultra-violet |
| VEGF | Vascular endothelial growth factor |

| | |
|---|---|
| WGA | Wheat germ agglutinin |
| WLS | Wntless |
| WNT | Wingless-related integration site |
| WT | Wild-type |
| YAP | Yes-associated protein |
| YS | Yolk-sac |

# Table of content

# List of Figures

# List of Tables

# Chapter 1: General Introduction

# 1.1 Myocardial infarction and heart failure

### *1.1.1 Adult MI and the development of heart failure, mechanisms.*

Myocardial infarction (MI) is most frequently caused by the rupture of an atherosclerotic plaque leading to the formation of a thrombus within the coronary vasculature. Blood flow is thereby interrupted in the myocardium distal to the clot leading to necrotic cardiomyocyte death (Thygesen *et al.*, 2013). The adult mammalian heart lacks significant regenerative capacities; myocardial damage therefore eventually leads to the formation of a non-contractile scar. The loss of functional myocardium associated with scarring triggers adaptive remodelling of the remaining healthy myocardium (Cohn *et al.*, 2000). This can become maladaptive and is a risk factor for the development of heart failure (HF) (Cohn *et al.*, 2000). The extent and severity of remodelling is determined by a combination of the degree of initial injury as well as the effectiveness of the repair (Frangogiannis, 2014). Due to the considerable improvement in reperfusion techniques the survival rate of patients following MI has been dramatically improved (Ezekowitz *et al.*, 2009; Behfar *et al.*, 2014). However, HF is a frequent complication of MI. Indeed, within 5 years of first MI, 16% of men and 22% of women over 45 years of age will have heart failure (Mozaffarian *et al.*, 2016). With increasing survival post-MI and an aging population, the prevalence of HF is expected to have risen 48% between 2012 and 2030 (Mozaffarian *et al.*, 2016).

#### *1.1.1.1* Overview of the immune response following MI in the adult

Following myocardial damage, endogenous 'danger signals' are released by the necrotic cells. Those include the wide family of danger-associated molecular patterns (DAMPs) (Timmers *et al.*, 2012). Release of DAMPs then activates innate immune cells thus starting the immune response associated with MI (Chan *et al.*, 2012; Frangogiannis, 2012). The first immune cell to be recruited to the site of infarction in the adult heart are neutrophils. Their number thus peaks rapidly at day 1 post-MI and by day 6-7 is back to low levels (McSweeney *et al.*, 2010). Neutrophil infiltration is rapidly followed by infiltration of blood circulating monocytes (K. Jung *et al.*, 2013). There are two populations of circulating blood monocytes: $Ly6C^{hi}$ and $Ly6C^{lo}$ (Geissmann *et al.*, 2003). Upon MI, the $Ly6C^{hi}$ population is preferentially recruited to the site of injury via the interaction of the chemokine/chemokine receptor couple CCL2/CCR2 (Dewald *et al.*, 2005; Nahrendorf *et al.*, 2007). Their number peaks in

the myocardium at day 3 post-MI. Their recruitment represents a hallmark of the inflammatory phase of MI as they secrete inflammatory cytokines and matrix metalloproteinases (MMPs) (Nahrendorf *et al.*, 2007; Frangogiannis, 2012). Ly6C$^{lo}$ monocytes were shown to dominate at a later stage between day 4 and 7 post-MI in the so called proliferative phase and to accumulate through CX3CR1 rather than CCR2. Those monocytes are considered anti-inflammatory; promoting matrix deposition and angiogenesis (Nahrendorf *et al.*, 2007).

Following tissue infiltration monocytes start differentiating into macrophages. Depending on the set of signals they receive, macrophages can adopt a wide range of phenotypes which allows them to acquire varied specific functions within a tissue (Davies *et al.*, 2013; Wynn *et al.*, 2013). Nevertheless, macrophages have been described as being able to broadly adopt two polarised phenotypes. Those were originally characterised by *in vitro* polarisation of bone-marrow derived macrophages using either LPS/TNFα or IL-4 yielding respectively to the so called M1 and M2 phenotypes (Stein *et al.*, 1992; Mills *et al.*, 2000; Gordon and Taylor, 2005). *In vivo*, due to the multitude of polarizing signals received by macrophages this nomenclature has been broaden to M1-like, pro-inflammatory, and M2 like, anti-inflammatory, macrophages. It is widely agreed that those two phenotypes are over simplified and do not take into account macrophage ontology (Wynn *et al.*, 2013; Murray *et al.*, 2014). They are nevertheless helpful in the description of macrophage function.

In the context of MI, 'M1-like' macrophages predominate during the early inflammatory phase between day 1 and 3 post-MI; whereas 'M2-like' macrophages are the dominant macrophage subset from day 5 post-MI (Yan *et al.*, 2013). This correlates with the changes between the inflammatory and proliferative/repair phases following MI described by Frangogiannis (2012). M1-like macrophages have been shown to be crucial in the phagocytosis of cell debris and matrix remodelling through the secretion of proteases; on the other hand, M2-like macrophages have pro-angiogenic, pro-resolution and pro-fibrotic capacities (Nahrendorf *et al.*, 2007; Murray and Wynn, 2011).

It is clear that the immune system and more specifically macrophages play a crucial role following MI in the adult. The time-line and specific roles of each phases of the

immune response as well as the role of the different cell types involved has been the focus of extensive research (Frangogiannis, 2014). This has helped further our understanding of the mechanisms involved in cardiac repair following MI. Nevertheless, myocardial damage such as MI invariably leads to the formation of scar which can impede cardiac function.

#### *1.1.1.2* Scar formation and the development of heart failure

During the inflammatory phase following MI (day 1-3), extra-cellular matrix (ECM) is actively degraded through the activity of MMPs (Zamilpa and Lindsey, 2010). MMP-9, which is present on neutrophils and macrophages, noticeably peaks during this phase (Vanhoutte *et al.*, 2006). In the proliferative/repair phase post-MI (from day 4), collagen is actively deposited within the infarcted area and remains high for at least 3 weeks in rats (Holmes *et al.*, 2005). Deposition of a scar helps maintain cardiac structural integrity following MI and is regulated by a tight balance of ECM-degrading and preserving signals that are likely to play key roles in successful cardiac repair. It is known that myofibroblasts actively lay down ECM following MI (Nahrendorf *et al.*, 2007; van den Borne *et al.*, 2010; Murray and Wynn, 2011). Myofibroblasts are mainly thought to differentiate from cardiac fibroblasts although other cell types in the heart have been shown to trans-differentiate, e.g. endothelial cells, pericytes, epicardial cells (van den Borne *et al.*, 2010) and 'fibrocytes' may be recruited from the bone marrow. Cardiac fibroblasts are present in the steady state within the myocardium (Camelliti *et al.*, 2005; Porter and Turner, 2009). Following injury, disruption of tissue integrity triggers their activation and differentiation into myofibroblasts (Tomasek *et al.*, 2002; Hinz and Gabbiani, 2003). Other signals contribute to their differentiation including TGFβ1 which stimulate their production of collagen (Petrov *et al.*, 2002). Myofibroblasts have mostly been characterised based on their expression of α-smooth muscle actin (αSMA). In the context of MI, following their activation and differentiation, they are known to migrate within the infarcted area where they secrete both MMPs and collagen thereby increasing matrix turnover. This migratory process was notably shown in rats to be dependent on their expression of the Wnt signalling receptor *Frizzled-2* (Blankesteijn *et al.*, 1997). Following resolution of inflammation, the number of myofibroblasts decrease leaving an acellular mature scar in place mostly composed of collagen (Holmes *et al.*, 2005).

Following MI in the adult mammal, there is therefore a pattern of structural remodelling involving removal of cell debris and formation of a non-contractile scar. This remodelling can be considered a beneficial event as it helps maintain structural integrity and even improve cardiac function following injury. The loss of contractile tissue and alteration in tissue architecture however puts stress on the remaining viable myocardium. These changes can lead to further remodelling that can become maladaptive with associated functional and structural detrimental changes leading to heart failure progression (Cohn *et al.*, 2000; van den Borne *et al.*, 2010; Frangogiannis, 2014).

Multiple strategies have been developed to promote better repair leading to improved outcome following MI. Those have included modulation of inflammation (Frangogiannis, 2012) or fibrosis (Gourdie *et al.*, 2016). However, the most valuable goal is to promote cardiomyocyte replenishment whilst limiting fibrosis thereby achieving tissue regeneration.

### *1.1.2 Regenerative strategies*

The adult mammalian heart was long considered as devoid of regenerative capacities with cardiomyocytes having exited the cell cycle. Nevertheless, in the recent years evidence for slow renewal of cardiomyocyte changed this perspective (Bergmann *et al.*, 2009). This suggests that the adult mammalian heart does harbour regenerative capacities that may have the potential to be instructed over scar formation following MI (Porrello and Olson, 2014). It is however very clear that those capacities are not sufficient for cardiomyocyte replenishment following MI. Several approaches have been undertaken in an effort to favour cardiomyocyte replenishment over scar formation including cell-based therapies.

The first reports of cell-based therapeutic strategies following MI started with the transplantation of autologous bone-marrow-derived mononuclear stem cells (BMMNCs). Those were shown to integrate within the myocardium and differentiate into cardiomyocytes and endothelial cells (Jackson *et al.*, 2001; Orlic *et al.*, 2001; Deb *et al.*, 2003). Those initial results were disproved by fate mapping experiments showing no trans-differentiation of BMMNCs into cardiomyocytes. They were however able of promoting endogenous cardiomyocyte replenishment following MI

(Loffredo *et al.*, 2011). Meta-analysis of original clinical trials suggested minor but beneficial effects of BMMNCs-based therapy on functional recovery following acute MI (Kuswardhani and Soejitno, 2011; Delewi *et al.*, 2013). Those meta-analyses were however obtained from the collection of published summaries. A later meta-analysis using individual-patient data was unable to report the previous beneficial effects (Gyongyosi *et al.*, 2015). In the recent years, translation to humans of the benefits originally observed following BMMNCs-based therapy in mice has therefore been controversial with poorly understood mechanisms.

Human mesenchymal stem cells (MSCs) also yielded promising pre-clinical results as studies suggested that they could trans-differentiate into cardiomyocytes *in vitro* and *in vivo* (Toma *et al.*, 2002; Xu *et al.*, 2004). Following MI in a porcine model, MSCs were shown to integrate within the injured myocardium and to have a beneficial effect on functional recovery (Shake *et al.*, 2002). Later a clinical trial showed a beneficial effect of MSCs transplantation in humans following MI (Hare *et al.*, 2009). However, following injection, MSCs are known to mostly accumulate in the spleen, liver, and lung with only 0.44% to be found in the myocardium (Toma *et al.*, 2002). Such low engraftment frequency has raised doubt on whether engraftment is the main mechanism of action of MSCs. Others have suggested that MSCs could exert their beneficial effect through the secretion of growth factors such as vascular endothelial growth factor (VEGF) or fibroblast growth factor (FGF) promoting proliferation of endothelial cells and smooth muscle cells thereby increasing blood flow in a hind limb ischaemia model (Kinnaird *et al.*, 2004). Other mechanisms of action such as expansion of cardiac stem cells or differentiation into endothelial cells have been proposed but are still questioned (reviewed in Williams & Hare (2011)).

Further cell-based therapies that are being investigated in clinical trials involve cardiopoeitic stem cells (reviewed by Behfar *et al.* 2014). Cardiopoietic stem cells are derived from MSCs and instructed towards a cardiac phenotype with a differentiation cocktail (Behfar *et al.*, 2010). Those cells were shown preclinically to integrate the injured myocardium, differentiate into cardiomyocytes and endothelial cells, and improve cardiac function compared to animals that received regular MSCs (Behfar *et al.*, 2010). Those cells are showing encouraging results by improving cardiac function in patients with chronic heart failure following an ischaemic insult (Bartunek *et al.*,

2013). Whether differentiation of those cells into cardiomyocyte and endothelial cells is the sole mechanism of action is unclear. However, cardiac function does not return to normal following the treatment suggesting that cardiomyocyte replenishment is not complete.

In 2003, Beltrami *et al.* showed that the adult mouse heart contained a population of $KIT^{+ve}$, $Lin^{-ve}$ cells expressing markers of cardiomyocyte progenitors with clonogenic, self-renewing capacities and able to differentiate into cardiomyocytes, endothelial cells, and smooth muscle cells *in vitro* and *in vivo*. Those cells were argued to represent an adult cardiac stem cells population (Beltrami *et al.*, 2003). The regenerative potential of $KIT^{+ve}$ cells is however controversial. A study by Ellison *et al.* (2013) showed, using a Cre-reporter mouse, that a population of $KIT^{+ve}$ cells could act as cardiomyocyte progenitors in the adult mouse following injury by injection of isoproterenol. Later, a study by (van Berlo *et al.*, 2014) showed that following MI, $KIT^{+ve}$ cells differentiation into cardiomyocyte was extremely limited and that most of their contribution to the cardiomyocyte pool was through cell fusion. However, KIT is expressed in a number of other cell types present in the adult myocardium (Santini *et al.*, 2016) which may render precise cell lineage and tracking difficult. This may explain the discrepancies observed in the published work. Further work will be needed to determine the exact identity and origin of those cells and whether they have the capacity to sufficiently differentiate into cardiomyocyte to replenish the injured myocardium following MI in the adult.

Promising *in vivo* and *in vitro* pre-clinical studies showed the potential of multiple stem-cell populations to differentiate into cardiomyocytes and to improve outcome following MI. Nevertheless, engraftment and differentiation efficiency are low and most of the effect of those cells seems mediated through paracrine effects and promotion of angiogenesis following MI in the adult (Santini *et al.*, 2016).

Another avenue involves the study of cardiac regeneration in models retaining such capacities. Indeed, understanding how an organism can spontaneously regenerate its myocardium following injury may provide tools of crucial importance to support promotion of myocardial regeneration following injury in the adult human.

## 1.2 Cardiac regeneration in lower vertebrates

Organ regeneration has been the focus of scientific research for over a century. It is however only recently that formal investigation of cardiac regeneration was conducted in lower vertebrate models. Despite the first evidence of cardiac regeneration being reported in amphibian models (Rumyantsev, 1966; Oberpriller and Oberpriller, 1974), the zebrafish has imposed itself as the standard model for investigation of cardiac regeneration. This is partly due to its straightforward genetic manipulation and short generation time.

Zebrafish (*Danio rerio*), a member of the teleost infraclass of bony fish, was first reported to harbour potent cardiac regenerative capacities by Poss *et al.* (2002). Their experiment consisted of surgically removing about 20% of the ventricular myocardium in adult fish. Following resection, a blood clot was rapidly formed. This was replaced by a fibrin cap by 9 days post-resection. Over the next 60 days the fibrin cap was shown to regress as cardiomyocytes replenished the resected area. By that time point the ventricular area had recovered to baseline levels. The authors were also able to show evidence of cm proliferation following resection and that cell proliferation was essential to scar-free regeneration of the adult zebrafish heart. Later, it was formally proven that cm replenishment of the resected myocardium in the adult zebrafish occurred through existing cm de-differentiation and subsequent proliferation using lineage tracing and electron microscopy techniques (Jopling *et al.*, 2010).

## 1.3 Mammalian cardiac regeneration: Lessons from development

It is commonly believed that following injury, developmental pathways such as Wnt, Notch and Hedgehog are re-activated in an effort to restore tissue integrity (Oka *et al.*, 2007; Bollini *et al.*, 2011; Bielefeld *et al.*, 2013). It is however very clear that successful regeneration is both age-dependent and organ-specific (Poss, 2010; Porrello and Olson, 2014). For example, unlike other regenerative organs such as the liver (Forbes and Newsome, 2016), the adult mammalian heart is mostly considered non-regenerative.

### *1.3.1 Age dependency of mammalian cardiac regeneration*

#### *1.3.1.1* In humans

There is evidence that the human heart exhibits potent regenerative capacity during early post-natal life. Minimal myocardial scarring along with normal function was observed in adults having had cardiac corrective surgery for anomalous origin of the left coronary artery from the pulmonary artery (ALPACA) as children (Fratz *et al.*, 2011). Moreover, full functional recovery was reported following thrombolytic therapy in a new-born child presenting with severe MI (Haubner *et al.*, 2016). These observations have supported the concept that regenerative capacities could be re-activated in the adult after injury.

#### *1.3.1.2* In mice

Mammalian models of cardiac regeneration were non-existent until the description in 2011 by Porrello *et al.* that 1 day old neonatal mice could fully regenerate their myocardium by 21 days following apical resection. Synchronously, Porrello *et al.* (2013) and Haubner *et al.* (2012) developed model of left anterior descending (LAD) coronary artery ligation in 1 day old mice, leading to MI. As with the resection model, neonatal mice could regenerate the injured myocardium by 21 days following MI. This was also accompanied by full recovery of cardiac function. Similarly to the zebrafish, neonatal mice were shown to achieve cardiac regeneration through de-differentiation and proliferation of cardiomyocytes, rather than through a stem-cell based mechanism(Porrello *et al.*, 2011, 2013; Haubner *et al.*, 2012). MI in neonatal mice was shown to be associated with increased markers of cell death such as cleaved caspase 3, functional decrease in the days following surgery, and decreased proportion of viable myocardium (Haubner *et al.*, 2012; Porrello *et al.*, 2013). At day 3 post-MI, Porrello *et al.* (2013) observed extensive cm loss and immune cell infiltration. By day 7, a scar had formed within the injured myocardium. This scar was then gradually removed as the myocardium regenerated leading to minimal interstitial fibrosis by day 21 post-MI. A small area of fibrosis was noted by both Porrello *et al.* (2013) and Haubner *et al.* (2012) at the site of the suture which did not have any effect on the functional recovery observed by day 21. Importantly, those regenerative capacities were strictly limited to the first week after birth. Neonatal mice undergoing CAL at post-natal day 7 (P7) were unable to regenerate the lost myocardium and instead formed a scar, similar to the adult.

Studying what controls both cardiac development and regeneration during the regenerative window (P1-P7) therefore appears crucial in advancing our understanding of cardiac regeneration. This could in turn provide tools to favour regeneration over scar formation in the adult following MI

### *1.3.2 Mammalian cardiac development and maturation*

#### *1.3.2.1* Organogenesis

The heart is the first organ to form in vertebrates. It originates from cardiogenic precursors within the epiblast on either side of the primitive streak (PS) (Wu *et al.*, 2008; Vincent and Buckingham, 2010). Those precursors then migrate through the PS to give rise to cardiogenic mesoderm which will subsequently migrate in a rostro-lateral fashion to form the primitive heart tubes (~E6.5) (Buckingham *et al.*, 2005). Following formation of a coelom the mesoderm is split into a dorsal (somatic) and ventral (splanchnic) section. The embryo's folding then begins bringing the 2 heart tubes together. Those start fusing cranially thereby creating the cardiac crescent of first heart field (FHF) (Buckingham *et al.*, 2005). In the early 2000s another source of cardiac precursors named the second heart field (SHF) was shown to be located posteriorly to the FHF in the developing embryo. Both FHF and SHF participate in embryonic cardiac organogenesis. Fusion of the cardiac crescent then extend caudally to form a single heart tube (E7.5) (Buckingham *et al.*, 2005). Following a series of looping and segmentation a four-chambered heart composed of right and left atria (RA, LA) and ventricles (RV, LV) is formed in mammals. The FHF and SHF specifically give rise to the LV and outflow-tract (OFT) respectively. The rest of the myocardium is composed of a combination of cells originating from both heart fields.

From E9.5 onwards a group of coelomic cells start proliferating on the pericardial side of the *septum transversum* to give rise to the pro-epicardium organ (PEO). The PEO then extends villi which migrate cranially to cover the myocardium. A subset of epicardial cells can then undergo epithelial to mesenchymal transition (EMT) and are the main source of vascular smooth muscle cells (Wilm *et al.*, 2005).

An illustration of this process can be found on Figure 1-1.

By E14.5 the foetal heart has acquired most of its adult structural characteristics (Buckingham *et al.*, 2005). The circulation is however slightly different. Most of the

blood is diverted away from the lungs and systemic and pulmonary circulations are not isolated. Following birth and interruption of maternal oxygenation, the lungs inflate and both circulations segregate.

#### *1.3.2.2* Cardiac structural maturation

The adult mammalian heart is composed of three main cell types: cardiomyocytes, endothelial cells, and fibroblasts. The exact proportion of each cell type is likely to vary according to species, age, and in disease. Until recently fibroblasts had been considered the most numerically abundant cell type in the heart (Banerjee *et al.*, 2007). This view was however challenged by a recent publication by Pinto *et al.* (2016) showing that in the adult mouse and human hearts endothelial cells are the most abundant cell type, followed by cardiomyocytes, and finally fibroblasts.

##### (a) Cardiomyocytes

As the foetus develops, the heart is faced with an increasing work load which in turn stimulates its growth. Cardiomyocyte growth can be achieved through hyperplasia (cell division), or hypertrophy (increased cell size) (Oparil *et al.*, 1984). Hyperplastic growth was shown to be at its highest at foetal and early post-natal stages in mammals (Soonpaa and Field, 1998; Leu *et al.*, 2001). In the rodent, early post-natal cardiomyocyte cell division is acytokinetic and leads to bi-nucleation of 80-90% of cells. Binucleated cardiomyocytes are mostly unable of completing cytokinesis in the highly regenerative newt (Matz *et al.*, 1998) linking binucleation to the loss of regenerative capacities in the mouse (Porrello and Olson, 2014). In mice, hyperplastic growth was shown to stop around P4 (Leu *et al.*, 2001). Even though it is clear that cardiomyocyte growth is mostly hyperplastic at this stage it is important to note that cardiomyocytes do also increase in size. Hirschy *et al.* (2006) showed that cm length increased 3-fold between E8.5 and P4 whilst their width remained stable. From P4 onwards most of cm growth is described as hypertrophic; growing first mostly in length and from P24 mostly in width (Leu *et al.*, 2001). Even though those studies have provided the field with a relatively good understanding of the different phases of cardiomyocyte growth some caveats are worth noting. Leu *et al.* (2001) performed their experiments on isolated cardiomyocytes which does not provide information of their role in tissue architecture and interaction with other cell types. Whilst Hirschy *et al.* (2006) investigated cardiomyocyte growth pattern on heart sections thereby preserving tissue architecture, their study focused on foetal development with limited investigation during the neonatal stages and how it relates to other cell types. A comprehensive analysis of postnatal

cardiomyocyte growth patterns, focusing on the neonatal period, and how those relate to tissue architecture is therefore missing. An in-depth understanding of normal postnatal growth patterns of the neonatal mouse heart would provide a strong basis for interpretation of the mechanisms involved following injury and during regeneration.

(b) Coronary vasculature

Pioneering anatomical studies such as the one performed by Bennett (1936) in the pig heart recognised that the coronary vasculature sprouted from the aorta into the myocardium. Later, those observations would be questioned as a study on quail embryos suggested that coronary vessels grew into rather than out of the aorta (Bogers *et al.*, 1989). Further experiments on avian models proposed a model by which the coronary vasculature was to originate from the pro-epicardial organ (PEO) (Mikawa and Gourdie, 1996; Männer, 1999; Perez-Pomares *et al.*, 2002). This model was then itself challenged with lineage tracing studies showing that the PEO only gave rise to few cardiac endothelial cells whilst being the main source of smooth muscle cells (SMC) (Wilm *et al.*, 2005). Red-Horse *et al.* (2010) elegantly settled this controversy regarding the origin of the coronary vasculature. Using a coronary endothelial specific LacZ reporter the authors were able to show the invasion of endothelial cells from the *sinus venosus* onto the dorsal side of the heart from E11.5. Those cells were then shown to migrate in a caudal-ventral manner thereby wrapping around the developing heart (Figure 1-1). At the onset of this PhD, coronary vasculature growth in the post-natal mammal was thought to be achieved through angiogenesis of those existing vessels. Formal proof of this concept was however lacking.

(c) Cardiac fibroblasts

Cardiac fibroblasts (CF) play essential roles in the deposition and remodelling of extra-cellular matrix (ECM) both during development (Ieda *et al.*, 2009) and disease (Porter and Turner, 2009; Turner and Porter, 2013). Due to the lack of specific markers of CF the field has been lacking a formal proof of their origin within the embryo at the onset of the PhD. It was however thought that they originate mostly from the PEO (Mikawa and Gourdie, 1996; Acharya *et al.*, 2012).

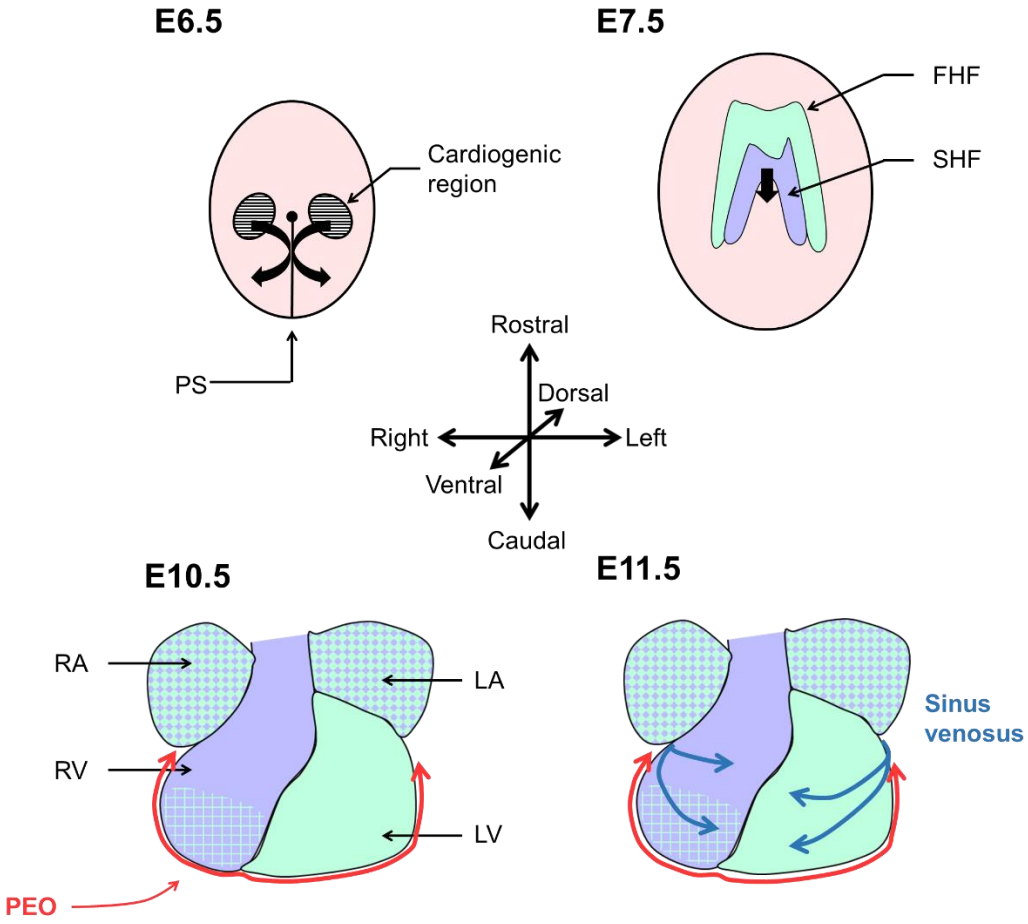


**Figure 1-1: Cardiac organogenesis schematic.** Cardiogenic precursors start migrating through the primitive streak (PS) at E6.5 to give rise to cardiogenic mesoderm which produces the primitive heart tubes. Those will then start fusing giving rise to the cardiac crescent or first heart field (FHF-green). The fusion of the primitive heart tubes starts then expands caudally from the cardiac crescent at E7.5 to form a single heart tube with the participation of a second progenitor population known as the second heart field (SHF-purple). After a series of looping the heart acquires 4 distinct regions; right and left atria (RA, LA) and ventricles (RV, LV) by E10.5 with the FHF giving rise to the LV whilst the SHF gives the outflow tract. The rest of the myocardium is made of a mixture of the two precursor populations. From E10.5 the pro-epicardial organ (PEO) starts migrating rostrally to cover the heart (red arrows). This will give rise to vascular smooth muscle cells. From E11.5, cells from the sinus venosus start migrating in a caudal-ventral manner to wrap around the developing heart giving rise to endothelial cells (blue arrows). Adapted from Buckingham *et al.* (2005).

*1.3.2.3* Functional maturation of the heart

During one cardiac cycle, the blood-filled ventricles start systole by a period of isovolumetric contraction (IVCT). It is during the IVCT that pressure within the ventricle rises until it reaches levels above that within the pulmonary artery and aorta. At this point the aortic and pulmonary valves open letting blood into the circulation. The ventricles then start relaxing thereby decreasing ventricular pressure. Once it has

reached levels below the arterial pressure the aortic and pulmonary valves close. This is followed by an isovolumetric relaxation time (IVRT) until the ventricular pressure drop induces the mitral and tricuspid valves to open leading to the passive filling (E-wave) of the ventricle. The atria then contract ejecting the remainder of the blood into the ventricles performing the so called active filling (A-wave) (Godfrey *et al.*, 2012). Passive and active filling of the ventricles can be measured by pulse-wave Doppler ultrasound (Godfrey *et al.*, 2012)

Cardiac systolic function, or the ability to eject blood within the circulation, is thought to be relatively stable throughout foetal development and to decline slightly after birth albeit within the physiological range (Corrigan *et al.*, 2010). Those measurements were acquired using pulse-wave Doppler and motion-mode (M-mode) ultrasound which are 1-dimensional (D) measurements of cardiac function. At the onset of this PhD, 2-D measurements of cardiac systolic function routinely performed in the adult mouse were not available for application to neonatal mice. Those not only provide functional readouts but also structural information such as cavity size and wall thickness.

Cardiac diastolic function is drastically different in the foetus compared to the postnatal animal. In the foetus, most of the filling of the ventricle is due to the active filling or A wave; whereas in the adult the passive filling (E wave) predominates. Reversal of the E/A wave ratio occurs during the first post-natal week (Zhou *et al.*, 2003a; Corrigan *et al.*, 2010).

Altogether, thanks to advances in lineage tracing techniques the understanding of cardiac organogenesis has made considerable progress. Cellular origins and composition has indeed been scrutinised with a new light over the past 25 years. In comparison, characterisation of early post-natal cardiac structure and function has not received similar attention. Nevertheless, the recent discovery of the ability of the neonatal mouse to fully regenerate its myocardium has placed early post-natal growth in a new light. Characterisation of structural and functional changes of the neonatal heart could thus provide important clues regarding the mechanisms behind cardiac regeneration.

High-resolution *in-vivo* ultrasound has been extensively used to characterise functional and structural maturation of the foetal heart *in-utero* (Phoon and Turnbull, 2003; Yu

*et al.*, 2008). This was achieved through pulse-wave Doppler, a non-electrocardiogram (ECG)-gated visualisation method. In the post-natal heart, ultrasound is well described as a powerful method to investigate functional effects of MI in both adults and neonates (Haubner *et al.*, 2012; Moran *et al.*, 2013; Porrello *et al.*, 2013). This is possible using M-mode visualisation. In the adult, the ultrasound set up allows ECG-gated visualisation of the mouse heart, but this has not previously been achieved in the neonatal mouse. Establishing a set-up of ECG-gated visualisation in neonatal mice would therefore allow collection of novel information on the structural and functional maturation of the heart in that period. It would also allow quantification of the functional effect of MI on neonatal mice.

## 1.4 Macrophages in development and regeneration

### *1.4.1 Overview of the immune system*

The mammalian immune system has been classically divided into innate immunity, activated rapidly following exposure to a pathogen or after injury; and adaptive immunity which specifically targets pathogens with a stronger, more focused response. Leukocytes are primary effector cells of the immune system.

Broadly, leukocytes originate in the bone marrow from pluripotent haematopoietic stem cells. Those then give rise to 2 main categories of multipotent stem cells: common lymphoid and myeloid progenitors. Common lymphoid progenitors yield all lymphocytes (B, T, and Natural Killer (NK) cells). On the other hand, the common myeloid precursors will give rise to all myeloid cells. These include platelet-producing megakaryocytes, erythrocytes, granulocytes (neutrophils, basophils, eosinophils), mast cells precursors, and monocytes. Monocytes are mostly found in the blood. They can however enter tissues where they differentiate into macrophages (MΦ). MΦ, from the Greek μακροσ (large) and φαγειν (to eat), are large phagocytic cells that sample the environment and are capable of activating other immune cells thereby participating in innate immunity. Resident MΦ populations are found in all adult mammalian tissues where they exert non-immunological roles in homeostasis (Davies *et al.*, 2013; Wynn *et al.*, 2013).

### *1.4.2 Tissue resident macrophages origin*

Understanding how tissue resident MΦ are established, their origins, as well as the pathways involved in their maintenance would provide tools for the manipulation of their function in a context such as cardiac injury.

All tissue resident MΦ populations were thought to be derived through the so-called mononuclear phagocytic system (MPS). The MPS established resident MΦ as directly differentiated from bone marrow-derived blood monocytes that have entered the tissue (van Furth *et al.*, 1972). However, this system was challenged with the evidence that some organs contain MΦ populations established prior to the onset of definitive haematopoiesis within the bone-marrow that persists into adulthood.

A first population of maternally-derived MΦ arises in the yolk-sac as early as E7.5. This population does not however present haematopoietic capacities. Subsequently, two populations of myeloid cells precursors with haematopoietic capacities are established in the yolk-sac (Bertrand *et al.*, 2005). The first population, described as 'primitive' is thought to bypass the monocyte stage of differentiation and to only give rise to MΦ. Between E8.5 and E10.5 a second population of erythro-myeloid precursors arises from the haemogenic endothelium. This population is able to give rise to erythrocytes and megakaryocytes thereby carrying a wide myeloid potential. Yolk-sac derived progenitors then populate the foetal liver making it the main source of definitive haematopoiesis by E12.5. They also seed the bone marrow where definitive haematopoiesis will be relocated postnatally. Following birth, haematopoiesis is relocated to the bone marrow where it will remain (Bertrand *et al.*, 2005; Pollard, 2009).

Using a combination of lineage tracing and genome-wide expression arrays, Schulz *et al.* (2012) were able to show that YS derived MΦ persist postnatally in organs such as the lung, the kidney, or the skin. They were also able to show that, depending on their origins, tissue MΦ differentially express the canonical MΦ marker F4/80 and leukocyte marker CD11b. Typically, YS derived MΦ were shown to be mostly F4/80$^{hi}$, CD11b$^{lo}$ whereas macrophages derived from definitive haematopoiesis were F4/80$^{lo}$, CD11b$^{hi}$ (Schulz *et al.*, 2012).

The exact composition of tissue resident MΦ in regards to their origins is thought to be organ specific. The brain is thought to mostly be populated prenatally by YS derived MΦ prior to the closure of the blood-brain barrier (Alliot *et al.*, 1999; Ginhoux *et al.*, 2013). Contrastingly, the gut contains a resident MΦ population that is continuously replenished by bone marrow derived monocytes (Bain and Mowat, 2014; Bain *et al.*, 2014). Finally, the lung contains distinct macrophage populations originating in the yolk sac as well as through definitive haematopoiesis in the foetal liver or bone-marrow (Kopf *et al.*, 2015). The exact composition and origin of cardiac resident MΦ as well as their function in the steady state was unclear at the onset of this PhD.

### *1.4.3 The role of MΦ in organ growth and regeneration*

Macrophages were historically described in non-sterile and sterile inflammation. Over the past 20 years it has become increasingly clear that MΦ also play essential roles in tissue homeostasis, growth, and regeneration.

#### *1.4.3.1* MΦ in organ growth

The importance of MΦ in growth has been in part demonstrated using a mouse model homozygous for a null mutation of the colony stimulating factor -1 (*Csf1*$^{op/op}$) (Yoshida *et al.*, 1990). CSF-1 and its receptor CSF1R are essential in the differentiation and survival of MΦ. The *Csf1*$^{op/op}$ mouse lacks many tissue MΦ populations and presents a range of developmental abnormalities, including growth retardation (Chitu and Stanley, 2006). Mice homozygous for an inactivating mutation of the *Csf1r* (*Csf1r*-null) lead to a similar phenotype albeit more severe (Dai *et al.*, 2002). IL-34 was proposed as an alternative ligand of the CSF1-R which would explain the phenotype discrepancies (Lin *et al.* 2007).

##### (a) MΦ and angiogenesis

Angiogenesis is essential to support growth of all vertebrates. It has been clear for decades that MΦ play important roles in both physiological and pathological angiogenesis (Sunderkötter *et al.*, 1994; Pollard, 2009; James A. Stefater *et al.*, 2011). MΦ are indeed able to produce growth factors (Fantin *et al.*, 2010; Rymo *et al.*, 2011) and matrix remodelling proteins (Moldovan *et al.*, 2000; Hiratsuka *et al.*, 2002; Murdoch *et al.*, 2008) thereby facilitating angiogenesis. In the retina, MΦ have also been shown to regulate regression of the hyaloid vasculature which is essential for normal retinal development (Lobov *et al.*, 2005). Macrophages have also been shown

to associate with tip cells and promote anastomosis of newly formed vessels in the retina (Fantin *et al.*, 2010).

(b) MΦ and the central nervous system

In the brain, microglia depletion (*Csf1*$^{op/op}$, or *Csf1r*-null) in the embryo leads to postnatal defects in brain development (Michaelson *et al.*, 1996; Erblich *et al.*, 2011). Microglia depletion was also shown to diminish neuronal pruning which is essential in adequate brain development (Pow *et al.*, 1989; Paolicelli *et al.*, 2011).

(c) MΦ in bone development

The most striking phenotype of the *Csf1*$^{op/op}$ is osteopetrosis which is a defect of bone remodelling. This is due to bone resident MΦ depletion which requires CSF-1 for development and maturation (Dougall *et al.*, 1999; Pollard, 2009). Macrophage depletion also leads to a failure to develop bone cavity and therefore haematopoiesis defects (Begg *et al.*, 1993).

(d) MΦ and cardiac growth

As described in section 1.1.1.1 MΦ play critical roles following MI in the adult. Interestingly, morpholino-induced depletion of MΦ in xenopus was shown to impair heart tube formation (Smith and Mohun, 2011). Pinto *et al.* published in 2012 the first formal report of cardiac resident MΦ in the adult mouse. The authors proposed a role in immune regulation for those MΦ which was supported by gene expression analysis. Since then resident cardiac macrophages have received considerable attention which will be discussed later in this thesis. At the onset of this PhD their origins and role during murine cardiac development, growth and homeostasis was however mostly unclear.

*1.4.3.2* MΦ in regeneration

MΦ depletion using clodronate loaded liposomes completely abrogates limb regeneration in the adult salamander (Godwin *et al.*, 2013). Interestingly, MΦ depletion was associated with extensive fibrosis and increased expression of collagen I and IV at the site of amputation. This phenotype was completely reversible after macrophage replenishment. Using the same MΦ ablation approach showed their requirement for neuron regeneration in a sciatic nerve injury model (Salegio *et al.*, 2011) as well as during hepatocyte regeneration in a chronic liver injury model (Boulter *et al.*, 2012). At the onset of this PhD the role of macrophages in neonatal

cardiac regeneration following MI was suggested by the Olson lab based on the deleterious effect of clodronate-mediated macrophage ablation. This work was subsequently published by Aurora *et al.* (2014) showing complete abrogation of cardiac regeneration and extensive scar formation by 21 days following injury. A role for MΦ in the angiogenic response following injury was proposed. These observations formed the basis for development of a hypothesis around the role of MΦ derived WNT ligands in myocardial post-natal growth and neonatal regeneration.

## 1.5 The Wnt signalling pathway in development and regeneration

### *1.5.1 The Wnt signalling pathway*

Since the discovery of *Wnt* genes, over 30 years ago, Wnt signalling has been shown to play crucial roles in key biological phenomena such as development, regeneration and disease.

The first *Wnt* gene, *Wnt1*, was discovered through the work of Dr Roel Nusse and Harold Varmus. Their work focused on elucidating the oncogenic mechanism of the retrovirus, Mouse Mammary Tumour Virus (MMTV) (Nusse and Varmus, 1982) in the hope of identifying new proto-oncogenes. These studies led to the discovery of integration site 1 (*Int1*) of the MMTV which proved to possess a great degree of conservation across species, notably with drosophila (Nusse and Varmus, 1982). *Int1* was eventually revealed to be the same gene as well-known segment polarity gene in drosophila; Wingless (Rijsewijk *et al.*, 1987).

Later on the *int* nomenclature was judged inadequate and the int family of genes was renamed: Wingless-related integration site '*Wnt*' and *Int1* became *Wnt1*.

Since then, researchers have identified most of the protagonists of the Wnt signalling pathway. However, many aspects of their interactions and roles remain unclear.

#### *1.5.1.1* Overview of the pathway

The Wnt signalling pathway has been classically divided into the 'canonical', β-catenin dependent, and 'non-canonical', β-catenin independent pathways.

(a) Canonical Wnt signalling pathway

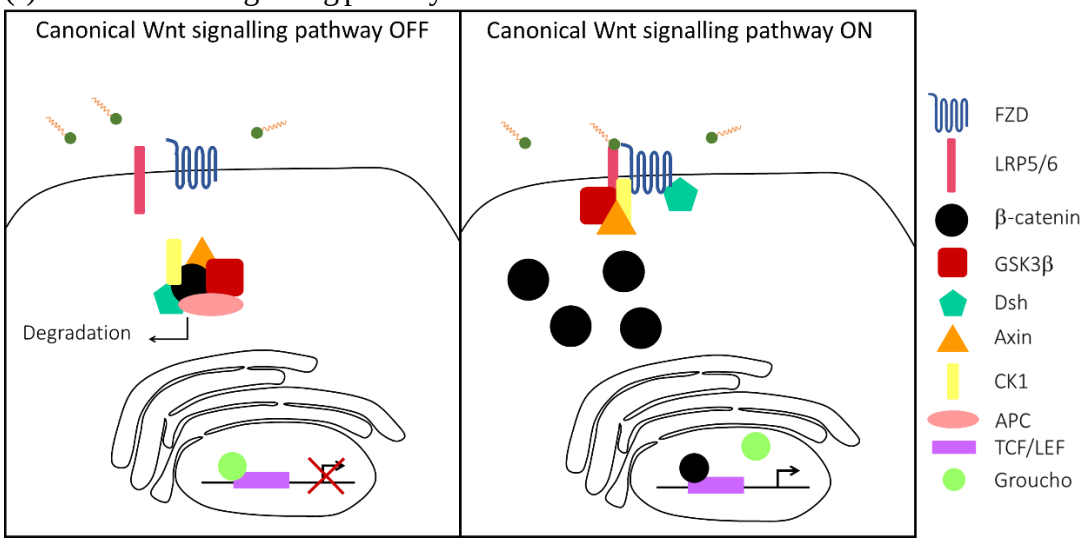


**Figure 1-2: Overview of the canonical Wnt signalling pathway.** Binding of WNT to a frizzled receptor (FZD) and its co-receptor, LRP5/6, leads to the stabilisation and cytosolic accumulation of β-catenin. β-catenin then translocates to the nucleus where it displaces Groucho from TCF/LEF transcription factor allowing activation of target genes' transcription. (Adapted from Dawson *et al.* (2013))

In the absence of WNT (Figure 1-2, left panel), β-catenin is targeted for ubiquitination and subsequent degradation by its destruction complex. The destruction complex is composed of Dishevelled, Casein Kinase 1 (CK1), Glycogen Synthase Kinase 3 β (GSK3β), Adenomatous Polyposis Coli (APC) and Axin. It acts through a series of phosphorylation (Clevers and Nusse, 2012).

Upon binding of a WNT (Figure 1-2, right panel) to its receptor, frizzled (FZD), and co-receptor, LRP5/6, the cytoplasmic tail of the latter is phosphorylated. This is mediated by interaction with CK1, GSK3β and Axin (Rao & Kühl, 2010). In this process FZD interacts with Dishevelled but is thought to mainly serve as an anchor for WNTs (MacDonald *et al.*, 2009). β-catenin destruction complex is thus disassembled leading to the stabilisation and accumulation of β-catenin in the cytoplasm. β-catenin then translocates to the nucleus were it interacts with TCF/LEF transcription factor displacing the corepressor Groucho leading to activation of transcription of target genes involved in cell proliferation and differentiation (Clevers and Nusse, 2012).

(b) Non-canonical Wnt signalling pathway

Non-canonical or β-catenin independent signalling is classically divided into two separate pathways; the Wnt/$Ca^{2+}$, and the Wnt/planar cell polarity (PCP) pathway. Both pathways still involve the Frizzled receptor but not its co-receptor LRP5/6.

In the Wnt/$Ca^{2+}$ pathway (De, 2011), binding of a WNT ligand to its FZD receptor triggers activation of phospholipase C (PLC) and thereby accumulation of inositol 1,4,5 triphosphate (IP3) and 1,2 diacylglycerol (DAG). IP3 triggers the release of $Ca^{2+}$ from the ER and therefore activation of CaMKII while DAG activates PKC and both of these can lead to activation of the transcription factor nuclear factor of activated T cells (NFAT). NFAT is involved in cardiac development as well as cardiac hypertrophy (Schulz and Yutzey, 2004; Komiya and Habas, 2008).

The Wnt/PCP pathway, on the other hand, requires recruitment at the membrane of DVL, which then transduces the signal through the small GTPases, Rho and Rac. In the Rho branch, binding of a WNT ligand to its FZD receptor leads the recruitment of DVL and activation of dishevelled associated activator of morphogenesis 1 (Daam1) which itself activates Rho. Rho then activates Rho-associated kinase (ROCK) to modulate actin cytoskeleton stability and polarity. In the Rac branch, interaction between WNT and FZD leads to the activation of c-Jun-N-terminal kinase (JNK). The downstream effectors of WNT/FZD activated JNK are however less clear (Komiya and Habas, 2008; Rao and Kühl, 2010).

*1.5.1.2* WNT ligands post-translational modifications and secretion

In mammals, the WNT ligand family is composed of 19 members. All 19 proteins possess common features such as a signal peptide at the N-terminus end targeting them for secretion, highly conserved cysteine residues, and numerous glycosylation sites.

(a) WNT post-translational modifications

Most of the research investigating the mechanisms of WNT post-translational modifications as well as secretion has been focused on WNT3a. Therefore, the following paragraphs refer mainly to this particular ligand. Nevertheless, the information is applicable to most WNT proteins.

WNTs glycosylation and acylation are essential for their secretion and activity. Regulation of these modifications permits control over their release into the extracellular medium.

(i) Glycosylation

Mutation of both Asn87 and Asn298, preferential glycosylation sites on WNT3a, into Gln led to extremely low levels of its secretion in the extracellular medium. The mutations also impaired WNT3a's capacity to induce accumulation of β-catenin (Komekado *et al.,* 2007). Briefly, WNT3a binding to its appropriate receptor on a target cell leads to dissociation of the β-catenin destruction complex and thereof its accumulation in the cytosol. How WNT3a stimulation leads to accumulation of cytosolic β-catenin will be described in subheading 1.5.1.1(a).

(ii) Acylation

WNT3a was shown to be acylated on two different residues. A palmitic acid is added on Cys77 and a palmitoleic acid is attached on Ser209 as revealed by mass spectrometry (Takada *et al.*, 2006). Acylation of Ser209 was shown to be mediated by the multi-pass transmembrane protein Porcupine (PORCN) of the membrane bound O-acyltransferase (MBOAT) family (Takada *et al.*, 2006). PORCN was first described as many members of the Wnt signalling pathway in drosophila where it was known to be crucial for the maintenance of Wingless signalling (Mikels & Nusse, 2006). In mice deletion of *Porcn* is embryonic lethal. These mice failed to secrete functional WNTs and exhibited defective gastrulation (Herr *et al.*, 2012). Moreover, anti-Porcn siRNA treatment led to abolished Ser209 acylation and abrogated secretion of WNTs along with their retention in the cytoplasm. On the other hand, C77A mutation eradicated canonical Wnt signalling but had no impact on secretion of WNT (Willert *et al.*, 2003).Furthermore, treatment of WNTs with acyl protein thioesterase, an enzyme catalysing deacylation, leads to non-hydrophobic, inactive ligands (Willert *et al.*, 2003). Figure 1-3 recapitulates the succession of WNTs acylation modifications.

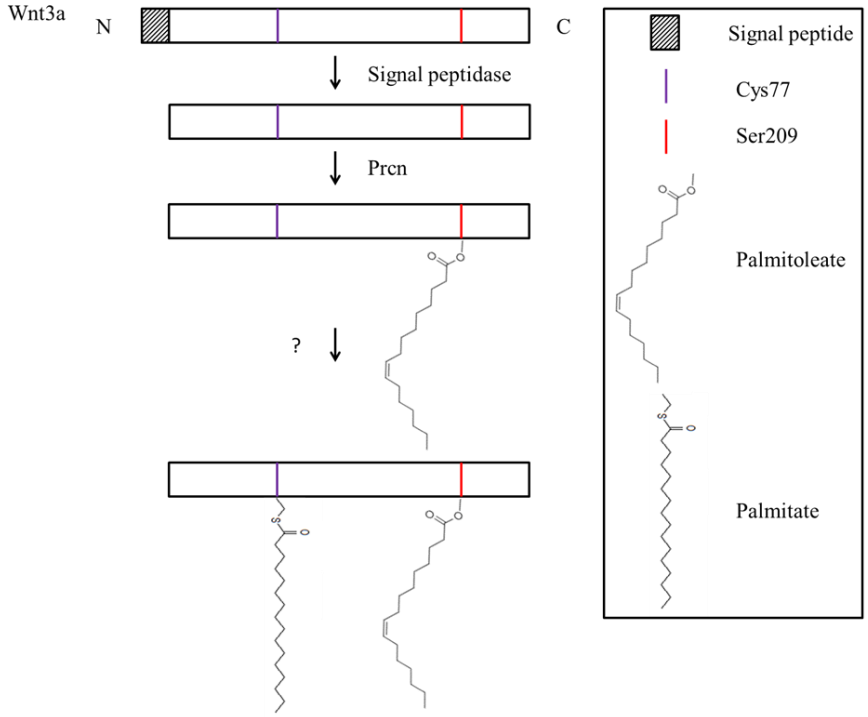


**Figure 1-3: WNT acylation.** Following translation, the N-terminal signal sequence is removed. WNTs are subsequently glycosylated in the endoplasmic reticulum (ER). This step is required for acylation of Ser209 in the ER by porcupine and of Cys77 by a yet unknown enzyme. Adapted from Resh (2012)

(b) Wntless and the retromer complex

Wntless (Wls) is a relatively recently discovered multi-pass transmembrane protein. The extent of Wls participation in the Wnt signalling remains unclear, nevertheless it is widely accepted that it is essential in the secretion of WNTs. Indeed, deletion of Wls in the mouse leads to embryonic lethality (Herr *et al.*, 2012). The interaction between Wls and WNT3a proved to be dependent of acylation of Ser209 but not Cys77 (Takada *et al.*, 2006). Following delivery of WNT ligand to the cell membrane Wls is then recycled and shipped back to the Golgi by the Retromer complex (Herr *et al.*, 2012). Figure 1-4 recapitulates the secretory steps of Wnt proteins.

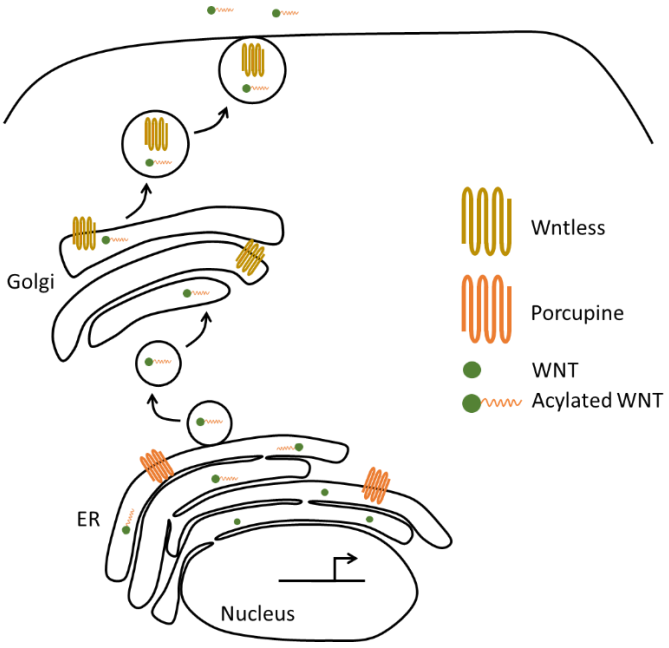


**Figure 1-4: Secretion of Wnt ligands into the extracellular medium.** Following post-translational modifications in the endoplasmic reticulum, glycosylated and acylated WNTs travel to the Golgi apparatus where they interact with wntless which escorts them to the cellular membrane where they are released into the extracellular medium. Wntless is then thought to be recycled by the retromer complex. Adapted from Herr *et al.* (2012)

(c) WNT extracellular transport and delivery

Due to their hydrophobicity, WNTs are thought to remain partly bound to the cellular membrane of the secretory cells. This would imply that activation of the Wnt signalling pathway in the target cell would require its close proximity to the secreting cell. However, *in vitro* studies on human cells showed that WNTs can also be secreted in association with exosomes which were able to induce Wnt signalling activation in target cells. Thus, WNTs are likely to have longer-range signalling capacity than previously thought (Gross *et al.*, 2012).

### *1.5.2 Wnt signalling and MΦ-derived WNTs in development*

#### *1.5.2.1* Wnt signalling in cardiac development

As described in 1.3.2.1, the heart is the first organ to form during embryogenesis following a well described succession of events. WNTs and their receptor FZDs are expressed throughout cardiac development within the relevant tissues as reviewed by Gessert & Kühl (2010). Early during cardiac organogenesis, cardiac precursors arise from the mesoderm. Mesoderm formation, therefore a prerequisite of cardiac

organogenesis, has been shown to be highly dependent on the activity of the canonical Wnt signalling pathway. Deletion of β-catenin and the canonical ligand WNT3a is associated with absence of mesodermal layer (Liu *et al.,* 1999; Huelsken *et al.,* 2000). Furthermore, down-regulation of β-catenin within the SHF leads to a reduced number of progenitors whereas its overexpression leads to their expansion (Ai *et al.* 2007; Klaus *et al.* 2007; Cohen *et al.* 2007; Kwon *et al.* 2007; Lin *et al.* 2007). Altogether these studies highlight the importance of the canonical Wnt signalling pathway in the early formation of cardiogenic mesoderm through its ability to promote expansion of precursor populations.

The canonical pathway was however shown to be detrimental to cardiac specification. Indeed, up-regulation of canonical Wnt pathway inhibitors was able to promote instruction of mesoderm to the cardiac lineage in a Notch signalling dependent manner. This was reversible with the addition of the canonical ligand WNT3a (Chen *et al.*, 2008). On the other hand, non-canonical Wnt signals have been shown to promote cardiac specification. The non-canonical ligand WNT11 indeed promotes expression of cardiac specific genes as well as prevents cytoplasmic accumulation of β-catenin thereby inhibiting the canonical pathway (Pandur *et al.*, 2002; Abdul-Ghani *et al.*, 2011). Other non-canonical WNTs are up-regulated in cardiac progenitors including the prototypical WNT5a which promotes formation of troponin positive cells, a key marker of cardiomyocytes (Chen *et al.*, 2008). Both WNT5a and WNT11 have then been shown to be important in cardiac organogenesis (Cohen *et al.*, 2012). WNT11 was shown to act through a JNK/PKC dependent pathway during cardiac organogenesis (Pandur *et al.*, 2002; Koyanagi *et al.*, 2005).

The literature highlights the importance of the Wnt signalling pathway during the various phases of cardiac organogenesis. In summary, it is widely accepted that in the foetal heart, canonical signals promote proliferation of cardiac progenitors whilst its inhibition in concert with non-canonical signals promotes their specification. The tight regulation of the series of Wnt signals regulating cardiac organogenesis is crucial to adequate outcome. The role of the Wnt signalling in the post-natal maturation of the mammalian heart is however less clear.

#### *1.5.2.2* MΦ-derived WNTs in development

As previously mentioned (1.4.3.1) MΦ play central roles in organ growth. MΦ have also been shown to be a source of WNTs in injury and regenerative contexts as will be further detailed below.

The roles of MΦ-secreted WNTs in development remains poorly understood. Nevertheless, they have been shown to play critical roles during angiogenesis, a process crucial to the support of growth and development. This was shown in both models of wound repair and retinal angiogenesis (Stefater *et al.* 2013; Stefater *et al.* 2011). In both cases, blockade of MΦ secretion of WNTs with a targeted deletion of *Wls* using a *Csf1r* promoter driven *Cre* led to vasculature patterning defects. More precisely, release of WNTs from MΦ induced tissue expression of Flt1, a VEGF-A receptor with limited signalling capacities, thereby titrating angiogenic signals necessary to promote adequate patterning of the vasculature.

### *1.5.3 Wnt signalling and MΦ-derived WNTs in regeneration*

#### *1.5.3.1* Wnt signalling in regeneration

The Wnt signalling pathway not only plays well described roles during development it is also known to be essential in the regeneration of some organs. In lower vertebrates, members of the canonical pathway were shown to be expressed during limb regeneration (Caubit *et al.*, 1997; Poss *et al.*, 2000) whilst its inhibition prevented regeneration (Kawakami *et al.*, 2006). In mammals, the pathway is known to play a role in skeletal muscle (Otto *et al.*, 2008), hair follicle (Ito *et al.*, 2007), and intestinal crypt (Miyoshi *et al.*, 2012) regeneration. As described in section 1.5.2.1 modulation of the Wnt signalling pathway is known to be crucial for cardiac organogenesis and is also known to promote formation of functional cardiomyocytes from human pluripotent stem cells (hPSC) (Lian *et al.*, 2012). Nevertheless, its role in neonatal cardiac regeneration is unclear. The Hippo signalling pathway, which controls organ size and cell proliferation during development (Pan, 2010; Zhao *et al.*, 2011), was identified as a regulator of neonatal cardiac regeneration. Briefly, activity of the pathway leads to phosphorylation of Yes associated protein (YAP) thereby preventing its nuclear translocation and activation of genes controlling cell growth. Inhibition of the pathway was shown to promote cm proliferation in a Wnt signalling-dependent manner in the mouse embryo (Heallen *et al.*, 2011), as well as promoting scar free

regeneration 21 days following LAD ligation in P7 and P28 mice (outside of the regenerative window) (Xin *et al.*, 2013). These reports therefore suggest a potential role of the Wnt signalling pathway in neonatal cardiac regeneration.

#### *1.5.3.2* MΦ -derived WNTs in regeneration

In the kidney, ischaemia-reperfusion injury was shown, using Axin2-LacZ and BATGal reporter mouse lines, to induce a clear increase in canonical Wnt signalling activity. It was also shown that MΦ were a major source of WNTs during the repair phase following injury and that they were able to robustly induce canonical Wnt activity *in vitro* in a reporter cell line. In the tissue, MΦ ablation was associated with decreased Wnt activity following injury. Furthermore, MΦ-specific deletion of *Wnt7b* was shown to impair kidney repair and regeneration by affecting progression of epithelial cells through the G2 phase of the cell cycle preventing advancement into mitosis (Lin *et al.*, 2010). In the liver, following injury using a model of choline-deficient, ethionine supplemented diet (CDE) known to specifically cause hepatocyte regeneration (Yang *et al.*, 2008), MΦ were shown to strongly up-regulate *Wnt3a*. Clodronate liposome mediated ablation of MΦ was also shown to prevent hepatocyte regeneration in this model, a process that is known to depend on canonical Wnt activity (Boulter *et al.*, 2012).

At the onset of this PhD, these two studies had established role of MΦ-secreted WNTs in tissue regeneration. Since then, further evidence of the involvement of this axis in regeneration has been provided, as discussed later in the thesis.

It is therefore clear that modulation of the Wnt signalling pathway following injury can participate in tissue regeneration. More precisely, MΦ-derived WNTs have been shown to promote scar-free regeneration of multiple organs. Whether they play a role in cardiac regeneration of the neonatal mouse remains unknown.

## 1.6 Hypotheses

Understanding how an organ grows can help identify factors to promote regeneration in the adult tissue.

**Hypothesis 1**: New insights on structural and functional maturation of the murine heart will be provided by a combination of ECG-gated high-resolution *in-vivo* ultrasound and histological technique. Emphasis will be placed upon the neonatal period, when the heart is capable of regeneration

MΦ and the Wnt signalling pathway are known to play roles in normal organ growth. MΦ are able of secreted WNT ligands. This secretion is dependent on the activity of the enzyme Porcupine.

**Hypothesis 2**: Macrophage depletion and preventing secretion of WNTs from macrophages through specific deletion of Porcupine will impair normal cardiac functional and structural maturation.

MΦ have been shown to be essential in scar-free regeneration of the neonatal murine heart. MΦ-derived WNTs are essential in the scar-free regeneration of the kidney, liver, and gut.

**Hypothesis 3**: Preventing secretion of WNTs from macrophages through specific deletion of Porcupine will impair scar-free cardiac regeneration in neonatal mice.

# Chapter 2: Methods

A list of reagents, consumables and equipment can be found in Section 2.7 with their suppliers. Recipes for in-house buffers are in Section 2.8

## 2.1 Animals

All animals were mice aged post-natal day 1 (P1) to P42. Both males and females were used. Mice were kept under a 12-hour light/12-hour dark cycle mimicking circadian rhythm. Temperature of the environment was maintained at 21±2$^{o}$C and humidity at 50±10%. Animals had access to chow diet and water *ad libitum*.

### *2.1.1 United Kingdom – Edinburgh*

Animal work was approved by the University of Edinburgh Preclinical Animal Welfare and Ethical Review Board, and by the UK Home Office, project licence 60/4247 and 70/8933 and personal licence IC353799.

#### *2.1.1.1* C57BL/6J mice

C57BL/6J mice were bred in-house from stock originally obtained from Harlan (UK).

#### *2.1.1.2* MacGreen mice

(a) Colony

Tg(*Csf1r-Egfp*), or 'MacGreen', mice express enhanced green fluorescent protein (EGFP) under the control of the colony-stimulating factor 1 receptor gene (*Csf1r*) promoter (Sasmono *et al.*, 2003). CSF-1 and its receptor CSF1R are essential in the differentiation and survival of macrophages (Dai *et al.*, 2002; Chitu and Stanley, 2006). *Csf1r* is mostly expressed by monocytes and macrophages. *Csf1r* mRNA can also be found in neutrophils but is not translated (Sasmono *et al.*, 2007). Nevertheless, this indicates an active *Csf1r* promoter in neutrophils which also express EGFP in Tg(*Csf1r-Egfp*) mice. Animals containing the transgene were noted as GFP$^{+ve}$ and used for visualisation of *Csf1r*-expressing cells. Animals devoid of the transgene were noted as GFP$^{-ve}$. This mouse line is on an incomplete C57BL/6J background. Males positive for the transgene were kindly donated by Prof Philippa Saunders (MRC Centre for Inflammation Research, Edinburgh, UK) and crossed with WT C57BL/6J in-house females to establish a colony. A heterozygous breeding strategy was then applied for this colony by backcrossing GFP$^{+ve}$ males from each new generation to wild type (WT) C57BL/6JOla females.

(b) Genotyping

Ear clips were collected for identification and genotyping purposes of each MacGreen animal at weaning by the BRR-LF2 staff. DNA was extracted on column using a DNeasy blood and tissue kit according to manufacturer's instructions.

Genotyping of the MacGreen mouse was performed by PCR using the following primers: EGFP Forward 5' GCA CGA CTT CTT CAA GTC CGC CAT GCC 3', EGFP Reverse 5' GCG GAT CTT GAA GTT CAC CTT GAT GCC 3' and internal control primers: Fabpi Forward 5' CCT CCG GAG AGC AGC GAT TAA AAG TGT CAG 3', Fabpi Reverse 5' TAG AGC TTT GCC ACA TCA CAG GTC ATT CAG 3' (Final concentration: 1 μM). This leads to 267 bp and 500 bp products for EGFP and Fabpi respectively. Each PCR reaction contained the following:

- 5.0 μL 2X Biomix
- 1.0 μL Forward Primer EGFP
- 1.0 μL Reverse Primer EGFP
- 1.0 μL Forward Primer Fabpi
- 1.0 μL Reverse Primer Fabpi
- 1.0 μL DNA

The PCR reaction was then run on a thermocycler using the following programme:

1) 94°C, 3min
2) 94°C, 30s
3) 65°C, 30s
4) 72°C, 1min
5) 72°C, 7min

35 cycles

6) 4°C, forever

To the PCR product was added 5 μL of sucrose gel-loading dye which was then run on a 1.5% agarose gel containing 1x gel-red dye in 1X TBE, for 1h at 100 V. The gel was then examined under an ultra-violet (UV) lamp and a picture of the result taken. Mice containing the transgene Tg(*Csf1r-Egfp*) produce a 267 bp product. Mice devoid of the transgene do not produce a 267 bp product.

Ear clipping is not possible until the second post-natal week in mice. Neonatal MacGreen mice were therefore genotyped *post mortem* by crushing a small amount of spleen or skin between slide and coverslip in fluoromount G and assessing the presence of $GFP^{+ve}$ cells in the sample using an Axiovert200 fluorescent microscope.

Figure 2-1 shows both genotyping methods and their correlation.

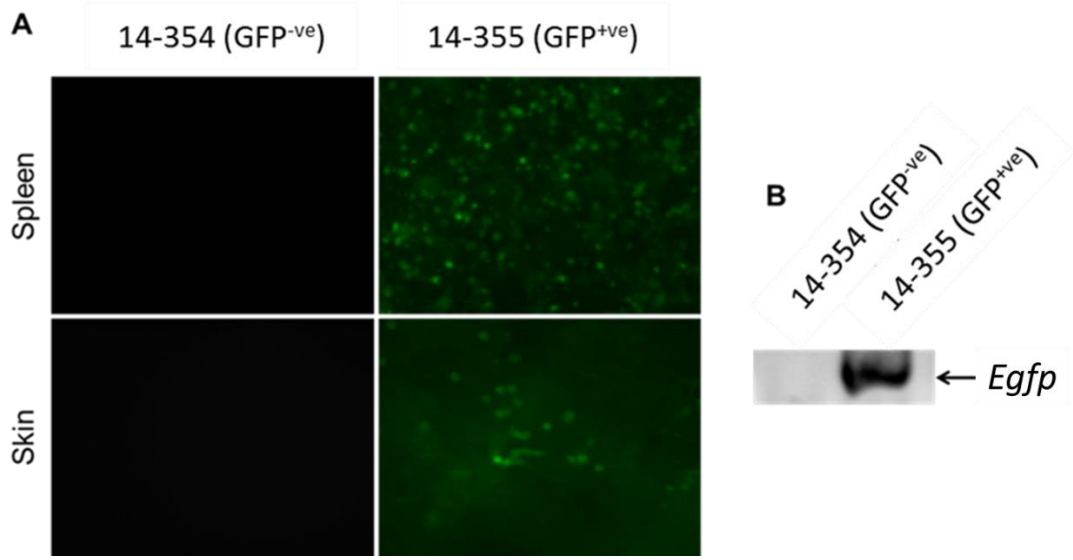


**Figure 2-1: Genotyping of MacGreen mice.** Spleens and skin were collected and mounted on a slide in Fluoromount G and observed under a fluorescent microscope for GFP detection (*A*). *Egfp* DNA was detected by PCR (*B*). Mouse 14-354 was identified as $GFP^{-ve}$ and 14-355 as $GFP^{+ve}$ with both methods.

### *2.1.2 United States of America – New York*

Animal work was reviewed and approved by the Einstein College of Medicine's Institutional Animal Care and Use Committee (IACUC) under animal protocol #20150408 and performed in accordance to the guide for the care and use of laboratory animals in line with the National Institute of Health (NIH) Office of Laboratory Animal Welfare (OLAW).

*2.1.2.1 Csf1r*-null mice

(a) Colony

This mouse line was kindly provided by Prof J.W. Pollard. Mice homozygous for a targeted deletion of exon 5 of the *Csf1r* gene express a truncated *Csf1r* mRNA and lack functional CSF1R protein (Li *et al.*, 2006). Those mice are referred to as *Csf1r*-null. Mice lacking CSF1R had previously been shown to lack many tissue macrophages and to present a range of developmental abnormalities (Dai *et al.*, 2002). Parents heterozygous for the deleted allele of *Csf1r* were used for breeding. Progeny contained homozygotes for the deleted allele (*Csf1r*-null), heterozygotes, and homozygotes for the wild-type (WT) allele (WT animals). *Csf1r*-null mice were compared to their aged matched WT littermates as control. Those mice were aged between P1 and P20 and were on a complete C57BL/6J background.

(b) Genotyping

Tail clips were collected for genotyping by Dr Liyin Zhu. Tails were digested in 180 μL of tail buffer and 20 μL of proteinase K solution and placed at 55$^{o}$C overnight. DNA was then precipitated by adding 2 volumes of 100% ethanol, samples spun at max speed for 10 min at 4$^{o}$C. Supernatant was removed and pellet rinsed with 500 μL of 70% ethanol. Supernatant was discarded and pellet air-dried and re-suspended in 30 μL of Milli-Q water.

Deletion of exon 5 of the *Csf1r* gene was assessed by PCR by Mrs Liyin Zhu using the following primers: Csf1r-intron 4 Forward 5' ATC CCA GCA TTA GGC AGC CT 3'and Csf1r-intron 5 Reverse 5' GCC ACC ATG TGT CCG TGC TT 3'. This leads to a 1.3 kb product for the WT allele and 600 bp for the deleted allele. Each PCR reaction contained the following:

- 15.3 μL $H_2O$
- 2.5 μL 10 X Buffer with Mg
- 2.0 μL dNTP (2.5 mM)
- 1.5 μL Primer Csf1r-intron 4 Forward (1.0 μM)
- 1.5 μL Primer Csf1r-intron 5 Reverse (1.0 μM)
- 0.2 μL Takara Taq polymerase
- 2 μL DNA

The PCR reaction was then run on a thermocycler using the following programme:

1) 95ºC, 4 min
2) 95ºC, 30 s
3) 58ºC, 30 s
4) 72ºC, 30 s
5) 72ºC, 7 min

(2–5) 40 cycles

6) 4ºC, forever

To the PCR product was added 5 μL of sucrose gel-loading dye which was then run on a 1.5% agarose gel containing 0.5% ethidium bromide in 1X TBE, for 1h at 100 V. The gel was then examined under a UV lamp and a picture of the result taken. Mice homozygous for the deleted allele of *Csf1r* (*Csf1r*-null) produced a single 600bp product. Mice homozygous for the WT allele produced a single 1.3kb fragment. Mice heterozygous for the deleted allele of *Csf1r* produced both 600bp and 1.3kb fragments.

#### *2.1.2.2* Porcupine mouse

(a) Colony

This mouse line was kindly provided by Prof J.W. Pollard. Mice homozygous for a floxed allele of the Porcupine gene (*Porcn*$^{fl/fl}$) were used for breeding and generation of experimental animals. Those were originally generated from embryos kindly provided by Dr J. Rossant (Hospital for Sick Children Research Institute, Toronto, Canada) to Prof J.W. Pollard's lab (Biechele *et al.*, 2013). Here, the male breeders were also heterozygous for a transgene containing the improved Cre (iCre)-recombinase under the control of the *Csf1r* promoter (Tg(*Csf1r-iCre*)) (Deng *et al.*, 2010). The off-spring of such breeding are homozygous for *Porcn*$^{fl/fl}$, and a subset also express cre-recombinase in *Csf1r*-expressing cells (Saha *et al.*, 2016). This mouse line is referred to as the Porcupine mouse. Animals expressing iCre were referred to as Cre$^{+ve}$ and compared to iCre-deficient (Cre$^{-ve}$) animals as littermate controls. Those mice were aged between P1 and P41 and were on an incomplete FVB background.

(b) Genotyping

Tail clips were obtained by either Mr Mark Thompson or myself. DNA was obtained as described in 2.1.2.1(b)

Homozygosity for the floxed allele of the Porcupine gene was assessed in the mice used for the breeding and generation of experimental animals by Mr Mark Thompson. The following primers were used: RecF1: 5' CTG TTA AAC CAA GAC ATG ACC TTC A 3', RecR1: 5' TAA CTA GGA CGC TTT GGG ATA GGA T 3' and RecR3: 5' GTT CTG CCT TCC TAA CCC ATA TAA C 3'. Primer combination RecF1 and RecR1 was used to determine the presence of the floxed allele. This leads to a 138 bp product for the WT allele and 248 bp for the floxed allele. Primers RecF1 and RecR3 were used to confirm the deletion of Porcupine in cells expressing iCre. This produces a large fragment (> 1.4 kb) for the WT or floxed allele and 386 bp for the deleted allele. A schematic representation of the primers location can be found on (Figure 2-2). Each PCR reaction contained the following:

- 13.8 μL $H_2O$
- 2.5 μL 10 X Buffer with Mg
- 2.0 μL dNTP (2.5 mM)
- 1.5 μL PorcnRecF1 (1.0 μM)
- 1.5 μL PorcnRecR1 (1.0 μM)
- 1.5 μL PorcnRecR3 (1.0 μM)
- 0.2 μL Takara Taq polymerase
- 2 μL DNA

The PCR reaction was then run on a thermocycler using the following programme:

1) 95°C, 5 min
2) 95°C, 45 s
3) 60°C, 45 s
4) 72°C, 45 s
5) 72°C, 5 min

30 cycles

6) 4°C, forever

To the PCR product was added 5 μL of sucrose gel-loading dye which was then run on a 1.5% agarose gel containing 0.5% ethidium bromide in 1X TBE, for 1 hour at 100V. The gel was then examined under a a UV lamp and a picture of the result taken. Mice homozygous for the floxed

allele of Porcupine (*Porcn*$^{fl/fl}$) produced a single 248bp product. Mice homozygous for the WT allele produced a single 138 bp fragment. Mice heterozygous for the floxed allele of the Porcupine gene produced both 248bp and 138 bp fragments.

Females *Porcn*$^{fl/fl}$; Cre$^{-ve}$ were crossed with males *Porcn*$^{fl/fl}$; Cre$^{+ve}$. Presence of iCre was assessed by Mr Mark Thompson and myself using the following set of primers: iCre779 Forward 5' CAG GGC CTT CTC CAC ACC AG C 3', and iCre386 Reverse 5' CTG GCT GTG AAG ACC ATC 3'. Mice containing the transgene produce a 393bp product. Mice devoid of the transgene do not yield a 393bp product.

It was reported by Prof J.W. Pollard's lab that bone marrow derived macrophages (BMMΦ) from Cre$^{+ve}$ animals of this mouse line contain 80% of the deleted allele of Porcupine by PCR using the RecF1 and RecR3 primers set (Figure 2-2) (Saha *et al.*, 2016). The authors also showed that the culture medium from Cre$^{+ve}$ BMMΦ was unable to activate the β-catenin pathway in the TCF/LEF (TOPFLASH) reporter assay (Korinek *et al.*, 1997). Culture medium from Cre$^{-ve}$ littermates BMM could induce activity. This indicates that the macrophage-targeted deletion of Porcupine can prevent secretion of WNTs into the extracellular space as expected.

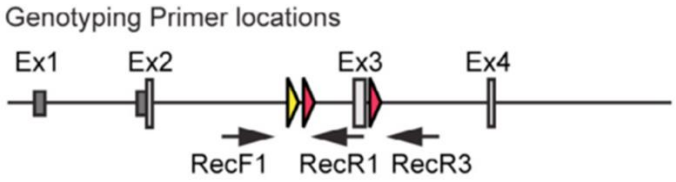


**Figure 2-2: Porcupine floxed allele genotyping strategy.** A set of three primers were used to determine the mice genotype for the floxed and wild-type (WT) allele of Porcupine gene (*Porcn*) as well as the deleted allele. RecF1, RecR1, and RecR3 are the primers used for this genotyping. The yellow triangle represents the flippase (Flp) recognition target (FRT) site left from the Flp-FRT site directed recombination to remove the neomycin cassette originally present in the construct used to introduced LoxP sites (red triangles) around exon 3 of *Porcn*. RecF1 and RecR1 primer combination was used for identification of the floxed and WT alleles. These lead to the amplification of a 248 bp fragment for the floxed allele and a 138 bp fragment for the WT as the FRT and LoxP site are absent. RecF1 and RecR3 primer combination was used to control for cell specific deletion. These leads to the amplification of a large fragment (>1.4 kb) for the WT or floxed allele and a 386 bp fragment for the deleted allele. Schematic taken from Biechele *et al.* (2013)

### *2.1.3 Sexing*

Mice on the C57BL/6 back ground are easily sexed in the neonatal period as male mice present with a typical dark patch of skin on their scrotum. Mice on the FVB background do not present an easy external way of sexing in the neonatal period. Genotyping was therefore used to sex the Porcupine mouse as it was the only one on an FVB background.

Tail clips were obtained by either Mr Mark Thompson or myself. DNA was obtained as described in 2.1.2.1(b).

Sex was determined using a forward primer: 5' TGA AGC TTT TGG CTT TGA G 3' and a reverse primer: 5' CCA CTG CCA AAT TCT TTG G 3'. This leads to the amplification of a single 300 bp fragment for females. Males lead to the amplification of a 280 bp and 300 bp fragment. Each PCR reaction contained the following:

- 15.3 μL $H_2O$
- 2.5 μL 10 X Buffer with Mg
- 2.0 μL dNTP (2.5 mM)
- 1.5 μL Forward (1.0 μM)
- 1.5 μL Reverse (1.0 μM)
- 0.2 μL Takara Taq polymerase
- 2 μL DNA

The PCR reaction was then run on a thermocycler using the following programme:

1) 95°C, 3 min
2) 95°C, 30 s
3) 50°C, 30 s
4) 72°C, 30 s
5) 72°C, 5 min

(2–5: 35 cycles)

6) 4°C, forever

To the PCR product was added 5 μL of sucrose gel-loading dye which was then run on a 2.5% agarose gel containing 0.5% ethidium bromide in 1X TBE, for approximately 5 hours. The gel was then examined under a UV lamp, a picture of the result taken, and sex identified.

## 2.2 *In vivo* work

### *2.2.1 Echocardiography from early postnatal to adult stages*

#### *2.2.1.1* Procedure

When imaging neonatal mice, all pups from a litter were taken away from the dams at the same time to prevent maternal cannibalisation (Mahmoud *et al.*, 2014) . The mice were placed into a box lined with tissue and bedding which was placed onto a heat mat set between 37-40ºC. Each animal was weighed and anaesthesia induced with 5% (neonates) or 2.5% (juvenile and adult) isoflurane in medical $O_2$ for approximately 2 min before being placed in a supine position onto a heated ultrasound table (40ºC). Anaesthesia was maintained through a nose cone with 4-5% (neonates) or 2-3% (juvenile and adult) isoflurane during the procedure. When imaging neonatal mice, adapters were attached to the end of a standard nose cone (P2 & P4: Ø5 mm, P8: Ø8 mm) as shown on Figure 2-3. This allowed adequate fitting of the nose cone around the neonatal mice airways and effective delivery of anaesthesia throughout the procedure. Thoracic hair was removed from juvenile and adult mice using commercially available electric shavers and depilatory cream. Conductive ultrasound gel was then applied to each paw that were then secured onto copper electrodes to allow recording of electrocardiogram (ECG) signals. As shown on Figure 2-3 the set up was adapted by Mr Adrian Thomson and myself to be able to record ECG signals from neonatal mice. Copper tape was wrapped twice around the body of a resized cotton bud and used to extend the ECG electrodes present on the ultrasound table to reach the neonatal mouse limbs. The animal's body temperature was monitored throughout the procedure using rectal probes. A heating lamp was used to maintain the body temperature between 36.5-37.5ºC. Pre-warmed Aquasonic® 100 ultrasound transmission gel was applied onto the abdomen avoiding bubble formation.

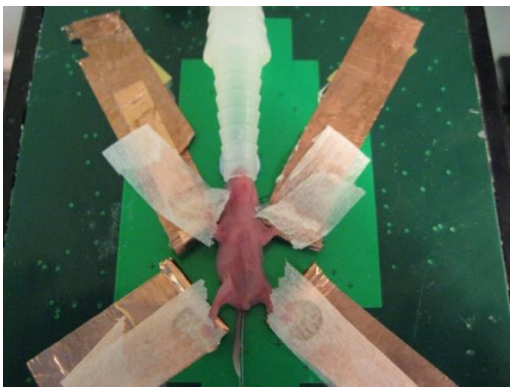

**Figure 2-3: Set-up for assessing neonatal cardiac function and structure using high-resolution in-vivo ultrasound imaging.**

Ultrasound acquisition was performed by Mr. Adrian Thomson (Chapter 3) or myself (Chapter 4 & 5) using a Visualsonics Vevo® 770 ultrasound biomicroscope. The details about the different ultrasound probes used in this thesis are listed in Table 2-1. Different probes were used to optimise the resolution of the acquired images. Animals' cardiac function was assessed through analysis of standard pulse wave Doppler data and of parasternal long axis (PLAX) images of the left ventricle using B and M-mode.

| Animal stage | Probe name | Centre frequency (MHz) | Axial resolution (μm) | Focal length (mm) |
|---|---|---|---|---|
| E18.5 | RMV 708 | 55 | 30 | 4.5 |
| P2, P4, P8 | RMV 704 | 40 | 40 | 6 |
| P21, P42 | RMV 707B | 30 | 55 | 12.7 |

**Table 2-1: Ultrasound probes.**

*2.2.1.2* Ultrasound traces acquisition and analysis

(a) EKV PLAX B-mode

This specific method allows for electrocardiogram (ECG) gated Kilo-Hertz Visualisation (EKV) of the parasternal long axis (PLAX) of the left ventricle (LV). Images were acquired with very high temporal resolution over a full cardiac cycle. This method allows identification of the LV endocardial and epicardial limits at the end of systole and diastole using the cardiac measurement- LV package of the Vevo770® software. Representation of the measurements obtained with this method can be found in Figure 2-4. The software allows calculation of the parameters listed

in Table 2-2. Notably, left ventricular end systole and diastole area (LVESA, LVEDA) were used to calculate the functional readout of fractional area change (FAC).

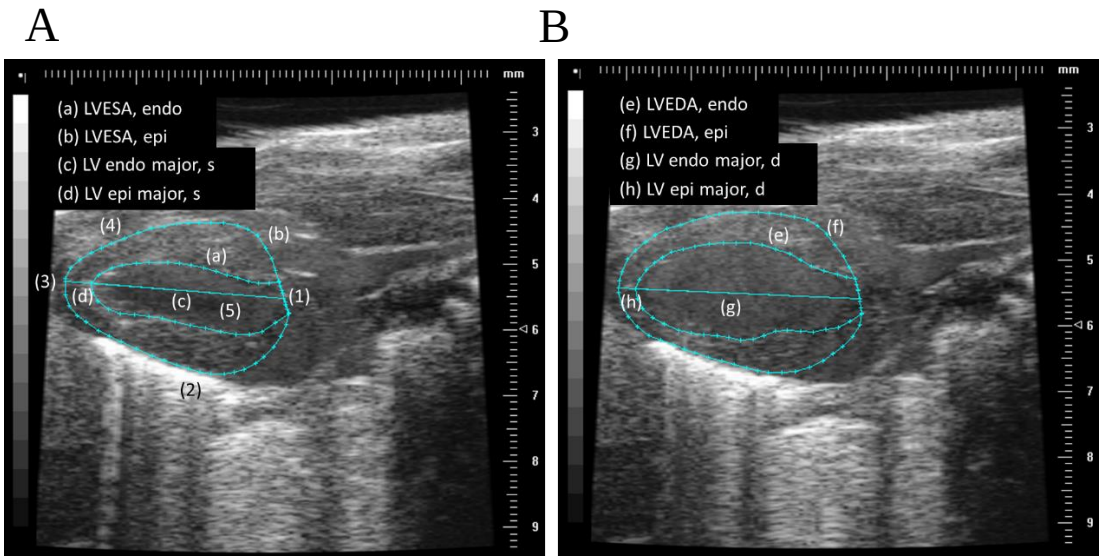


**Figure 2-4: Representative EKV PLAX B-mode still images.** Parasternal long axis (PLAX) view of the left ventricle (LV) was imaged throughout a cardiac cycle using electrocardiogram gated kilohertz visualisation (EKV) B-mode ultrasound. Representative images of a 1 day old mouse left ventricle (LV) at the end of systole (*A*) and diastole (*B*). The Vevo770 software was used to identify: left ventricular end systole and diastole areas of the endocardium (LVESA, endo (a) & LVEDA, endo (e)) and epicardium (LVESA, epi (b) & LVEDA, epi (f)), LV endocardial and epicardial majors at the end of systole (LV endo major, s (c) & LV epi major, s (d)) and at the end of diastole (LV endo major, d (g) & LV epi major, d (h)). Anatomical features are: (1) Aortic valve, (2) LV posterior wall, (3) Apex, (4) LV anterior wall, (5) LV cavity.

| Parameter Short Name | Parameter Long Name | Formula | Units |
|---|---|---|---|
| LVESA, epi | Epicardial Left Ventricular End Systole Area | N/A | $mm^2$ |
| LVESA, endo | Endocardial Left Ventricular End Systole Area | N/A | $mm^2$ |
| LVEDA, epi | Epicardial Left Ventricular End Diastole Area | N/A | $mm^2$ |
| LVEDA, endo | Endocardial Left Ventricular End Diastole Area | N/A | $mm^2$ |
| LV Epi major, s | Left Ventricle Epicardial Major, End Systole | N/A | mm |
| LV Epi major, d | Left Ventricle Epicardial Major, End Diastole | N/A | mm |
| LV Endo major, s | Left Ventricle Endocardial Major, End Systole | N/A | mm |
| LV Endo major, d | Left Ventricle Endocardial Major, End Diastole | N/A | mm |
| LV Vol, d | Left Ventricle Volume, End Diastole | $LV\ Vol,d = \left({}^{4\pi}/_{3}\right) x \left({}^{LV\ endo\ major,d}/_{2}\right) x \left({}^{LVEDA,endo}/_{\pi\left({}^{LV\ endo\ major,d}/_{2}\right)}\right)^2$ | µL |
| LV Vol, s | Left Ventricle Volume, End Systole | $LV\ Vol,s = \left({}^{4}/_{3}\right) x \left({}^{LV\ endo\ major,s}/_{2}\right) x \left({}^{LVESA,endo}/_{\pi\left({}^{LV\ endo\ major,s}/_{2}\right)}\right)^2$ | µL |
| LV SV | Left Ventricle Stroke Volume | $LV\ Vol,d\ - LV\ Vol,s$ | µL |
| FAC | Fractional Area Change | $FAC = \left({}^{(LVEDA,endo\ - LVESA,endo)}/_{LVEDA,endo}\right) x\ 100$ | % |
| EF | Ejection Fraction | $EF = \left({}^{LV\ SV}/_{LV\ Vol,d}\right) x\ 100$ | % |
| WT | Average Wall Thickness | $WT = \sqrt{{}^{LVEDA,epi}/_{\pi}} - \sqrt{{}^{LVEDA,endo}/_{\pi}}$ | mm |
| LV mass | Left Ventricle Mass | $LV\ mass = 1.05\ x \left(\left({}^{5}/_{6}\right) x\ LVEDA,epi\ x\ (LV\ epi\ major,d + WT) - \left({}^{5}/_{6}\right) x\ LVEDA,endo\ x\ LV\ endo\ major,d\right)$ | mg |

**Table 2-2: EKV PLAX B-mode measurements.**

Measurements obtained from parasternal long axis (PLAX) view of the left ventricle on electrocardiogram-gated kilohertz visualisation (EKV) B-mode movies.

(b) PLAX M-mode

From the PLAX B-mode view (Figure 2-4) the M-mode cursor was placed to span across the left ventricular anterior wall, cavity, and posterior wall (Figure 2-5A). This method allows visualisation of wall movement along a single line as shown on Figure 2-5B which was obtained from a 1 day old mouse. Those traces were used to determine end diastolic and systolic distances (EDD & ESD). Those were used by the Vevo® 770 software to calculate the functional readout of fractional shortening (FS). Description of this measurement can be found in Table 2-3. Importantly, note the electrocardiogram recording of the 1 day old mouse on Figure 2-5B (green line).

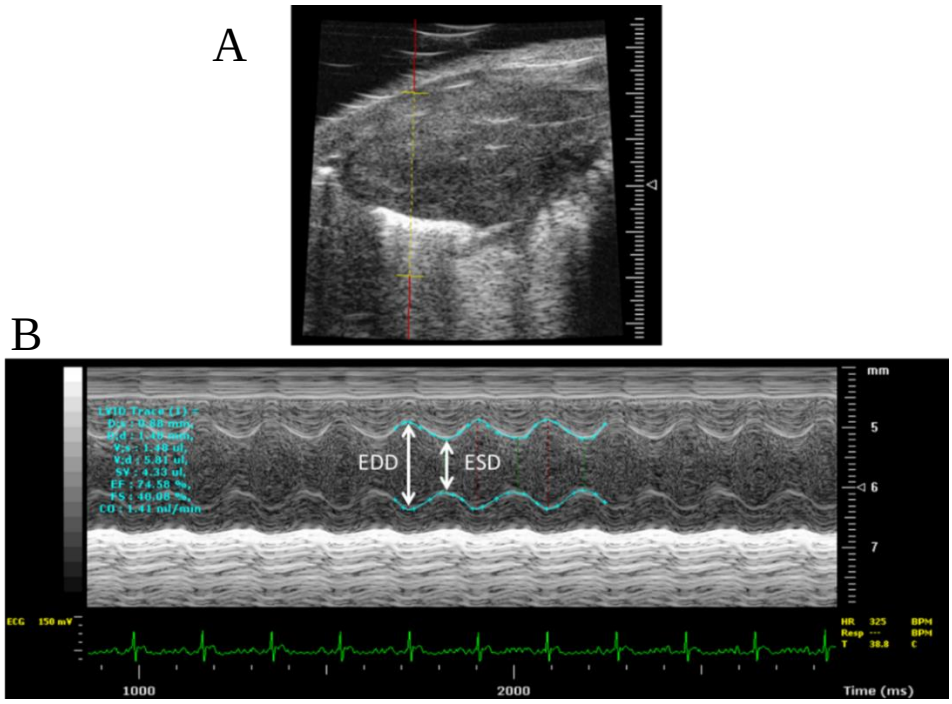


**Figure 2-5: Representative PLAX M-mode still image.** Parasternal long axis (PLAX) view of the left ventricle (LV) wall movement was imaged using M-mode with the cursor (yellow dotted line) spanning across the left ventricular anterior wall, cavity, and posterior wall (*A*). Posterior and anterior endocardial wall movement along the cursor was traced as indicated by the blue lines on (*B*) across 3 cardiac cycles. End diastolic and systolic distances (EDD & ESD) are used to calculate the fractional shortening (FS). Those are representative images of a 1 day old mouse LV.

(c) Standard pulse wave Doppler

The ultrasound probe was placed to achieve an apical 4 chamber view of the heart and the Doppler cursor placed within the left ventricular cavity below the aortic and mitral valves Figure 2-6A. Representative Doppler traces can be found on Figure 2-6B, C

and schematic representation on Figure 2-6D. The E wave represents the velocity of the blood coming from the left atrium passively filling the left ventricle. This passive filling is due to a fall of pressure in the left ventricle at the end of systole as it relaxes during diastole. The A wave represents the velocity of the blood that is actively pumped out of the left atrium into the left ventricle due to the atrial kick. E/A ratios are used to identify diastolic dysfunction. On each Doppler trace, Myocardial Performance Index (MPI) of the left ventricle was obtained by measurement of isovolumic contraction and relaxation times (IVCT, IVRT) and ejection time (ET) Figure 2-6D. Description of the measurements and formula used can be found on Table 2-7.

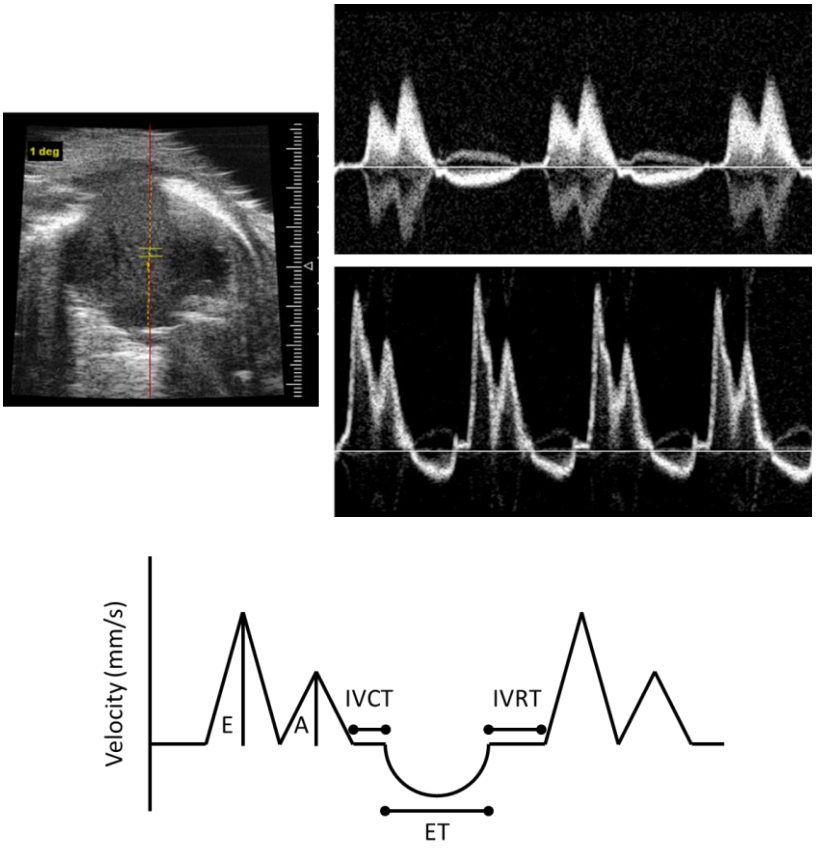


**Figure 2-6: Representative neonatal and adult transmitral pulse wave Doppler traces.** Pulse wave Doppler traces were obtained from 4 chamber apical view of the left ventricle by placing the cursor within the left ventricle (LV) cavity under mitral and aortic valves (*A*). (*B*) shows a typical neonatal (postnatal day 1 -P1-) Doppler trace with A > E wave. (*C*) shows a typical adult (P42) Doppler trace with A < E wave. (*D*) Schematic representation of an adult transmitral Doppler trace with designation of the peak E wave velocity (E), peak A wave velocity (A), isovolumic contraction time (IVCT), ejection time (ET), and isovolumic relaxation time (IVRT).

A

| Parameter Short Name | Parameter Long Name | Formula | Units |
|---|---|---|---|
| ESD | Left Ventricle End Systole Distance | N/A | mm |
| EDD | Left Ventricle End Diastole Distance | N/A | mm |
| FS | Fractional Shortening | $FS = \left({}^{(EDD\ -\ ESD)}/_{EDD}\right)\ x\ 100$ | % |

B

| Parameter Short Name | Parameter Long Name | Formula | Units |
|---|---|---|---|
| IVCT (LV) | Left Ventricle Isovolumic Contraction Time | N/A | ms |
| IVRT (LV) | Left Ventricle Isovolumic Relaxation Time | N/A | ms |
| ET (LV) | Left Ventricle Ejection Time | N/A | ms |
| MV E | Mitral Valve Peak E Velocity | N/A | mm/s |
| MV A | Mitral Valve Peak A Velocity | N/A | mm/s |
| MPI | Myocardial Performance Index | $MPI = {}^{(IVCT\ (LV)\ +\ IVRT(LV))}/_{ET\ LV}$ | N/A |
| E/A ratio | Mitral Valve E to A wave ration | $E/A\ ratio = {}^{MV\ E}/_{MV\ A}$ | N/A |

**Table 2-3: M-mode and Transmitral Pulse Wave Doppler Measurements.**

Measurements obtained from M-mode visualisation (*A*) and transmitral pulse wave Doppler (*B*).

### *2.2.2 Induction and evaluation of cardiac injury in neonatal mice*

#### *2.2.2.1* Preparation for Coronary artery ligation (CAL) surgery in neonatal mice

The surgical area was first cleaned with 70% ethanol. A sterile zone was created by laying of a sterile surgical sheet. A pre-cooled ice pack was then wiped thoroughly with 70% ethanol and placed onto the surgical sheet. A new, sterile surgical sheet was cut and secured onto the ice pack.

The male breeder mouse was removed from the cage containing the females and post-natal day 1 (P1) pups (maternal cage) and placed in a new clean cage. Material from the maternal cage was then collected into a petri dish for later use. The entire litter was placed into a separate box lined with tissue and placed onto a heat mat and under a regular lamp to ensure adequate warmth. Distance of the lamp was adjusted depending on the temperature of the room at the time of the surgery. The pups would be kept in this holding box for a maximum of ~ 3 h depending on litter size.

#### *2.2.2.2* CAL surgery in neonatal mice

Anaesthesia was first induced using isoflurane (4-5%) in medical $O_2$ for 2 min. The pup was then wrapped in tissue and placed in crushed ice for 5 min to induce hypothermia. Adequate anaesthesia was then checked by lack of movement, lack of toe-pinch reflex, and apnoea. The pup was placed and secured in a supine position onto the ice pack to maintain anaesthesia throughout the procedure. In a pilot study pups were maintained under hypothermia for approximately 15min and the following recovery assessed. 100% survival was confirmed at 30min following recovery from hypothermia.

A 5 mm skin incision was placed over the left thorax above the $5^{th}$ rib and the skin was blunt dissected to expose the pectoral muscle using blunt bent forceps. The $5^{th}$ intercostal space was identified and a small opening was created laterally through the pectoral and intercostal muscles with sharp bent forceps. Straight forceps were then used to open the thorax and visualise the left pulmonary lobes and heart. Blunt bent forceps were then used to grab the $5^{th}$ rib and lift it slightly to allow adequate visualisation of the left ventricle and atrium. The left anterior descending (LAD) coronary artery was then identified and ligated using 9-0 Ethilon suture. The ribs and pectoral muscles were then closed with 1 single stich using 8-0 Prolene suture. A first single stich was placed on the skin incision, analgesia was administrated with one drop

of 1/50 bupivacaine in saline onto the wound, a second single stich was placed to fully close the skin wound using 8-0 Prolene suture.

The pup was then returned to the rest of the litter on the heat mat and under the lamp to stimulate recovery and raise body temperature. Full recovery was assessed by restoration of movements, regular breathing patterns, and return of pink colour.

In order to be able to longitudinally follow individual animals each pup was tattooed by injecting a small quantity of dye under the skin of the paws using a 27G needle.

Once the entire litter had undergone surgery and tattooing the pups were rolled in warm and rehydrated material from the maternal cage in an effort to avoid maternal cannibalisation. The entire litter was then returned at once to the maternal cage to the location of the nest. The litter was not checked again for a few hours to avoid maternal stress, which increases risks of cannibalisation (Mahmoud *et al.*, 2014). In a pilot study pups were anaesthetised (isoflurane + hypothermia) and maintained under hypothermia for approximately 15min, recovered and then re-introduced to their mother. 100% survival was confirmed at 24h post-re-introduction.

#### *2.2.2.3* Confirmation of injury and assessment of regeneration

To confirm the presence of injury, cardiac function was assessed the day following the surgery (day 1) using high-resolution *in vivo* ultrasound imaging as described in 2.2.1. Cardiac functional decrease in the first days following LAD ligation has previously been shown to correlate with signs of myocardial injury (Haubner *et al.*, 2012; Porrello *et al.*, 2013). A pilot study was designed to confirm that, in our hands, functional decrease following LAD ligation correlated with signs of myocardial damage. As shown on Figure 2-7A reduced fractional area change (FAC) at day 1 was used to characterise successful LAD ligation leading to myocardial infarction (MI). This correlated with signs of myocardial injury on cardiac sections as shown on Figure 2-7E (black outline) as well as raised plasma cardiac troponin I (cTnI) levels Figure 2-7G. Plasma cTnI levels were measured as described in section 2.3.1 in blood collected from decapitation wounds at day 1 following MI. Functional recovery was also observed at day 21 following LAD ligation (Figure 2-7B) as previously described (Haubner *et al.*, 2012; Porrello *et al.*, 2013) which was associated with normal left ventricular morphology (Figure 2-7F)

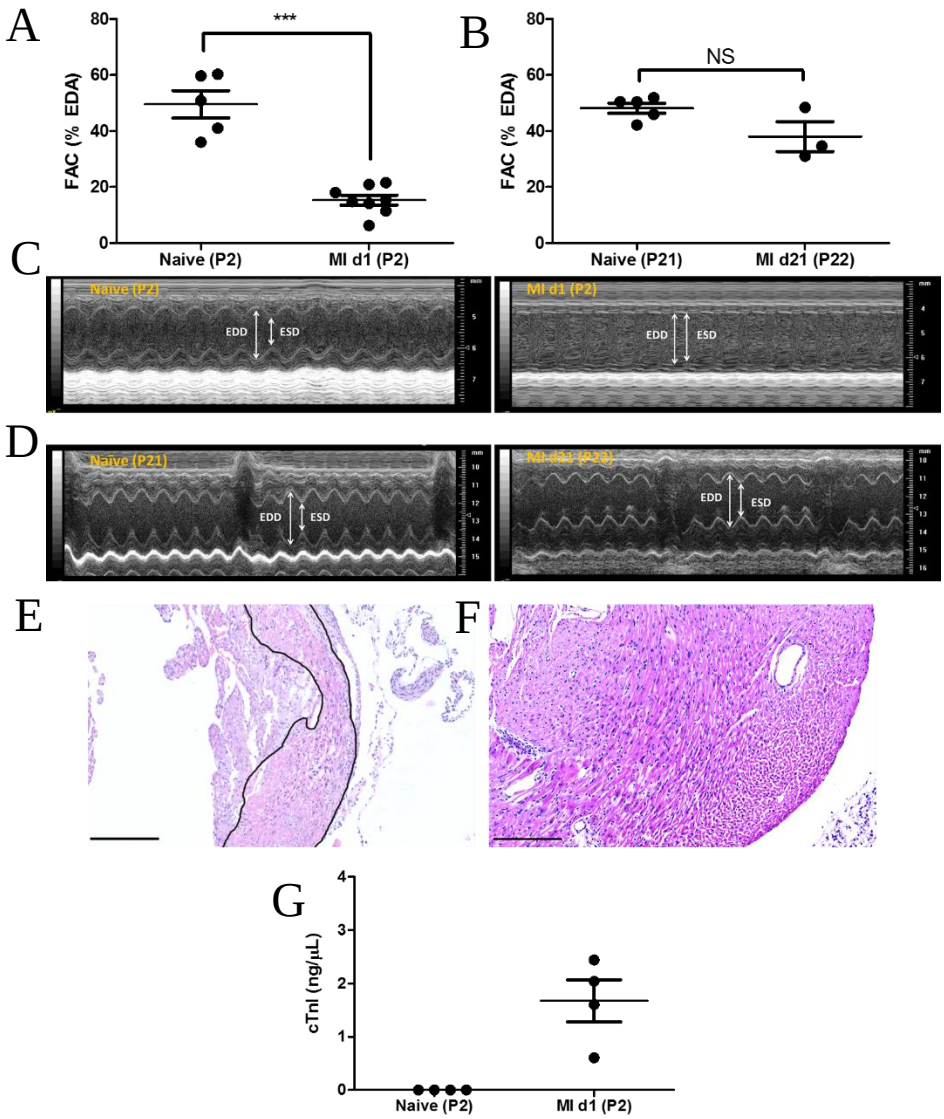


**Figure 2-7: High-resolution *in vivo* ultrasound can be used to confirm presence of injury and regeneration following LAD ligation in P1 mice.** Mice underwent left anterior descending (LAD) coronary artery ligation at postnatal day 1 (P1). At day 1 (P2), cardiac function was assessed on parasternal long axis (PLAX) view of the left ventricle (LV) using M-mode and electrocardiogram gated kilohertz visualisation (EKV) B-mode. Functional decrease was used to characterise successful LAD ligation at day 1 (*A*). Functional recovery was also observed at day 21 as previously described in the literature (Haubner *et al.*, 2012; Porrello *et al.*, 2013) (*B*). Representative LV M-mode traces at day 1 (*C*) and day 21 (*D*) showing absence and recovery of wall movement respectively in the MI group. Arrows represent End Diastolic and Systolic Distances (EDD, ESD) Functional decrease and recovery were respectively associated with signs of injury (black outline-*E*) and normal morphology (*F*) within the LV on H&E stained 4 µm thick cardiac sections. Plasma cardiac troponin I (cTnI) were measured and showed increased levels at day 1 following LAD ligation compared to naïve animals indicative of cardiac injury (*G*). Data are shown as mean ± SEM. ***p < 0.001, Student *t*-test. Scale bars = 200 µm

If the pups were to return to the maternal cage following ultrasound imaging, material from the maternal cage would be collected into a petri dish to use at the time of re-introduction. The entire litter was then placed into a separate box lined with tissue and placed onto a heat mat and under a regular lamp to ensure adequate warmth. Distance from the lamp was adjusted depending on the temperature of the room at the time of the scanning. At the end of the imaging session the pups were returned as described in 2.2.2.2 or culled using a schedule 1 method and relevant tissue collected.

#### *2.2.2.4* Blood sampling

Blood was collected at day 1 following LAD ligation subsequently to ultrasound imaging for analysis of plasma cardiac troponin I levels as described in 2.3.1. Briefly, following decapitation, 50 μL of blood was collected from the open wound from each neonatal mouse (P2) and placed into a 0.5 mL Eppendorf tube containing 50 μL of 3.2% sodium citrate solution to prevent coagulation. The blood sample was thoroughly mixed by pipetting up and down and kept on ice until centrifuged at 6000 g for 10 min at 4$^{o}$C. The plasma was then collected and placed into a new 0.5 mL Eppendorf and the sample stored at -80$^{o}$C until further processing.

### *2.2.3 Termination and tissue harvesting*

At the end of each study, mice were weighed and culled using a schedule 1 method. The chest was then opened and the heart perfused with approximately 2 mL of heparinised saline through the right and left ventricle using a 27G needle. Efficiency of the perfusion could be assessed by discolouration of the liver and lungs. The heart and other relevant organs were harvested and further processed for fluorescence assisted cell sorting (FACS), snap frozen for later RNA extraction, or placed in 10% Formalin in phosphate buffered saline (PBS) for 24h at room temperature (RT) and then for at least another 24h in 70% ethanol before processing for histology.

Organs from MacGreen animals were harvested in the same way but then placed in 4% PFA over-night at 4$^{o}$C on a roller. The organs were then rinsed 3 times for 5 min in PBS and placed in 10% sucrose for 1 hour at RT, 20% sucrose for 2 hours at RT, and 30% sucrose over-night at 4$^{o}$C. Organs were then embedded in optimal cutting temperature (OCT) compound and stored at -80$^{o}$C until further processing.

## 2.3 *In vitro* work

### *2.3.1 Cardiac troponin I (cTnI) enzyme-linked immunosorbent assay (ELISA)*

Cardiac troponin I (cTnI) levels were measured in plasma samples obtained as described in section 2.2.2.4 using a high sensitivity kit following manufacturer's instructions. Plasma cTnI levels have long been identified as a powerful marker of cardiac injury (Adams *et al.*, 1993). Briefly, plasma was further diluted 1:2 with the provided plasma diluent. The sample was then incubated with two antibodies directed against cTnI: one attached to the microtiter wells for solid phase immobilisation and the second horseradish peroxidase (HRP)-conjugated. This result in a so-called sandwich ELISA, with cTnI being secured between the solid phase and HRP-conjugated antibodies. Samples were then incubated at room temperature for 1 hour on a plate shaker, washed with wash solution, and incubated for 20 min with tetramethylbenzine, a substrate of HRP. This leads to the development of a blue colour stopped by the addition of 1N HCl turning the colour yellow. The absorbance of the samples at 405 nm was then obtained on a plate reader. A standard curve was used to quantitatively determine the concentration of plasma cTnI.

This protocol is designed for adult mice which present with levels of plasma troponin above 10 ng/mL following MI. As the samples are diluted 1:4 overall, this falls within the usual standard curve done with the assay (Figure 2-8A). However, the optical density (OD) of the plasma samples from naïve and post-MI neonatal animals were lower than those usually obtained from adults and fell at the extremity of the standard curve where the linear regression is not most accurate (Figure 2-8A). A new standard curve was obtained from the OD values of the standards with the lowest concentrations (Figure 2-8B). The samples' OD fell within the new standard curve's linear regression which had a good coefficient of determination ($R^2$) (Figure 2-8B).

A

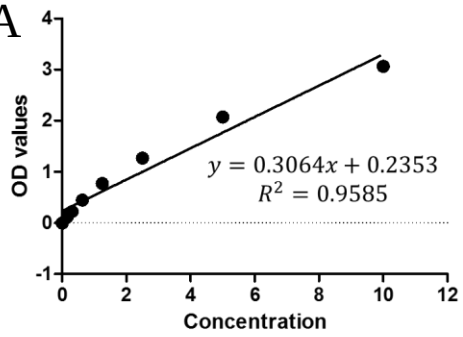


B

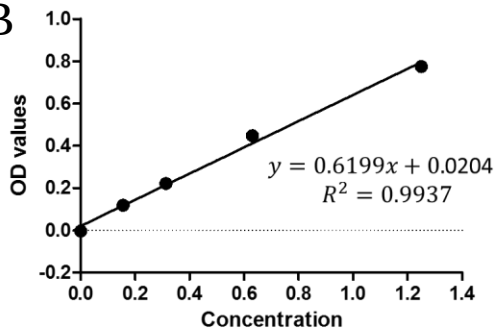


C

| Samples | OD values |
|---|---|
| Naïve (P2) | 0.007 |
| Naïve (P2) | 0.01 |
| Naïve (P2) | 0.005 |
| Naïve (P2) | 0.003 |
| MI d1 (P2) | 0.399 |
| MI d1 (P2) | 0.337 |
| MI d1 (P2) | 0.269 |
| MI d1 (P2) | 0.114 |

**Figure 2-8: Determination of plasma cTnI levels in naïve and post-MI neonatal mice.** Plasma samples were obtained and cTnI concentration measured using a high-sensitivity kit. The original standard curve (*A*) presented with a good coefficient of determination (R2) but the samples fell at one extremity of the linear regression which had poor correlation. A new standard curve was made from the standards with the lowest concentration and a linear regression produced (*B*). Linear regressions' equations and R2 are present on each graph. (*C*) is the list of optical density (OD) values obtained for each naïve and post-myocardial infarction (MI) samples. Linear regression was performed on GraphPad Prism 5.

### *2.3.2 Fluorescence Assisted Cell Sorting (FACS)*

#### *2.3.2.1* Cell suspension preparation from neonatal myocardium

Unless stated otherwise, due to the amount of tissue available from a neonatal heart and according to previous work (Aurora *et al.*, 2014) it was decided to pool multiple neonatal hearts in order to perform FACS. The hearts were harvested as described in 2.2.3. The hearts would then be placed into cold Hank's balanced salt solution (HBSS) in a 1.5 mL Eppendorf tube. All FACS experiments were performed on $GFP^{+ve}$ MacGreen mice. Expression of GFP was assessed prior to further processing as described in 2.1.1.2(b).

Hearts were cut into small pieces and placed in a MACs tube C containing 7.5 mL of warm HBSS supplemented with 1.25 g/L collagenase D and 60 U/mL of DNase I. The tissue was consecutively processed on a gentleMACs dissociator and placed in an incubator for 30 min at 37°C. The tissue was then processed on the gentleMACs

dissociator once more and the digest was strained through a 70 μm mesh filter into a 50 mL falcon tube. 20 mL of cold PBS without calcium or magnesium (PBS-/-) was then used to rinse the MACs tube. The liquid was then used to flush the filter. The sample was centrifuged (300 g, 5 min, 4°C), re-suspended in 10 mL PBS-/-, and centrifuged again. The supernatant was discarded again and cells were re-suspended in 1 mL PBS -/-.

*2.3.2.2* Cardiac mononuclear phagocytes isolation from neonatal myocardium

Cells were spun at 300g for 5 min at 4°C, supernatant was discarded and 10 μL of mouse serum was added to each sample containing 100 μL of PBS-/- for 20 min at 4°C. 50 μL of antibody solution was subsequently added to the stained sample and incubated for 30 min at 4°C in the dark. Antibody solution was as described in Table 2-7.

| Antigen | Fluorochrome | Dilution |
|---|---|---|
| CD45 | PE/Cy7 | 1/100 |
| Ly6G | Pacific Blue | 1/100 |
| CD11b | AF700 | 1/100 |
| F4/80 | PE | 1/100 |
| Ly6C | PerCP Cy5.5 | 1/100 |

**Table 2-4: Antibody panel and dilution for cardiac mononuclear phagocyte isolation from neonatal hearts.** Fluorochrome labelled antibodies were used against the antigen listed above to identify cardiac mononuclear phagocyte population in the neonatal mouse heart.

The cell suspension was consecutively rinsed with 1 mL of PBS-/- and cells re-suspended in PBS-/- supplemented with 2% foetal bovine serum (FBS).

Cells were sorted on a FACSAria II or FACS fusion into 2 mL tubes containing complete DMEM medium supplemented with 10% FBS. Figure 2-9 shows the gating strategies used for extraction of cardiac mononuclear phagocytes from neonatal hearts. On Figure 2-10 are the fluorescence minus one (FMO) negative controls for F4/80, CD11b, and Ly6C. Cardiac mononuclear phagocytes were collected from naïve and post-MI neonatal hearts. F4/80$^{lo}$, CD11b$^{hi}$, Ly6C$^{-ve}$ and F4/80$^{hi}$, CD11b$^{lo}$, Ly6C$^{-ve}$ populations were collected from naïve neonatal hearts. Following MI, the F4/80$^{hi}$,

CD11b$^{lo}$, Ly6C$^{-ve}$ was mostly gone (Section 5.4.1), F4/80$^{lo}$, CD11b$^{hi}$, Ly6C$^{-ve}$ were collected.

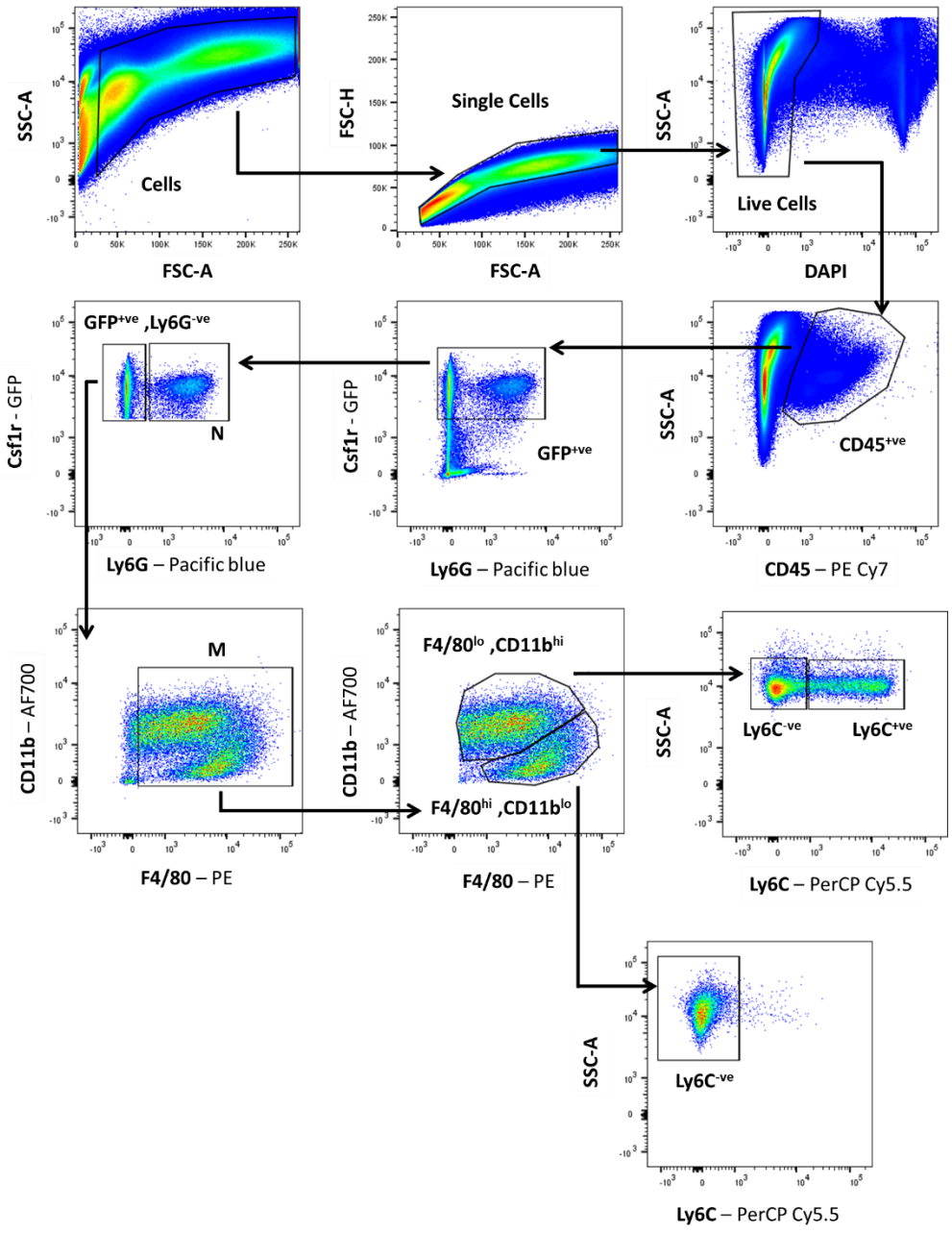


**Figure 2-9: Gating strategy for cardiac mononuclear phagocytes from neonatal MacGreen mice.** Cells were gated in the order indicated by the black arrows. SSC-A and FSC-A were used to exclude cell debris giving the gate named 'Cells'. Single cells were then gated using FSC-H and FSC-A. From the single cells gate, live cells were identified as DAPI$^{-ve}$. Leukocytes were then gated as CD45$^{+ve}$. GFP and Ly6G were then used to identify neutrophils as GFP$^{+ve}$, Ly6G$^{+ve}$ labelled N. The GFP$^{+ve}$, Ly6G$^{-ve}$ population was then gated on CD11b and F4/80 in order to identify mononuclear phagocytes (labelled M) as (F4/80, CD11b)$^{+ve}$. Mononuclear phagocytes could be

subdivided into F4/80$^{lo}$, CD11b$^{hi}$ and F4/80$^{hi}$, CD11b$^{lo}$ subsets. Those were further characterised based on expression of Ly6C (Ly6C$^{-ve}$ and Ly6C$^{+ve}$ populations). Abbreviations; SSC-A: side scatter-area, FSC-A: forward scatter-area, SSC-H: side scatter-height, FSC-H: forward scatter-height.

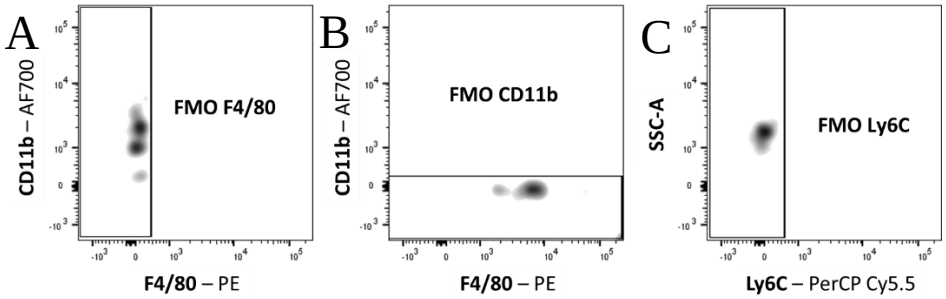


**Figure 2-10: Fluorescence minus one (FMO) negative controls for F4/80, CD11b, and Ly6C.** Cells obtained from cardiac digests were stained with all antibodies listed in Table 2-4 and DAPI except anti-F4/80 (*A*), anti-CD11b (*B*), or anti-Ly6C (*C*). Cells were gated as shown on Figure 2-9 and the negative population for F4/80 (*A*), CD11b (*B*), or Ly6C (*C*) identified.

## 2.4 Molecular biology

### *2.4.1 RNA extraction*

Prior to any work involving RNA samples a designated area of the bench, as well as pipettes and any consumables required, was wiped clean with 70% ethanol followed by RNase Zap. RNase free filtered tips were used.

#### *2.4.1.1* From cardiac mononuclear phagocytes

A cell suspension of cardiac mononuclear phagocyte subsets was isolated using FACS as described in 2.3.2. Cells were spun down at 1000 g for 5 min at 4$^{o}$C and RNA was extracted using an RNeasy® Micro Kit. Briefly, supernatant was removed and cells lysed with 75 µL of RLT buffer provided in the RNeasy® kit supplemented with 1% β-mercaptoethanol. One volume of 70% ethanol was added to the cell lysate. The mix was then loaded onto an RNeasy® Micro Kit column and processed according to manufacturer's instructions. Total RNA was pulled down in 14 µL of RNase free water and stored at -80$^{o}$C until further processing.

#### *2.4.1.2* From whole heart

Tissues were harvested as described in 2.2.3 and snap frozen until RNA extraction. Each whole heart (right and left ventricle) were placed in a labelled 2 mL tissue homogenizing tubes containing ceramic beads on dry ice and 1 mL of QIAzol® reagent added to the sample before placing it on wet ice. The samples were then

homogenised using a Precelly 24 tissue homogeniser 2 times at 6500 rpm for 30 s and immediately placed on wet ice to cool down. The homogenate was then transferred into an autoclaved 1.5 mL Eppendorf tube, incubated 5 min at RT, and 0.5 mL of chloroform added to the homogenate. Samples were shaken by hand for 15 s, incubated 5 min at RT, and centrifuged at 12,000g for 15 min at 4°C. The upper, aqueous, phase was then transferred into a new autoclaved 1.5 mL Eppendorf , 0.5 mL of isopropanol added, samples vortexed, and incubated 5 min at RT. Samples were then centrifuged at 12,000g for 10 min at 4°C, supernatant discarded, and RNA pellet rinsed with 1 mL of 70% ethanol. Samples were then centrifuged at 7,500g for 5 min at 4°C, supernatant discarded, and RNA pellet air-dried. Once dry, RNA pellet was dissolved in 30 µL of RNase free water and stored at -80°C until further use.

### *2.4.2 mRNA expression evaluation*

#### *2.4.2.1* In cardiac mononuclear phagocytes

Total RNA concentration was evaluated on a Nanodrop 1000 but was below the detection limit in all samples tested. RNA samples from naïve animals were therefore pooled, precipitated with 7.5 M of lithium chloride solution, rinsed with 70% ethanol and re-suspended in 14 µL of RNase free water to increase RNA concentration. RNA samples from post-MI animals were not pooled. Concentrations were however below the detection limit of the Nanodrop 1000. At this point, samples contained RNA of up to 18 neonatal hearts.

The total RNA concentration of the samples was then obtained using an Agilent RNA 6000 Nano kit. RNA concentrations were < 6 ng/ µL in a total volume of approximately 10 µL (Figure 2-11A). The intention has been to run these sample on an RT$^2$ Profiler™ PCR array specific to the mouse Wnt signalling, but the amount of RNA was below the minimum required (400 ng). Regular quantitative PCR (qPCR) was therefore performed on macrophage RNA from naïve and post-MI hearts to assess the presence of the *Wnt5b* and *Gapdh* transcripts. Briefly, cDNA was synthesised from 10 µL of RNA sample using the QuantiTect® reverse transcription kit according to manufacturer's instruction including a genomic DNA wipe-out step. Freshly synthesised cDNA was used for qPCR of *Wnt5b* and *Gapdh* using Taqman gene expression assays and prepared as follows:

- Taqman Universal Master Mix II (2x) 5 μL
- Taqman Gene Expression Assay 2 μL
- cDNA 2 μL
- Nuclease Free $H_2O$ 1 μL

The following programme was used to run the qPCR on a 7900HT Fast Real-Time PCR system:

1) 95°C, 1 min 20 s
2) 95°C, 1 s
3) 60°C, 20 s

] 40 cycles

The amount of RNA obtained from cardiac mononuclear phagocytes was also too low for regular qPCR. As shown on Figure 2-11B, the house-keeping gene *Gapdh* had threshold cycle (Ct) values around 30 indicating low amount of the transcript due to the low quantity of total RNA. The transcript for *Wnt5b* did not yield any amplification within the 40-cycle limit indicating that regular qPCR is unable to detect its expression in our sample.

A

| | [totalRNA] (ng/μL) | RIN | total RNA (ng) |
|---|---|---|---|
| **P2 (F4/80hi, CD11blo, Ly6C-ve)** | 0.29 | N/A | 2.9 |
| **P2 (F4/80lo, CD11bhi, Ly6C-ve)** | 1.38 | N/A | 13.8 |
| **P8 (F4/80hi, CD11blo, Ly6C-ve)** | 3.57 | N/A | 35.65489 |
| **P8 (F4/80lo, CD11bhi, Ly6C-ve)** | 3.36 | N/A | 33.56788 |
| **d7 post-MI(F4/80lo, CD11bhi, Ly6C-ve)** | 5.67 ± 0.68 | N/A | 56.73 ± 6.85 |

B

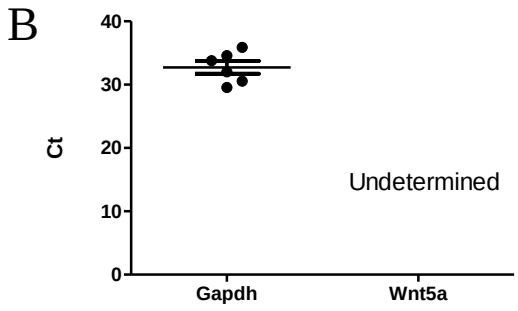


**Figure 2-11: Total RNA concentration is insufficient to use on RT2 Profiler™ PCR array.** Total RNA concentration of different cardiac mononuclear phagocyte populations was assessed on an Agilent nano chip (*A*). mRNA expression of *Gapdh* and *Wnt5a* was assessed using Taqman gene expression assays (*B*)

*2.4.2.2* In whole heart

(a) Samples

The expression levels of mRNA were assessed on a commercial RT$^2$ Profiler™ PCR array specific to the mouse Wnt signalling pathway in whole heart samples assigned to the following experimental groups:

- Naïve neonatal mice (P8), n=6
- Neonatal mice at day 7 post-MI (P8), n=6
- Adult mice at day 7 post-MI, n=4 (samples supplied by Dr Katie Mylonas)

(b) cDNA synthesis

Immediately after assessing whole heart total RNA quantity and quality using a Nanodrop 1000, cDNA was synthesised from each sample using the RT$^2$ First Strand Kit provided with the RT$^2$ Profiler™ PCR array specific to the mouse Wnt signalling pathway. Briefly, 400 ng of total RNA of each sample was incubated in a genomic DNA elimination mix at 42$^o$C for 5 min in a thermocycler (reaction volume: 10 μL). Reverse transcription mix was then added to each sample that were then incubated at 42$^o$C for 15 min (reaction volume: 20 μL). The reaction was stopped by a step at 95$^o$C for 5 min and 91 μL of RNase free water was added to each sample. At this point cDNA samples were kept at -20$^o$C for less than 48h.

(c) mRNA expression

To 102 μL of each cDNA sample was added 650 μL of 2x RT$^2$ SYBR Green Mastermix and 548 μL of RNase free water. Samples were then dispensed into RT$^2$ Profiler PCR Array plates pre-loaded with primers and probes for 84 genes related to the Wnt signalling pathway as well as controls. Figure 2-12 shows the RT$^2$ Profiler PCR Array layout. A list of each gene can be found in Appendix.

| | 1 | 2 | 3 | 4 | 5 | 6 | 7 | 8 | 9 | 10 | 11 | 12 | 13 | 14 | 15 | 16 | 17 | 18 | 19 | 20 | 21 | 22 | 23 | 24 |
|---|---|---|---|---|---|---|---|---|---|---|---|---|---|---|---|---|---|---|---|---|---|---|---|---|
| A | 1 | 1 | 2 | 2 | 3 | 3 | 4 | 4 | 5 | 5 | 6 | 6 | 7 | 7 | 8 | 8 | 9 | 9 | 10 | 10 | 11 | 11 | 12 | 12 |
| B | 1 | 1 | 2 | 2 | 3 | 3 | 4 | 4 | 5 | 5 | 6 | 6 | 7 | 7 | 8 | 8 | 9 | 9 | 10 | 10 | 11 | 11 | 12 | 12 |
| C | 13 | 13 | 14 | 14 | 15 | 15 | 16 | 16 | 17 | 17 | 18 | 18 | 19 | 19 | 20 | 20 | 21 | 21 | 22 | 22 | 23 | 23 | 24 | 24 |
| D | 13 | 13 | 14 | 14 | 15 | 15 | 16 | 16 | 17 | 17 | 18 | 18 | 19 | 19 | 20 | 20 | 21 | 21 | 22 | 22 | 23 | 23 | 24 | 24 |
| E | 25 | 25 | 26 | 26 | 27 | 27 | 28 | 28 | 29 | 29 | 30 | 30 | 31 | 31 | 32 | 32 | 33 | 33 | 34 | 34 | 35 | 35 | 36 | 36 |
| F | 25 | 25 | 26 | 26 | 27 | 27 | 28 | 28 | 29 | 29 | 30 | 30 | 31 | 31 | 32 | 32 | 33 | 33 | 34 | 34 | 35 | 35 | 36 | 36 |
| G | 37 | 37 | 38 | 38 | 39 | 39 | 40 | 40 | 41 | 41 | 42 | 42 | 43 | 43 | 44 | 44 | 45 | 45 | 46 | 46 | 47 | 47 | 48 | 48 |
| H | 37 | 37 | 38 | 38 | 39 | 39 | 40 | 40 | 41 | 41 | 42 | 42 | 43 | 43 | 44 | 44 | 45 | 45 | 46 | 46 | 47 | 47 | 48 | 48 |
| I | 49 | 49 | 50 | 50 | 51 | 51 | 52 | 52 | 53 | 53 | 54 | 54 | 55 | 55 | 56 | 56 | 57 | 57 | 58 | 58 | 59 | 59 | 60 | 60 |
| J | 49 | 49 | 50 | 50 | 51 | 51 | 52 | 52 | 53 | 53 | 54 | 54 | 55 | 55 | 56 | 56 | 57 | 57 | 58 | 58 | 59 | 59 | 60 | 60 |
| K | 61 | 61 | 62 | 62 | 63 | 63 | 64 | 64 | 65 | 65 | 66 | 66 | 67 | 67 | 68 | 68 | 69 | 69 | 70 | 70 | 71 | 71 | 72 | 72 |
| L | 61 | 61 | 62 | 62 | 63 | 63 | 64 | 64 | 65 | 65 | 66 | 66 | 67 | 67 | 68 | 68 | 69 | 69 | 70 | 70 | 71 | 71 | 72 | 72 |
| M | 73 | 73 | 74 | 74 | 75 | 75 | 76 | 76 | 77 | 77 | 78 | 78 | 79 | 79 | 80 | 80 | 81 | 81 | 82 | 82 | 83 | 83 | 84 | 84 |
| N | 73 | 73 | 74 | 74 | 75 | 75 | 76 | 76 | 77 | 77 | 78 | 78 | 79 | 79 | 80 | 80 | 81 | 81 | 82 | 82 | 83 | 83 | 84 | 84 |
| O | HKG | HKG | HKG | HKG | HKG | HKG | HKG | HKG | HKG | HKG | GDC | GDC | RTC | RTC | RTC | RTC | RTC | RTC | PPC | PPC | PPC | PPC | PPC | PPC |
| P | HKG | HKG | HKG | HKG | HKG | HKG | HKG | HKG | HKG | HKG | GDC | GDC | RTC | RTC | RTC | RTC | RTC | RTC | PPC | PPC | PPC | PPC | PPC | PPC |

**Figure 2-12: RT$^2$ PCR profiler array template.** Each 384-well plate had been pre-plated with 84 genes of interest to the Wnt signalling pathway, 5 house-keeping genes (HKG), genomic DNA controls (GDC), reverse transcription controls (RTC), and positive PCR controls (PPC). Each number from 1 to 84 represent each of the 84 genes tested and listed in Appendix. The primers and probes for each gene was plated in quadruplets allowing analysis of 4 samples per plate.

Each plate was then run onto a Roche Lightcycler 480 using the guidelines obtained from: http://www.sabiosciences.com/pcrarrayprotocolfiles.php. The following programme was used:

1) Heat activation
    - 95ºC, 10 min
2) PCR Cycling
    - 95ºC, 15 s
    - 60ºC, 1 min

    ] 40 cycles
3) Melt Curve
    - 60ºC, 15 s
    - 95ºC, 0.03ºC/s

(d) Analysis

The threshold cycle (Ct) was calculated for each well using the second derivative method on the Roche Lightcycler software and an excel spread sheet was formatted as shown on Figure 2-13 to compare expression data between experimental groups.

Quality controls were then run per manufacturer's instructions. The Ct value for the genomic DNA (gDNA) contamination controls were above 35 for all samples studied.

This indicates that the gDNA contamination is inexistent or too low to affect gene expression profiling. To assess efficiency of the reverse transcription the following formula was used for each plate:

$$\Delta Ct = average\ Ct^{RTC} - average\ Ct^{PPC}$$

The value was below 5 for each RT$^2$ Profiler™ PCR array plate indicating efficient reverse transcription. PCR reproducibility was assessed by comparing the Ct(PPC) values for each sample which should be 20 ± 2 on each RT$^2$ Profiler™ PCR array plate and between each plate. One sample belonging to the day 7 adult MI group was discarded as its Ct(PPC) value was 25.27. All other samples passed this quality control indicating good reproducibility and allows comparison of the results between plates.

samples →

| | 16-214 | 16-217 | 16-218 | 16-219 | 16-221 | 16-222 | 13-139 | 13-181 | 13-183 |
|---|---|---|---|---|---|---|---|---|---|
| | Test group 1 | Test group 1 | Test group 1 | Test group 1 | Test group 1 | Test group 1 | Control Group | Control Group | Control Group |
| A01 | 24.90 | 23.80 | 24.18 | 24.84 | 24.08 | 24.54 | 24.83 | 26.73 | 24.70 |
| A02 | 28.48 | 27.31 | 27.59 | 27.90 | 27.60 | 28.00 | 28.85 | 30.85 | 28.79 |
| A03 | 30.13 | 28.72 | 28.91 | 29.78 | 28.92 | 29.11 | 29.81 | 31.87 | 30.53 |
| A04 | 31.67 | 31.27 | 31.06 | 32.27 | 30.91 | 31.16 | 32.76 | 35.00 | 33.11 |
| A05 | 35.00 | 28.24 | 28.65 | 29.18 | 28.61 | 29.17 | 30.76 | 31.89 | 31.30 |
| A06 | 28.89 | 28.25 | 27.73 | 29.19 | 28.14 | 29.00 | 29.91 | 31.68 | 30.06 |
| A07 | 35.00 | 35.00 | 35.00 | 35.00 | 35.00 | 35.00 | 35.00 | 35.00 | 35.00 |
| A08 | 24.11 | 24.67 | 23.73 | 35.00 | 23.84 | 24.16 | 25.96 | 27.44 | 25.44 |
| A09 | 24.82 | 24.81 | 24.20 | 24.92 | 24.27 | 24.71 | 25.67 | 26.96 | 25.44 |
| A10 | 35.00 | 25.43 | 25.57 | 26.06 | 25.46 | 26.09 | 26.34 | 27.89 | 25.97 |
| A11 | 27.24 | 26.82 | 26.70 | 28.11 | 27.23 | 27.54 | 28.21 | 30.13 | 28.61 |
| A12 | 24.67 | 24.55 | 24.00 | 25.01 | 24.81 | 24.53 | 25.72 | 27.02 | 25.64 |

↑ wells

↖ Ct

**Figure 2-13: Example formatted Excel spread sheet for gene expression analysis.** Data from the RT$^2$ Profiler™ PCR array plates were formatted as shown above. The first column on the left indicates each well number corresponding to a gene of interest or control as shown in Figure 2-12. The first row lists the different samples identification numbers into distinct columns. The second row identifies each sample to an experimental group. One group was always designated as 'Control Group' (green outline) and one group as 'Test group 1' (orange outline). For each sample, the threshold cycle (Ct) was listed against the corresponding well.

The Ct value of the housekeeping genes (HKG) are used to normalise the Ct of each gene of interest (GOI) for each different sample using the following formula:

$$\Delta Ct(GOI)_{sample\ 1} = Ct(GOI)_{sample\ 1} - Ct(HKG)_{sample\ 1}$$

Identification of a HKG that is stably expressed across all samples of the compared experimental groups was performed prior to analysis of the RT$^2$ Profiler™ PCR array

results. Two comparisons were carried out. The first compared mRNA expression levels within whole heart at day 7 following induction of MI in neonatal mice to aged matched naïve samples as the reference. As shown on Figure 2-14 all five HKG displayed great stability between the two experimental groups. However, *Gapdh* presented with the closest match and was therefore chosen as the HKG for this comparison. The second comparison measured mRNA expression difference between whole hearts at day 7 following induction of MI in neonatal and adult mice. As shown on Figure 2-15, the genes had a slightly greater variability between the two experimental groups, *Gusb* was selected as it had the closest match between the two groups.

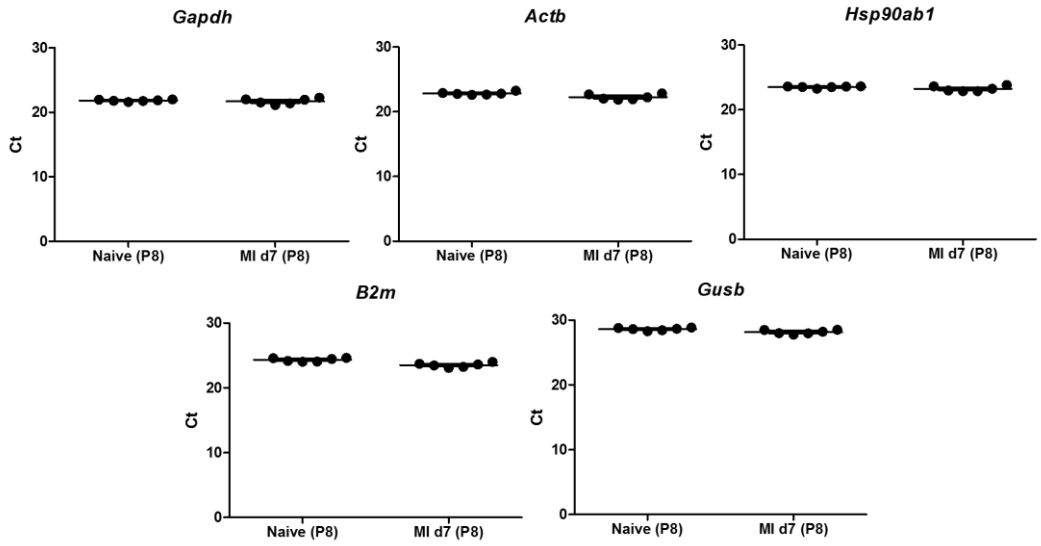


**Figure 2-14: Identification of best-fit housekeeping gene for comparing gene expression changes following MI in the neonatal mouse.** The Ct value of each housekeeping gene (HKG) for each experimental group were plotted and the HKG with the closest match between groups identified and selected for normalising expression data. Here *Gapdh* was selected. Data is mean ± SEM, n=6/group.

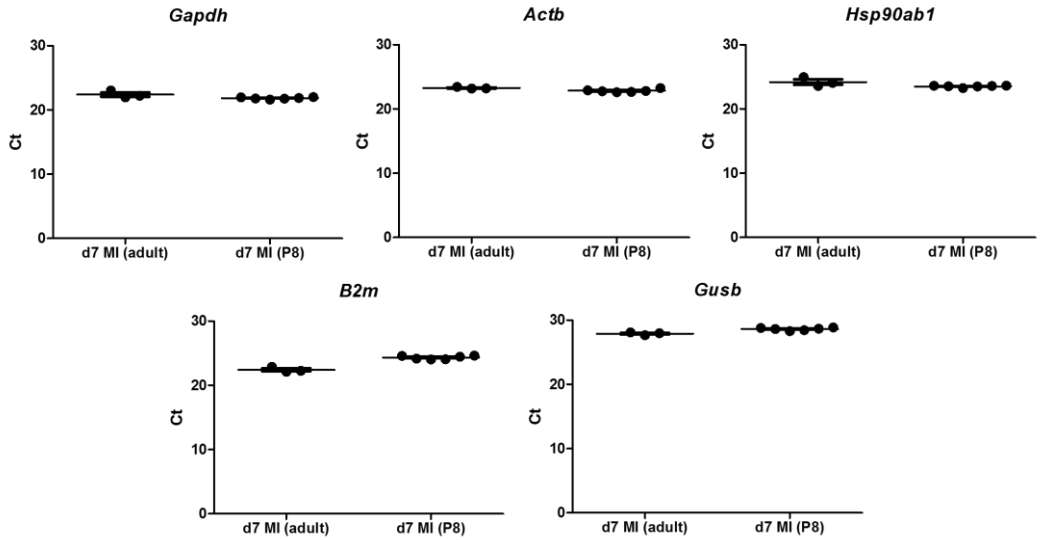


**Figure 2-15: Identification of best-fit housekeeping gene for comparing gene expression changes following MI between adult and neonatal mice.** The Ct value of each housekeeping gene (HKG) for each experimental group were plotted and the HKG with the closest match between groups identified and selected for normalising expression data. Here *Gusb* was selected. Data is mean ± SEM, n=3-6/group.

From the online data analysis centre of Qiagen (link below) the mouse RT$^2$ Profiler™ PCR array specific to the Wnt signalling pathway was selected. The formatted Excel spread sheet was then uploaded onto the online data analysis centre and the Ct cut off set to 35. All samples were quality checked again by the online platform and passed.

http://www.qiagen.com/shop/genes-and-pathways/data-analysis-center-overview-page/

The pre-selected HKG was then used to perform the normalisation of the expression values on the online data analysis centre. The volcano representation of the data was preferred with a boundary set to 1.5-fold change and the p-value to 0.05. This method considers a gene to be significantly differentially regulated between the experimental groups if it is changed by at least 1.5-fold and the p-value for the comparison is $\leq 0.05$. The volcano plot and the report created by the online data analysis centre were exported and saved.

## 2.5 Histology

### *2.5.1 Immunohistochemistry and Immunofluorescence on formalin fixed - paraffin embedded tissue*

Paraffin embedded samples were cut into sequential 4 µm thick sections on a Leitz microtome with disposable blades. Sections were orientated to achieve a short axis, 2 chamber view of the heart. Ribbons of sections were carefully transferred onto the surface of a 45$^{o}$C water bath and placed onto electrostatic slides. The slides were then labelled and dehydrated overnight at room temperature.

Prior to staining, slides were deparaffinised and rehydrated by sequential transfer into xylene (2 x 5 min), absolute ethanol (2 x 10 s), 90% ethanol (10 s), 80% ethanol (10 s), 70% ethanol (10 s), and finally washed in distilled water for 5 min.

#### *2.5.1.1* Haematoxylin and Eosin (H&E) staining

*Staining*. This staining was performed at the Queen's Medical Research Institute (QMRI) shared university research facility (SuRF) histology department by myself using standardised protocol. Briefly, following deparaffinisation and rehydration slides were immersed in Harris Haematoxylin solution (5 min), rinsed under running water (20 s), immersed in 1% acid alcohol solution (5 s), dipped into Scott's tap water (2 min), and placed in eosin solution (20s). Slides were finally rinsed under running water and dehydrated and cleared by sequential immersion in 70% ethanol (5s), 80% ethanol (5 s), 90% ethanol (5 s), absolute ethanol (2 x 5 s), and xylene (2 x 5 min). Slides were then mounted with coverslip and left to dry overnight at room temperature.

*Analysis.* Images were acquired on a Zeiss slide scanner at magnification x40.

#### *2.5.1.2* Picrosirius Red (PSR) staining

*Staining*. This staining was performed by Melanie McMillan at the QMRI's SuRF histology department using a standard protocol. Briefly, following deparaffinisation and rehydration slides were immerged in commercially available picric acid solution containing 0.1% direct red (picrosirius red -PSR- solution) for 2-4 hours. Slides are then dehydrated and cleared (2.5.1.1). Slides were then mounted with coverslip and left to dry overnight at room temperature.

*Analysis.* Pictures were then taken using either a Nikon Eclipse E800 microscope using a Prior proscan II stage at maginification x10 (Chapter 3) or using a Zeiss slide scanner at magnification x40 (Chapter 4 & 5). Analysis was either carried out in Adobe

Photoshop CS6 or Definiens software. When using Adobe Photoshop CS6, a region of interest (ROI) was selected encompassing the whole LV. A sample image was then used to create a colour range mask for the $PSR^{+ve}$ area and for the whole tissue area. This was done by identifying pixels falling into each category until a representative selection could be obtained and validated on multiple pictures. $PSR^{+ve}$ and whole tissue area were then exported into Excel for formatting before statistical analysis.

When using Definiens software, images were grouped into dark, light, and medium subsets to obtain more accurate identification of the PSR staining considering variability in the strength of the staining. Each subset was exported into Definiens Tissue Studio v2.4 and ROIs manually selected encompassing the whole LV. Each ROI was then saved into a workspace and opened in Definiens Developer XD v2.4. The image with the widest colour variation within the subset was chosen for sample training. A chessboard segmentation was applied to each image creating 5 x 5 pixels squares for analysis. A schematic representation can be found on Figure 2-16A. $PSR^{+ve}$, whole tissue, and background were assigned a class and the software trained on the sample image by selecting groups of pixels belonging to each class. The red-green-blue (RGB) value of each selected group of pixel for each class was recorded by the software and plotted. Groups of pixels were selected until a smooth distribution of RGB values for each class could be discerned. Representative distribution for each class can be found on Figure 2-16B. Each group of pixel on the entire image would then be assigned a class using built-in features of the software. This was then done automatically for all the images of the subset and total $PSR^{+ve}$ and whole tissue area exported into excel. This above protocol was designed in close collaboration with Daniel Soong who wrote and performed the algorithms in Definiens Developer XD v2.4.

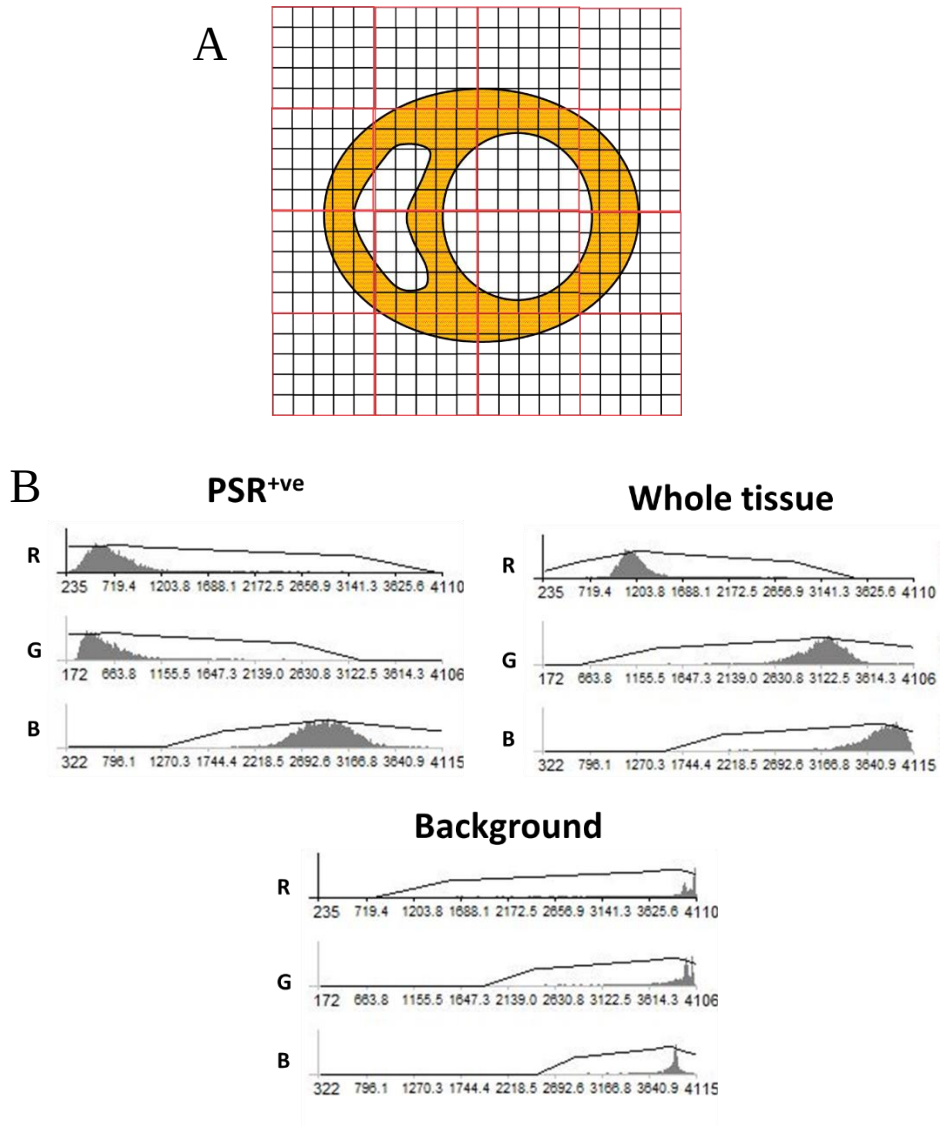


**Figure 2-16: Picrosirius red analysis using Definiens Developer XD v2.4 software.** Following region of interest selection in Definiens Tissue Studio v2.4 images a workspace was created and opened in Definiens Developer XD v2.4. A chessboard segmentation was applied to each image. (*A*) is a simplified representation of this method. Groups of 5 x 5 pixels were created from the original image for further analysis. Black squares are the original pixels and the red squares represent the chessboard segmentation grouping pixels. The functions presented in (*B*) were used to define $PSR^{+ve}$, whole tissue, and background classes using red (R), green (G), blue (B) (RGB) values obtained from a training sample.

### *2.5.1.3* Section processing for immunofluorescence

Following deparaffinisation and rehydration, an antigen retrieval was carried out by immersion and microwave heating of the slides in sodium citrate buffer (10 mM, pH6. Slides were allowed to cool down to RT for an hour. Slides were then rinsed twice in PBS for 3 min, and then mounted onto a Sequenza slide rack.

(a) Cardiomyocytes cross-sectional area (CMCSA)

*Staining*. Non-specific staining was blocked by 1-hour incubation in 150 μL of 10% normal goat serum at room temperature. Slides were incubated overnight at 4°C with 150 μL of 1/100 biotinylated Isolectin B4 (IB4) in PBS. The following day the slides were rinsed 3x with 1 mL of PBS and incubated with 150 μL of 1/100 streptavidin coupled Alexa Fluor® 488 and 1/75 rhodamine-coupled wheat germ agglutinin (WGA) in PBS for 1h at RT in the dark. IB4 and WGA are both lectins binding to carbohydrates found at the cell membrane. IB4 binds to carbohydrates mainly found on endothelial cells' membrane whilst WGA binds to all membranes. Slides were rinsed 3x with 1 mL of PBS. Slides were then stained with DAPI (nuclei) for 5 min at RT, rinsed and mounted with Fluoromount G and coverslips. Slides were left to dry overnight in the dark at RT and subsequently stored in the dark at 4°C.

*Analysis*. Pictures were then taken using either a Zeiss Axiovert200 microscope or a Zeiss slide scanner at magnification x40. Four fields of view within the outer myocardium were obtained as it is where the cardiomyocytes lay perpendicular to the short axis view. This view allows measurement of CMCSA. In each field of view, 10 cardiomyocytes' cross sectional area were measured using Adobe Photoshop CS6 software.

(b) Coronary vasculature

*Staining*. Non-specific staining was blocked by 1-hour incubation in 150 μL of 10% normal goat serum at room temperature. Slides were incubated overnight at 4°C with 150 μL of 1/100 biotinylated IB4 in PBS. The following day the slides were rinsed 3x with 1 mL of PBS and incubated with 150 μL of 1/100 streptavidin coupled Alexa Fluor® 488 and 1/75 Cyanin3 (Cy3) coupled anti-α smooth muscle actin (αSMA) antibody in PBS for 1h at RT in the dark. Slides were rinsed 3x with 1 mL of PBS. Slides were then stained with DAPI (nuclei) for 5 min at RT, rinsed and mounted with Fluoromount G and coverslips. Slides were left to dry overnight in the dark at RT and subsequently stored in the dark at 4°C.

*Analysis*. Pictures were then taken using either a Zeiss Axiovert200 microscope or a Zeiss slide scanner at magnification x40. Five fields of view within the outer myocardium were obtained. Neonatal outer myocardium is not entirely compacted

leading to regions without tissues. In comparison, the adult outer myocardium is dense. For the quantification of vascular density, regions only containing myocardium were drawn around and their areas measured. Counting of vessels was then performed within each region and normalised to its respective area. This allows quantification of vascular density, expressed in vessels per $mm^2$, and avoids skewing the result by including regions empty of myocardium. Vessels diameter were also measured within the selected regions. The number of $\alpha SMA^{+ve}$ vessels was counted within the whole left ventricle. All measurements were performed in Adobe Photoshop CS6 software.

(c) Cardiomyocytes proliferation

*Staining*. Cell membranes were permeabilised by incubating the slides with 150 µL of 0.2% triton x-100 in PBS for 10 min at RT, slides rinsed 3x with 1 mL of PBS, and incubated with 150 µL of blocking solution, 20% normal goat serum and 5% bovine serum albumin (BSA) in TBS, for 1h at RT. Slides were then incubated overnight at 4°C with 150 µL of 1/200 of mouse anti-cardiac troponin T (cTnT) and 1/200 of rabbit anti-Ki67 in blocking solution with 0.1% Tween. The following day the slides were rinsed 3x with 1 mL of TBS and incubated with 150 µL of goat anti-rabbit and goat anti-mouse secondary antibodies coupled with Alexa Fluor® 555 and Alexa Fluor® 488 respectively in TBS for 1h in the dark at RT. Slides were rinsed 3x with 1 mL of TBS. Slides were then stained with DAPI (nuclei) for 5 min at RT, rinsed and mounted with Fluoromount G and coverslips. Slides were left to dry overnight in the dark at RT and subsequently stored in the dark at 4°C.

*Analysis*. Pictures were then taken using either a Zeiss Axiovert200 microscope or a Zeiss slide scanner at magnification x40. For hearts from the C57BL/6Jola and *Csf1r*-null mouse lines, regions only containing myocardium were drawn around and their areas measured, as explained in (b)2.5.1.3(b). Counting of the number of $Ki67^{+ve}$ nuclei within $cTnT^{+ve}$ cardiomyocytes was performed within each region and normalised to its area. This analysis was performed on Adobe Photoshop CS6.

For hearts from the Porcupine mouse line, whole section images obtained with the Zeiss slide scanner were exported into Definiens tissue studio v2.4 software and ROIs manually selected encompassing the whole LV. Within each ROI, nuclei were detected at 10x using a built-in nuclear detection algorithm based on size and shape. Nuclei

detection was refined by indicating to the software 'real' and 'not real' nuclei. The workspace was then opened in Definiens Developer XD v2.4 software. An image with the widest colour variation was chosen for sample training. Cells cytoplasm were simulated by growing nuclei by 3 pixels (pix) at 10x. $Ki67^{+ve}$ cells were identified as having a nuclear to cytoplasmic ratio of Ki67 staining intensity of > 1.6 and a nuclear Ki67 intensity 1.3-fold brighter than the average of all cells. This allows elimination of the immediate background staining around the nucleus. The area positive for cTnT was identified using a thresholding method. $Ki67^{+ve}$ and $Ki67^{-ve}$ nuclei were counted within the $cTnT^{+ve}$ area and data exported for statistical analysis.

### *2.5.2 Immunofluorescence on frozen sections*

Tissues embedded in OCT compound were cut into 10 μm sequential sections on a Leitz cryostat with disposable blades. Sections were orientated to achieve a short axis, 2 chamber view of the heart. Sections were carefully placed onto electrostatic slides, labelled and stored at -80°C until further use. On the day of the staining, the slides were taken out of the -80°C freezer and placed in the dark on the bench top at room temperature for 1h. Slides were then rinsed twice in PBS for 3 min in the dark, excess PBS dabbed with tissue and hydrophobic pen was used to draw around the section.

#### *2.5.2.1* Identification of macrophages

*Staining*. Non-specific staining was blocked by 1-hour incubation in 70 μL of 10% normal goat serum at room temperature in the dark. Slides were briefly rinsed in PBS 1x to remove excess blocking solution and incubated overnight at 4°C with 150 μL of 1/1000 rabbit anti-GFP antibody in PBS. The following day the slides were rinsed 3x in PBS and incubated with 150 μL of 1/200 goat anti-rabbit secondary antibody coupled with Alexa Fluor® 488 in PBS for 1h at RT in the dark. Slides were rinsed 3x in PBS. Slides were then stained with DAPI (nuclei) for 5 min at RT, rinsed and mounted with Fluoromount G and coverslips. Slides were left to dry overnight in the dark at RT and subsequently stored in the dark at 4°C.

*Analysis.* Pictures were then taken using either a Zeiss slide scanner at magnification x40. Areas measuring 200 μm x 200 μm were selected within 5 different fields of view. The number of $GFP^{+ve}$ cells were counted within each area. This analysis was performed on Adobe Photoshop CS6.

## 2.6 Statistical analysis

Statistical analysis was performed using GraphPad Prism 5 software. Data are either expressed as mean SEM or median interquartile range depending on the observed distribution of the samples. Comparison between 2 samples was done using unpaired Student's *t*-test or Mann-Whitney test. Comparison between more than 2 samples was done using either 1 or 2-way ANOVA with post-hoc Bonferroni multi-comparison test. Significance level was set to $p < 0.05$.

## 2.7 List of reagents, consumables and equipment

**Table 2-5: List of reagents and their suppliers.**

| Reagents | Supplier | Catalogue number |
|---|---|---|
| 10X buffer with Magnesium | Sigma-Aldrich | P2192 |
| 16% PFA | Alfa Aesar | 43368 |
| 20% SDS | ThermoFisher scientific | AM9820 |
| Acquasonic 100 ultrasound transmission gel | Parker Labs | N/A |
| Agarose | Bioline | BIO41025 |
| Agilent reagents and chips | Agilent technologies | 5067-1511 |
| anti-Ly6C PerCP Cy5.5 | Biolegend | 128012 |
| anti-mouse CD11b AF700 | Biolegend | 101222 |
| anti-mouse CD45 PE/Cy7 | Biolegend | 109830 |
| anti-mouse F4/80 PE | Biolegend | 123110 |
| anti-mouse Ly6G Pacific blue | Biolegend | 127612 |
| Biomix | Bioline | BI025012 |
| Biotinylated Isolectin B4 | ThermoFisher Scientific | I21414 |
| b-mercaptoethanol | Merck Millipore | 444203 |
| Bovine serum albumin (BSA) | Sigma-Aldrich | A7906 |
| Calcium chloride (CaCL2) | Sigma-Aldrich | C3306 |
| Cardiac Troponin I ELISA kit | Life Diagnostics | CTNI-1-HSP |
| Chloroform | ThermoFisher Scientific | C/4960/17 |
| Collagenase D | Sigma-Aldrich | COLLD-RO |
| Conductive ultrasound gel | Parker Labs | N/A |
| Csf1r-null mouse genotyping primers | ThermoFisher scientific | N/A |

| | | |
|---|---|---|
| Cyanine 3 couple anti-a-smooth muscle actin | Sigma-Aldrich | C6198 |
| DAPI | Sigma-Aldrich | 11284932001 ROCHE |
| Direct red | Sigma-Aldrich | 365548 |
| DMEM | ThermoFisher Scientific | 31053028 |
| DNase I for FACS | Sigma-Aldrich | 11284932001 ROCHE |
| DNeasy Blood and Tissue kit | Qiagen | 69504 |
| dNTPs (2.5mM) | ThermoFisher scientific | R72501 |
| EDTA | Sigma-Aldrich | E8008 |
| Eosin | ThermoFisher Scientific | 6766009 |
| Ethanol | VWR Chemicals | 20821330 |
| Fluoromount G | Southern Biotech | 0100-01 |
| Foetal bovine serum (FBS) | ThermoFisher Scientific | 10500064 |
| Formalin (10%) | Sigma-Aldrich | HT501128 |
| *Gapdh* gene expression assay | ThermoFisher Scientific | Hs02786624 |
| Gel red dye | Biotium | 41003 |
| Glycerol | Sigma-Aldrich | C5516 |
| Goat anti-mouse AF488 | ThermoFisher Scientific | A11001 |
| Goat anti-rabbit AF555 | ThermoFisher Scientific | A32727 |
| Haematoxylin (Harris) | Pioneer Research Chemicals Limited | PRC/R/51 |
| HBSS | ThermoFisher Scientific | 14180046 |
| Heparin | ThermoFisher Scientific | 10639163 |
| Hydrochloric acid (HCl-1N) | ThermoFisher Scientific | SA48-4 |
| Isoflurane | Merial animal health ltd | N/A |
| Isopropanol | VWR Chemicals | 20821330 |

| | | |
|---|---|---|
| MacGreen mouse EGFP genotyping primers | ThermoFisher scientific | N/A |
| MacGreen mouse Fabpi genotyping primers | ThermoFisher scientific | N/A |
| Marcaine (bupivacaine) Polyamp Steripack 0.25% | AstraZeneca | N/A |
| Medical $O_2$ | BOC Medical | N/A |
| Mouse anti-cardiac troponin T | Abcam | Ab10214 |
| Mouse serum | Biosera | MO-340/500 |
| Sodium chloride (NaCl) | Sigma-Aldrich | S3014 |
| Normal Goat Serum | Biosera | GO605/500 |
| Nuclease free water | Qiagen | 1039480 |
| Optimal cutting temperature (OCT) compound | Cell Path | KMA-0100-00A |
| PBS (tablets) | Sigma-Aldrich | P-4417 |
| PBS without calcium without magnesium | ThermoFisher Scientific | 14190-094 |
| Porcupine mouse genotyping primers | ThermoFisher scientific | N/A |
| Proteinase K | ThermoFisher scientific | 25530-015 |
| Qiazol | Qiagen | 79306 |
| QuantiTect reverse transcription kit | Qiagen | 205311 |
| Rabbit anti-GFP | Abcam | Ab290 |
| Rabbit anti-Ki67 | Abcam | Ab15580 |
| RNase free water | Qiagen | N/A |
| RNase Zap | ThermoFisher scientific | AM9780 |
| RNeasy micro kit | Qiagen | 74004 |
| RT2 PCR Profiler array (Mouse Wnt signalling) | Qiagen | PAMM-043ZG-4 |

| | | |
|---|---|---|
| Scott's tap water | Sigma-Aldrich | S5134 |
| Sex genotyping primers | ThermoFisher scientific | N/A |
| Sodium acetate | ThermoFisher scientific | R1181 |
| Sodium citrate | Sigma-Aldrich | W302600 |
| Sterile Saline 0.9% | B Braun | 362 7632 |
| Streptavidin AF488 | ThermoFisher Scientific | S32354 |
| Sucrose | Scientific Laboratory Supplies | CHE3650 |
| Sucrose gel loading dye | ThermoFisher scientific | 10725104 |
| TaKaRa Taq polymerase | TaKaRa | R001 |
| Taqman universal Master Mix II | ThermoFisher Scientific | 4364103 |
| Tattooing dye | Scream Ink (the tattoo shop) | N/A |
| Tris base | ThermoFisher Scientific | BP152-1 |
| Tris borate EDTA (TBE) | National Diagnostics | EC860 |
| Tris HCl | Sigma-Aldrich | 10812846001 |
| Triton X-100 | Sigma | T-8787 |
| Tween 20 | Sigma | P-2287 |
| WGA - Rhodamine | Vectors laboratories | RL-1022 |
| *Wnt5a* gene expression assay | ThermoFisher Scientific | Hs00998537 |
| Xylene | VWR Chemicals | 28975-360 |

**Table 2-6: List of consumable and their suppliers.**

| Consumable | Supplier | Catalogue number |
|---|---|---|
| 27G needle | BD Microlance 3 | 300635 |
| Coverslips | Leica Biosystems | 3800171G |
| Disposable blades | ThermoFisher scientific | 3050835 |
| Eppendorf tubes | ThermoFisher scientific | N/A |
| Ethilon 9-0 | Ethicon | W2813 |

| | | |
|---|---|---|
| Falcon tubes | ThermoFisher scientific | N/A |
| gentleMACS C-tube | Miltenyi biotec | 130-093-237 |
| Prolene 8-0 | Ethicon | W2777 |
| Slides (electrostatic) | VWR | 100501-220 |
| Surgical sheet (sterile) | Vet direct | VGSD001 |
| Tissue homogenizing tubes | OMNI international | SKU 19-627 |

**Table 2-7: List of equipment and their suppliers.**

| Equipment | Supplier | Catalogue number |
|---|---|---|
| 7900HT Fast Real-Time PCR System | ThermoFisher Scientific | N/A |
| Agilent 2100 Bioanalyzer | Agilent Technologies | N/A |
| Animal scale | Ohaus | Traveller TA301 |
| AxioVert 200 | Zeiss | N/A |
| Bench top centrifuge | ThermoFisher Scientific | Heraeus Fresco 17 |
| Bent blunt forceps | Fine Science Tools | FST 11052-10 |
| Copper tape | BQLZR | N/A |
| FACS Aria II | BD biosciences | N/A |
| FACS fusion | BD biosciences | N/A |
| Genotyping thermocycler | MJ Research | PTC-200 |
| gentleMACS Dissociator | Miltenyi biotec | 130-093-235 |
| Large centrifuge (used for FACS protocol) | ThermoFisher Scientific | Heraeus Megafuge 16R |
| Lighcycler® 480 | Roche | N/A |
| Microtome | Leica | Leitz 1512 |
| Nanodrop 1000 | ThermoFisher Scientific | N/A |
| Needle holder | Fine Science Tools | FST 12075-12 |
| Nikon Eclipse E800 | Nikon | N/A |
| Precelly 24 tissue homogeniser | Bertin instruments | N/A |
| Prior proscan II | Prior scientific | N/A |

| | | |
|---|---|---|
| Sequenza slide rack | ThermoFisher Scientific | 73-310-017 |
| Sharp bent forceps | Fine Science Tools | FST 11251-35 |
| Slide scanner | Zeiss | Axio Scan Z1 |
| Small Scissors | Fine Science Tools | FST 15003-08 |
| Straight blunt forceps | Fine Science Tools | FST 11064-07 |
| Thermometer - Adult | Physitemp | RET-3 |
| Thermometer - Neonates | Physitemp | RET-4 |
| Vevo 770 preclinical ultrasound | Visualsonics | N/A |
| Water bath | Sakura Finetek Europe | N/A |

## 2.8 In-house buffer recipes

| In-house buffers | Composition |
|---|---|
| 3.2% sodium citrate buffer | 32.06 g sodium citrate in 1 L deionised water (pH6) |
| Acid alcohol | 1% hydrochloric acid in 70% ethanol |
| Heparinised saline | 10 U for 1 mL of PBS |
| Proteinase K solution | Proteinase K powder with 200 mL 1 M Tris HCl, 800 mL 0.5 M $CaCl_2$, 10 mL glycerol, 9 mL deionised water |
| Sodium citrate buffer (antigen retrieval) | 2.94 g sodium citrate in 1 L deionised water (pH6) |
| Tail buffer | 6.1 g Tris base, 5 mL EDTA, 5 mL 20% SDS, 5.8 g NaCl in 500 mL deionised water |
| Tris-buffered saline (TBS) | 2.42 g Tris base, 8 g NaCl, in 1 L deionised water (pH7.6) |

# Chapter 3: Normal growth and function of the postnatal murine heart

## 3.1 Introduction

In mammals, there is clear evidence that cardiac regeneration is age-dependent. Both the human and mouse neonates have potent cardiac regenerative capacities whilst adults do not (Section 1.3.1). In mice, these capacities are limited to the first postnatal week (Fratz *et al.*, 2011; Porrello *et al.*, 2011, 2013, Haubner *et al.*, 2012, 2016). Understanding the changes occurring in the neonatal period that could contribute to the loss of cardiac regenerative capacities therefore appears crucial. Embryonic cardiac organogenesis has been extensively studied (Section 1.3.2). Comparatively, studies focusing on neonatal cardiac functional and structural maturation are relatively sparse.

Cardiac structure is defined by morphometric measurements but also by the cellular content and architecture. The three major cell types present in the myocardium are cardiomyocytes, endothelial cells, and fibroblasts (Pinto *et al.*, 2016). Cardiomyocytes, making up most of the tissue volume, are known to rapidly lose their proliferative capacities after birth and to mostly grow through hypertrophy in the postnatal mouse (Soonpaa and Field, 1998; Leu *et al.*, 2001; Hirschy *et al.*, 2006). Early proliferative capacity has been linked to cardiac regeneration in the neonatal mouse (Haubner *et al.*, 2012; Porrello *et al.*, 2013). A recent report by Pinto *et al.* (2016) identified endothelial cells as the most abundant non-myocyte cell type in the heart. Angiogenesis is essential for the delivery of oxygen and nutrients to the growing cardiac muscle. At the start of this PhD the origin and development of the coronary vasculature in the embryo had been widely studied as described in Section 1.3.2.2(b). In the postnatal animal, coronary vasculature growth was thought to be achieved through angiogenesis of vessels formed in the embryo. Formal proof of this concept was however lacking. Angiogenesis defects have also been linked to failure of the neonatal mouse heart to regenerate (Aurora *et al.*, 2014).

Due to the size of neonatal mice, the literature linking cardiac functional and structural maturation is sparse. Trans-mitral Doppler imaging had been used to characterise diastolic function in the mouse embryo *in-utero* (Phoon and Turnbull, 2003; Yu *et al.*, 2008) and also postnatally (Zhou *et al.*, 2003b). It had also provided functional assessment following coronary artery ligation (CAL) induced MI in adult and neonatal mice (Haubner *et al.*, 2012; Moran *et al.*, 2013; Porrello *et al.*, 2013). In neonatal mice, however, only non-electrocardiogram (ECG) gated measurements were possible. This

made functional read-outs of fractional area change (FAC) and ejection fraction (EF) as well as structural information on cavity size, average wall thickness, and ventricular mass impossible.

A systematic analysis relating neonatal cardiac structural and functional maturation was thereby missing.

## 3.2 Hypothesis and aims

Hypothesis:

**'New insights on structural and functional maturation of the postnatal murine heart will be provided by a combination of electrocardiogram-gated high resolution *in vivo* ultrasound and histological techniques'**

Aims:

(i) To establish a method to permit collection of structural and functional data *in vivo* in neonatal mice using electrocardiogram-gated high-resolution ultrasound

(ii) To characterise cardiac structural and functional growth in mice from early postnatal to adult stages using histology and ultrasound.

## 3.3 Methods

### *3.3.1 Animals*

All mice used in this chapter were wild-type male C57BL/6J bred in-house from animals originally bought from Harlan, UK. Mice were aged between P2 and P42.

### *3.3.2 Histology*

All tissues were formalin-fixed, paraffin embedded, cut into 4 μm thick sections. Cardiomyocyte cross-sectional area (CMCSA), cardiomyocyte proliferation as well as vessel size, density, and maturation were measured using immuno-fluorescence as described in Section 2.5. Picrosirius red (PSR) staining for collagen content was performed by Miss Melanie McMillan at the Queen's Medical Research Institute histology facility using a standardised protocol.

### *3.3.3 Image acquisition and analysis*

Images used for calculation of CMCSA, vessel size, density and maturation were acquired on a Zeiss Axiovert200, magnification x 40. Images used for measurement of cardiomyocyte proliferation were imaged on a Zeiss slide scanner Axio Scan Z1, magnification x 40. Images used for quantification of collagen content were obtained on Nikon Eclipse E800 microscope using a Prior proscan II stage at magnification x 10. All image analysis was performed on Photoshop CS6 as described in Section 2.5.

### *3.3.4 Ultrasound*

Ultrasound was carried out as described in Section 2.2.1. All ultrasound imaging within this chapter was performed by Mr Adrian Thompson. Ultrasound analysis was carried out by myself as described in Section 2.2.1.

### *3.3.5 Statistical analysis*

Statistical analysis was performed as described in Section 2.6 using Graphpad Prism 5.

## 3.4 Results

### *3.4.1 Cardiac morphometric measurements from early postnatal to adult stages*

As shown on Figure 3-1A body weight significantly increased between each time point. Heart wet weight tended to increase but only increased significantly from P21 onwards (Figure 3-1B). The heart wet weight to body weight ratio was significantly increased when comparing P2 and P21 but at no other time point (Figure 3-1C). Ultrasound-extracted left ventricle (LV) mass followed the same pattern as heart wet weight but a significant increase was observed from P8 onwards (Figure 3-1D).

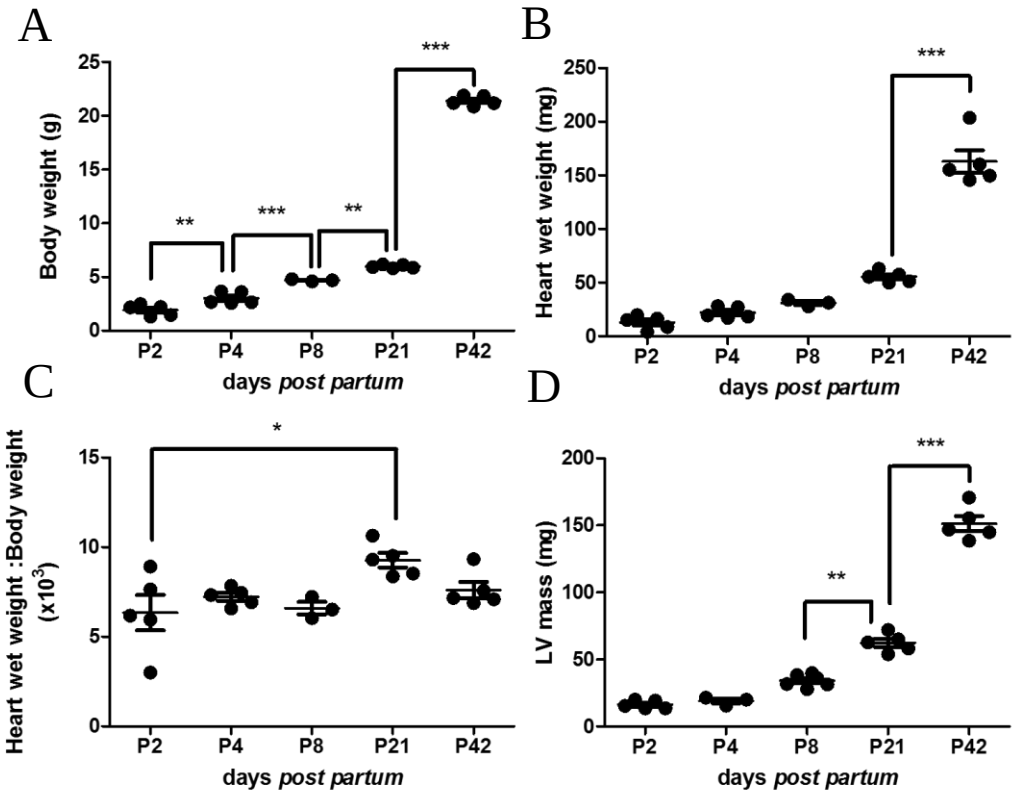


**Figure 3-1: Body and heart growth from early postnatal to adult stages.** Body weight (*A*) was measured prior to high-resolution *in vivo* ultrasound postnatal day 2 (P2), P4, P8, P21, and P42. Heart wet weight (*B*) was measured immediately after high-resolution *in vivo* ultrasound imaging following dissection and used to calculate heart to body weight ratio (*C*). Left ventricle (LV) mass (*D*) was extracted from electrocardiogram-gated kilohertz visualisation (EKV) parasternal long axis (PLAX) B-mode. n = 3-5/group. Results are presented as mean ± SEM. p-value determined with 1-way ANOVA with Bonferroni post hoc test. * $p < 0.05$, ** $p < 0.01$, *** $p < 0.001$.

Figure 3-2 shows that LV mass obtained from electrocardiogram-gated kilohertz visualisation (EKV) parasternal long axis (PLAX) B-mode ultrasound correlates with *ex vivo* postnatal heart wet weight.

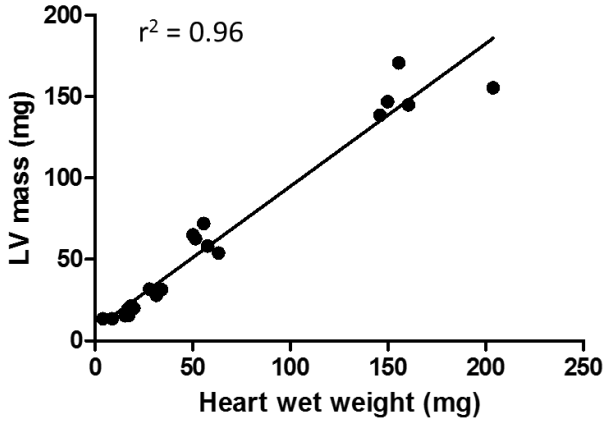


**Figure 3-2: Ultrasound-extracted left ventricle (LV) mass correlates with *ex vivo* heart wet weight.** Heart wet weight was measured immediately after high-resolution *in vivo* ultrasound imaging following dissection. left ventricle (LV) mass was extracted from electrocardiogram-gated kilohertz visualisation (EKV) parasternal long axis (PLAX) B-mode. LV mass was plotted against heart wet weight for each animal and linear regression applied to determine the coefficient of determination $r^2$. n = 21.

LV end systolic and diastolic area (LVESA & LVEDA) were both significantly increased from P8 onwards (Figure 3-3B, C).

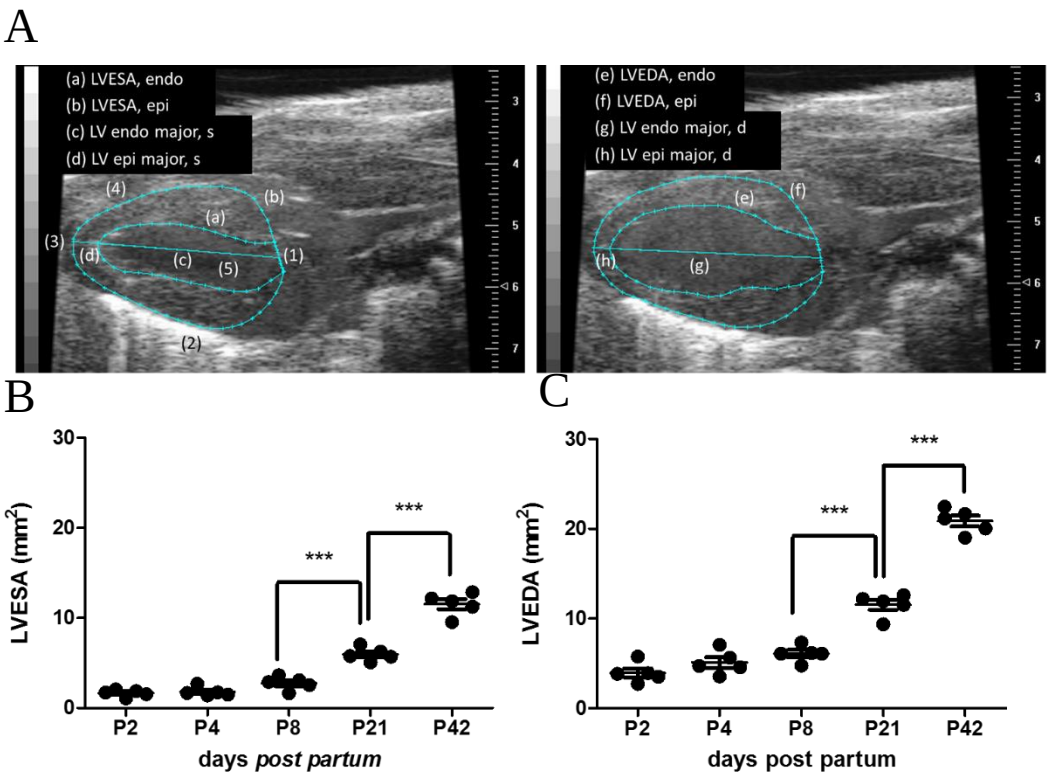


**Figure 3-3: Cardiac dimensions throughout postnatal growth.** Electrocardiogram-gated kilohertz visualisation (EKV) parasternal long axis (PLAX) B-mode (*A*) allowed calculation of left ventricle (LV) cavity size at the end of systole (LVESA-*B*) and diastole (LVEDA-*C*) at postnatal day 2 (P2), P4, P8, P21, and P42. n = 5/group. Results are presented as mean ± SEM. p-value determined with 1-way ANOVA with Bonferroni post hoc test. *** p <0.001.

### *3.4.2 Three phases of postnatal cardiac growth*

Cardiomyocyte cross-sectional area (CMCSA) was measured as an indicator of cardiomyocyte size (Figure 3-4A). CMCSA was unchanged between P2 and P8 whilst ultrasound extracted left ventricular (LV) wall thickness was significantly increased. Proliferative cardiomyocyte (cardiac troponin $T^{+ve}$, $Ki67^{+ve}$, $DAPI^{+ve}$) density within the left ventricle was shown to be highest at P2 and P4 Figure 3-5B.

Between P8 and P21 CMCSA increased 2.4-fold whilst LV wall thickness did not significantly change and proliferative cardiomyocyte density rapidly decreased to reach practically non-detectable levels by P21 (Figure 3-5B).

Finally, between P21 and P42 both CMCSA and LV wall thickness were significantly increased by 1.6-fold and 1.3-fold respectively (Figure 3-4B, C) whilst proliferative cardiomyocyte density was extremely low (Figure 3-5B).

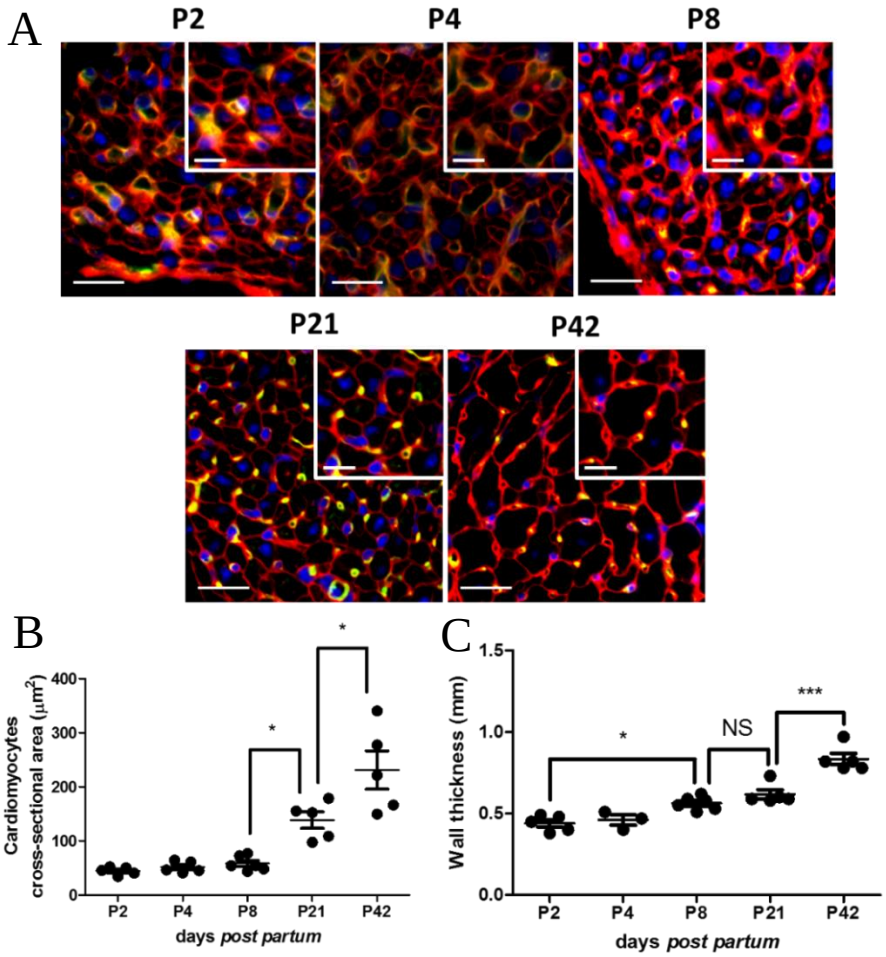


**Figure 3-4: Myocardial growth patterns identified by combining high-resolution *in vivo* ultrasound with histological techniques.** Cardiomyocytes cross sectional area (CMCSA) was investigated on Wheat Germ Agglutinin (WGA-red-membrane marker), isolectin B4 (IB4-green-endothelial cells marker), and DAPI (blue) stained 4μm thick sections at postnatal day 2 (P2), P4, P8, P21, and P42. Vessels appear yellow as double positive for IB4 and WGA. Quantification of CMCSA was performed on 5 different fields of view within the outer layer of the myocardium where cardiomyocytes are perpendicular to the plan of section. Representative images (*A*), scale bars = 20μm. Upper right corners are zooms, scale bars = 10μm. CMCSA quantification (*B*). Left ventricular (LV) wall thickness (*C*) was extracted from electrocardiogram-gated kilohertz visualisation (EKV) parasternal long axis (PLAX) B-mode. n = 3-5/group. Results are presented as mean ± SEM. p-value determined with 1-way ANOVA with Bonferroni post hoc test. NS $p > 0.05$, * $p < 0.05$, *** $p < 0.001$.

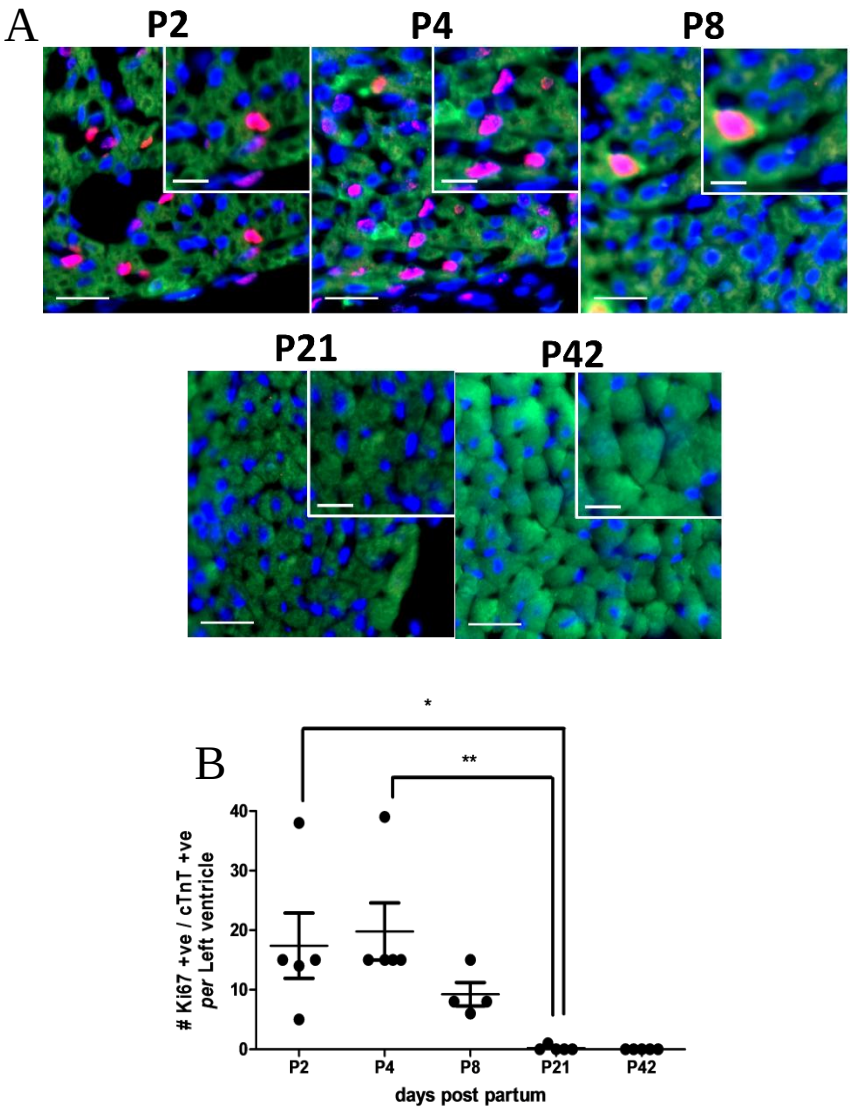


**Figure 3-5: Cardiomyocyte proliferation is at its highest in the neonate and rapidly decrease to low levels in the adult.** Proliferative cardiomyocytes (cm) were identified as positive for cardiac troponin T (green-cm marker) and containing a nucleus, DAPI (blue), positive for Ki67 (red-proliferation maker). Double positive nuclei appear pink. Quantification was performed on 5 different field of views across the whole left ventricle of 4 μm thick cardiac sections at postnatal day 2 (P2), P4, P8, P21, and P42. Representative images (*A*), scale bars = 20μm. Upper right corners are zooms, scale bars = 10μm. Cardiomyocytes proliferation quantification (*B*). n = 3-5/group. Results are presented as mean ± SEM. p-value determined with 1-way ANOVA with Bonferroni post hoc test

### *3.4.3 Vessel size, density, and maturation in the postnatal murine heart*

A left shift was observed in vessel size distribution from P2 to P42 (Figure 3-6A, B). Average vessel size was significantly reduced between P2 and P8. Vessel size was then unchanged between P8 and P42 (Figure 3-6B, C). On the other hand, vascular density was significantly increased between P2 and P8. Vascular density was not statistically different between P8 and P42 (Figure 3-6D). The number of α–smooth muscle actin (αSMA) positive vessels was significantly increased between neonatal mice (P2 & P8) and adult mice (P42) (Figure 3-6E).

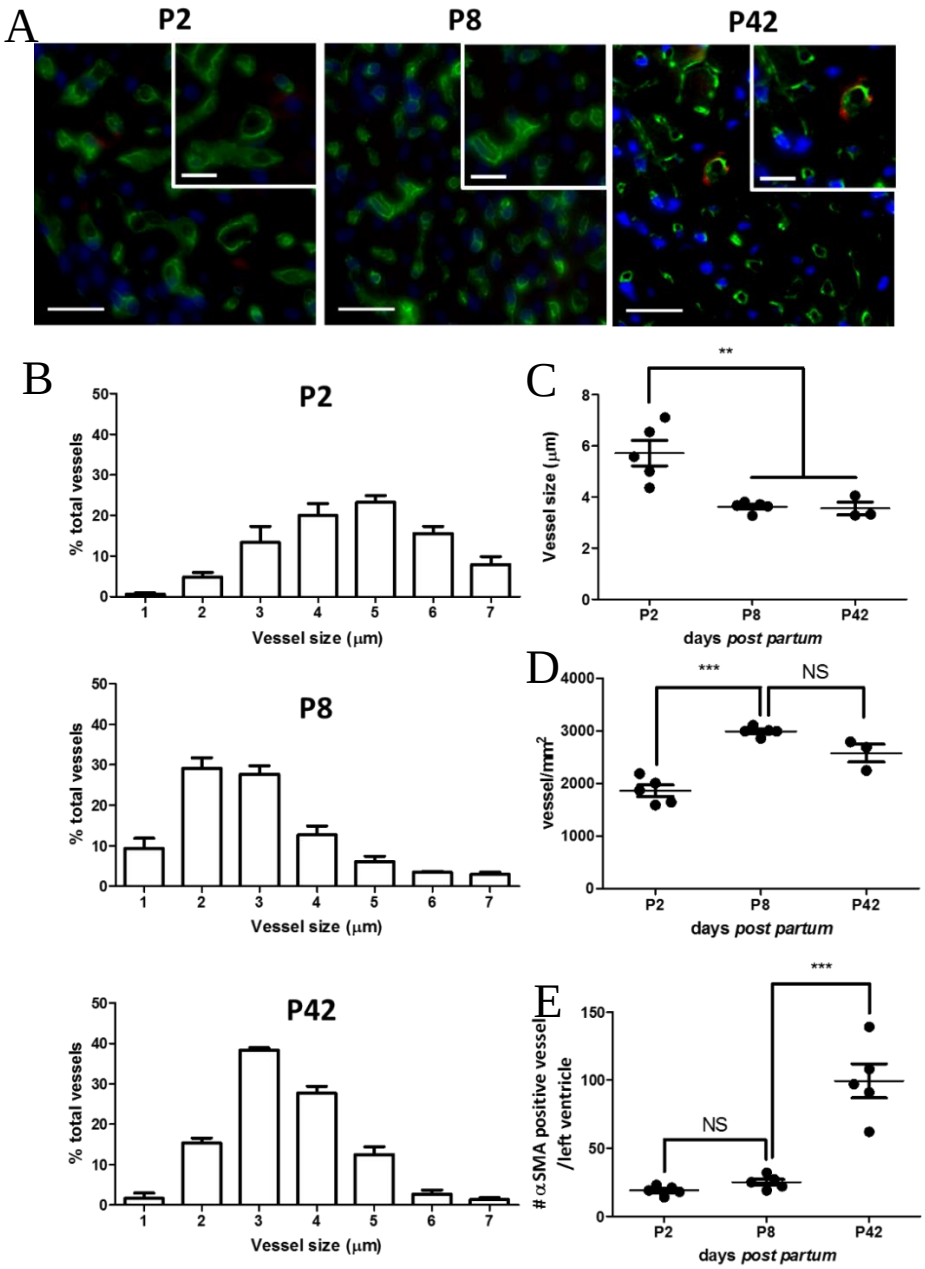


**Figure 3-6: Coronary vessel size, density and maturation during postnatal growth.** Vessel size, density, and maturation was investigated on isolectin B4 (IB4-green-endothelial cells), α smooth muscle actin (αSMA-red-mural cell coated vessels), and DAPI (blue). Quantification of vessel size and density was performed on 5 different field of views within the outer layer of the left ventricle on 4 μm thick stained sections at postnatal day 2 (P2), P8 and P42. Representative images (*A*), scale bars = 50μm. Upper right corners are zooms, scale bars = 10μm. Vessel size distribution was investigated at the 3 chosen time points (*B*). Average vessel size in μm (*C*). Vessel density was expressed /mm2 of myocardium (*D*). Number of $\alpha SMA^{+ve}$ vessels within the whole left ventricle (*E*). n = 3-5/group. Results are presented as mean ± SEM. p-value determined with 1-way ANOVA with Bonferroni post hoc test. *** p <0.001.

### *3.4.4 The heart contains stable levels of interstitial collagen throughout postnatal growth*

Left ventricle collagen content was stable from P2 to P42 (Figure 3-7).

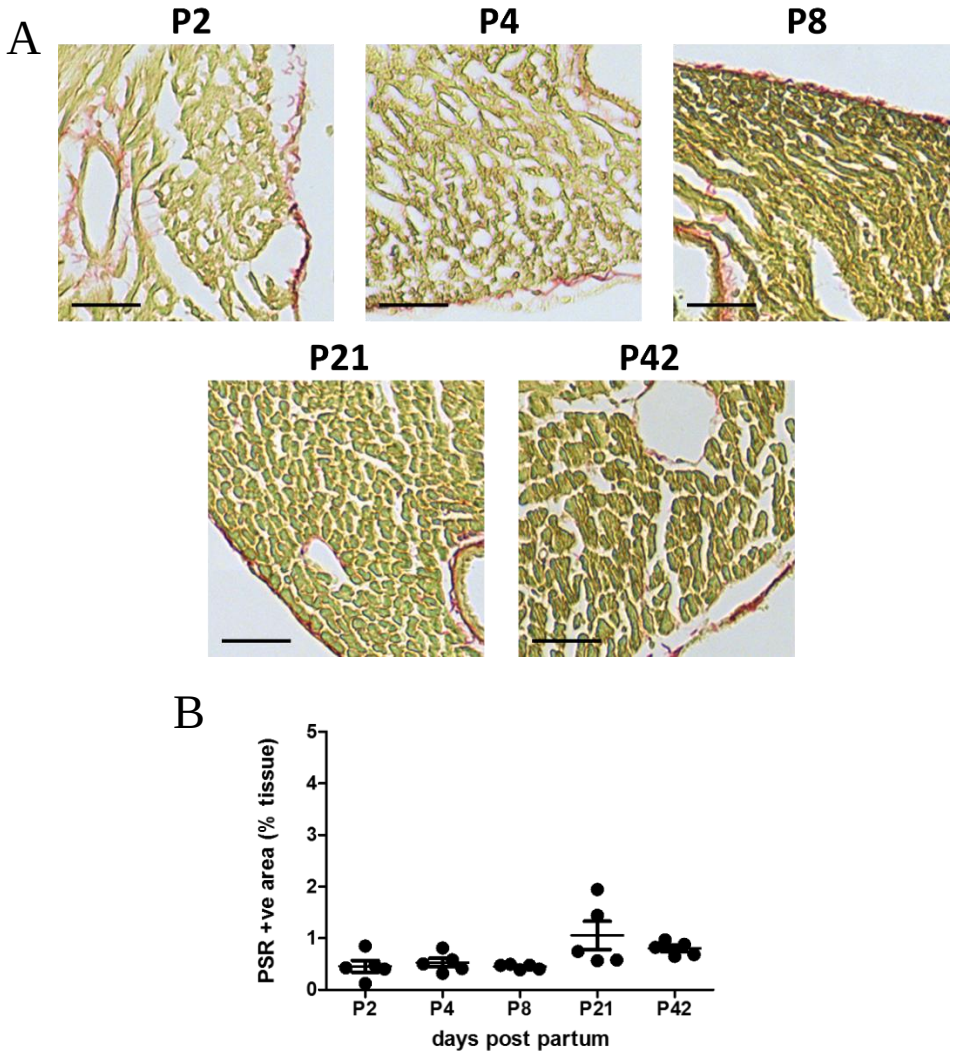


**Figure 3-7: Cardiac interstitial collagen content is unchanged throughout growth.** Interstitial collagen content was evaluated on picrosirius red (PSR-collagen marker) across the whole left ventricle on 4 μm thick section at postnatal day 2 (P2), P4, P8, P21, P42 with Photoshop CS6. Collagen fibres appear red, remaining tissue yellow. Representative images of PSR stained heart (*A*). Quantification of $PSR^{+ve}$ area (*B*). Black scale bars = 50 μm. n = 3-5/group. Results are presented as mean ± SEM. p-value determined by 1-way ANOVA with Bonferroni post hoc test.

### *3.4.5 Cardiac systolic function is maintained throughout all phases of murine myocardial growth.*

The systolic function read-outs of fractional area change (FAC), ejection fraction (EF), and fractional shortening (FS) were unchanged from P2 to P42 (Figure 3-8*A*, *B*, *C*). Myocardial performance index (MPI) was also unchanged except between P2 and P8 when it was decreased.

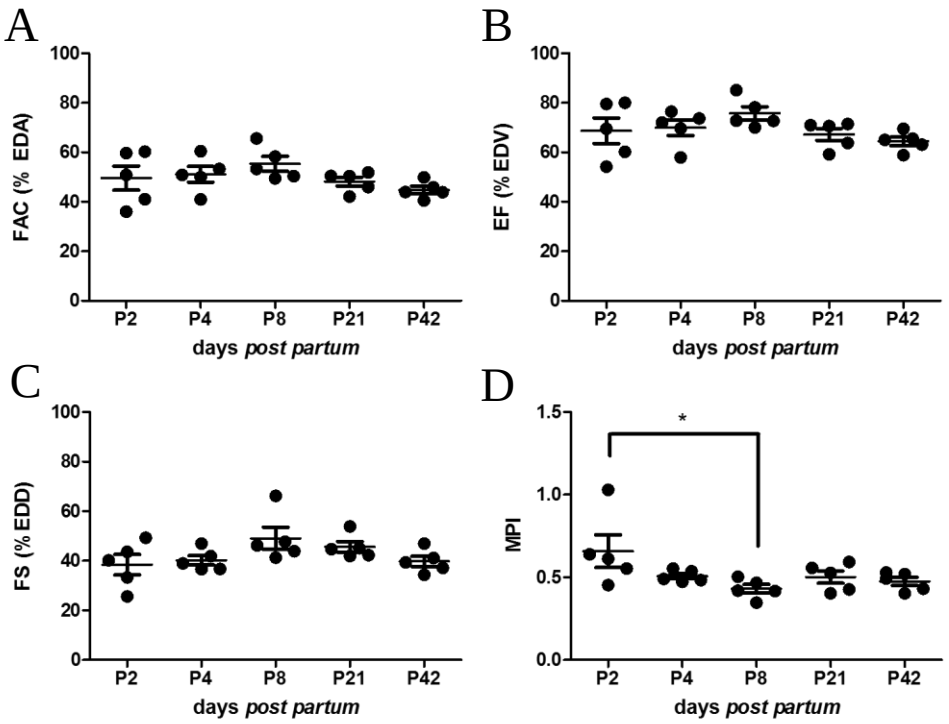


**Figure 3-8: Cardiac systolic function is stable throughout postnatal cardiac structural changes.** Cardiac systolic function was investigated using high-resolution *in vivo* ultrasound at postnatal day 2 (P2), P4, P8, P21, P42. Electrocardiogram-gated kilohertz visualisation (EKV) parasternal long axis (PLAX) B-mode allowed calculation of fractional area change (FAC-*A*) and ejection fraction (EF-*B*). PLAX motion-mode (m-mode) was used to obtain fractional shortening (FS-*C*). Trans-mitral pulse-wave Doppler allowed calculation of the myocardial performance index (MPI-*D*). n = 3-5/group. Results are presented as mean ± SEM. p-value determined with 1-way ANOVA with Bonferroni post hoc test. * $p < 0.05$.

### *3.4.6 Cardiac diastolic function increases drastically during the first postnatal week*

Figure 3-9 shows that at P2, the E to A wave ratio is < 1, it then significantly increases in P8 animals which have a ratio > 1. This reversal of the E to A wave ratio is then maintained between P8, P21 and P42 with no significant changes.

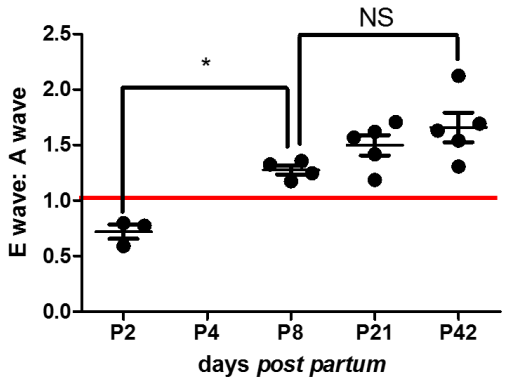


**Figure 3-9: Cardiac diastolic function matures over the first postnatal week.** Cardiac diastolic function was investigated using high-resolution *in vivo* ultrasound at postnatal day 2 (P2), P8, P21, P42. Trans-mitral pulse-wave Doppler allowed calculation of the E wave to A wave ratio. Red line represents a ratio of 1. A ratio < 1 is typical of foetal cardiac diastolic function. A ratio > 1 is typical of adult cardiac diastolic function. n = 3-5/group. Results are presented as mean ± SEM. p-value determined with 2-way ANOVA with Bonferroni post hoc test.

## 3.5 Discussion

Whilst foetal cardiac development has been extensively investigated in mice, relatively few have investigated postnatal structural and functional maturation. In this chapter a combination of high-resolution *in vivo* ultrasound and histological techniques were used to characterise murine postnatal cardiac growth and function.

*Growth pattern of the postnatal murine heart*

In this chapter, comparison of histological data with ultrasound assessment suggests three distinct phases of postnatal cardiac growth. First, between P2 and P8. This phase was characterised by unchanged CMCSA, increased cardiomyocyte proliferation and a small but significant increase in wall thickness. Consistent with observations of this chapter, the width of murine cardiomyocyte freshly isolated from the heart was previously reported to be unchanged in this period, (Leu *et al.*, 2001). The neonatal period is also known to characterised by high levels of cardiomyocyte proliferation, P1 mice contain a significant portion of cm in the G2/M phase of the cell cycle (Walsh *et al.*, 2010). This proportion decreases between P1 and P4 whilst proportion of cm in S-phase increases (Walsh *et al.*, 2010). Increased DNA synthesis without completion of mitosis has been linked to cm binucleation occurring within this time frame in rodents (Li *et al.*, 1996; Soonpaa *et al.*, 1996). Here, the density of cm positive for Ki67 is highest between P2 and P8 which correlates with the data from the literature as Ki67 is present at all active phases of the cell cycle (Gerdes *et al.*, 1984). EKV PLAX B-mode ultrasound allowed calculation of average LV wall thickness between P2 and P8 which was shown to significantly increase indicating myocardial tissue expansion. This observation along with active cm proliferation during the first postnatal week characterise a hyperplastic phase of growth of the postnatal murine heart. This can be linked to the ability of the neonatal mouse to regenerate its myocardium following injury (see Chapter 5) while the myocardium retains the ability to expand through cardiomyocyte proliferation (Porrello *et al.*, 2011, 2013; Haubner *et al.*, 2012; Porrello and Olson, 2014). Interestingly though, Leu *et al.* (2001) have demonstrated that mouse cardiomyocytes increase in length during the early postnatal period, suggesting that not all growth can be attributed to proliferation. Since the onset of this PhD considerable advances have been made in the understanding of the mechanisms behind early postnatal cardiomyocyte proliferation. Those have included

miRNAs, the transcription factors MEIS1, growth factor receptor ERB2, hypoxia, and the Hippo and Wnt signalling pathways (Heallen *et al.*, 2011; Chen *et al.*, 2013; Mahmoud *et al.*, 2013; Xin *et al.*, 2013; Puente *et al.*, 2014; H. Ma *et al.*, 2016). Modulation of these pathways have yielded promising translational results to the adult mouse by inducing cardiomyocyte proliferation. This highlights the benefits of understanding the mechanism of early postnatal growth for recapitulation in the adult.

Following the first postnatal week, cardiomyocyte volume, length, and width are known to increase whilst DNA synthesis decreases (Leu *et al.*, 2001; Walsh *et al.*, 2010). This is consistent with data from this chapter showing a decrease in the density of cardiomyocytes positive for Ki67 between P8 and P21 and a significant increase in CMCSA. The mouse heart has therefore switched from a hyperplastic to a hypertrophic mode of growth. Interestingly, ultrasound-extracted LV wall thickness did not significantly change between P8 and P21. This is unexpected considering the increase in CMCSA observed in that same time period. EKV PLAX B-mode ultrasound also allowed calculation of left ventricular end systolic and diastolic area (LVESA, LVEDA) which were both significantly increased between P8 and P21. The overall LV size is therefore increasing along with CMCSA but this does not translate into increased LV wall thickness. A possible explanation for this observation is the structural reorganisation of cardiomyocytes within the LV which could lead to a bigger chamber without significant increase in wall thickness. Investigating the cellular architecture of the myocardium across the whole tissue is however a challenging endeavour. In the myocardium, no anatomical structure matching the distinct fibres of skeletal muscle can indeed be observed. Instead cardiomyocytes are bound to each other in a mesh like structure (Jouk *et al.*, 2007). Groups of cardiomyocytes can be tracked along their long axis and have been proposed to form a spiralling structure called the ‘helical ventricular myocardial band’ (Stephenson *et al.*, 2016). To this day, the precise organisation of cardiomyocytes within the myocardium remains a source of debate and investigation (Stephenson *et al.*, 2016). Recently, Bensley *et al.* (2016) have been able to obtain precise information on cardiomyocyte size and bi or mono-nucleation status using 40 μm thick cardiac sections stained with wheat germ agglutinin (WGA) and DAPI in combination with confocal imaging. A similar

approach could be envisaged here to investigate the architecture of the myocardium from early postnatal to adult stages.

The biological significance of a phase of cardiomyocytes re-organisation is elusive. Intracellularly, cardiomyocytes are known to mature postnatally to achieve more efficient delivery of adenosine tri-phosphate (ATP) to myofibrils (Piquereau *et al.*, 2010). In this thesis, Heart to body weight ratio was shown to be constant between most time point studied albeit a significant increase at P21. Piquereau *et al.* (2010) have reported a similar change and a subsequent decrease in the ratio between P21 and 2 months old mice. They propose a link between this observation and an increased efficiency of cardiomyocyte contraction after P21. Whether intracellular changes are mirrored with changes in tissue architecture is less clear.

Finally, both CMCSA and LV wall thickness significantly increased between P21 and P42, in the absence of cardiomyocyte proliferation, indicative of a purely hypertrophic mode of growth. At the same time point Leu *et al.* (2001) have observed increased volume and width in cardiomyocytes freshly isolated from mouse heart.

*Coronary vasculature maturation in the postnatal mouse*

Angiogenesis is essential in supporting organ growth (Section 1.4.3.1(a)). At the onset of this PhD, the pattern of coronary vascular growth in postnatal mammals was relatively poorly characterised. Since then an elegant report on the origin and formation of the postnatal coronary vasculature was published by Tian *et al.* (2014). Their study used a tamoxifen inducible Cre driven reporter targeted to endothelial cells via the Apelin promoter, specifically expressed by endothelial cells, and not endocardial cells (Red-Horse *et al.*, 2010). A single injection of tamoxifen at E10.5 permanently labelled foetal coronary endothelial cells mostly derived from the *sinus venosus* and their progeny (Section 1.3.2.2(b)). Using this approach the authors identitied a 'first coronary vascular population' present throughout foetal and postnatal life, and observed only within the outermost layer of the myocardium (compact myocardium). During foetal life and until P0, the remaining inner myocardium receives nutrients and oxygen directly from the ventricular cavity. This trabeculated myocardium is characterised by finger-like projections into the ventricular cavity. Data from this chapter has shown that the average vessel size within the compact

myocardium decreases whilst vessel density increases during the first postnatal week, Interestingly, Tian *et al.* (2014) observed that as the heart grows from P0 to P7, the proportion of myocardium irrigated by the first coronary vascular population remains unchanged. This observation and the data from this chapter therefore suggests that vascularisation of the outermost layer of the myocardium is achieved through the expansion of pre-existing vessels: angiogenesis (Carmeliet 2000).

As for the trabeculated myocardium, part of it undergoes compaction shortly after birth which was associated with the appearance of new blood vessels (Tian *et al.*, 2014). Those vessels were not derived from the expansion of those present in the compact myocardium. The authors argued for an endocardial origin of those vessel through epicardial-to-mesenchymal transition (EMT). As the heart grows between P7 and P28, showed a moderate increase

Postnatal vascularisation of the myocardium is therefore not only achieved through expansion of pre-existing vessels but also *de novo* vessel formation. Whether vessels composed of endothelial cells from the *sinus venosus* or of endocardial origin have different biological functions is less clear.

Mural cells which include pericytes and smooth muscle cells provide structural support in the maturation of vascular beds (Carmeliet, 2003; Jain, 2003). They are also known to regulate angiogenesis by modulating endothelial cell proliferation and migration (Carmeliet, 2000; Cai and Schaper, 2008). Here we investigated the coating of the postnatal coronary vasculature by smooth muscle cells using α smooth muscle cell actin (αSMA) as marker. The number of $\alpha SMA^{+ve}$ vessels within the whole LV was shown to be highest in P42 mice when compared to neonatal mice (P2, P8). As the mouse grows, blood pressure increases which has previously been linked to mural cell coating of the vasculature (Cai and Schaper, 2008). This would therefore correlate well with the pattern observed here. Vessels positive for αSMA were sparsely distributed throughout the LV. Quantification was therefore performed within the whole LV as opposed to selecting fields of view in order to accurately represent the total number of $\alpha SMA^{+ve}$ vessels. As hearts are larger in P42 mice compared to neonatal mice, this quantification means that $\alpha SMA^{+ve}$ vessels were counted across a bigger surface area in P42 mice which can skew the quantification. Further investigation would consider

another method of quantification, potentially normalising the amount of $\alpha SMA^{+ve}$ vessels to the area of the LV thereby giving a paramter expressed per $mm^2$.

*Cardiac functional maturation of the postnatal mouse*

Trans-mitral pulse wave Doppler is used to determine the pattern of LV filling by comparing the ratio of the passive phase due to LV relaxation (E-wave) to the active phase of atrial contraction (A-wave). This ratio reflects diastolic function by indicating the portion of ventricular filling performed by ventricular relaxation as opposed to atrial contraction (Zhou *et al.*, 2003b; Corrigan *et al.*, 2010). In foetal mice and humans, atrial contraction filling of the left ventricle predominates over passive filling. This ratio was shown by (Zhou *et al.*, 2003b) to reverse over the course of the first postnatal week in mice. The data presented in this chapter supports this observation as the E:A wave ratio reverses between P2 and P8 when it acquires the typical adult pattern of E > A.

EKV PLAX B-mode ultrasound was performed for the first time in neonatal mice to our knowledge. This allowed measurements of left ventricular end systolic and diastolic area (LVESA, LVEDA) across all postnatal stages which increased synchronously with body and heart weights. LVESA and LVEDA are used for the calculation of the systolic functional read-outs of fractional area change (FAC) and ejection fraction (EF). Kulandavelu *et al.* (2006) had previously reported the recording of ECG signal in neonatal mice but not in combination with high-resolution *in vivo* ultrasound. Cardiac systolic function was also assessed on PLAX M-mode and transmitral Doppler and showed to be mostly unchanged at the time point studied. A significant decrease in myocardial performance index (MPI), collected from pulse-wave Doppler ultrasound, was however observed when comparing P2 and P8 mice. A decreased MPI is indicative of better systolic function. This increased systolic function was not observed in any of the 3 other measurements. Corrigan *et al.* (2010) performed a similar study where MPI was measured from foetal to adult stages and saw no significant difference between the late foetal stage of E18.5 and 1 week old mice. An outlier with a clearly high MPI can be identified in the P2 group. Removal of this outlier eliminates the significant difference previously observed between P2 and P8. Overall, cardiac systolic function therefore seems unchanged from neonatal to adult

stages, despite the significant changes in cardiomyocyte growth and arrangement taking place during this period.

Overall data from this chapter, from both *in vivo* ultrasound and *ex vivo* histology, have suggested three phases of postnatal growth of the mouse heart. Whilst cardiomyocytes had been shown to undergo different phases of growth in the postnatal mouse heart (Soonpaa *et al.*, 1996; Leu *et al.*, 2001), how it related to the growth of the whole heart was previously unclear. The phases identified here were: a first hyperplasic phase characterised by cardiomyocyte proliferation and increased wall thickness between P2 and P8; a second phase between P8 and P21 of hypertrophic growth in association with potential structural rearrangement characterised by CMCSA increase, low cardiomyocyte proliferation, and no change in LV wall thickness; and finally, a hypertrophic phase characterised by CMCSA and LV wall thickness increase and low cm proliferation between P21 and P42. This was allowed with the use of Electrocardiogram-gated kilohertz visualisation (EKV) parasternal long axis (PLAX) B-mode ultrasound for the first time to our knowledge in neonatal mice. It was also shown to provide reliable structural measurements as LV mass obtained using this method were shown to strongly correlate with *ex vivo* measured heart wet weight. This technique therefore constitutes a strong tool that can be used in the study of cardiac structure and function from early postnatal stages.

# Chapter 4: The role of macrophages and macrophage-secreted WNTs in normal cardiac postnatal growth and function

## 4.1 Introduction

Macrophages (MΦ) are found in all adult mammalian tissues where they exert known roles in homeostasis (Davies *et al.*, 2013; Wynn *et al.*, 2013). MΦ progenitors first arise during development as early as E7.5 in the yolk-sac. These progenitors then populate various organs including the foetal liver where definitive haematopoiesis is established from E12.5 (Schulz *et al.*, 2012). Until birth, the foetal liver remains the primary source of circulating monocytes which can give rise to tissue MΦ. After birth haematopoiesis relocates from the liver to the bone marrow making it the main haematopoietic organ in mammals (Ginhoux and Guilliams, 2016). Depending on their origin, tissue MΦ have also been shown through fate mapping experiments to differentially express the canonical MΦ marker F4/80 and leukocyte marker CD11b. Yolk-sac derived and foetal liver/bone marrow derived MΦ are typically F4/80$^{hi}$, CD11b$^{lo}$ and F4/80$^{lo}$, CD11b$^{hi}$ respectively (Schulz *et al.*, 2012).

In mammals, each organ contains phenotypically distinct subsets of tissue MΦ thought to have various origin (Ginhoux and Guilliams, 2016). For example, brain tissue MΦ, microglia, are primarily yolk-sac derived whereas the gut epithelium is populated almost entirely with bone-marrow derived MΦs in the adult. At the outset of this PhD cardiac MΦ origin and dynamic in the steady state was unclear.

The importance of MΦ in growth has been in part demonstrated using a mouse model homozygous for a null mutation of the colony stimulating factor -1 (*Csf1*$^{op/op}$) (Wiktor-Jedrzejczak *et al.*, 1990; Yoshida *et al.*, 1990). CSF-1 and its receptor CSF1R are essential in the differentiation and survival of MΦ. The *Csf1*$^{op/op}$ mouse lacks many tissue MΦ populations and present a range of developmental abnormalities including growth retardation (Chitu and Stanley, 2006). At the start of this PhD project it was however unknown whether MΦ played specific roles in the postnatal maturation of the heart discussed in Section 3.5.

The highly conserved Wnt signalling pathway is known to play crucial roles during development (Wynn *et al.*, 2013) (Section 1.5.2). WNT ligands are secreted proteins that are acylated by the member of the membrane bound O-acyltransferase (MBOAT) family: porcupine (PORCN). Without acylation, WNTs cannot bind the cargo protein wntless (Wls) which is essential for their secretion into the extracellular space (Mikels

and Nusse, 2006). WNTs act on the receiving cell by binding to their receptors, members of the frizzled (FZD) family. By involving different partners at the membrane and intracellularly, WNTs can act through 3 major pathways described in Section 1.5.1.1. The most well characterised and so called canonical Wnt signalling pathway acts through stabilisation of cytoplasmic β-catenin that can then translocate to the nucleus and regulate gene expression.

In the embryonic heart, the Wnt signalling pathway has been shown to play stage specific roles in cardiac specification (Gessert and Kühl, 2010). In the adult myocardium it is however thought to be quiescent and only re-activated upon injury (as reviewed by Dawson *et al.* 2013). The activity of the Wnt signalling pathway in the neonatal heart is however unknown. At the onset of this PhD a brief analysis of RNAseq data kindly provided by Prof. Tim Aitman showed that naïve hearts differentially expressed Wnt signalling related genes between postnatal day 1 and 10. This may indicate a role of the pathway in early postnatal growth.

Formation of an adequate vasculature is known to be essential in normal organ growth. As shown in the previous chapter, vessel size, density and maturation change during postnatal growth. Evidence has shown over the years that the Wnt signalling pathway is a modulator of angiogenesis (Dejana, 2010). Indeed, endothelial cells express a wide range of *Fzd* receptors at their surface (Goodwin *et al.*, 2006). Additionally, loss of function of FZD4 is associated with decreased vascularisation of the heart and kidney (Descamps *et al.*, 2012). Interestingly, MΦ-derived WNTs were shown to modulate vascular patterning of the retina by controlling apoptosis of endothelial cells (James A Stefater *et al.*, 2011). MΦ-derived WNTs were also shown to regulate angiogenesis by titrating local VEGF (Stefater *et al.*, 2013). Whether they play a role in postnatal vascular expansion and patterning in the myocardium is unclear.

Collectively, the studies presented above argue for a role of both macrophages and WNTs during cardiac growth and its associated mechanisms.

## 4.2 Hypothesis and aims

Hypothesis:

'**Macrophage depletion and preventing secretion of WNTs from macrophages through specific deletion of Porcupine will impair normal cardiac growth and function'**

Aims:

(i) Characterise the presence of cardiac macrophages and their behaviour during cardiac postnatal growth.

(ii) Characterise the impact of constitutive macrophage depletion on normal cardiac postnatal growth with a focus on the neonatal period

(iii) Study the mRNA expression profile of Wnt signalling pathway genes in cardiac mononuclear phagocytes in the steady state

(iv) Characterise the effect of macrophage specific deletion of *Porcn* on normal postnatal cardiac growth and function

## 4.3 Methods

### *4.3.1 Animals*

Three mouse lines were used in the studies reported in this chapter:

- Tg(*Csf1r-Egfp*) mice express enhanced green fluorescent protein under the control of the colony-stimulating factor 1 receptor gene (*Csf1r*) promoter. Animals expressing the transgene were noted as $GFP^{+ve}$. This mouse line is referred to as the MacGreen mouse and is on an incomplete C57BL/6J background. Male and female mice aged between P2 and P42 were used. Further details on the mouse line can be found in Section 2.1.1.2.

These were bred and housed in Edinburgh in the Central Bioresearch Services local facility.

- Male and female mice homozygous for an inactivating deletion of exon 5 of *Csf1r* (further details in Section 2.1.2.1) were used and referred to as *Csf1r*-null animals. Wild-type (WT) littermates were used as controls and compared to *Csf1r*-null animals aged between P1 and P20. Those mice were on a C57BL/6J background. Genotyping as well as body and heart weight measurements were carried out by Dr Liyin Zhu at the Albert Einstein College of Medicine, NY.
- Male and female mice homozygous for a floxed allele of the Porcupine gene ($Porcn^{fl/fl}$) were used for breeding and generation of experimental animals. The male breeders were heterozygous for a transgene containing the cre-recombinase under the control of the *Csf1r* promoter (Tg(*Csf1r-icre*)). The off-spring of such breeding are homozygous for $Porcn^{fl/fl}$, and a subset also express cre-recombinase in *Csf1r*-expressing cells. This mouse line is referred to as the Porcupine mouse. Cre-expressing animals were referred to as $Cre^{+ve}$ and compared to cre-deficient ($Cre^{-ve}$) animals as littermate controls. These mice are on an incomplete FVB background. Further details on the mouse line can be found in Section 2.1.2.2. Both male and female mice aged between P1 and P41 were used in this chapter. Breeding and part of the genotyping and weight measurements were carried out by Mr Mark Thompson.

These animals were bred and housed at the Einstein College of Medicine (New York, Bronx).

### *4.3.2 FACS*

Cardiac leukocytes including, granulocytes, monocytes and macrophages were measured in heart digest of P2 and P8 $GFP^{+ve}$ MacGreen animals. Hearts of $GFP^{+ve}$ animals of the same litter, typically 3-4, were pooled in an effort to increase yield. Heart digests were stained with DAPI, CD45 PE-Cy7, Ly6G Pacific blue, CD11b Alexa fluor 700, F4/80 PE, and Ly6C PerCP Cy5.5 and assessed as described in Section 2.3.2. Gating strategy is shown in Section 2.3.2.

### *4.3.3 Histology*

10 μm thick frozen sections of male and female MacGreen tissues were stained with anti-GFP antibody for MΦ visualisation. All other tissues were formalin-fixed paraffin embedded and cut into 4 μm thick sections as described in Section 2.5. Cardiomyocyte cross-sectional area (CMCSA), cardiomyocyte proliferation as well as vessel size, density, and maturation were measured using immuno-fluorescence as described in Section 2.5. Both male and females were used in the histological characterisation of the *Csf1r*-null and their wild-type littermates. Only males were used in the histological characterisation of the Porcupine mouse. Picrosirius red (PSR) staining for identification of collagen content was performed by Miss Melanie McMillan at the Queen's Medical Research Institute histology facility using a standardised protocol.

### *4.3.4 Ultrasound*

Ultrasound was carried out as described in Section 2.2.1 on male and female Porcupine mice aged between P1 and P41 to assess cardiac structure and function. All ultrasound measurements within this chapter were acquired by myself.

### *4.3.5 Image acquisition and analysis*

Images were acquired on a Zeiss slide scanner Axio Scan Z1, magnification x 40 for heart sections of MacGreen and Porcupine mice as well as P1 *Csf1r*-null mice and their corresponding WT littermates. Images were acquired on a Zeiss Axiovert200, magnification x 40 for heart sections of P7 *Csf1r*-null mice and their WT littermates. All image analysis was performed on Adobe Photoshop CS6 except cardiomyocyte proliferation quantification in Porcupine mice which was performed using Definiens

software as described in Section 2.5. The algorithm was written and performed by Dr Daniel Soong.

### *4.3.6 Statistical analysis*

Statistical analysis was performed as described in Section 2.6 using Graphpad Prism 5.

## 4.4 Results

### *4.4.1 Cardiac mononuclear phagocytes during postnatal growth*

Image analysis of heart frozen sections from GFP$^{+ve}$ MacGreen mice showed that the density of *Csf1r*-expressing cardiac mononuclear phagocytes was constant between postnatal day 2 (P2) and P42 (Figure 4-1).

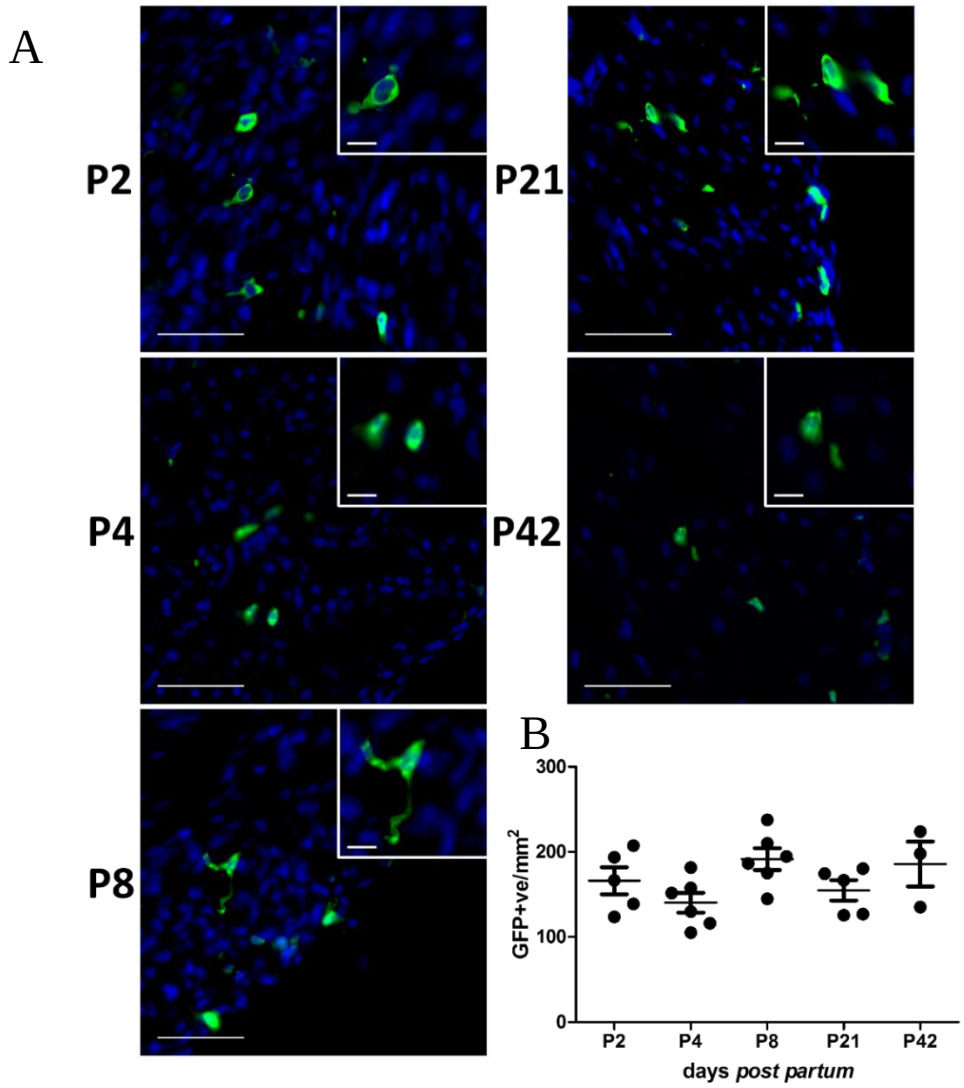


**Figure 4-1: The density of *Csf1r*-GFP expressing cells is stable throughout growth in the myocardium of MacGreen mice.** Representative images (*A*) of 4 μm thick cardiac sections from GFP$^{+ve}$ MacGreen mice stained for GFP (green) at postnatal day 2 (P2), P4, P8, P21, P42. Quantification of the number of GFP$^{+ve}$ cells was performed on 5 different fields of view across the whole left ventricle (*B*). Scale bars = 50 μm. Upper right corners are zooms, scale bars = 10 μm. Results are presented as mean ± SEM. p-value determined with 1-way ANOVA with Bonferroni post hoc test.

Flow cytometry analysis in hearts from $GFP^{+ve}$ MacGreen mice revealed 3 distinct populations of mononuclear phagocytes at both P2 and P8. Those 3 populations differentially expressed F4/80, CD11b and Ly6C. A first population of $F4/80^{hi}$, $CD11b^{lo}$, $Ly6C^{-ve}$ mononuclear phagocyte. A second of $F4/80^{lo}$, $CD11b^{hi}$, $Ly6C^{-ve}$ and a third of $F4/80^{lo}$, $CD11b^{hi}$, $Ly6C^{+ve}$ mononuclear phagocytes (Figure 4-3A, B).

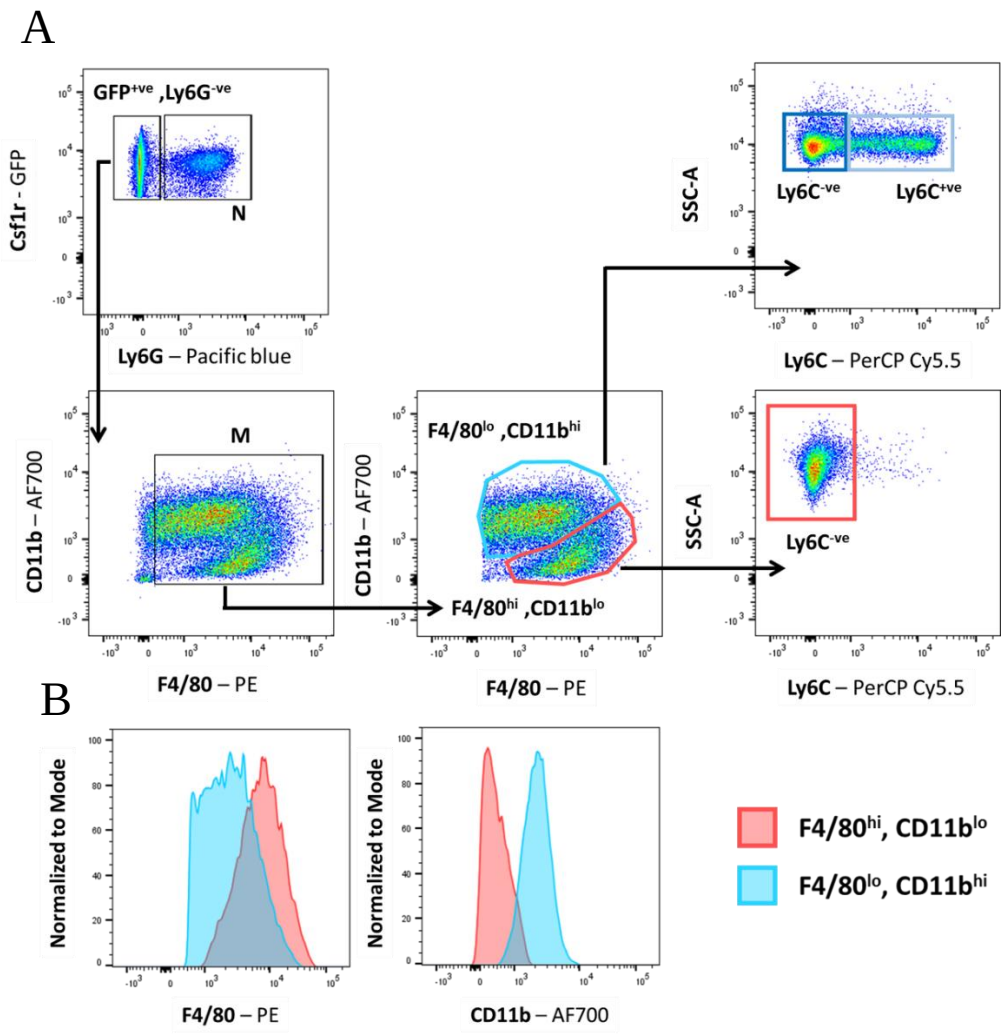


**Figure 4-2: The neonatal heart contains distinct mononuclear phagocyte populations.** Single, Live, $CD45^{+ve}$ cells were gated on. Neutrophils (N) were identified as $GFP^{+ve}$, $Ly6G^{+ve}$. The $Csf1r^{+ve}$, $Ly6G^{-ve}$ population was then gated on CD11b and F4/80 in order to identify total mononuclear phagocytes (labelled M) as $(F4/80, CD11b)^{+ve}$. Mononuclear phagocytes could be subdivided into $F4/80^{lo}$, $CD11b^{hi}$ and $F4/80^{hi}$, $CD11b^{lo}$ subsets. $F4/80^{hi}$, $CD11b^{lo}$ contained a single $Ly6C^{-ve}$ population whereas $F4/80^{lo}$, $CD11b^{hi}$ contained both a $Ly6C^{-ve}$ and $Ly6C^{+ve}$ population (*A*). Differential expression of F4/80 and CD11b by flow cytometry of the two mononuclear phagocyte subsets (*B*). Abbreviations; SSC-A: side scatter-area.

The proportion of F4/80$^{hi}$, CD11b$^{lo}$, Ly6C$^{-ve}$ mononuclear phagocyte within the total mononuclear phagocyte population ((F4/80, CD11b)$^{+ve}$) was unchanged between P2 and P8. F4/80$^{lo}$, CD11b$^{hi}$, Ly6C$^{-ve}$ and F4/80$^{lo}$, CD11b$^{hi}$, Ly6C$^{+ve}$ cells' proportion of total mononuclear phagocyte was not significantly changed. However, a trend to an increased proportion of F4/80$^{lo}$, CD11b$^{hi}$, Ly6C$^{-ve}$ cells and decreased proportion of F4/80$^{lo}$, CD11b$^{hi}$, Ly6C$^{+ve}$ cells can be noted.

As shown on Figure 4-3C, the proportion of total leukocytes, as measured using CD45 (pan-leukocyte marker) and expressed as a percentage of live cells, was unchanged between P2 and P8. This was also true of neutrophils, identified as (Csf1r, Ly6G)$^{+ve}$ (Figure 4-3D).

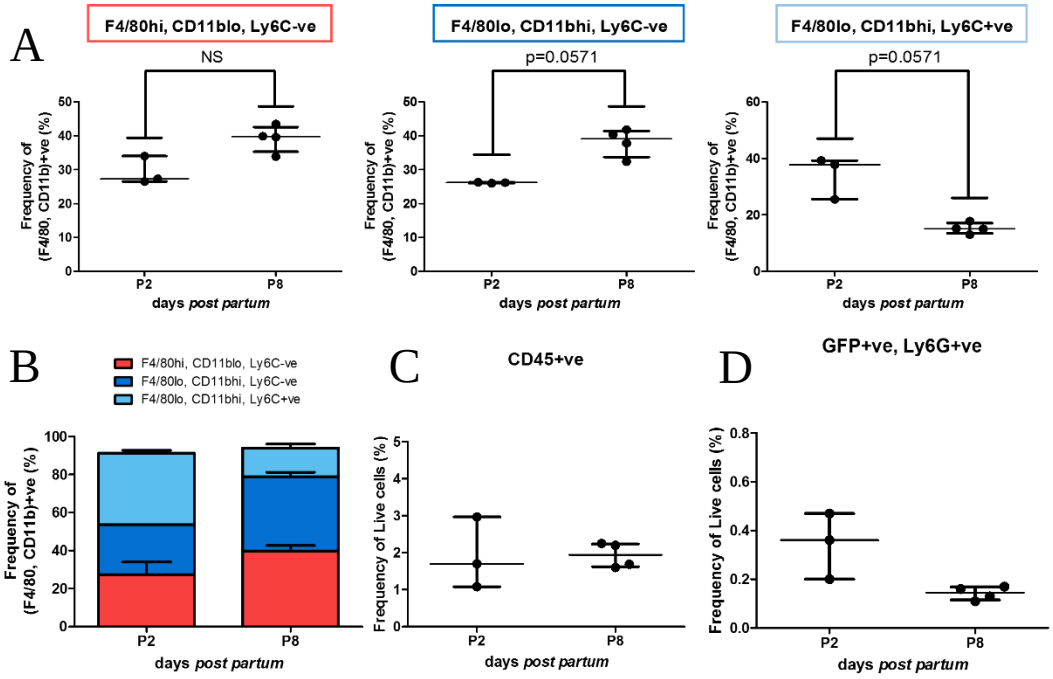


**Figure 4-3: Cardiac mononuclear phagocyte populations during the first postnatal week.** Gating strategy on Figure 4-2A was used to quantify the frequency of F4/80$^{hi}$, CD11b$^{lo}$, Ly6C$^{-ve}$ - F4/80$^{lo}$, CD11b$^{hi}$, Ly6C$^{-ve}$ - F4/80$^{lo}$, CD11b$^{hi}$, Ly6C$^{+ve}$ mononuclear phagocytes as a proportion of total mononuclear phagocytes each subset is expressed as a proportion of the total mononuclear phagocyte ((F4/80, CD11b)$^{+ve}$) in GFP+ve MacGreen mice hearts at postnatal day 2 (P2) and P8 (*A*). Summary of subsets frequencies (*B*) Total CD45$^{+ve}$ (*C*) and GFP$^{+ve}$, Ly6G$^{+ve}$ (*D*) cells were expressed as a proportion of live cells. n=3-4/group. Data are expressed as median ± interquartile range. p-value was determined with two-tailed Mann-Whitney tests.

### *4.4.2 Constitutive genetic depletion of macrophages impairs body and cardiac growth*

Body and heart wet weight were not significantly different prior to P7 between groups (Figure 4-4A, B). However, in P7 and P20 animals both body and heart wet weight were significantly reduced in *Csf1r*-null animals when compared to WT littermates. Heart wet weight to body weight ratio (Figure 4-4C) was not significantly different between groups at any age, apart from P1, when heart weight was significantly increased relative to body weight in *Csf1r*-null compared to WT littermates.

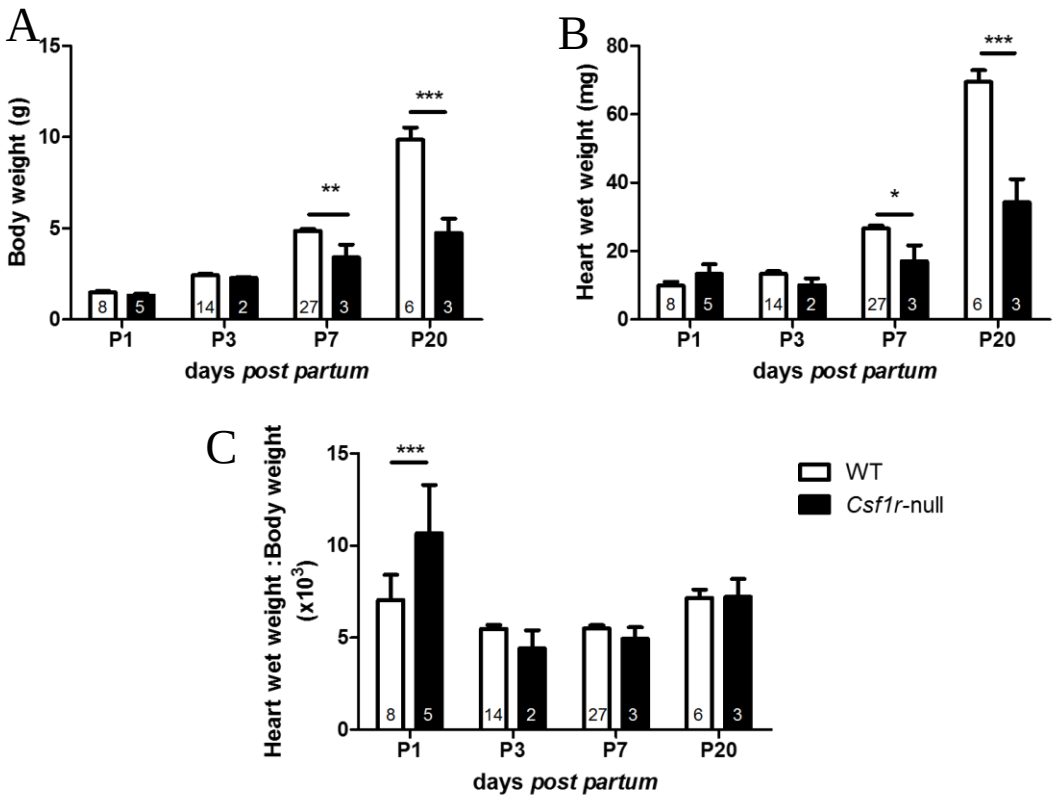


**Figure 4-4: Body and cardiac growth impairment of *Csf1r*-null animals.** Body weight (*A*) as well as heart wet weight (*B*) were recorded in *Csf1r*-null animals and WT littermates used as controls. Heart wet weight to body weight ratio was then calculated (*C*). Results are presented as mean ± SEM. p-value determined with 2-way ANOVA with Bonferroni post hoc test. * p <0.05, ** p <0.01 *** p <0.001.

### *4.4.3 Constitutive genetic depletion of macrophages does not impair cardiomyocytes cross sectional area or proliferation in the neonatal mouse*

Cardiomyocyte cross sectional area (CMCSA) wasn't significantly different in *Csf1r*-null mice relative to WT during the neonatal period within (P1) and outside (P7) of the regenerative window, relative to WT (Figure 4-5).

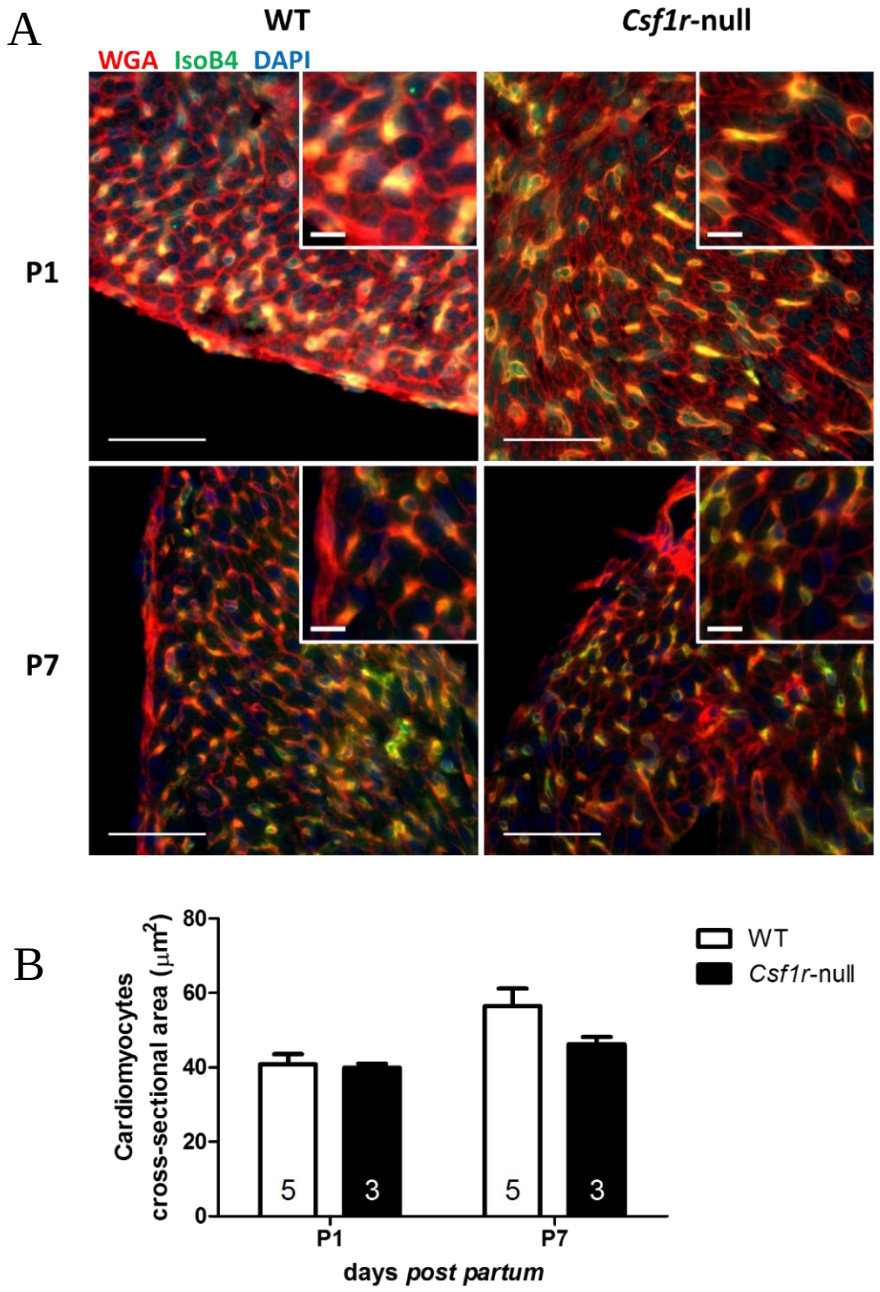


**Figure 4-5: Constitutive genetic depletion of macrophages does not influence CMCSA in the neonatal mouse.** Cardiomyocytes cross sectional area (CMCSA) was investigated on Wheat Germ Agglutinin (WGA-red-membrane marker), isolectin B4 (IB4-green-endothelial cells marker), and DAPI (blue) stained 4 μm thick sections at postnatal day 1 (P1) and P7. Vessels appear yellow as double positive for IB4 and WGA. Quantification of CMCSA was performed on 5 different fields of view within the outer layer of the myocardium where cardiomyocytes are perpendicular to the plan of section. Representative images (*A*), scale bars = 50μm. Upper right corners are zooms, scale bars = 10μm. CMCSA quantification (*B*). Clear bars are WT and black bars *Csf1r*-null animals. Results are presented as mean ± SEM. p-value determined with 2-way ANOVA with Bonferroni post hoc test.

Proliferative cardiomyocyte (cardiac troponin $T^{+ve}$, $Ki67^{+ve}$, $DAPI^{+ve}$) density within the left ventricle of *Csf1r*-null animals and their WT littermates was significantly increased between mice aged P1 and P7 (Figure 4-6B). Density of proliferative cardiomyocytes was not significantly different between *Csf1r*-null animals and their WT littermates at either time points (Figure 4-5B).

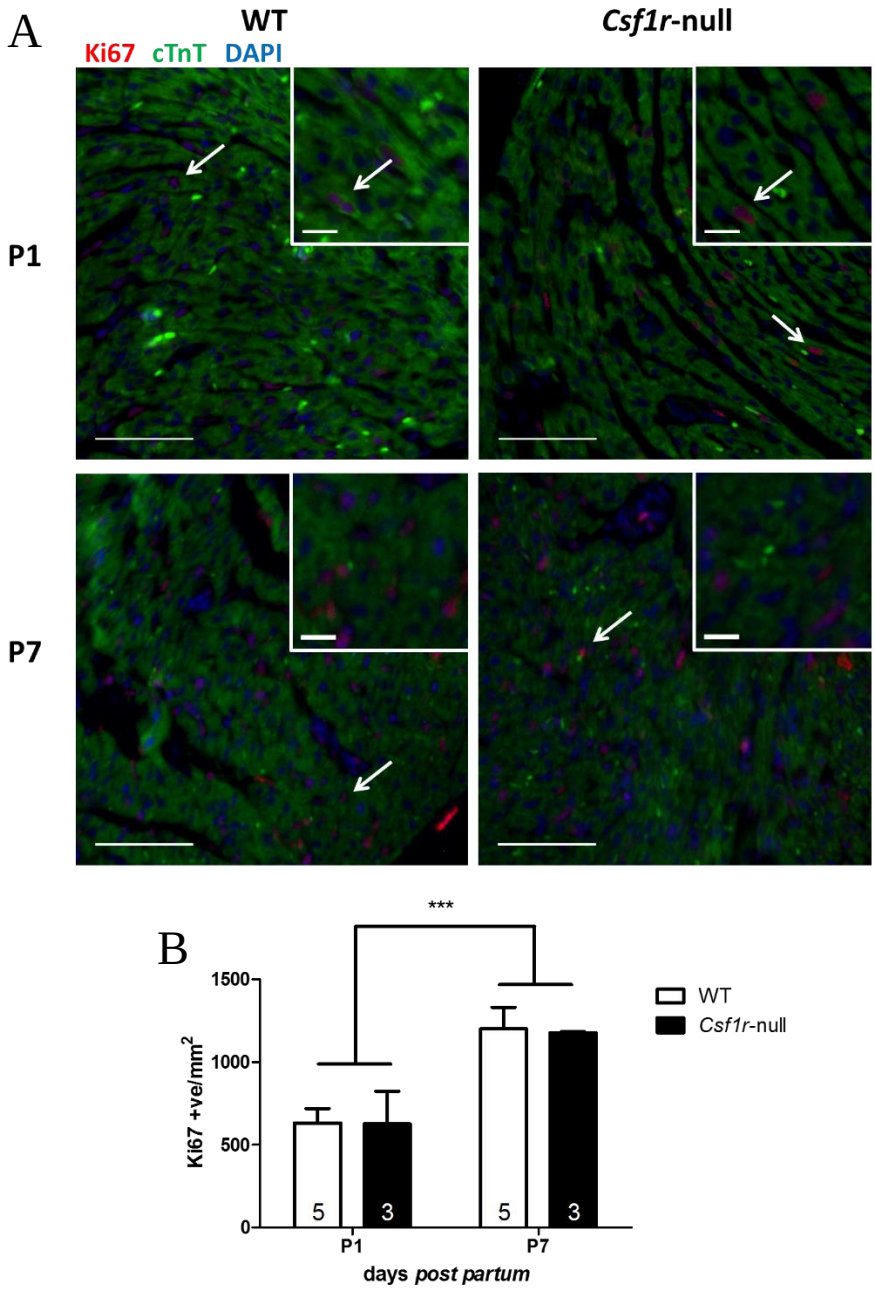


**Figure 4-6: Constitutive genetic depletion of macrophages does not influence cardiomyocyte proliferation in the neonatal mouse.** Proliferative cardiomyocytes (cm) were identified as positive for cardiac troponin T (green-cm marker) and containing a nucleus, DAPI (blue), positive for Ki67 (red-proliferation maker). Double positive nuclei appear pink (white arrows). Quantification was performed on 5 different field of views across the whole left ventricle of 4 μm thick cardiac sections at postnatal day 1 (P1) and P7 in *Csf1r*-null mice and compared to their wild-type littermates as controls. Representative images (*A*), scale bars = 50μm. Upper right corners are zooms, scale bars = 10μm. Cardiomyocytes proliferation quantification (*B*). Clear bars are WT and black bars *Csf1r*-null animals. Results are presented as mean ± SEM. p-value determined with 2-way ANOVA with Bonferroni post hoc test.

### *4.4.4 Constitutive genetic depletion of macrophages does not impair vessel density or size in neonatal mice*

A left shift was observed in vessel size distribution from P1 to P7 (Figure 4-7D). Average vessel size was significantly reduced between those time points (Figure 4-7B). Vascular density was significantly increased between P1 and P7 (Figure 4-7C).

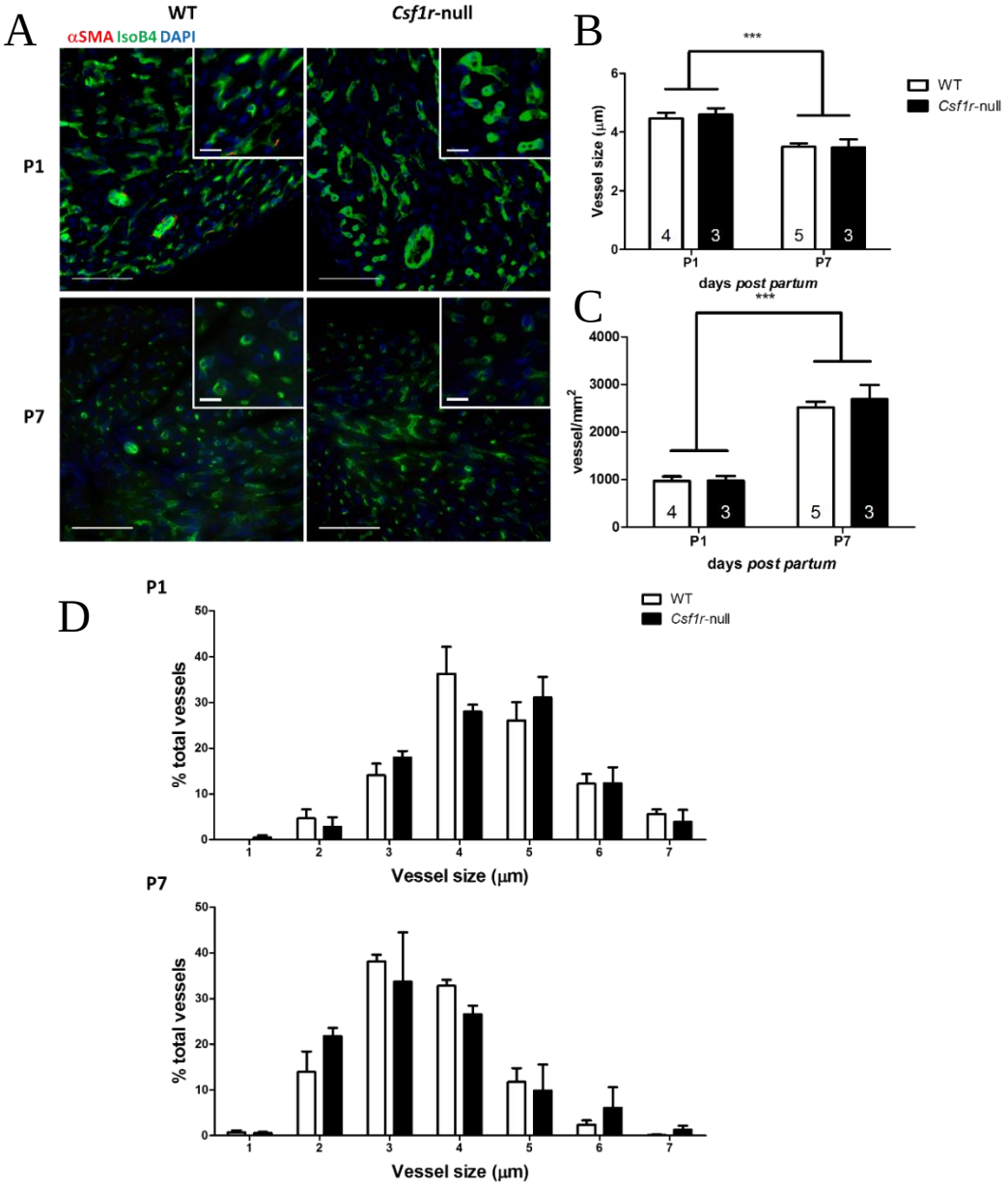


**Figure 4-7: Constitutive genetic depletion of macrophages does not influence vessel size or density in the neonatal mouse.** Vessel size and density was investigated on isolectin B4 (IB4-green-endothelial cells), α smooth muscle actin (αSMA-red-mural cell coated vessels), and DAPI (blue). Quantification of vessel size and density was performed on 5 different field of views within the outer layer of the left ventricle on 4μm thick stained sections at postnatal day 1 (P1) and P7 in *Csf1r*-null mice and compared to their wild-type littermates as controls. Representative images (*A*), scale bars = 50μm. Upper right corners are zooms, scale bars = 10μm. Average vessel size in μm (*B*). Vessel density was shown as expressed per $mm^2$ of myocardium (*C*). Vessel size distribution was investigated at the 2 chosen time points (*D*). Clear bars are WT animals and black bars are *Csf1r*-null. Results are presented as mean ± SEM. p-value determined with 2-way ANOVA with Bonferroni post hoc test. *** $p < 0.001$.

### *4.4.5 Does Csf1r-icre mediated depletion of Porcn affect normal postnatal cardiac growth and function?*

#### *4.4.5.1 Csf1r-icre* mediated depletion of *Porcn* does not influence normal postnatal cardiac growth

Body and heart weight increased from P1 to P41 in Cre-expressing ($Cre^{+ve}$) and Cre-deficient ($Cre^{-ve}$) Porcupine mice (Figure 4-8A, B). Body weight was significantly increased in $Cre^{+ve}$ animals at P41 when compared to age-matched $Cre^{-ve}$ littermates (Figure 4-8A). No effect of the genotype on body weight at earlier time points could be seen. Neither heart wet weight nor the heart to body weight ratio were significantly affected by the genotype (Figure 4-8B, C). Although LV mass determined by high-resolution *in vivo* ultrasound was significantly increased in $Cre^{+ve}$ animals at P41 when compared to age-matched $Cre^{-ve}$ littermates (Figure 4-8D), this is not reflected in actual heart weight.

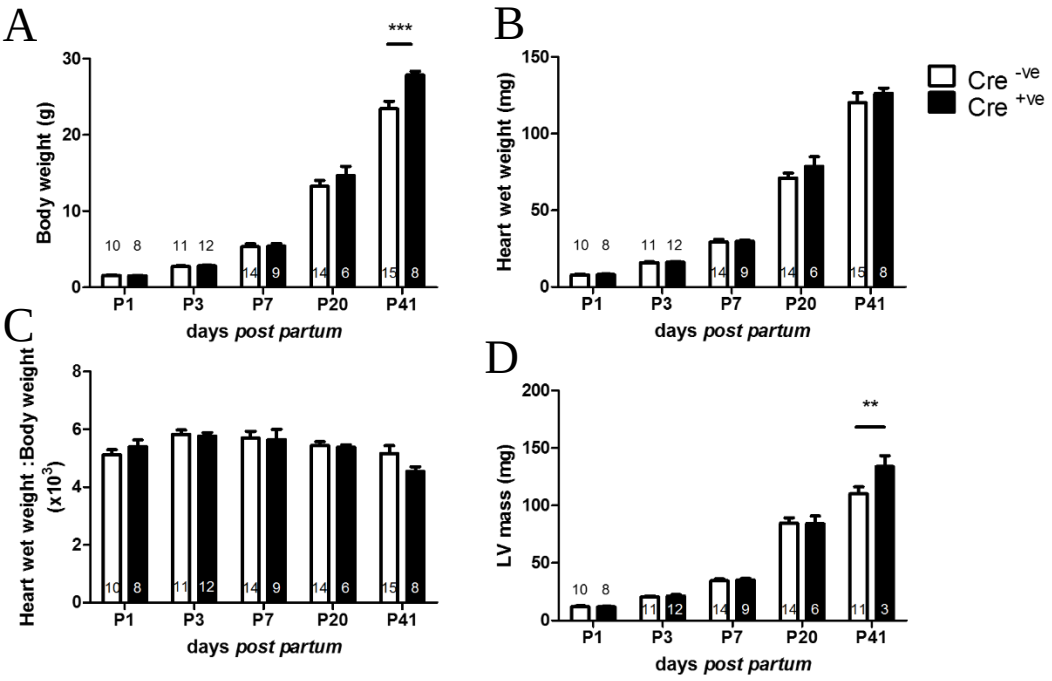


**Figure 4-8: *Csf1r-icre* mediated depletion of *Porcn* does not impair body or cardiac growth.** Body weight (*A*) was measured prior to high-resolution *in vivo* ultrasound. Heart wet weight (*B*) was measured immediately after high-resolution *in vivo* ultrasound imaging following dissection and used to calculate heart to body weight ratio (*C*). Left ventricle (LV) mass (*D*) was extracted from electrocardiogram-gated kilohertz visualisation (EKV) parasternal long axis (PLAX) B-mode. Measurements were performed at postnatal day 1 (P1), P3, P7, P20, and P41 in Cre-expressing ($Cre^{+ve}$ - black bars) and Cre-deficient ($Cre^{-ve}$ - clear bars) Porcupine mice. Results are presented as mean ± SEM. p-value determined with 2-way ANOVA with Bonferroni post hoc test. ** $p < 0.01$, *** $p < 0.001$.

#### *4.4.5.2 Csf1r-icre* mediated depletion of *Porcn* does not impair cardiomyocyte size or proliferation

CMCSA was significantly increased in $Cre^{+ve}$ mice at P41 when compared to age-matched $Cre^{-ve}$ littermates as controls. No effect of the genotype on CMCSA at earlier time points could be seen (Figure 4-9B). High-resolution *in vivo* ultrasound extracted LV wall thickness was increased from P1 to P41 with no effect of the genotype (Figure 4-9C).

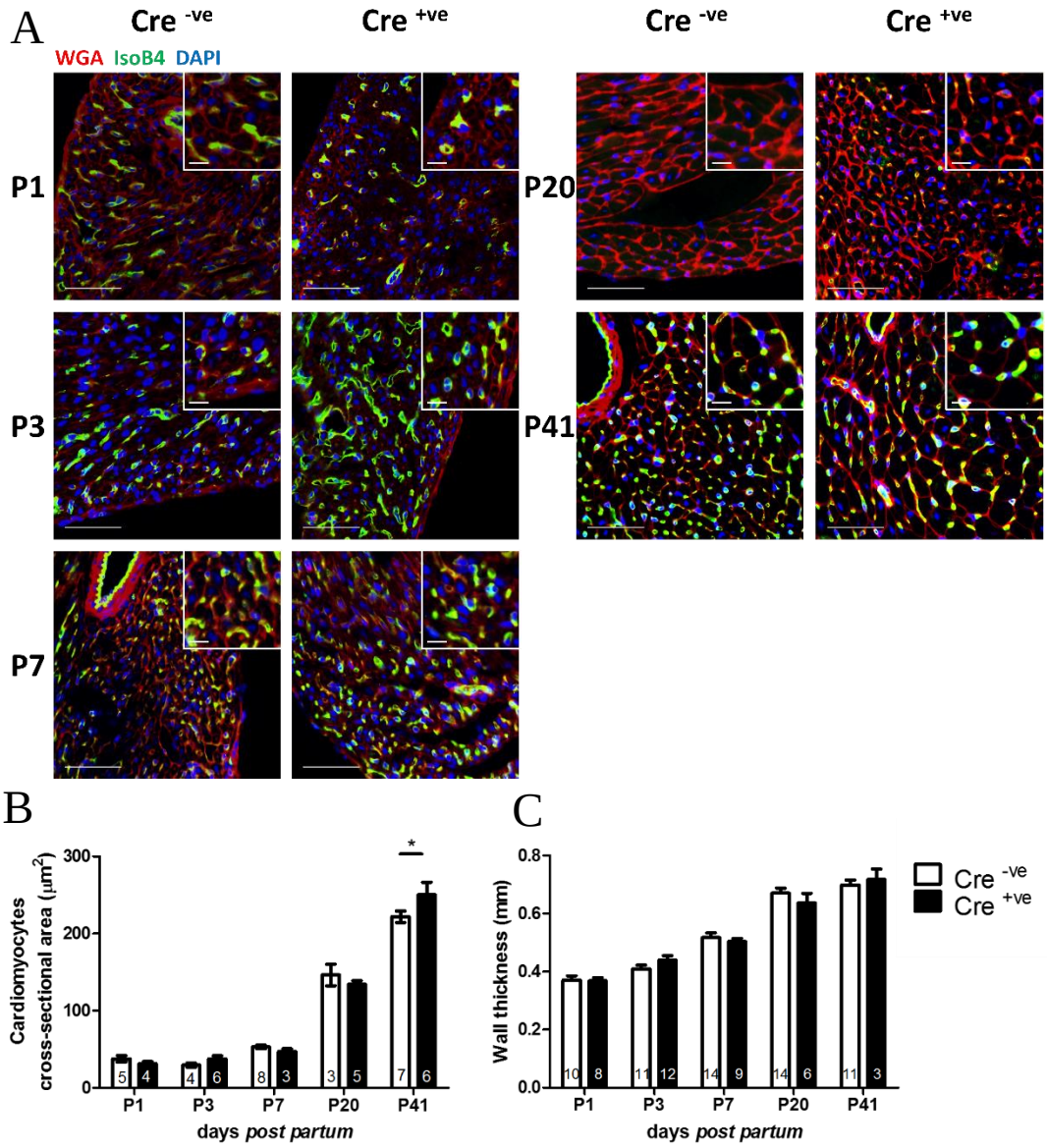


**Figure 4-9: *Csf1r-icre* mediated depletion of *Porcn* does not impair CMCSA.** Cardiomyocytes cross sectional area (CMCSA) was investigated on Wheat Germ Agglutinin (WGA-red-membrane marker), isolectin B4 (IB4-green-endothelial cells marker), and DAPI (blue) stained 4 μm thick sections at postnatal day 1 (P1), P3, P7, P20, and P41 in Cre-expressing ($Cre^{+ve}$ - black bars) and Cre-deficient ($Cre^{-ve}$ - clear bars) Porcupine mice. Representative images (*A*), scale bars = 50μm. Upper right corners are zooms, scale bars = 10μm. CMCSA quantification (*B*). Left ventricular (LV) wall thickness (*C*) was extracted from electrocardiogram-gated kilohertz visualisation (EKV) parasternal long axis (PLAX) B-mode. Results are presented as mean ± SEM. p-value determined with 2-way ANOVA with Bonferroni post hoc test. * $p < 0.05$.

Proliferative cardiomyocyte (cardiac troponin $T^{+ve}$, $Ki67^{+ve}$, $DAPI^{+ve}$) density within the left ventricle of Porcupine mice was highest in mice aged P1, P3, and P7 (Figure 4-10B). This density drops to low levels at P20 and P41 (Figure 4-10B). No significant difference between Cre+ve mice and their Cre-ve control littermates was observed.

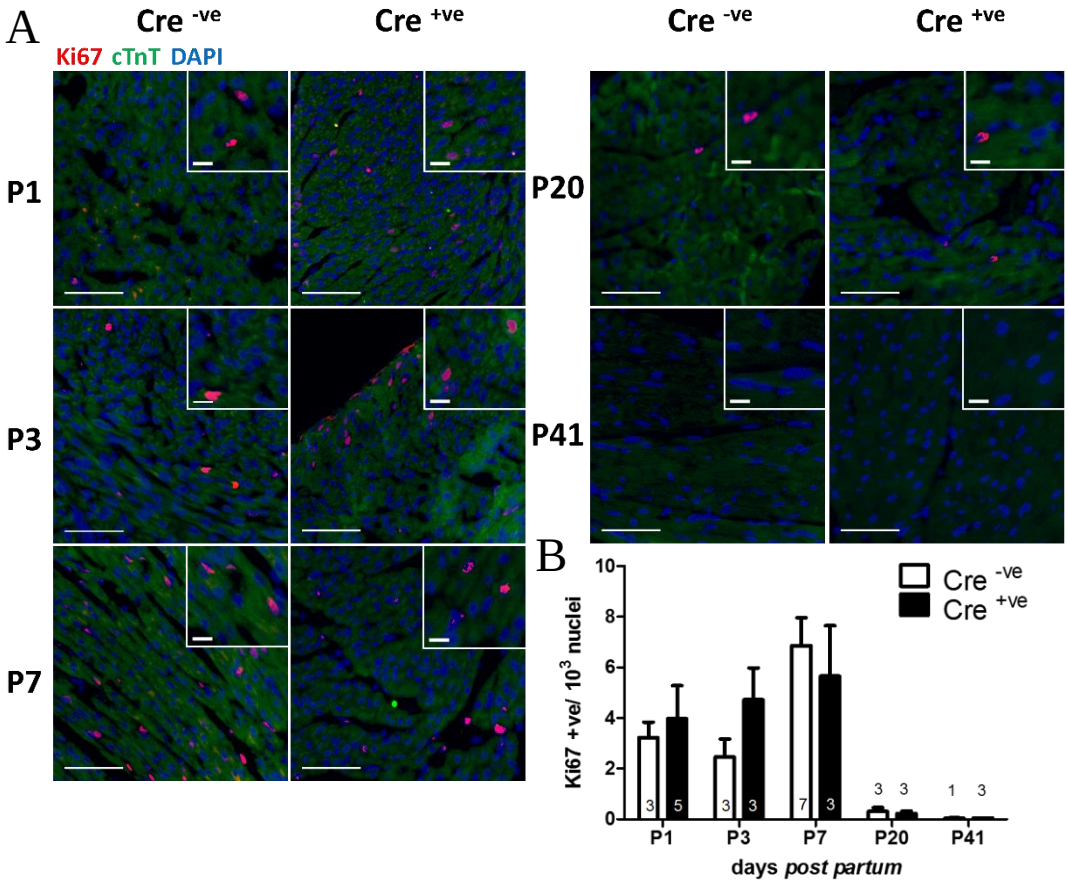


**Figure 4-10: *Csf1r-icre* mediated depletion of *Porcn* does not influence cardiomyocytes proliferation.** Proliferative cardiomyocytes (cm) were identified as positive for cardiac troponin T (green-cm marker) and containing a nucleus, DAPI (blue), positive for Ki67 (red-proliferation maker). Double positive nuclei appear pink. Quantification was performed across the whole left ventricle of 4 μm thick cardiac sections at postnatal day 1 (P1), P3, P7, P20, and P41 in Cre-expressing ($Cre^{+ve}$ - black bars) and Cre-deficient ($Cre^{-ve}$ - clear bars) Porcupine mice. Representative images (*A*), scale bars = 50μm. Upper right corners are zooms, scale bars = 10μm. Cardiomyocytes proliferation quantification (*B*). Results are presented as mean ± SEM. p-value determined with 2-way ANOVA with Bonferroni post hoc test.

#### *4.4.5.3 Csf1r-icre* mediated depletion of *Porcn* does not influence vessel size, density, or maturation

Vessel size distribution was not significantly affected by the genotype at any of the 3 time points investigated (Figure 4-11B). Average vessel size was decreased and vessel density increased from P1 to P7 and P41 with no effect of the genotype (Figure 4-11C-D). As shown on Figure 4-11E the number of $\alpha SMA^{+ve}$ vessels throughout the LV was drastically increased in adult animals (P41) when compared to neonates (P1, P7). No effect of the genotype could be noted.

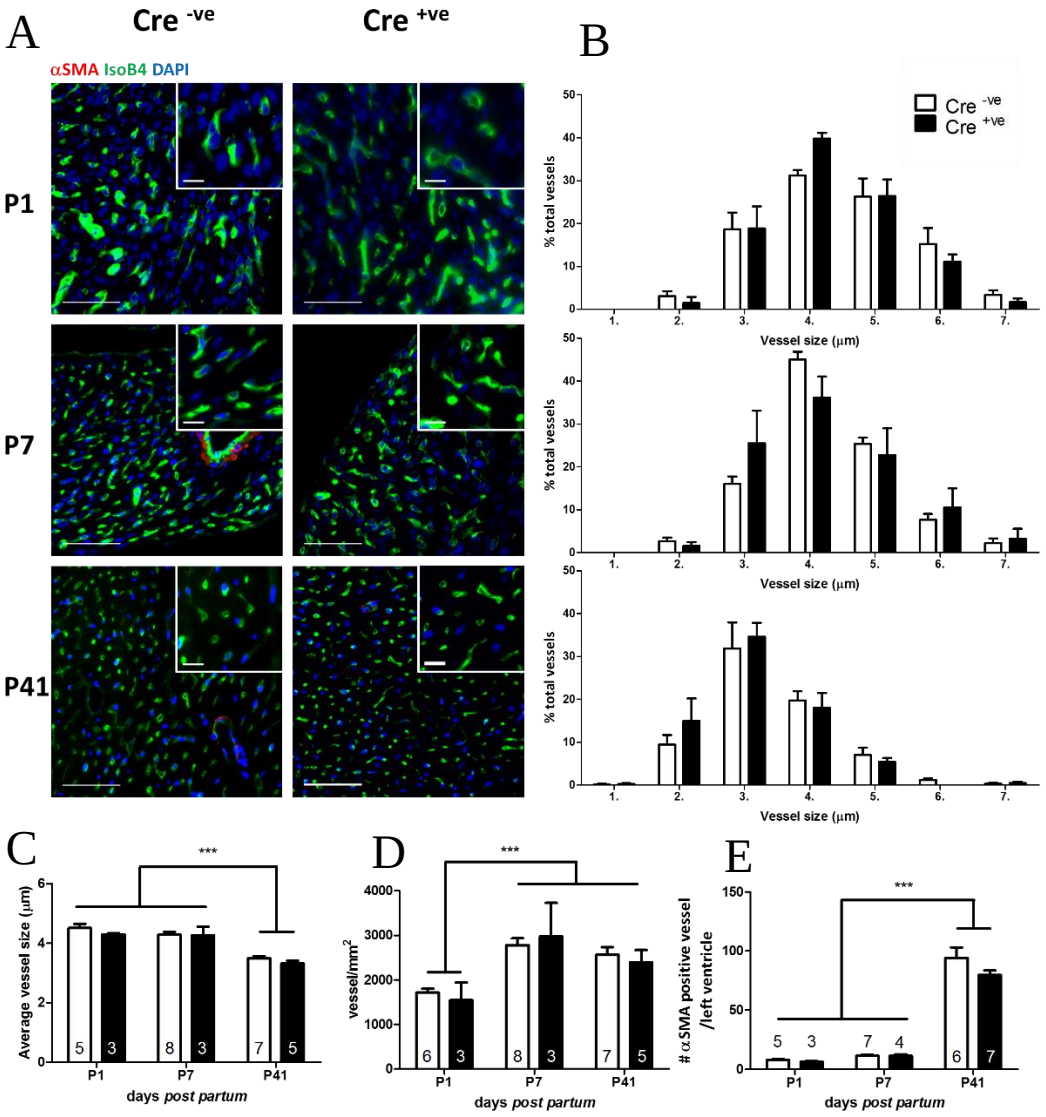


**Figure 4-11: *Csf1r-icre* mediated depletion *Porcn* does not influence cardiac vessel size, density, or maturation.** Vessel size, density, and maturation was investigated on isolectin B4 (IB4-green-endothelial cells), α smooth muscle actin (αSMA-red-mural cell coated vessels), and DAPI (blue). Quantification of vessel size and density was performed on 5 different field of views within the outer layer of the left ventricle on 4 μm thick stained sections at postnatal day 1 (P1), P7, and P41 in Cre-expressing ($Cre^{+ve}$ - black bars) and Cre-deficient ($Cre^{-ve}$ - clear bars) Porcupine mice. Representative images (*A*), scale bars = 50μm. Upper right corners are zooms, scale bars = 10μm. Vessel size distribution was investigated at the 3 chosen time points (*B*). Average vessel size in μm (*C*). Vessel density was shown as expressed /mm2 of myocardium (*D*). Number of $αSMA^{+ve}$ vessels within the whole left ventricle (*E*). Results are presented as mean ± SEM. p-value determined with 2-way ANOVA with Bonferroni post hoc test. *** p <0.001.

*4.4.5.4 Csf1r-icre* mediated depletion of *Porcn* does not influence cardiac interstitial fibrosis

Cardiac interstitial fibrosis was investigated on picrosirius red (PSR) stained sections. The amount of fibrosis appeared stable across all time-point studied. The genotype did not have an effect (Figure 4-12B).

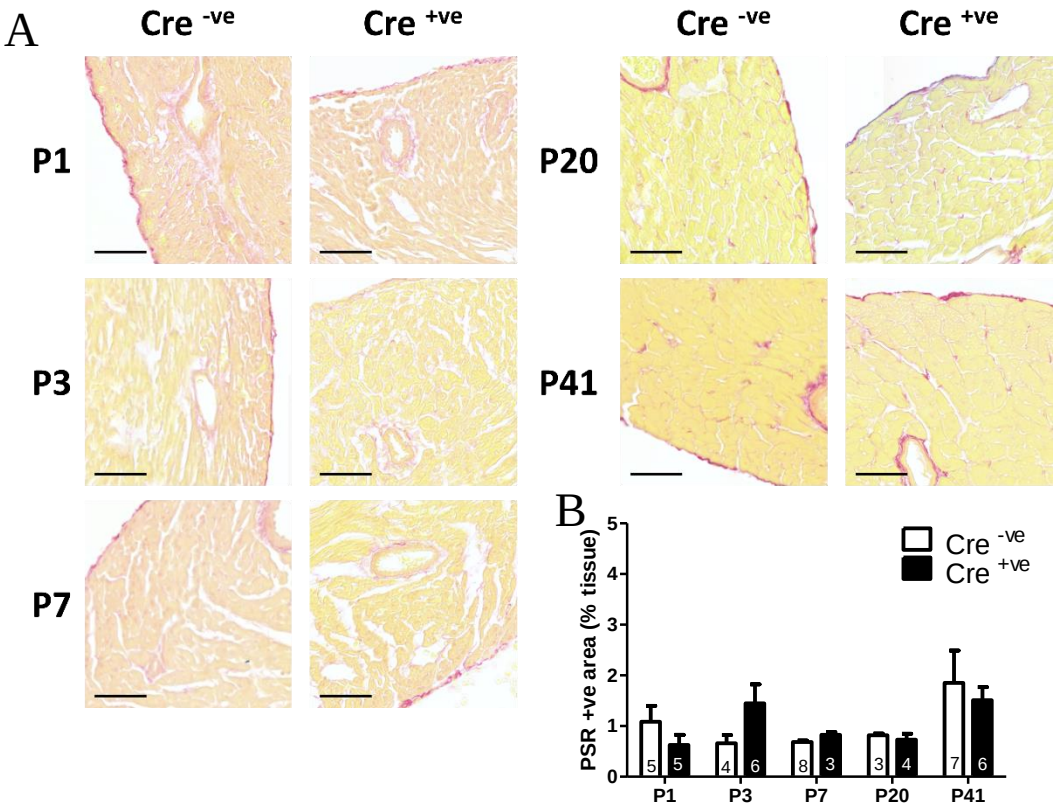


**Figure 4-12: *Csf1r-icre* mediated depletion of Porcn does not influence cardiac interstitial collagen content.** Interstitial collagen content was evaluated on picrosirius red (PSR-collagen marker) across the whole left ventricle on 4 μm thick section at postnatal day 1 (P1), P3, P7, P20, P41 in Cre-expressing ($Cre^{+ve}$ - black bars) and Cre-deficient ($Cre^{-ve}$ - clear bars) Porcupine mice with Photoshop CS6. Collagen fibres appear red, remaining tissue yellow. Representative images of PSR stained heart (*A*). Quantification of $PSR^{+ve}$ area (*B*). Scale bars = 50 μm. Results are presented as mean ± SEM. P-value determined by 2-way ANOVA with Bonferroni post hoc test.

#### *4.4.5.5 Csf1r-icre* mediated depletion of *Porcn* does not influence cardiac dimensions at systole or diastole

LV end systolic area (LVESA) was increased from P1 to P41 with no effect of genotype (Figure 4-13B). LV end diastolic area (LVEDA) was increased from P1 to P41. LVEDA was significantly increased in $Cre^{+ve}$ animals at P41 when compared to age-matched $Cre^{-ve}$ control littermates No effect of the genotype on LVEDA at earlier time points could be seen (Figure 4-13C).

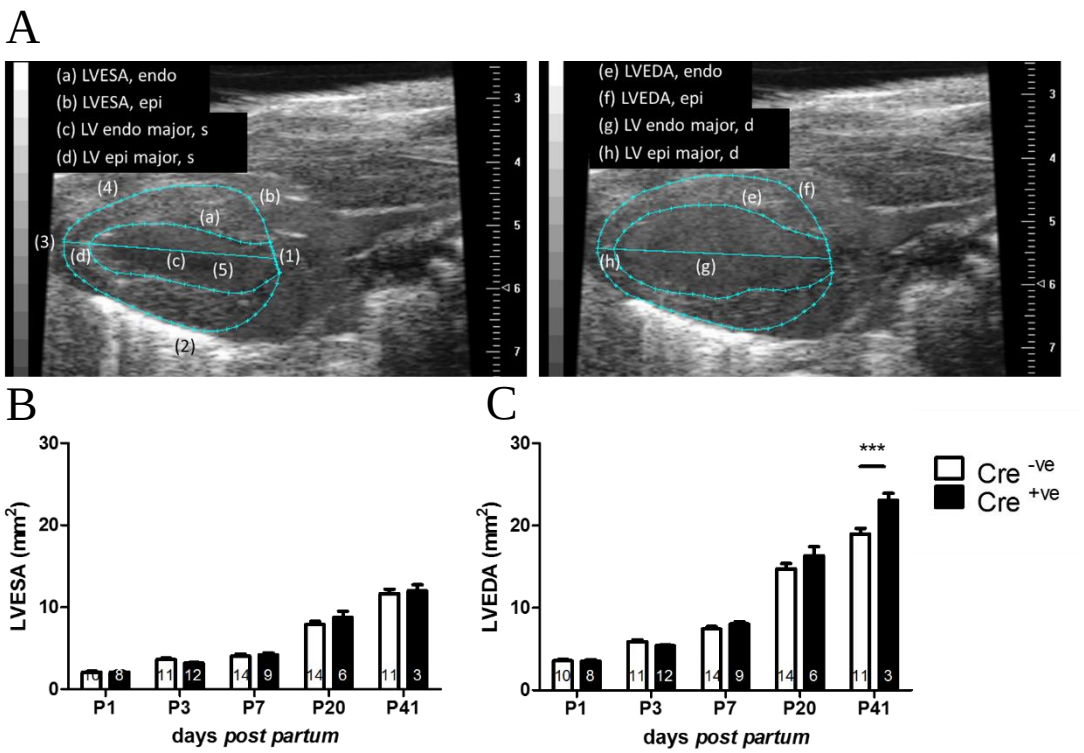


**Figure 4-13: *Csf1r-icre* mediated depletion of *Porcn* does not impair cardiac dimensions.** Electrocardiogram-gated kilohertz visualisation (EKV) parasternal long axis (PLAX) B-mode (*A*) allowed calculation of left ventricle (LV) cavity size at the end of systole (LVESA-*B*) and diastole (LVEDA-*C*) at postnatal day 1 (P1), P3, P7, P20, P41 in Cre-expressing ($Cre^{+ve}$ - black bars) and Cre-deficient ($Cre^{-ve}$ - clear bars) Porcupine mice. Results are presented as mean ± SEM. p-value determined with 2-way ANOVA with Bonferroni post hoc test. *** p <0.001.

#### *4.4.5.6 Csf1r-icre* mediated depletion of *Porcn* does not impair cardiac diastolic function

Both functional measurements of fractional area change (FAC) and ejection fraction (EF), obtained with electrocardiogram-gated kilohertz visualisation (EKV) parasternal long axis (PLAX) B-mode ultrasound, were similar at all time points up to P20 between $Cre^{+ve}$ animals and $Cre^{-ve}$ control littermates. At P41, both FAC and EF were

significantly increased in Cre$^{+ve}$ animals when compared to Cre$^{-ve}$ control littermates. No effect of the genotype on FAC or EF at earlier time points could be seen (Figure 4-14A, B). No effect of the genotype could be observed at any time point with the additional functional measurements of fractional shortening (FS) and myocardial performance index (MPI) obtained from PLAX M-mode and pulse-wave Doppler respectively (Figure 4-14C, D).

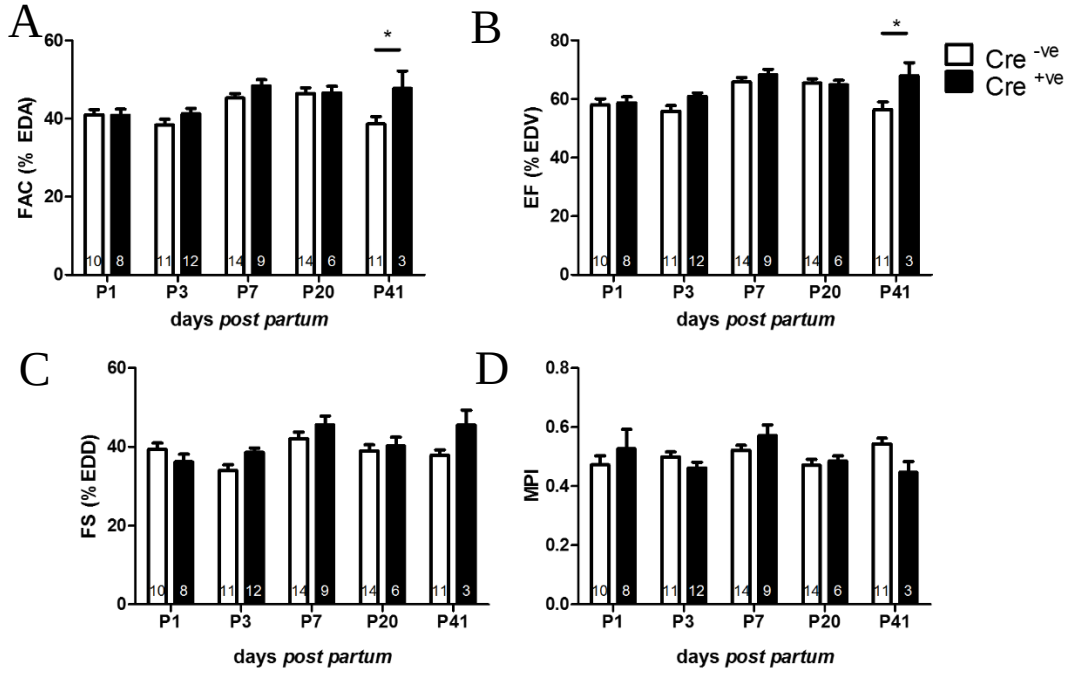


**Figure 4-14: *Csf1r-icre* mediated depletion of *Porcn* does not impair cardiac systolic function.** Cardiac systolic function was investigated using high-resolution *in vivo* ultrasound at postnatal day 2 (P2), P4, P8, P21, P42 in Cre-expressing (Cre$^{+ve}$ - black bars) and Cre-deficient (Cre$^{-ve}$ - clear bars) Porcupine mice. Electrocardiogram-gated kilohertz visualisation (EKV) parasternal long axis (PLAX) B-mode allowed calculation of fractional area change (FAC-*A*) and ejection fraction (EF-*B*). PLAX motion-mode (m-mode) was used to obtain fractional shortening (FS-*C*). Trans-mitral Doppler allowed calculation of the myocardial performance index (MPI-*D*). Results are presented as mean ± SEM. p-value determined with 2-way ANOVA with Bonferroni post hoc test. * $p < 0.05$.

*4.4.5.7 Csf1r-icre* mediated depletion of *Porcn* does not influence cardiac diastolic function

A normal pattern of E to A wave ratio reversal was observed in Porcupine mice. Mice prior to P7 had a ratio below 1, and mice from P7 had a ratio above 1 (Figure 4-15). No significant difference between the two genotypes could be noted.

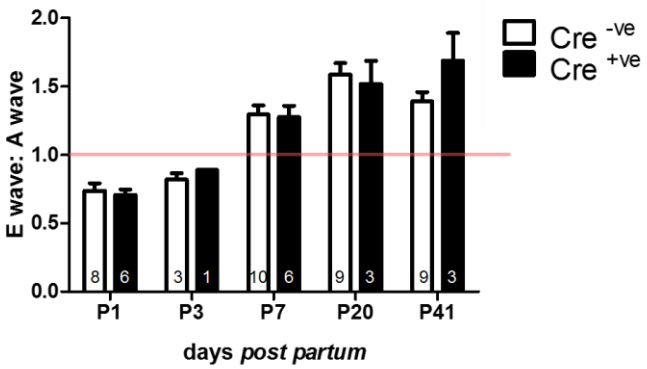


**Figure 4-15: *Csf1r-icre* mediated depletion of *Porcn* does not impair cardiac diastolic function.** Cardiac diastolic function was investigated using high-resolution *in vivo* ultrasound at postnatal day 2 (P2), P8, P21, P42 in Cre-expressing ($Cre^{+ve}$ - black bars) and Cre-deficient ($Cre^{-ve}$ - clear bars) Porcupine mice. Trans-mitral pulse-wave Doppler allowed calculation of the E wave to A wave ratio. Red line represents a ratio of 1. A ratio < 1 is typical of foetal cardiac diastolic function. A ratio > 1 is typical of adult cardiac diastolic function. Results are presented as mean ± SEM. p-value determined with 2-way ANOVA with Bonferroni post hoc test.

## 4.5 Discussion

Macrophages have well described roles in tissue homeostasis (Davies *et al.*, 2013; Wynn *et al.*, 2013). In the heart, they have mostly been described in the context of injury such as myocardial infarction (MI) (Frangogiannis, 2014) and their role during normal cardiac growth remains unclear (Pinto *et al.*, 2014). Whilst the Wnt signalling pathway has been demonstrated to play key roles during foetal cardiac development and following injury in adults (Gessert and Kühl, 2010; Dawson *et al.*, 2013), its role during early postnatal cardiac growth is unknown. It is becoming increasingly clear that macrophages express and secrete WNTs that are then able to modulate angiogenesis (James A Stefater *et al.*, 2011; Stefater *et al.*, 2013). The present study therefore aimed at shedding light on the role of macrophages and macrophage-secreted WNTs on murine postnatal cardiac growth.

*Mononuclear phagocyte populations in the murine heart*

In this chapter the MacGreen mouse, that expresses GFP under the control of the *Csf1r* promoter (Sasmono *et al.*, 2003), was used to visualise the mononuclear phagocyte population within the myocardium. *Csf1r* mRNA can also be found in neutrophils but is not translated (Sasmono *et al.*, 2007). Nevertheless, this indicates an active *Csf1r* promoter in neutrophil which also express GFP in the MacGreen mouse model. Flow cytometric analysis allowed to determine that, on average, 30% of $GFP^{+ve}$ cells are neutrophils based on their expression of Ly6G. The density of *Csf1r*-expressing cells within the myocardium of MacGreen mice was shown to be constant between P2 and P42 averaging at 170 $GFP^{+ve}$ cells/$mm^2$. The average mononuclear phagocytes content of the murine myocardium can therefore be estimated at 120 cells/$mm^2$ excluding neutrophils. Lavine *et al.* (2014) had identified an approximate number of 125 mononuclear phagocytes per milligram of heart tissue in neonatal mice. How this compares to our findings is less clear. The neonatal population of *Csf1r*-expressing cells was evenly distributed across the myocardium. Consistent with this data, Mylonas *et al.* (2015) previously reported that cardiac macrophages were also evenly distributed in the adult mouse.

Flow cytometric analysis of neonatal hearts revealed 3 clearly distinct populations of mononuclear phagocytes: $F4/80^{hi}$, $CD11b^{lo}$, $Ly6C^{-ve}$ - $F4/80^{lo}$, $CD11b^{hi}$, $Ly6C^{-ve}$ - $F4/80^{lo}$, $CD11b^{hi}$, $Ly6C^{+ve}$.

The foetal heart contains multiple cardiac mononuclear phagocyte populations that are ontologically distinct. F4/80$^{hi}$, CD11b$^{lo}$ macrophages are detected in the heart at E10.5 (Epelman *et al.*, 2014) and E12.5 (Leid *et al.*, 2016), and are believed to be yolk-sac derived as they appear prior to the formal establishment of foetal liver haematopoiesis (Schulz *et al.*, 2012). From E12.5 to E16.5 (Epelman *et al.*, 2014) and at E14.5 (Leid *et al.*, 2016), data from the literature shows the appearance of a second population with the characteristic foetal liver F4/80$^{lo}$, CD11b$^{hi}$ pattern. This latter population was also shown to be positive for C-C chemokine receptor type 2 (CCR2) suggesting a monocytic origin (Leid *et al.*, 2016). F4/80$^{hi}$, CD11b$^{lo}$ macrophages were however CCR2$^{-ve}$ (Leid *et al.*, 2016). Leid *et al.* (2016) showed that in the foetal heart both CCR2$^{+ve}$ and CCR2$^{-ve}$ populations co-expressed MER proto-oncogene tyrosine kinase (MertTK) indicating their macrophage identity. Lavine *et al.* (2014) however showed that in the neonatal heart the CCR2$^{+ve}$ population did not co-express MerTK and classed this population as monocytes. In the present study, cells with characteristics of yolk-sac and foetal liver derived macrophages were found in neonatal hearts.

Data from this chapter showed that in the neonatal mouse heart, the F4/80$^{lo}$, CD11b$^{hi}$ population of mononuclear phagocytes contains both Ly6C$^{-ve}$ and Ly6C$^{+ve}$ cells. Additional markers such as CCR2 and MerTK would help formally compare this population with the published literature. It however possesses the typical foetal liver/bone marrow derived pattern of F4/80$^{lo}$, CD11b$^{hi}$ (Epelman *et al.*, 2014; Lavine *et al.*, 2014; Leid *et al.*, 2016). Whether the Ly6C$^{-ve}$ population correspond to the CCR2$^{+ve}$, MerTK$^{+ve}$ population (Leid *et al.*, 2016); and the Ly6C$^{+ve}$ population to the CCR2$^{+ve}$, MerTK$^{-ve}$ population (Lavine *et al.*, 2014) is unclear but should be investigated further for better comprehension of the present data. The F4/80$^{hi}$, CD11b$^{lo}$ population of mononuclear phagocytes observed in this chapter only contained Ly6C$^{-ve}$ cells. Yolk-sac derived, F4/80$^{hi}$, CD11b$^{lo}$ cardiac macrophages were shown by Leid *et al.* (2016) to also be Ly6C$^{-ve}$. This may indicate that the population observed in this chapter arise from the yolk-sac. Lineage tracing experiments should be considered as formal proof of the origin of the mononuclear phagocyte populations observed in this chapter. The precise identification of different cardiac resident mononuclear phagocyte population is crucial as they have been shown to play different roles during

normal cardiac growth and following injury (Epelman *et al.*, 2014; Lavine *et al.*, 2014; Leid *et al.*, 2016).

Furthermore, the data presented here suggests that the population of yolk-sac derived macrophages is stable at least during the first week after birth which is in accordance to the literature showing that yolk-sac derived macrophages can still be found in the myocardium of adult mice (Epelman *et al.*, 2014). Even though it didn't reach significance some trends are worth noting in the F4/80$^{lo}$, CD11b$^{hi}$ population. Ly6C$^{+ve}$ cells, which likely represent bone-marrow derived monocytes, seemed present in a higher proportion at P2 when compared to P8. The opposite was true for Ly6C$^{-ve}$ cells, likely to be macrophages. This could indicate that following birth, monocytes are recruited to the myocardium where they will then differentiate into macrophages. This indeed coincides with a time where the heart undergoes important changes as described in Chapter 3. A formal investigation of those populations in the first days after birth including the CCR2 marker would help understand their dynamics and provide better understanding of the published literature. Measuring levels of chemokines and chemokine receptor as well as performing lineage tracing would also provide further proof of the recruitment of monocytes to the myocardium shortly after birth. Having established this phenotype would then provide a basis for the role of those newly recruited macrophages in early postnatal cardiac growth.

*Macrophages in cardiac growth*

In this chapter, the effect of macrophage depletion was investigated using a murine model lacking exon 5 of the *Csf1r* gene. This has previously been shown to reduce tissue macrophages numbers (Dai *et al.*, 2002) including microglia in the brain, a prime example of yolk-sac derived tissue resident macrophages (Erblich *et al.*, 2011). In the heart, tissue macrophages were also reduced using a similar genetic depletion model; the *Csf1*$^{op/op}$ mouse which presents an inactivating mutation within the *Csf1* gene (Leid *et al.*, 2016). Both ablation of the Csf1r gene and its ligand CSF1 are associated with osteopetrosis and reproductive deficiencies along with other defects leading to global growth retardation (Dai *et al.*, 2002; Pollard, 2009).

Consistent with these observation, *Csf1r*-null animals presented with both body and cardiac growth impairment from P7. Heart wet weight to body weight ratio was

comparable between *Csf1r*-null and WT littermates except at P1 where it appeared to be increased in mice depleted of macrophages. Further investigation at this time point showed that neither CMCSA or cardiomyocyte proliferation were increased which could have participated in an increased heart weight via hypertrophy and hyperplasia respectively. This correlates with data from Lavine *et al.* (2014) showing that clodronate mediated depletion of cardiac macrophages in the neonatal mouse does not affect either CMCSA or cardiomyocyte proliferation. The mechanism behind increased heart to body weight ratio at P1 is therefore unclear. It may be due to oedema or accumulation of another cell type not investigated. This however needs to be studied in a larger cohort of mice. The heart largely continues to grow in proportion to the body in these mice.

There is substantial amount of evidence showing an involvement of macrophages in angiogenesis during development and in pathology (Pollard, 2009; Nucera *et al.*, 2011). In the foetal heart, *Csf1*$^{op/op}$ mice contain significantly more vessels of a larger size compared to WT littermates at E17.5 (Leid *et al.*, 2016). In this chapter, *Csf1r*-null mice showed a trend to an increased proportion of larger vessels at P2 although this failed to reach statistical significance, due to the small number of hearts that were available to use for analysis. Vessel size distribution and density were normal at P8 in *Csf1r*-null compared to WT littermates. (Leid *et al.*, 2016) also observed that their phenotype of increased vessel size and density in the foetal heart at E17.5 disappears in P21 animals. This suggests that the effect of constitutive macrophage depletion may be compensated by alternative mechanisms that allow normal vessel development postnatally. Leid *et al.* (2016) argued for a role of IGF1 as a macrophage secreted factor that was shown by them and others to regulate angiogenesis (Bach, 2015). Interestingly IGF1 is also known to be produced by cardiac fibroblasts *in vitro* (Takeda *et al.*, 2010) and these cells could represent an alternative compensatory source of the growth factor in the absence of macrophages. Further investigation on the role of macrophages during coronary vasculature formation would greatly benefit from the use of inducible models; that would allow temporal control over macrophage depletion, which appears crucial in their function.

Interestingly, Leid *et al.* (2016) saw that foetal liver-derived CCR2$^{+ve}$ macrophage primarily localised within the trabeculated myocardium in the foetal heart. The phenotype observed in *Csf1*$^{op/op}$ mice of increased vessel size and density in the foetal heart at E17.5 was however not reproduced in a CCR2 KO mouse model (Leid *et al.*, 2016). Nevertheless, Tian *et al.* (2014) have shown that prior to P3 the trabecular myocardium does not contain any vessels and is supplied in nutrients and oxygen through exchange with the blood present in the ventricular cavity. Following birth and the increased pressure and demand on the LV, compaction of the trabecular myocardium occurs (Sedmera *et al.*, 2000). This is concurrent to the formation of a new coronary vasculature to supply the newly compacted myocardium (Tian *et al.*, 2014). Whether CCR2$^{+ve}$ macrophages play a role in the postnatal vascularisation of the newly compacted myocardium is less clear. Using an inducible CCR2 KO mouse model could help investigate this further by preventing recruitment of monocytes and macrophages to the myocardium at this key time point.

Even though *Csf1*$^{op/op}$ mice were shown by Leid *et al.* (2016) to lack cardiac macrophages, and that *Csf1*$^{op/op}$ and *Csf1r*-null mice are phenotypically close, a formal proof of cardiac macrophages ablation in *Csf1r*-null animals is lacking the present study and prevents conclusive statements to be drawn. Cardiac macrophages visualisation on sections has been endeavoured throughout this PhD using the specific marker F4/80. This was however inconclusive in our hands. Other markers that may be envisaged for immunostainings include Mac-3 or CD68 (Aurora *et al.*, 2014; Lavine *et al.*, 2014). Alternatively flow cytometry could also be carried out to confirm cardiac macrophage ablation.

Altogether evidence in the literature suggests that macrophages play a role in patterning and maturation of the coronary vasculature during foetal development. Their role postnatally is however less clear and may necessitate more refined ablation approaches. Their constitutive ablation indeed seems to induce compensatory mechanisms.

*Macrophages-derived WNTs and cardiac growth*

The Wnt signalling pathway is known to play and essential biphasic role during cardiac organogenesis promoting proliferation and then differentiation of cardiac precursors

(Section 1.5.2.1). WNT ligands are secreted proteins that are acylated by the member of the membrane bound O-acyltransferase (MBOAT) family: porcupine (PORCN). Without acylation, WNTs cannot bind the cargo protein wntless (Wls) which is essential for their secretion into the extracellular space (Mikels and Nusse, 2006).

Macrophages have been identified as a source of WNTs in several organs following injury in the adult mouse. These have included the kidney (Lin *et al.*, 2010), the liver (Boulter *et al.*, 2012; Irvine *et al.*, 2015; Planas-Paz *et al.*, 2016), the gut (Saha *et al.*, 2016), and recently in the heart (Palevski *et al.*, 2017). Whether macrophage-derived WNTs play a role in normal postnatal heart growth was however less clear.

Identifying whether cardiac mononuclear phagocytes express WNTs in the steady state is evidently crucial to our understanding of their potential role and has been endeavoured throughout this PhD. It was however not possible to collect sufficient RNA due to the low number of cells collected by FACS for analysis as described in Section 2.4.2. Detecting expression of *Wnts* from cells is notoriously difficult. The ability of tissue MΦ to express *Wnts* has previously been shown using nested PCR on freshly FACS isolated cells (Lin *et al.* 2010) or laser capture of F4/80$^{+ve}$ MΦ followed by total RNA amplification and qRT-PCR (Boulter *et al.*, 2012). Saha *et al.* (2016) were also able to show that culture medium from bone marrow derived MΦ (BMMΦ) is able to induce a positive response in a reporter that is activated when stimulated by the WNT/β-catenin pathway (Jho *et al.*, 2002).

One avenue that could be considered for future work is the amplification of the RNA collected from sorted mononuclear phagocytes. Nevertheless, mRNA expression does not necessarily mean protein expression or secretion. Another way to assess WNTs presence and secretion is the use of the reporter cell line mentioned above. This was not pursued in the current study due to time constraints but should be revisited. The literature shows that for extraction of tissue MΦ for cell culture, the preferred method is column extraction (Meznarich *et al.*, 2013). If this method is to be envisaged for future work, optimisation for cardiac MΦ will be necessary in order to confirm purity and yield of the population extracted.

WNT ligands family consist of 19 members in mammals (Section 1.5.1.1). As no specific candidate could be identified with cardiac mononuclear phagocyte expression data, a general depletion approached was chosen. As mentioned above, secretion of WNTs is dependent on their acylation by PORCN and transport to the membrane by Wls (Willert *et al.*, 2003; Port *et al.*, 2008; Herr and Basler, 2012; Saha *et al.*, 2016; Palevski *et al.*, 2017). Without either protein, WNTs are not secreted into the extracellular space. Two mouse models of mononuclear phagocyte-targeted depletion of *Porcn*, the Porcupine mouse, and *Wls*, the Wntless mouse, exist using cre-recombinase expressed from the *Csf1r* promoter. Both models have been shown to effectively delete their targeted genes specifically in macrophages which prevented secretion of WNTs into the extracellular space (Saha *et al.*, 2016; Palevski *et al.*, 2017). However, as mentioned above, neutrophils express *Csf1r* mRNA indicative of an active promoter (Sasmono *et al.*, 2007). They would therefore also be targeted by the *Csf1r-icre*. Neutrophils have been shown to express a number of *Fzd* receptors and to respond to Wnt signals (Y. S. Jung *et al.*, 2013) but unlike MΦ, whether they produce WNTs is unclear. As the Porcupine mouse could be kindly provided by Prof J.W Pollard's lab at the Einstein College of Medicine, New York, it was chosen in order to investigate the role of macrophage-derived WNTs on normal postnatal growth (Biechele *et al.*, 2013; Saha *et al.*, 2016).

In this chapter, the Porcupine mouse had normal heart and body weight, CMCSA, cardiac vascular size and density, ultrasound extracted cardiac dimensions and normal function up until P41 when body weight, LV mass, CMCSA, and LV end diastolic area were increased in $Cre^{+ve}$ mice compared to the $Cre^{-ve}$ control littermates. This may suggest cardiac hypertrophy (Maillet *et al.*, 2013). This phenotype was also associated with increased cardiac function measured with electrocardiogram-gated high-resolution ultrasound which might be suggesting physiological hypertrophy (Maillet *et al.*, 2013). A similar trend of increased cardiac function was observed in adult Wntless mice, albeit not statistically significant (Palevski *et al.*, 2017). However, further characterisation would be required investigating the molecular pathways typically involved with cardiac hypertrophy such as increased expression of *Igf1*, and phosphorylation of AKT and GSK3β (Μαιλλετ *ετ αλ.*, 2013). Atrial natriuretic peptide (ANP) and brain natriuretic peptide (BNP) are two proteins encoded by *Nppa*

and *NppB* respectively that are known to be up-regulated during cardiac hypertrophy (Rohini *et al.*, 2010); determination of their expression should also be envisaged.

Contrary to the original hypothesis, the Porcupine mouse has a mostly normal postnatal growth suggesting little role for macrophage-derived WNTs in the changes described in Chapter 3. Even though literature has shown that macrophages are able to express and secrete WNTs (Lin *et al.*, 2010; Boulter *et al.*, 2012; Saha *et al.*, 2016), it has not been possible in our hands to show their expression in cardiac macrophages. Saha *et al.* (2016) have however shown that *Csf1r-iCre* mediated depletion of Porcupine in the same mouse used in this chapter specifically depleted Porcupine in bone-marrow derived macrophages and prevented activation of a Wnt signalling reporter cell line. Direct evidence of expression and secretion of WNTs from cardiac macrophages, and confirmation of Porcupine depletion in cardiac macrophages as well as its effect on WNTs secretion is lacking from this thesis. This represents a major challenge experienced during this PhD.

Altogether data from this chapter has suggested a role for macrophages in normal postnatal growth of the whole animal. No specific link between macrophage depletion and a heart phenotype could however be established. Even though macrophage depletion had been shown to be associated with increased vessel size and density in the foetal heart, compensatory mechanisms seem put in place postnatally (Leid *et al.*, 2016). No effect of macrophage-derived WNTs on cardiac vessel size and density could be observed either. However, preventing secretion of WNTs from macrophages increases vascular density and branching in the postnatal retina (James A Stefater *et al.*, 2011). This may suggest a potential role for macrophage-derived WNTs in the effect of macrophage depletion on vascular maturation in the foetal heart.

# Chapter 5: The role of macrophage-secreted WNTs in neonatal cardiac regeneration

## 5.1 Introduction

Unlike other organs such as the liver (Forbes and Newsome, 2016) that are capable of a well-described regenerative response, the adult mammalian heart has thus far been considered largely non-regenerative. Following injury such as myocardial infarction (MI) a non-contractile scar is therefore formed to replace lost myocardium leading to remodelling of the remaining healthy tissue (Cohn *et al.*, 2000; Frangogiannis, 2014). Remodelling can in turn become maladaptive and lead to the development of heart failure (Section 1.1).

In contrast, neonatal humans and mice have been shown to retain potent regenerative capacities (Fratz *et al.*, 2011; Porrello *et al.*, 2011, 2013, Haubner *et al.*, 2012, 2016). Briefly, following induction of MI by permanently ligating the left anterior descending (LAD) coronary artery the neonatal mouse is able of full functional recovery and regeneration of the lost myocardium following 21 days (Haubner *et al.*, 2012; Porrello *et al.*, 2013). For further details see Section 1.3.1.

In other organs, macrophages (MΦ) are key to provision of a suitable environment for regeneration (Forbes and Rosenthal, 2014).At the outset of this PhD project a role for macrophages in neonatal heart regeneration had been proposed by the Olson lab (ISHR conference 2013) based on the detrimental effect of MΦ depletion on neonatal heart regeneration. This work has subsequently been published (Aurora *et al.* 2014) and presented a role of MΦ in angiogenesis post-MI in the neonate. Distinct populations of MΦ were also shown to participate in the response to cardiac injury in the adult and neonatal mouse (Lavine *et al.*, 2014). These studies demonstrate a pivotal role of MΦ in scar free neonatal cardiac regeneration, but the signalling pathways involved are not yet clear.

Importantly, MΦ-secreted WNTs were shown prior to the start of this PhD to be essential in regeneration of the kidney. MΦ-specific deletion of Wnt7b was indeed associated with increased interstitial fibrosis following hypoxia-induced injury of the kidney (Lin *et al.*, 2010). Since then a role of MΦ-secreted WNTs has been shown in the liver where prevention of secretion of WNTs from MΦ was also associated with increased fibrosis following thioacetamide-induced injury (Irvine *et al.*, 2015); and in the gut where prevention of secretion of WNTs from MΦ prevented stem cell

Chapter 5: The role of macrophage-secreted WNTs in neonatal cardiac regeneration proliferation in the crypt villi regeneration following radiation-induced injury (Saha *et al.*, 2016).

The Wnt signalling pathway (Section 1.5) is known to be crucial during cardiac development (Gessert and Kühl, 2010) and is also involved in mechanisms essential to regeneration such as cell proliferation, angiogenesis (Dejana, 2010), and fibrosis (Henderson *et al.*, 2010; Laeremans *et al.*, 2010). Of specific interest, WNT5a was shown to participate in vascular patterning in a skin wound model (Stefater *et al.*, 2013) whilst loss of function of the WNT receptor FZD4 diminished vascular networks in the heart and kidney (Descamps *et al.*, 2012). WNT5a and WNT3a were also shown to regulate proliferation and differentiation of immortalised cardiac fibroblasts into myofibroblasts (Laeremans *et al.*, 2010).

WNTs are highly hydrophobic secreted proteins. Acylation by the member of the membrane bound O-acyltransferase (MBOAT) family: porcupine (PORCN), is essential to their secretion into the extracellular space (Mikels and Nusse, 2006). PORCN, encoded by the gene *Porcn*, has therefore been used as a tool to prevent secretion of WNTs from selected cell populations using cell-type specific cre recombinase expression. Notably, macrophage-specific deletion of *Porcn* was shown to prevent secretion of WNTs using expression of cre-recombinase from the colony stimulating factor – 1 receptor (*Csf1r*) promoter (Saha *et al.*, 2016).

Altogether these observations support a positive role of MΦ and specifically MΦ-derived WNTs during organ regeneration. WNT5a could indeed promote adequate vascular patterning following MI in the neonate thereby supporting regeneration. This ligand along with WNT3a could also regulate proliferation and differentiation of cardiac fibroblasts and by that play a key role in the scar-free regeneration of the myocardium.

## 5.2 Hypothesis and aims

Hypothesis:

**'Preventing secretion of WNTs from macrophages through specific deletion of Porcupine will impair scar free cardiac regeneration in neonatal mice'**

Aims:

(i) Investigate the impact of MI on the cardiac mononuclear phagocyte populations described in Chapter 4.

(ii) Study the mRNA expression profile of Wnt signalling genes in the steady state and post-MI in cardiac macrophages and whole heart tissue.

(iii) Characterise the effect of macrophage-specific abrogation of WNTs secretion on functional recovery and regeneration 21 days post-MI.

## 5.3 Methods

### *5.3.1 Animals*

Three mouse lines were used in this chapter:

- Tg(*Csf1r-Egfp*) mice express enhanced green fluorescent protein under the control of the colony-stimulating factor 1 receptor gene (*Csf1r*) promoter. Animals expressing the transgene were noted as $GFP^{+ve}$. This mouse line is referred to as the MacGreen mouse and is on an incomplete C57BL/6J background. Male and female mice aged P8 (naïve or day 7 post-MI). Further details on the mouse line can be found in Section 2.1.1.2.
- C57BL/6J in-house male and female mice aged P8 (naïve and day 7 post-MI). (Section 2.1.1.1)

Both MacGreen and C57BL/6J mouse lines were bred and housed in Edinburgh in the Central Bioresearch Services local facility.

- Male and female mice homozygous for a floxed allele of the Porcupine gene ($Porcn^{fl/fl}$) were used for breeding and generation of experimental animals. The male breeders were heterozygous for a transgene containing the cre-recombinase under the control of the *Csf1r* promoter (Tg(*Csf1r-icre*)). The off-spring of such breeding are homozygous for $Porcn^{fl/fl}$, and a subset also express cre-recombinase in *Csf1r*-expressing cells. This mouse line is referred to as the Porcupine mouse. Cre-expressing animals were referred to as $Cre^{+ve}$ and compared to cre-deficient ($Cre^{-ve}$) animals as littermate controls. These mice are on an incomplete FVB background. Further details on the mouse line can be found in Section 2.1.2.2. Both male and female mice aged between P1 and P22 were used in this chapter. Breeding and part of the genotyping and weight measurements were carried out by Mr Mark Thompson.

These animals were bred and housed at the Einstein College of Medicine (New York, Bronx).

### *5.3.2 Coronary Artery Ligation (CAL) surgery in neonatal mice*

Animals at postnatal day 1 (P1) underwent CAL surgery to induce MI with naïve animals serving as controls as described in Section 2.2.2.

### *5.3.3 Ultrasound*

In order to confirm effective ligation of the LAD, high-resolution *in vivo* ultrasound was carried out at day 1 post-MI as described in Section 2.2.1. Animals that did not show functional decrease at day 1 were excluded from the study. Body weights were recorded at this time. Before termination, each animal underwent ultrasound at day 21 post-MI. Body and heart weights were recorded at this time. All ultrasound measurement within this chapter were acquired by myself.

### *5.3.4 FACS*

Cardiac leukocytes including, granulocytes, monocytes and macrophages were measured in heart digest of age-matched naïve and post-MI $GFP^{+ve}$ MacGreen animals at day 7. Naïve hearts of $GFP^{+ve}$ animals of the same litter were pooled in an effort to increase yield. Hearts of $GFP^{+ve}$ animals at day 7 post-MI were not pooled. Heart digests were stained with DAPI, CD45 PE-Cy7, Ly6G Pacific blue, CD11b Alexa fluor 700, F4/80 PE, and Ly6C PerCP Cy5.5 and assessed as described in Section 2.3.2.

### *5.3.5 mRNA extraction and expression analysis*

Whole heart total RNA of neonatal C57BL/6J was extracted using the Qiazol™/chloroform technique as described in Section 2.4.1.2. mRNA was then reverse transcribed and RT-qPCR was performed using the kits provided with the $RT^2$ Profiler™ PCR array mouse WNT signalling pathway from Qiagen (Section 2.4.2.2). Total RNA from adult C57BL/6J at day 7 post-MI were donated by Dr Katie Mylonas who performed the adult CAL surgery and RNA extraction.

### *5.3.6 Histology*

10 μm thick frozen sections of MacGreen tissues were stained with anti-GFP for MΦ visualisation. All other tissues were formalin-fixed paraffin embedded and cut into 4 μm thick sections as described in Section 2.5. Sections at 3 different levels below the ligation were collected at regular interval. At least 2 levels were used for image analysis. Picrosirius red (PSR) staining for identification of collagen content was performed by Miss Melanie McMillan at the Queen's Medical Research Institute histology facility using a standardised protocol.

### *5.3.7 Image acquisition and analysis*

Images were acquired on a Zeiss slide scanner Axio Scan Z1, magnification x 40 and analysed as described in Section 2.5 using either Definiens Developer XD or Adobe Photoshop CS6. Analysis using Definiens Developer XD was performed by Dr Daniel Soong.

### *5.3.8 Statistical analysis*

Statistical analysis was performed as described in Section 2.6 using Graphpad Prism 5.

## 5.4 Results

### *5.4.1 Changes in mononuclear phagocytes subsets post-MI*

*Csf1r*-expressing cells were shown to accumulate in the regenerating area of the myocardium at day 1 and 7 post-MI in heart sections from MacGreen mice (Figure 5-1A, B).

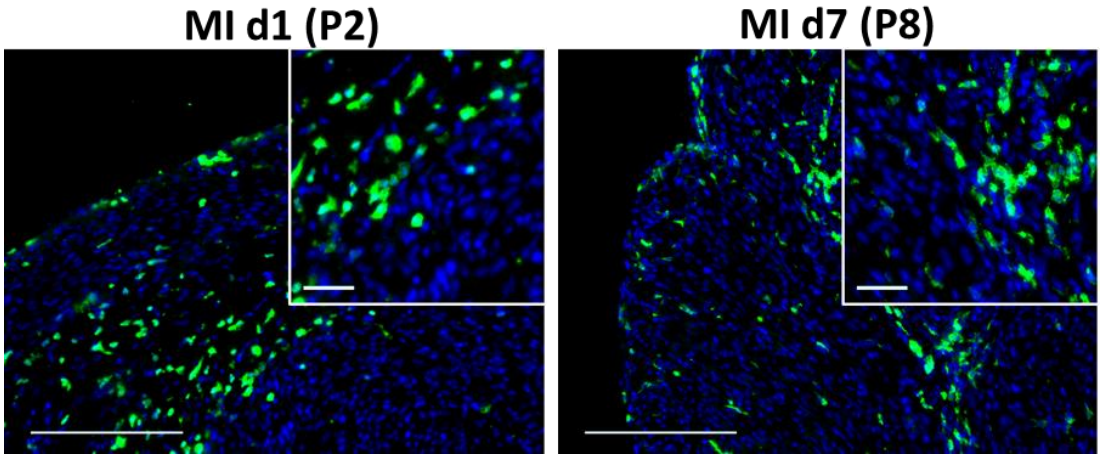


**Figure 5-1: *Csf1r*-expressing cells accumulate in the regenerating myocardium during the first week post-MI.** MacGreen mice underwent CAL surgery at postnatal day 1 (P1), 10 μm thick cardiac sections below the ligature were obtained and stained with an anti-GFP antibody (green) and DAPI (nuclei-blue) at day 1 (A), and day 7 (B) thereby identifying *Csf1r*-expressing cells. Gold outline marks the regenerating area. Scale bars = 100 μm. Upper right corners are zooms, scale bars 20 μm.

Flow cytometric analysis revealed that at day 7 post-MI the F4/80$^{hi}$, CD11b$^{lo}$, Ly6C$^{-ve}$ population of cardiac mononuclear phagocytes appears to have greatly diminished as shown on Figure 5-2B. Contrastingly, the F4/80$^{lo}$, CD11b$^{hi}$, Ly6C$^{-ve}$ and F4/80$^{lo}$, CD11b$^{hi}$, Ly6C$^{+ve}$ populations could still be observed within the neonatal heart at day 7 post-MI (Figure 5-2B).

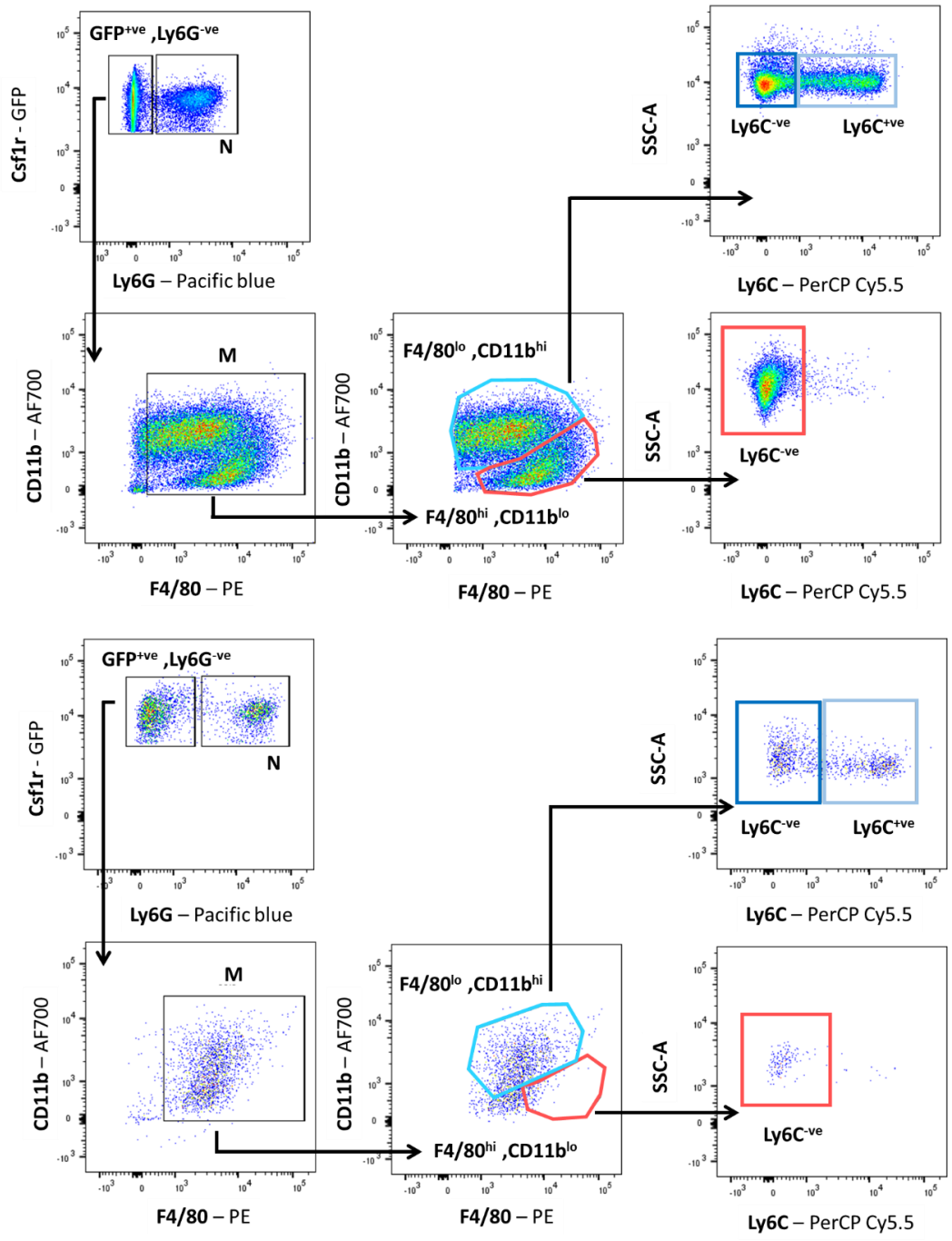


**Figure 5-2: Cardiac mononuclear phagocyte populations at day 7 post-MI.** Single, Live, CD45$^{+ve}$ cells were gated as described. Neutrophils (N) were identified as GFP$^{+ve}$, Ly6G$^{+ve}$. The Csf1r$^{+ve}$, Ly6G$^{-ve}$ population was then gated on CD11b and F4/80 in order to identify total mononuclear phagocytes (labelled M) as (F4/80, CD11b)$^{+ve}$. Mononuclear phagocytes could be subdivided into F4/80$^{lo}$, CD11b$^{hi}$ and F4/80$^{hi}$, CD11b$^{lo}$ subsets. F4/80$^{hi}$, CD11b$^{lo}$ contained a single Ly6C$^{-ve}$ population whereas F4/80$^{lo}$, CD11b$^{hi}$ contained both a Ly6C$^{-ve}$ and Ly6C$^{+ve}$ population. Flow charts of neonatal heart digest of naïve postnatal day 8 (P8) (*A*) and day 7 post-MI animals (*B*). Differential expression of F4/80 and CD11b by flow cytometry of the two mononuclear phagocyte subsets (*B*). Abbreviations; SSC-A: side scatter-area.

As shown on Figure 5-3A, the proportion of total leukocytes, as measured using CD45 (pan-leukocyte marker) and expressed as a percentage of live cells, was significantly increased in the myocardium at day 7 post-MI when compared to age-matched naïve hearts. This was also true of neutrophils, identified as (Csf1r, Ly6G)$^{+ve}$ (Figure 5-3B). Quantification also showed that the proportion of the F4/80$^{hi}$, CD11b$^{lo}$, Ly6C$^{-ve}$ population of cardiac mononuclear phagocytes is diminished at day 7 post-MI (Figure 5-3C) whereas that of the F4/80$^{lo}$, CD11b$^{hi}$, Ly6C$^{-ve}$ and F4/80$^{lo}$, CD11b$^{hi}$, Ly6C$^{+ve}$ populations are expanded (Figure 5-3D, E)

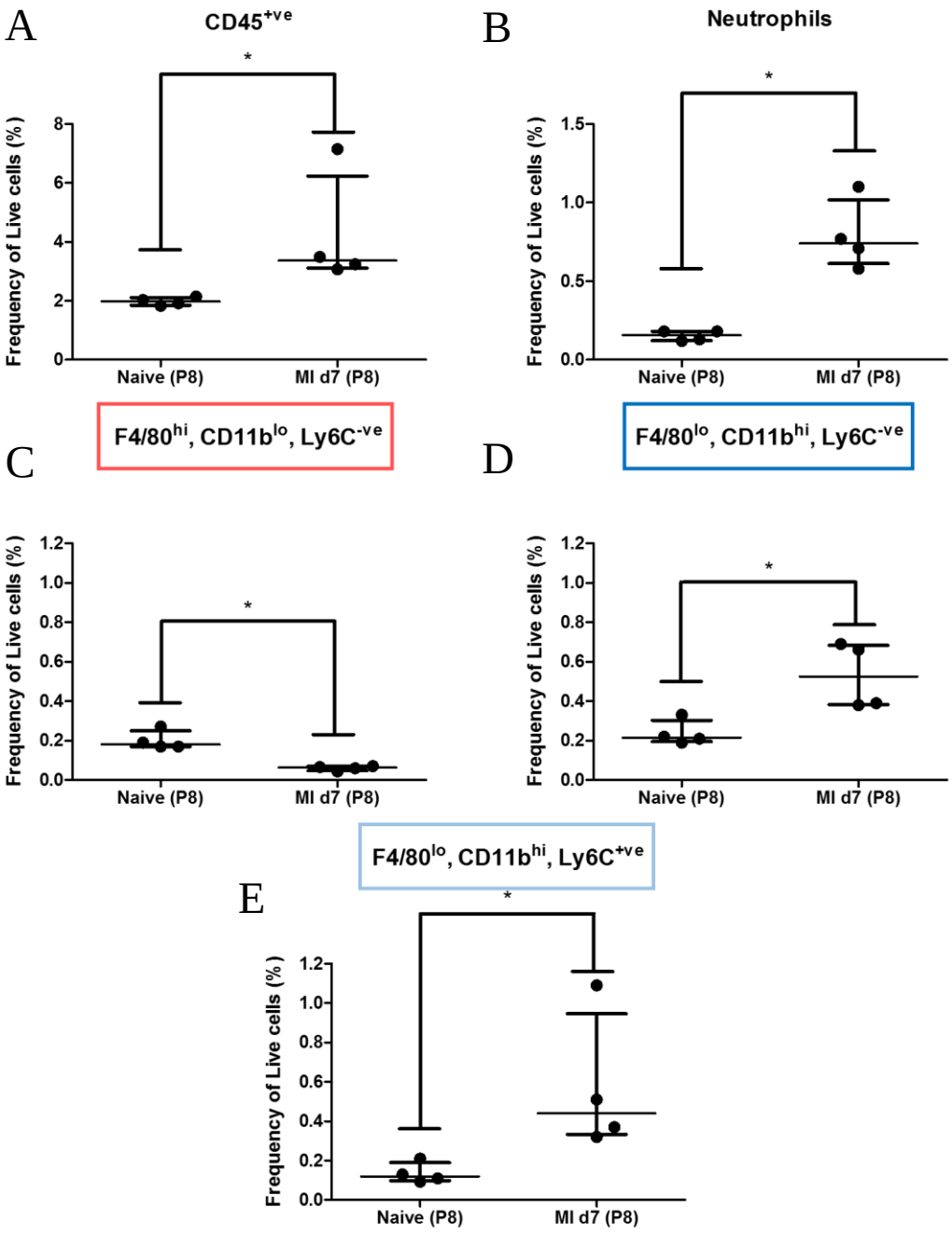


**Figure 5-3: Increased immune infiltrate at day 7 post-MI.** Quantification of the frequency of each immune cell population in the neonatal heart at day 7 following MI and in aged-matched naïve postnatal day 8 (P8) animals. Population size was expressed as a percentage of live cells. Populations are: total leukocytes as $CD45^{+ve}$ (*A*), neutrophils (*B*) as well as $F4/80^{hi}$, $CD11b^{lo}$, $Ly6C^{-ve}$ (*C*), $F4/80^{lo}$, $CD11b^{hi}$, $Ly6C^{-ve}$ (*D*), and $F4/80^{lo}$, $CD11b^{hi}$, $Ly6C^{+ve}$ (*E*) mononuclear phagocytes. n=4/group. Data are expressed as median ± interquartile range. p-value was determined with two-tailed Mann-Whitney tests. * $p < 0.05$.

### *5.4.2 Assessment of Wnt signalling pathway gene expression*

mRNA expression was assessed on a RT2 Profiler™ PCR array specific to the mouse Wnt signalling pathway. Whole neonatal heart tissue at day 7 post-MI in neonatal mice was compared to age-matched naïve animals as reference. 9 genes were shown to be significantly up-regulated post-MI (Figure 5-4). The upregulated gene expression included the *Wnt16* and *5b*, the receptor *Fzd2*, and the pathway inhibitors *Sfrp1* and *Dkk3*. Interestingly, out of the 12 Wnt target genes only *Axin2* was significantly up-regulated.

A

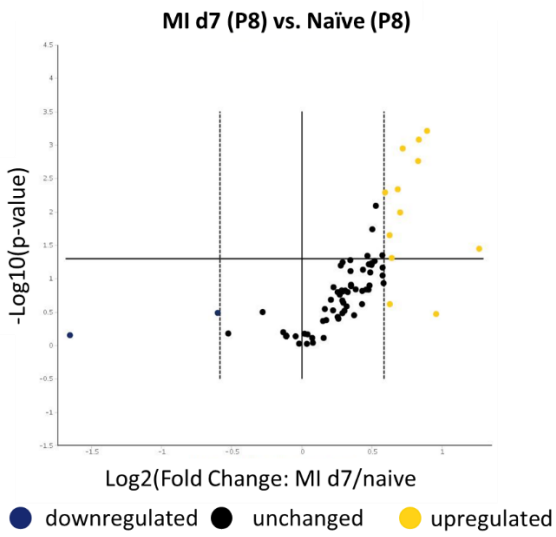


B

**Up-regulated genes**

| Gene symbol | Fold change | p-value |
|---|---|---|
| Axin2 | 1.5404 | 0.022482 |
| Daam1 | 1.5565 | 0.049304 |
| Dkk3 | 1.7736 | 0.001746 |
| Fzd2 | 1.6434 | 0.001131 |
| Rhou | 1.7797 | 0.000832 |
| Sfrp1 | 1.8532 | 0.000616 |
| Wisp1 | 1.604 | 0.004618 |
| Wnt16 | 2.3977 | 0.035863 |
| Wnt5b | 1.507 | 0.005139 |

**Figure 5-4: Cardiac mRNA expression of Wnt signalling genes in neonatal mice at day 7 post-MI compared to age-matched naïve mice.** mRNA expression of 84 genes was assessed on a $RT^2$ Profiler™ PCR array specific for the mouse Wnt signalling pathway. mRNA expression levels in whole heart tissue at day 7 post-MI was expressed as a fold-change compared to expression levels in age-matched naïve whole heart tissue as the reference. A volcano plot was used to present differentially expressed genes (*A*). Significantly differentially expressed genes are listed in (*B*). Boundaries were set at ±1.5 fold-change and significance at p-value < 0.05. n=6/group.

Using the same approach, whole neonatal heart tissue was compared to adult infarct plus border zone tissue (reference) at day 7 post-MI. Over 40 genes were significantly up-regulated and only 2 genes significantly down-regulated in the neonatal mouse compared to the adult following MI. Up-regulated genes included *Wnt2b* and *5b*, the receptors *Fzd1*, *2*, *3*, *4*, *5*, *6*, and *8*, and pathway inhibitors *Dkk3*, *Ctnnbip1* and *Sox17*. Out of the target genes, *Bcl9*, *Axin2*, and *Jun* were all significantly up-regulated in the neonate relative to the adult. Expression the pathway inhibitors Sfrp1 and Sfrp2 was significantly down-regulated in neonatal mice. Notably, *Sfrp2* was the most differentially expressed gene between the two groups being down 180.18-fold in neonatal mice when compared to adults at day 7 post-MI.

A

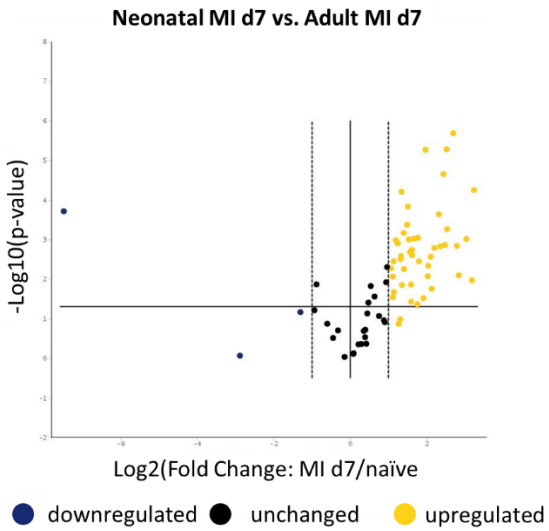


B

**Up-regulated genes**

| Gene symbol | Fold change | p-value |
|---|---|---|
| Aes | 2.1685 | 0.008658 |
| Apc | 3.4105 | 0.000907 |
| Axin1 | 2.9519 | 0.002067 |
| Axin2 | 4.9933 | 0.000233 |
| Bcl9 | 3.0209 | 0.037256 |
| Btrc | 4.297 | 0.002733 |
| Csnk1a1 | 2.8056 | 0.000424 |
| Ctbp1 | 3.4742 | 0.003555 |
| Ctnnb1 | 3.0702 | 0.002485 |
| Ctnnbip1 | 5.7358 | 0.000005 |
| Daam1 | 5.579 | 0.001379 |
| Dab2 | 3.0667 | 0.001832 |
| Dixdc1 | 7.1519 | 0.008018 |
| Dkk3 | 1.9185 | 0.011968 |
| Dvl2 | 6.9083 | 0.001455 |
| Ep300 | 3.1675 | 0.000952 |
| Fbxw11 | 2.8879 | 0.000997 |
| Frat1 | 3.3831 | 0.043132 |
| Fzd1 | 2.6512 | 0.005574 |
| Fzd2 | 5.4264 | 0.000022 |
| Fzd3 | 9.437 | 0.000056 |
| Fzd4 | 2.8514 | 0.000147 |
| Fzd6 | 3.9177 | 0.000005 |
| Fzd8 | 3.7755 | 0.030246 |
| Gsk3b | 2.1962 | 0.003584 |
| Jun | 4.3822 | 0.017509 |
| Kremen1 | 2.161 | 0.028732 |
| Lrp5 | 2.488 | 0.003104 |
| Lrp6 | 2.3702 | 0.001251 |
| Nfatc1 | 2.0898 | 0.005337 |
| Nkd1 | 4.1125 | 0.004608 |
| Nlk | 4.6001 | 0.001638 |
| Ppard | 2.2842 | 0.001039 |
| Prickle1 | 6.483 | 0.000002 |
| Pygo1 | 2.555 | 0.014213 |
| Rhoa | 1.9521 | 0.004949 |
| Ruvbl1 | 2.636 | 0.000682 |
| Sox17 | 4.0793 | 0.008462 |
| Tcf7 | 3.007 | 0.013794 |
| Tcf7l1 | 8.2154 | 0.000978 |
| Vangl2 | 9.0945 | 0.010716 |
| Wisp1 | 1.5547 | 0.027526 |
| Wnt2b | 5.1278 | 0.00149 |
| Wnt5b | 5.7958 | 0.000551 |

C

**Down-regulated genes**

| Gene symbol | Fold change | p-value |
|---|---|---|
| Sfrp1 | -1.8425 | 0.013577 |
| Sfrp2 | -180.1848 | 0.000193 |

**Figure 5-5: Cardiac mRNA expression of Wnt signalling genes at day 7 post-MI in neonatal mice compared to adult.** mRNA expression of 84 genes was assessed on a RT2 Profiler™ PCR array specific for the mouse Wnt signalling pathway. mRNA expression levels in neonatal whole heart tissue at day 7 post-MI was expressed as a fold-change compared to expression levels in infarct and border zone of adult mice at day-7 post-MI as the reference. A volcano plot was used to present differentially expressed genes (*A*). Significantly up-regulated genes are listed in (*B*) and down-regulated genes in (*C*). Boundaries were set at ±1.5 fold-change and significance at p-value < 0.05. n=6 neonatal, n=3 adult.

### 5.4.3 *Csf1r-icre mediated depletion of Porcn impairs scar free cardiac regeneration post-MI in the neonatal mouse*

Out of 26 Porcupine mice operated 3 mice did not present any signs of systolic dysfunction and 2 could not be classified at day 1 post-MI. This represents an 81% success rate of the surgery.

#### 5.4.3.1 *Csf1r-icre* mediated depletion of *Porcn* does not affect body weight, LV mass or wall thickness at day 1 post-MI.

At day 1 post MI (P2) both body weight and ultrasound extracted LV mass were significantly increased respectively by 30 and 20% when compared to naïve animals at P1 (Figure 5-6 A, B). LV wall thickness did not significantly change between those two time points (Figure 5-6 C). No effect of the genotype could be noted.

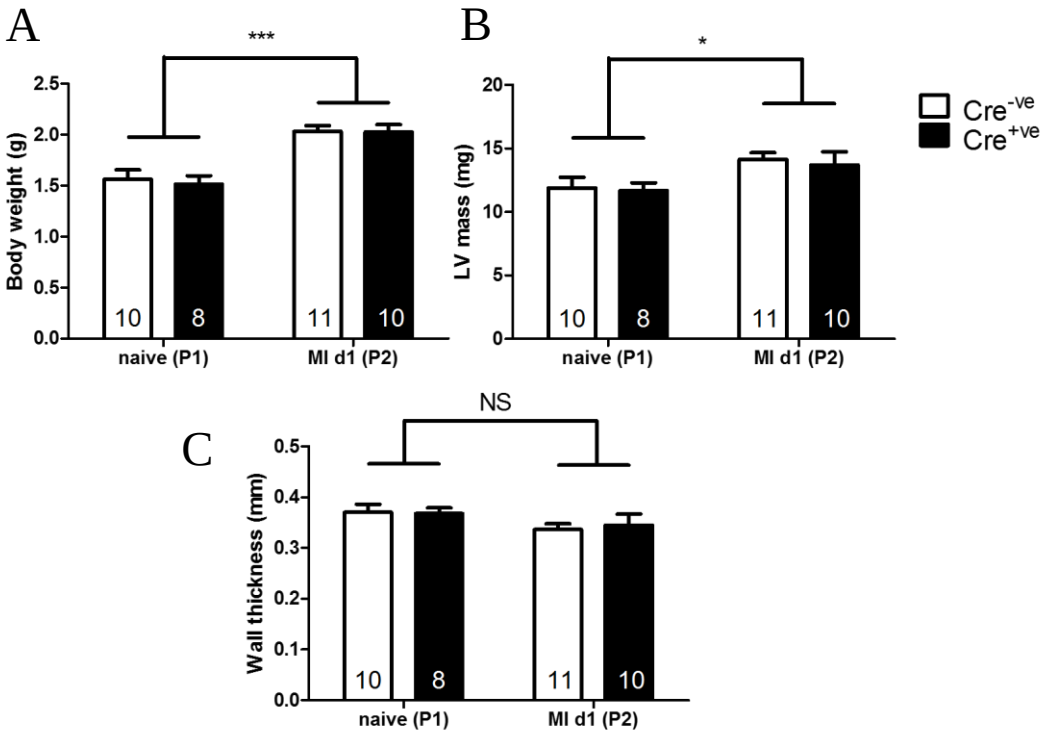


**Figure 5-6: *Csf1r-icre* mediated depletion of *Porcn* does not influence body weight, LV mass or wall thickness at day 1 post-MI.** Body weight (*A*) was measured prior to *in vivo* high-resolution ultrasound imaging. Both left ventricle (LV) mass (*B*) and wall thickness (*C*) were extracted from electrocardiogram-gated kilohertz visualisation (EKV) parasternal long axis (PLAX) B-mode in naïve animals at postnatal day 1 (P1) and at day 1 post-MI (P2) in Cre-expressing ($Cre^{+ve}$ - black bars) and Cre-deficient ($Cre^{-ve}$ - clear bars) Porcupine mice. Results are presented as mean ± SEM. p-value determined with 2-way ANOVA with Bonferroni post hoc test. * $p < 0.05$, *** $p < 0.001$.

#### *5.4.3.2* Cardiac function dramatically decreases at day 1 post-MI

Left ventricular end systolic and diastolic areas (LVESA, LVEDA) were respectively increased by around 100% and 40% between P1 and P2 (day 1 post-MI) (Figure 5-7 A, B). Cardiac function as evaluated by fractional area change (FAC), ejection fraction (EF), and fractional shortening (FS) was decreased by half at day 1 post-MI when compared to P1 naïve animals (Figure 5-7 C, D, E). Motion mode (M-mode) stills show a clear lack of movement from both anterior and posterior LV walls at day 1 post-MI (P2) when compared to naïve P1 animals (Figure 5-7 F). No effect of the genotype was noted.

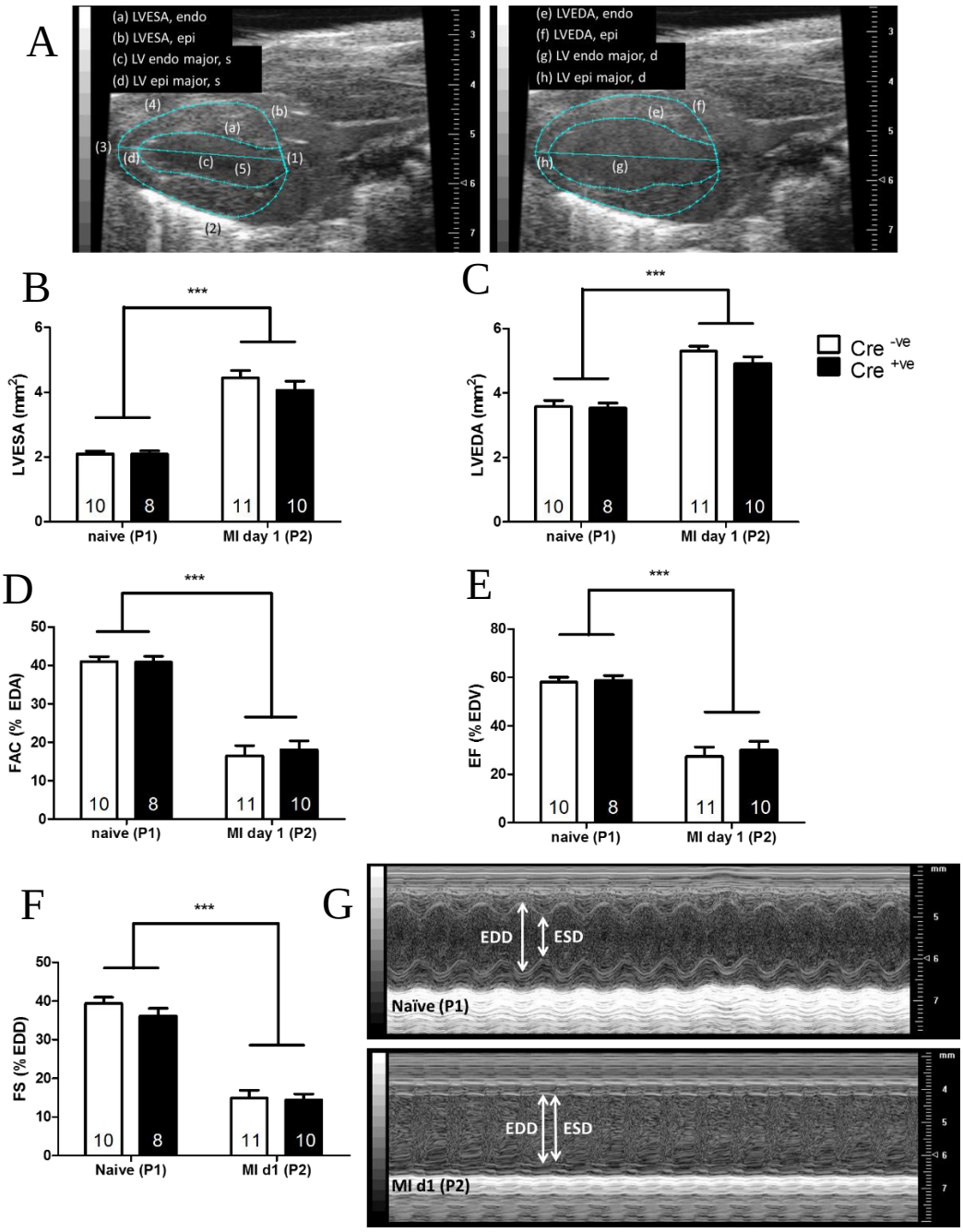


**Figure 5-7: CAL surgery results in functional impairment at day 1 post-MI with no effect of the genotype.** Cardiac function was assessed using *in vivo* high-resolution ultrasound in Cre-expressing ($Cre^{+ve}$ - black bars) and Cre-deficient ($Cre^{-ve}$ - clear bars) Porcupine mice. Electrocardiogram-gated kilohertz visualisation (EKV) parasternal long axis (PLAX) B-mode (*A*) allowed calculation of left ventricular end systole (LVESA-*B*) and diastole (LVEDA-*C*) area. These were used to calculate cardiac function with fractional area change (FAC-*D*) and ejection fraction (EF-*E*). Function was also assessed with fractional shortening (FS-*F*) using motion-mode (M-mode). M-mode stills showing akinetic anterior and posterior walls at day 1 post-MI (*G*). Results are presented as mean ± SEM. P-value determined with 2-way ANOVA with Bonferroni post hoc test. *** p <0.001.

#### *5.4.3.3* Normal cardiac and body growth at day 21 post-MI

As shown on Figure 5-8 A, no effect of the genotype on survival after MI could be noted. Body weight, heart wet weight, and their ratio at day 21 post-MI (P22) were normal when compared to naïve animals at P20 (Figure 5-8 B, C, D). Ultrasound extracted LV wall thickness was also identical between those groups whereas LV mass was decreased by 20% (Figure 5-8 E, F). No effect of the genotype could be noted on any of those measurements.

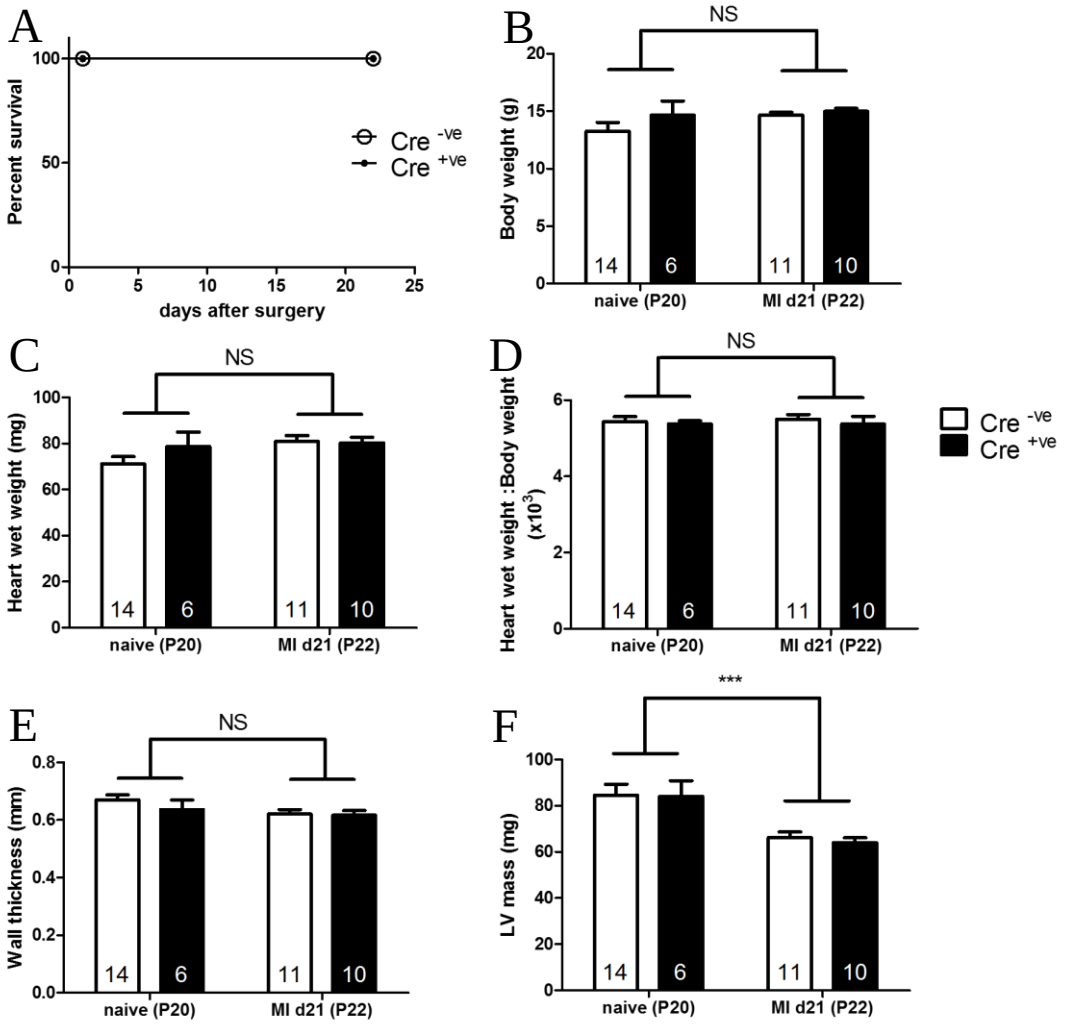


**Figure 5-8: CAL surgery at P1 does not impair survival or normal growth at day 21 post-MI with no effect of the genotype.** Survival at day 1 and day 21 following CAL surgery at postnatal day 1 (P1) in Cre-expressing ($Cre^{+ve}$ - black bars and circles) and Cre-deficient ($Cre^{-ve}$ - clear bars and circles) Porcupine mice (*A*) at day 21 following MI (postnatal day 22 -P22-) and in naïve P20 animals. Body weight (*B*) was measured prior to *in vivo* high-resolution ultrasound imaging. Heart wet weight (*C*) was measured immediately after *in vivo* high-resolution ultrasound imaging following dissection and used to calculate heart to body weight ratio (*D*). Both wall thickness (*E*) and LV mass (*F*) were extracted from electrocardiogram-gated kilohertz visualisation (EKV) parasternal long axis (PLAX) B-mode. Results are presented as mean ± SEM. P-value determined with 2-way ANOVA with Bonferroni post hoc test. *** $p < 0.001$.

### *5.4.3.4 Csf1r-icre* mediated depletion of *Porcn* does not influence cardiac function recovery at day 21 post-MI

Cardiac function as measured by FAC, EF, and FS was dramatically increased between day 1 and day 21 post-MI by over 100% (Figure 5-9 A, B, C). M-mode stills show recovery of movement of both LV anterior and posterior walls by day 21 post-MI (Figure 5-9 D). No effect of the genotype could be noted.

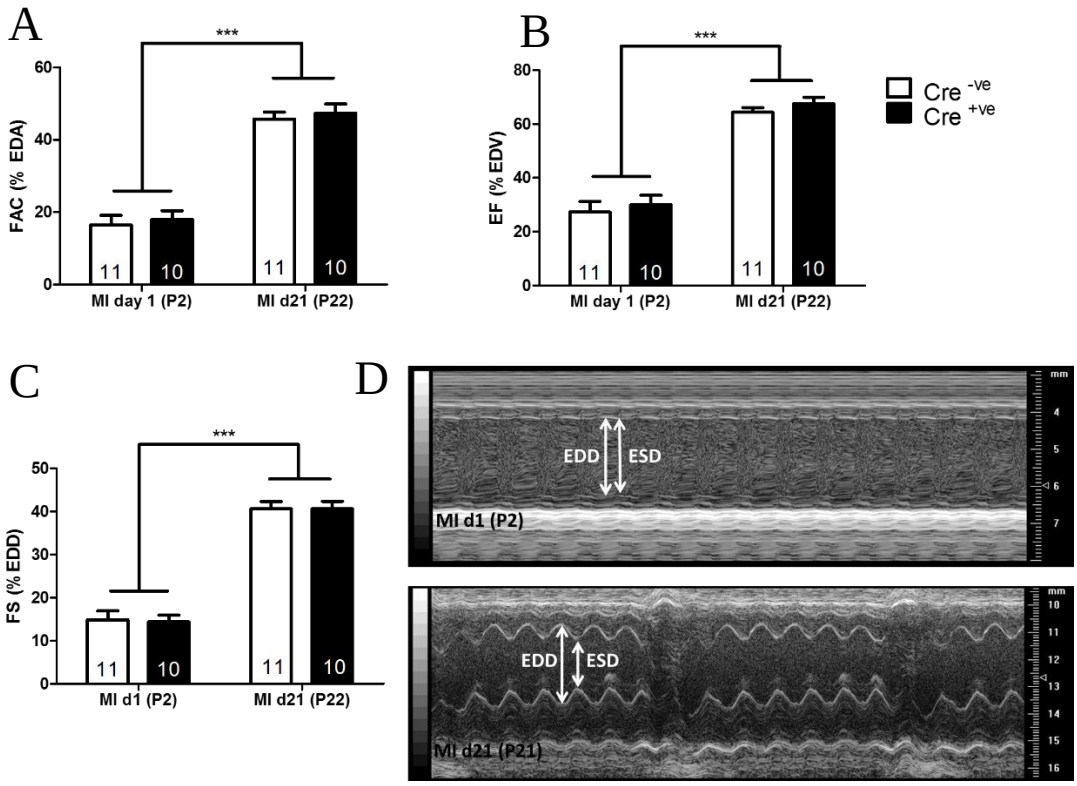


**Figure 5-9: Cardiac function is increased at day 21 when compared to day 1 post-MI at P1 with no effect of the genotype.** Cardiac function was assessed using *in vivo* high-resolution ultrasound in Cre-expressing ($Cre^{+ve}$ - black bars) and Cre-deficient ($Cre^{-ve}$ - clear bars) Porcupine mice at day 1 and 21 post-MI. Electrocardiogram-gated kilohertz visualisation (EKV) parasternal long axis (PLAX) B-mode allowed calculation of fractional area change (FAC-*A*) and ejection fraction (EF-*B*). Function was also assessed with fractional shortening (FS-*C*) using motion-mode (M-mode). M-mode stills showing recovery of movement of the anterior and posterior walls at day 21 post-MI (*D*). Results are presented as mean ± SEM. p-value determined with 2-way ANOVA with Bonferroni post hoc test. *** p <0.001.

### *5.4.3.5* Complete recovery of cardiac function by day 21 post-MI

LVESA and LVEDA were marginally, but significantly lower in animals at day 21 post-MI (P22) when compared to naïve animals of a similar age (P20) (Figure 5-10 A, B). However, cardiac function as assessed by FAC, EF and FS were identical between those two groups (Figure 5-10 C, D). No effect of the genotype could be noted on either cardiac dimensions or in functional recovery at day 21 post-MI.

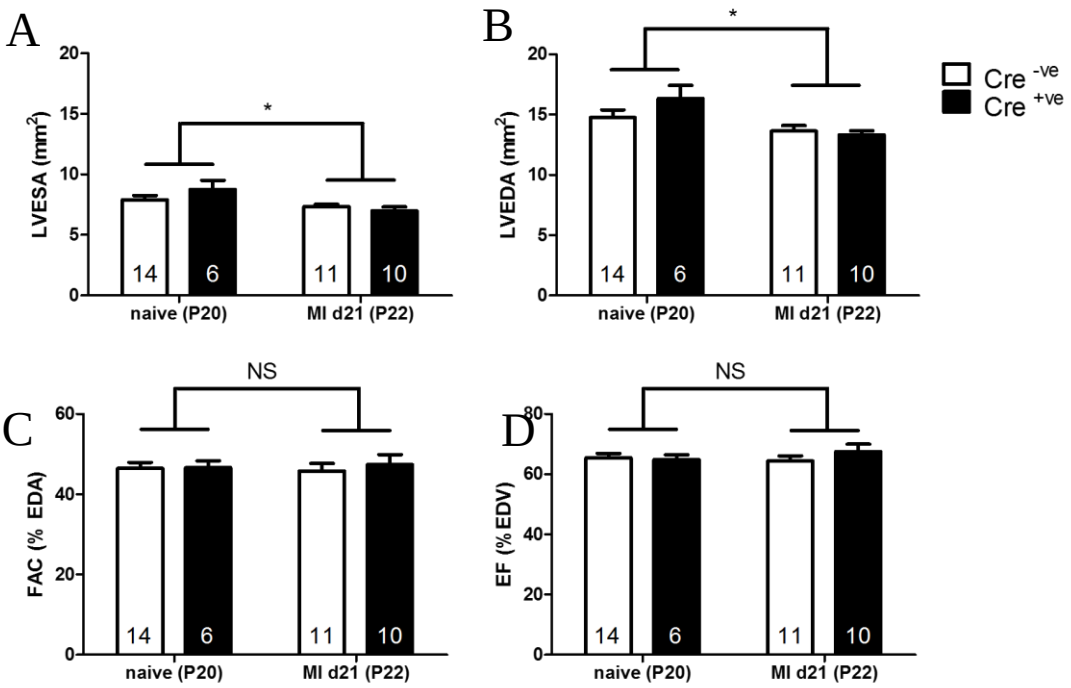


**Figure 5-10: Cardiac function is completely recovered by day 21 post-MI at P1 with a slight decrease in LV cavity size but no effect of the genotype.** Cardiac function was assessed using *in vivo* high-resolution ultrasound in Cre-expressing ($Cre^{+ve}$ - black bars) and Cre-deficient ($Cre^{-ve}$ - clear bars) Porcupine mice at day 21 following MI (postnatal day 22 -P22-) and in naïve P20 animals. Electrocardiogram-gated kilohertz visualisation (EKV) parasternal long axis (PLAX) B-mode allowed calculation of left ventricular end systole (LVESA-*A*) and diastole (LVEDA-*B*) area, and cardiac function with fractional area change (FAC-*C*) and ejection fraction (EF-*D*). Results are presented as mean ± SEM. P-value determined with 2-way ANOVA with Bonferroni post hoc test. * $p < 0.05$.

### *5.4.3.6* Macrophage-specific deletion of Porcn does not influence vascularisation of the infarcted area at day 21 post-MI

As shown on Figure 5-11 both $Cre^{+ve}$ and $Cre^{-ve}$ control littermates had normal looking myocardial vascularisation at day 21 post-MI.

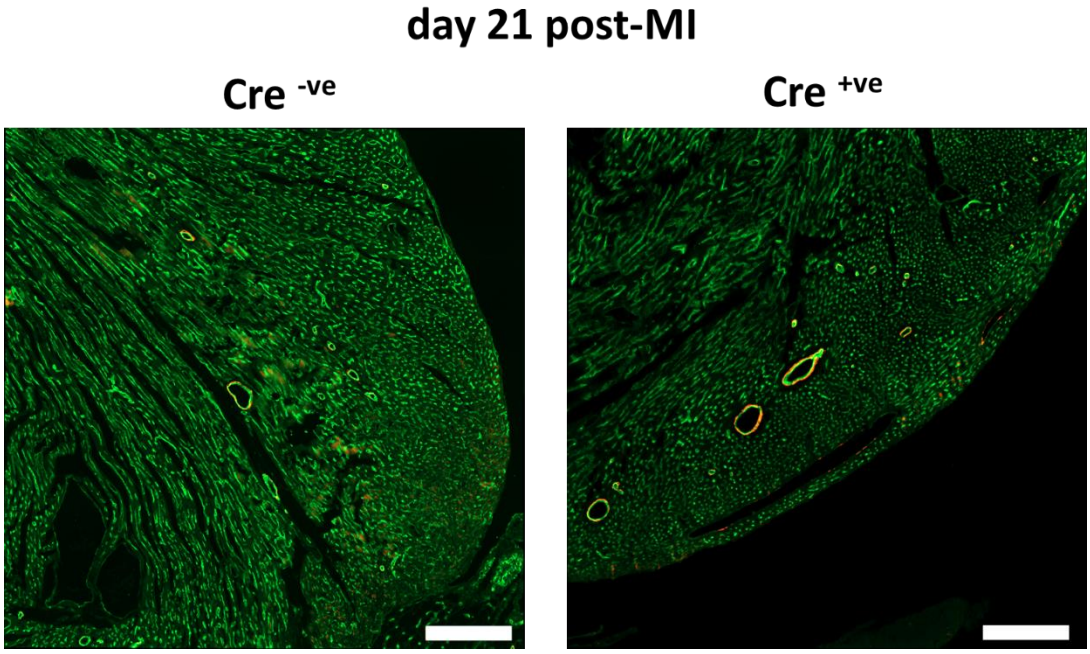


**Figure 5-11: Myocardial vascularisation is not influenced by macrophage-specific deletion of Porcn at day 21 post-MI.** Myocardial vascularisation was investigated on isolectin B4 (IB4-green-endothelial cells), α smooth muscle actin (αSMA-red-mural cell coated vessels), and DAPI (blue). DAPI was left out of above representative images for clarity. Staining was performed on 4μm thick stained sections at day 21 post-MI in Cre-expressing ($Cre^{+ve}$ - black bars) and Cre-deficient ($Cre^{-ve}$ - clear bars) Porcupine mice. Scale bars = 100 μm.

### *5.4.3.7 Csf1r-icre* mediated depletion of *Porcn* resulted in increased myocardial fibrosis at day 21 post-MI

All animals that had undergone surgery presented with an expanded pericardium as shown by the blue arrows on Figure 5-12A, B. Picrosirius red (PSR) staining identified a clear fibrotic area in the direct vicinity of the ligation in $Cre^{-ve}$ animals with limited interstitial fibrosis Figure 5-12A. On the other hand, fibrotic tissue also infiltrated the myocardium away from the suture in $Cre^{+ve}$ animals which presented with increased fibrotic area Figure 5-12B, C, D. It is important to note that the percentage of tissue detected as $PSR^{+ve}$ is much higher when using Definiens than in Photoshop. This is true for both $Cre^{-ve}$ and $Cre^{+ve}$ groups and did not affect the level of significance.

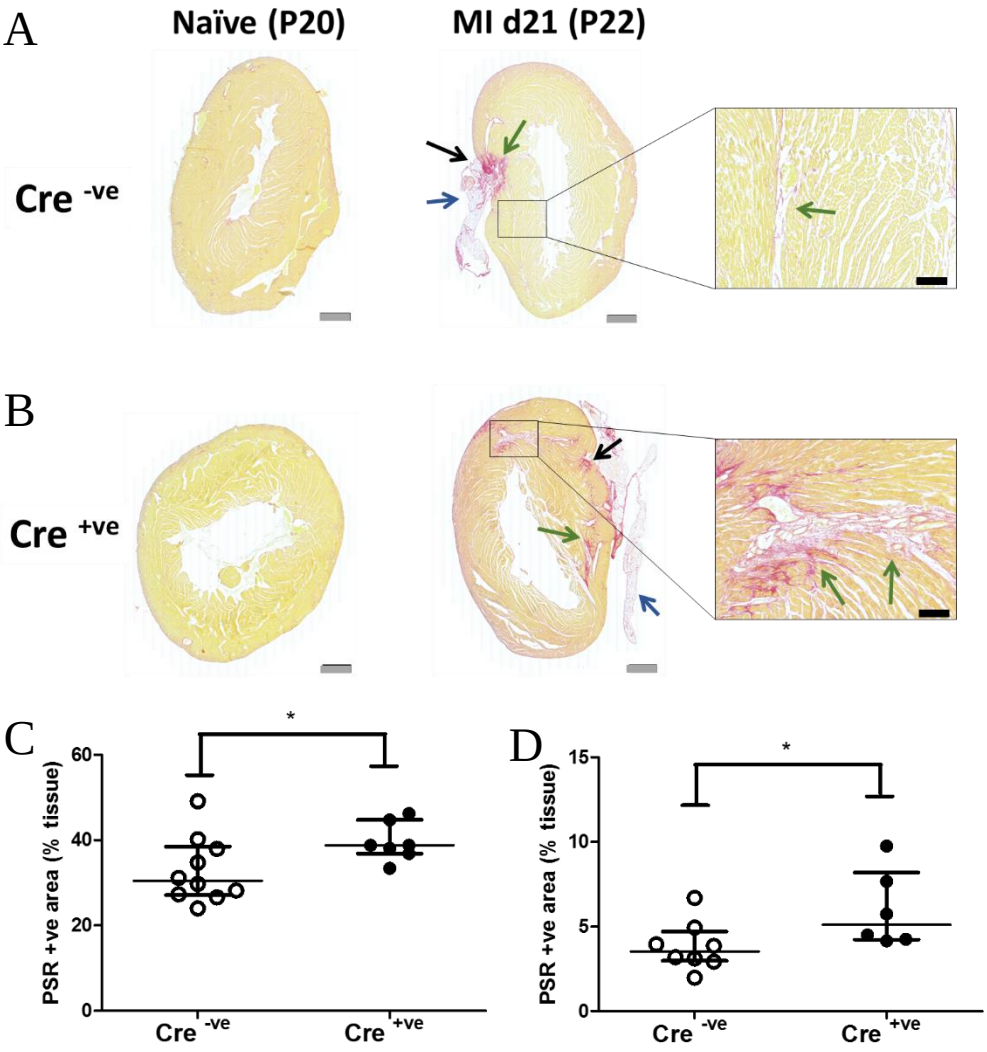


**Figure 5-12: Macrophage-specific abrogation of WNTs secretion increases fibrosis at day 21 post-MI at P1.** Collagen accumulation was evaluated on picrosirius red (PSR-collagen marker) across the whole left ventricle below the suture excluding the pericardium on 4 μm thick section at postnatal day 20 (P20) and at day 21 post-MI in Cre-deficient ($Cre^{-ve}$ - clear circles) (*A*) and Cre-expressing ($Cre^{+ve}$ - black circles) (*B*) Porcupine mice. Collagen fibres appear red, remaining tissue yellow. Fibrotic area was evaluated with Definiens software (*C*) and Adobe Photoshop CS6 (*D*) at day 21 post-MI (P22) and $Cre^{+ve}$ animals compared to $Cre^{-ve}$ control littermates. Black arrows indicate location of suture, green arrows indicate myocardial fibrosis, blue arrows indicate expanded pericardium. Grey scale bar = 500μm, black scale bar = 100μm. Results are presented as median ± inter-quartile range. P-value determined with Mann-Whitney test. * $p < 0.05$.

## 5.5 Discussion

It is becoming increasingly clear that macrophages and macrophage-derived WNTs play a central role in the regeneration of organs such as the kidney (Lin *et al.*, 2010), the liver (Boulter *et al.*, 2012), and the gut (Saha *et al.*, 2016). Although Aurora *et al.* (2014) have shown that macrophage depletion prevented neonatal cardiac regeneration it is not clear whether macrophage-derived WNTs are part of this process. The present study aimed to investigate the effect of MI on the neonatal cardiac mononuclear phagocyte populations described in chapter 4. Determining the expression profile at the mRNA level of Wnt signalling related genes in both cardiac macrophages and whole heart tissues was also endeavoured. The final aim of this study was to characterise the impact of preventing WNTs secretion from macrophages on neonatal cardiac regeneration. This was achieved through a macrophage-specific (*Csf1r* promoter driven cre recombinase) deletion of *Porcn*. *Porcn* encodes for the O-acyltransferase porcupine (PORCN) which is essential in the secretion of all WNTs (Mikels and Nusse, 2006).

*The role of immune cells following induction of MI in neonatal mice*

In this chapter, *Csf1r*-expressing cells were shown to accumulate within the regenerating myocardium at day 1 and day 7 post-MI using the MacGreen mouse. Day 7 was previously identified by Aurora *et al.* (2014) as the peak abundance of mononuclear phagocytes in the myocardium following MI in neonatal mice. This is consistent with the data from this chapter. This experiment was however designed as a pilot study to provide supporting evidence of the interaction between *Csf1r*-expressing cells and the regenerating myocardium. Further work should involve a full size investigation of the distribution and density of *Csf1r*-expressing cells at both day 1 and day 7 post-MI. This work should also incorporate double staining with a more specific mononuclear phagocyte marker. As discussed in Chapter 4 *Csf1r*-expressing cells are a mixed population of mononuclear phagocytes and neutrophils. Double staining for GFP and F4/80 in MacGreen mice has been attempted under multiple conditions during this PhD but has not worked. Other makers that could be used in the future include Mac-3 and CD68 as they have been shown to identify macrophages and monocytes on heart sections (Aurora *et al.*, 2014; Lavine *et al.*, 2014).

In the adult mouse, inflammatory cells content is increased following MI primarily as a result of recruitment of neutrophil and monocytes from the bone marrow and spleen (Frangogiannis, 2014; Chen and Frangogiannis, 2016). In the present study, total leukocytes ($CD45^{+ve}$) proportion was increased relative to live cells by approximately 2-fold at day 7 post-MI. This correlates with the published literature showing a crucial involvement of the immune system in the response to MI in the neonatal mouse (Aurora *et al.*, 2014).

In the adult, neutrophils are the first leukocyte population to accumulate in the myocardium after MI. Their number peaks 24h-48h post-MI to then decline to very low levels at day 6 post-MI (McSweeney *et al.*, 2010; Nahrendorf and Swirski, 2013). As presented in further detail in Section 1.1.1.1, this decline of neutrophils is known as a hallmark of inflammation resolution (reviewed in Frangogiannis 2014). The time course of inflammation and its subsequent resolution is however less clear in the neonatal mouse following MI. Data from this chapter has showed that neutrophils ($(Csf1r, Ly6G)^{+ve}$) were more abundant within the myocardium at day 7 post-MI when compared to naïve hearts. This correlates with data from Aurora *et al.* (2014) which showed that neutrophils were significantly more abundant at day 7 in mice that underwent CAL surgery at P1 compared to those operated at P14. Induction of MI in P14 mice yielded similar response to adult with formation of a non-contractile scar and no functional recovery at day 21 post MI. It therefore appears that a prolonged presence of neutrophils correlates with the capacity to regenerate a scar free myocardium.

Neutrophils are known to express proteases following MI in the adult (Ma *et al.*, 2013). This particular property may participate in regulating scar free regeneration of the neonatal heart. Neutrophils have also been shown to exhibit distinct phenotypes depending on the time post-MI in the adult (Y. Ma *et al.*, 2016). At day 1, they expressed high levels of *IL1β* and *Tnfα* which are classical pro-inflammatory markers. Whereas, at day 7, they expressed high levels of *IL10* and *Cd206* and low levels of *IL1β* and *Tnfα* which would indicate a more anti-inflammatory phenotype. The presence and dynamics of these two phenotypes following MI in the neonatal mouse is unknown. Their balance could however be important in scar free regeneration and

Chapter 5: The role of macrophage-secreted WNTs in neonatal cardiac regeneration should be included in further investigations. Ma et al (2016) have indeed shown that the pro-inflammatory phenotype correlates with wall thinning and thereby matrix degradation.

In the present study, cardiac mononuclear phagocyte populations behaviour was also investigated following MI in neonatal mice. The data has suggested that the F4/80$^{hi}$, CD11b$^{lo}$, Ly6C$^{-ve}$ population disappears from the heart at day 7 post-MI. As discussed in Chapter 4, this population may reflect yolk-sac derived macrophages (MΦ) observed by (Lavine *et al.*, 2014) in the neonatal heart. In their paper, Lavine *et al.* (2014) demonstrate that this population of MΦ expands immediately after genetic ablation of cardiomyocytes in the neonatal mouse. They were also shown to promote cardiomyocyte proliferation, angiogenesis, and have anti-fibrotic capacities. As discussed in Chapter 4, a more comprehensive investigation of the different cardiac mononuclear phagocyte populations would be required for a better comparison to the literature. It is also not clear whether the different types of injury, cardiomyocyte depletion vs. MI, has a significant influence on the ensuing immune response. A time course experiment of the immune response following MI would therefore be required to determine whether yolk-sac derived macrophages also expand immediately after injury as observed by Lavine *et al.* (2014), and then reduce by day 7 as suggested here.

The data showed in this chapter suggests an expansion in both F4/80$^{lo}$, CD11b$^{hi}$, Ly6C$^{-ve}$ and F4/80$^{lo}$, CD11b$^{hi}$, Ly6C$^{+ve}$ populations at day 7 post-MI in the neonate when compared to naïve mice. This failed to reach statistical significance due to the low sample size. As discussed in Chapter 4, these populations may correspond to the CCR2$^{+ve}$ mononuclear phagocytes of foetal liver/bone marrow origin described by Lavine *et al.* (2014) and Leid *et al.* (2016). It therefore may suggest that recruitment of cells of monocytic origin may be required later on during neonatal cardiac regeneration. Further investigation of this should be incorporated in the time course experiment of the immune response following MI.

Interestingly, neutrophil recruitment to the myocardium was recently shown to be dependent on resident CCR2$^{+ve}$ cardiac MΦ following syngeneic cardiac transplant in the adult mouse (Li *et al.*, 2016). Lavine *et al.* (2014) also reported a decreased neutrophil influx following cardiac injury in mice treated with CCR2 inhibitor. Aurora

*et al.* (2014) did not report any effect of macrophage depletion using clodronate-loaded liposomes on neutrophil presence in the heart following CAL at P1. The specific cardiac MΦ population that was depleted in this model is however unknown. Lavine *et al.* (2014) suggest that in their model, clodronate specifically depletes $CCR2^{-ve}$ cardiac MΦ. Using an inducible CCR2 KO model could help understanding the role of $CCR2^{+ve}$ cardiac MΦ in the recruitment of neutrophils following neonatal MI. As discussed above, neutrophils may indeed play a key role in scar free regeneration of the neonatal heart.

Together, data from this chapter and published studies have highlighted differences in the immune response following MI between the neonatal and adult mouse (Epelman *et al.*, 2014). Neonatal mice, compared to adult, appear to be utilising a population of yolk-sac derived resident MΦ which have better pro-angiogenic and anti-fibrotic capacities in the first days following injury (Lavine *et al.*, 2014). Our data may suggest that this population then subsides in favour of the expansion of a bone-marrow derived population, although more work is required. Neutrophils were then hypothesised as crucial regulators of scar free regeneration through their expression of proteases. Further work should investigate the relationship between bone-marrow derived MΦ and neutrophil recruitment following MI in the neonatal mouse. Neutrophil phenotype and protease expression dynamics should also be part of such study.

*Wnt signalling genes expression in MΦ and whole heart tissue*

The second aim was to show that cardiac MΦ express *Wnts* and to identify changes post-MI in the neonatal mouse. However, as discussed in Section 4.5, extraction from neonatal hearts and mRNA expression analysis of cardiac mononuclear phagocytes proved extremely challenging. The amount of total RNA obtained from the low number of cells collected by FACS was unfortunately not sufficient to use on the $RT^2$ Profiler™ PCR array specific to the mouse Wnt signalling pathway, or for regular RT-qPCR.

Aurora *et al.* (2014) performed microarray analysis on cardiac MΦ isolated at day 3 post-MI in the neonate. The data did not show any significant differential expression of *Wnts* between the MI and sham group. This however does not constitute a proof that neonatal cardiac MΦ do not express *Wnts*. Macrophages have however been shown to

be a source of WNTs in several organs following injury in the adult mouse. These have included the kidney (Lin *et al.*, 2010), the liver (Boulter *et al.*, 2012; Irvine *et al.*, 2015; Planas-Paz *et al.*, 2016), the gut (Saha *et al.*, 2016), and recently in the heart (Palevski *et al.*, 2017). Whether neonatal cardiac macrophages express and secrete WNTs is however less clear.

Identifying the exact set of *Wnts* expressed and secreted following neonatal MI by cardiac MΦ populations would provide insight on their potential effect on the immune response described in the previous section. The avenues that could be undertaken are described in Section 4.5.

It was however possible to study mRNA expression on the RT$^2$ Profiler™ PCR array specific to the mouse Wnt signalling pathway using whole tissue samples. First, day 7 post-MI (P8) was compared to age-matched naïve tissue as reference. Out of 84 genes tested only 9 were significantly differentially expressed between the two groups. These included 1 target gene: *Axin2*. *Axin2* is commonly used as a reporter of Wnt signalling as it lies downstream of WNT/β-catenin/TCF/LEF elements (Jho *et al.*, 2002). It has notably been used to show pathway activation following MI in adult mice (Oerlemans *et al.* 2010; Palevski *et al.* 2017; Mizutani *et al.* 2016). AXIN2 is also a potent negative regulator of the canonical Wnt signalling pathway by promoting phosphorylation and degradation of β-catenin (Stamos and Weis, 2013). No other target genes were significantly up-regulated in the neonate at day 7 post-MI relative to naive mice, suggesting that pathway activity may not be particularly increased post-MI relative to normal Wnt pathway activation in the growing neonatal heart.

In contrast, expression of pathway inhibitors *Dkk3* and *Sfrp1* were up-regulated post-MI in the neonate. To date, no studies have investigated their role in neonatal cardiac regeneration. In the adult, it is however known that overexpression of *Sfrp1* as well as *Dkk3* reduces inflammation and improves function following MI (Barandon *et al.*, 2003, 2011; Bao *et al.*, 2015). Contrastingly to the neonatal mouse, *Dkk3* expression was reduced in adult mice post-MI (Bao *et al.*, 2015). Up-regulation of those inhibitors may therefore be associated with the regenerative response of the neonate to MI and could be investigated further using KO models.

Chapter 5: The role of macrophage-secreted WNTs in neonatal cardiac regeneration

Out of the 19 mammalian *Wnt* genes, only 2 were significantly up-regulated after neonatal MI relative to naïve controls: *Wnt16* and the prototypical non-canonical *Wnt5b* (Hardy *et al.*, 2009; Bradley and Drissi, 2011). *Wnt16* preferential pathway is less clear. It has been shown to be both a weak activator of the canonical pathway whilst also being able to act through the non-canonical pathway (Clements *et al.*, 2011; Movérare-Skrtic *et al.*, 2014). Interestingly *Wnt5b* is up-regulated in human bone marrow derived macrophages, when stimulated with IL-4 (Derlindati *et al.*, 2015), a stimulus that promotes alternative activation (Gordon, 2003). WNT5b also reduces collagen X production in chondrocytes, a type of mesenchymal cell related to fibroblasts (Bradley and Drissi, 2011). Interestingly, *Fzd2*, which encodes a receptor known to interact with WNT5b (Gujral *et al.*, 2015), was also up-regulated in the neonatal heart post-MI. *Fzd2* is also known to be up-regulated on fibroblasts following adult MI (Blankesteijn *et al.*, 1997). Those genes are thus upregulated at a time where fibrotic tissue has accumulated within the myocardium and prior to scar regression which is thought to largely take place between day 7 and day 14 post-MI (Porrello *et al.*, 2013). Whether WNT5b secreted by cardiac macrophages following MI in the neonate interacts with FZD2 on fibroblasts to regulate collagen deposition/removal is not clear but should be investigated further.

Wnt activity is essential to cardiac development (Ueno *et al.*, 2007) but is thought to be quiescent in the adult myocardium (Dawson *et al.*, 2013; Palevski *et al.*, 2017). The exact time course of Wnt activity decrease is not clear in the heart. It is however thought to be higher in growing organs. It is therefore likely that Wnt activity is higher in neonatal mice than it is in adults at baseline. Upon a stressor such as injury, the pathway is however re-activated in the adult mouse (Dawson *et al.*, 2013; Palevski *et al.*, 2017) and inhibition has been generally shown as beneficial following MI (Barandon *et al.*, 2003, 2011; Zelarayán *et al.*, 2008; He *et al.*, 2010; Laeremans *et al.*, 2010).

The second comparison of Wnt pathway genes that was performed in this thesis was between neonatal and adult hearts at day 7 post-MI. This comparison revealed significant upregulation of over 40 genes in neonates relative to adults and downregulation of 2. The stronger contributor to these differential expression levels is

however most likely to be the age of the animal. As mentioned above, the Wnt pathway is most active in growing organs.

The up-regulated genes included the target genes *Axin2*, *Bcl-9*, and *Jun*, but also various suppressors of the pathway including *Ctnnbip1*. Genes encoding a number of receptors (FZD) and co-receptors (LRP5/6) were also up-regulated in neonatal mice post-MI consistent with increased Wnt activity. However, of the ligands only *Wnt2b* (5.1 fold) and *Wnt5b* (5.8 fold) were differentially expressed in neonatal mice relative to adults following injury. This consolidate the potentially important role of *Wnt5b* in regulating fibrosis. Interestingly, *Wnt2b* has recently been linked to epithelial to mesenchymal transition (EMT) of epicardial cells into cardiac fibroblasts (Mizutani *et al.* 2016). Altogether these observations are consistent with a stronger Wnt pathway activity at neonatal stages compared to the adult.

The only two down-regulated genes both encoded SFRPs which bind to WNTs extracellularly therefore competitively inhibiting their interaction with FZD receptors at the target cell membrane. Notably, *Sfrp2* was the most differentially expressed gene of the 84 tested with a down-regulation of 180.2-fold in neonates relative to adults post-MI. Interestingly, *Sfrp2* was shown to be up-regulated 2.3-fold at day 4 post-MI in the adult mouse (Palevski *et al.*, 2017). *Sfrp2* was not significantly differentially expressed in neonates at day 7 post-MI when compared to naïve controls but was significantly down-regulated in neonates relative to adults post-MI. This suggests that neonatal mice express considerably less *Sfrp2* at basal state and do not utilise it in the response to MI; whereas adults express higher levels of *Sfrp2* in the steady state and further increase its expression following MI. In adults, the role of SFRP2 in fibrosis has been receiving attention but remains unclear and highly dependent on the experimental design. Thus while fibrosis was reduced in *Sfrp2*-deficient mice following MI, resulting in improved systolic function (Kobayashi *et al.*, 2009), administration of SFRP2 2 days post-MI in the adult rat decreased fibrosis 14 days later (He *et al.*, 2010). Incubation of cardiac fibroblasts with SFRP2 *in vitro* promoted proliferation whilst increasing expression levels of *Mmp13*, consistent with promotion of ECM turn-over (Lin *et al.*, 2016). Those contradictory observation could be due to a concentration dependent effect of SFRP2 (He *et al.*, 2010). In their study, He *et al.* (2010) proposed that low concentrations of SFRP2 could promote deposition and

maturation of collagen whereas higher concentrations would inhibit it. It is however not clear what role SFRP2 plays in the response following neonatal MI. According to He *et al.* (2010) biphasic model, neonatal mice would therefore promote deposition and maturation of collagen which correlates with the scarring observed by Porrello *et al.* (2013) at day 7 post-MI. This scar is however then removed. Neonatal mice low levels of *Sfrp2* expression could also be better compared to *Sfrp2*-deficient mice and their lack of fibrosis following MI in the adult (Kobayashi *et al.*, 2009). SFRP2 injection following neonatal MI would help determine whether its absence is necessary to scar-free regeneration of the myocardium.

Altogether the data presented in this chapter suggests that, at day 7 following MI, the neonatal mouse presents a higher Wnt pathway activity when compared to adult mice which may not be solely due to the developmental stage. Indeed, neonatal mice did appear to utilise the Wnt pathway following MI as shown by up-regulation of *Wnt5b* and its receptor *Fzd2* as well as the target gene *Axin2* relative to naïve neonate. This data was also proposed as a potential link between regulation of fibrosis and the Wnt pathway following neonatal MI. Further investigation is however needed to determine the validity of this link. In order to gain insight on the contribution of cardiac macrophages to these changes in gene expression, alternative approach for their isolation should also be considered

*Csf1r-icre mediated depletion of Porcn does not influence functional loss at day 1 or recovery at day 21 post-MI*

In order to study the role of macrophage-secreted WNTs a mouse line with mononuclear phagocyte targeted depletion of the *Porcn* gene using cre-recombinase expression from the *Csf1r* promoter. *Porcn* encodes Porcupine (PORCN) which is essential in the secretion of WNTs (Section 1.5.1.1). As discussed in Section 4.5, conditional gene depletion from the *Csf1r* promoter would also target neutrophils. Neutrophils have however scarcely been described as WNTs producers. Moreover, recent work from the Pollard lab has shown that this results in specific *Porcn* deletion and prevention of WNT secretion by adult bone marrow derived macrophages (Saha *et al.*, 2016).

Prior to surgery, $Cre^{+ve}$ mice were shown to be normal up until P41 where they exhibited mild cardiomyocyte hypertrophy with slightly increased cardiac function

when compared to $Cre^{-ve}$ control littermates Section 4.4. No difference in any of the parameters tested could be noted prior to P41. No difference in mortality was observed between $Cre^{+ve}$ mice and $Cre^{-ve}$ littermates at either day 1 or day 21 post-MI

At day 1 post-MI, both $Cre^{+ve}$ and $Cre^{-ve}$ control littermates experienced significant functional decrease when compared to naïve P1 mice. The genotype did not have any statistical significance on the functional decrease observed at day 1. This suggests similar extent of injuries in both $Cre^{-ve}$ and $Cre^{+ve}$ animals as well. However, the exact degree of injury at day 1 post-MI in those mice could not be evaluated *in vivo*. This is classically done by measuring plasma troponin but it is impossible to sample sufficient blood in neonatal mice *in vivo* for analysis using current methods of detection. As shown in Section 2.2.2.3, functional decrease however correlated with signs of myocardial injury and increased plasma troponin in terminal blood at day 1 post-MI in neonatal C57BL/6J mice. In an effort to gather sufficient numbers and because of a limited access to these mice while in New York, all animals were assigned to a study looking at the effect of MΦ-specific deletion of *Porcn* on regeneration at day 21 post-MI. No animals were therefore pulled out of this study at day 1 to investigate the exact injury size.

Full recovery of function was observed at day 21 to levels comparable to un-operated mice (P20), consistent with regeneration, as previously reported (Haubner *et al.*, 2012; Porrello *et al.*, 2013). Again, no effect of the genotype was observed on recovery of cardiac function following MI. A decreased LV mass was suggested with no LV wall thinning by ultrasound in all post-MI mice. This was accompanied by a reduction in LVESA and LVEDA which can indicate smaller hearts. However, since heart wet weight and heart to body weight ratio were not significantly different between post-MI animals (P22) and mice of a similar age (P20) it is unclear whether it has significance.

Due to the limited access to the mouse line, it was decided to use the animals generated in the study presented in Chapter 4 as un-injured, naïve controls to the MI groups of Chapter 5. Time-points are therefore not exactly matching which represents a limitation to the interpretation of the results presented here. The study in Chapter 4 has however shown that cardiac function was not significantly changing at least between

P1 and P20. The differences observed in this chapter are therefore most likely due to the treatment rather than an age difference (1-2 days). This small age difference is likely to have an effect on structural measurements such as LVESA, LVEDA, and LV mass. The data presented here however suggests that mice at P22, that received MI at P1, have smaller hearts as measured on the ultrasound when compared to slightly younger naïve animals (P20). Considering that cardiac dimensions have been shown to increase between P20 and P41 in Chapter 4 it is also unlikely that this effect is due to the age difference. Exactly matching time-points however represent a more robust control group and should be envisaged for publication of this thesis' work

*Csf1r-icre mediated depletion of Porcupine results in increased interstitial fibrosis following regeneration*

Even though cardiac function was not changed between the naïve and MI groups 21 days after induction of MI, clear histological differences could be observed in tissue sections. Notably, the location of suture could be identified as a clear depression in the LV wall on the epicardial side, accompanied by scarring irrespective of the genotype, which has been reported by other groups using this model (Porrello *et al.*, 2013; Konfino *et al.*, 2015). Within the myocardium, Porrello *et al.* (2013) reported significant scar formation at day 7 post-MI, that is largely regressed by day 21 when regeneration is complete. Furthermore, MΦ were shown to play a central role in the scar-free regeneration of the myocardium following injury (Aurora *et al.*, 2014; Lavine *et al.*, 2014). In the present study, interstitial fibrosis distant from the ligature site in $Cre^{-ve}$ animals was largely similar to naïve animals at 21 days, although there was evidence of very limited residual fibrosis in the myocardium. Importantly, the extent of this interstitial fibrosis was significantly greater in $Cre^{+ve}$ mice, suggesting that MΦ-derived WNTs may participate in MΦ-mediated promotion of scar-free regeneration following neonatal MI.

As reported by (Konfino *et al.*, 2015), the type and extant of injury is likely to play a role on cardiac repair and regeneration following MI in the neonate. There is therefore a need to determine the time course of scar formation and regression following neonatal MI in our hands; this will also allow further understanding on the role of MΦ-derived WNTs on this process. Starting with the readily available day 21 samples this would be the opportunity to evaluate the presence of proteases MMP12 and MMP13

Chapter 5: The role of macrophage-secreted WNTs in neonatal cardiac regeneration as well as protease inhibitor TIMP1 in the regenerating myocardium as they were shown to be affected in a model of liver injury in mice unable to secrete WNTs from MΦ (Irvine *et al.*, 2015). Furthermore, expression analysis has identified two fibrosis related genes: *Wnt5b* and *Fzd2* (Laeremans *et al.*, 2010; Bradley and Drissi, 2011) as being up-regulated at day 7 post-MI when compared to naïve controls. WNT5b has also been shown to be produced by MΦ (Derlindati *et al.*, 2015) and FZD2 present on migrating myofibroblasts (Blankesteijn *et al.*, 1997). Studying the expression levels of those Wnt pathway genes in MΦ as well as fibroblasts would provide preliminary data on their involvement in scar free regeneration of the neonatal heart post-MI. Specific KO models could then be envisaged to further our understanding of their role if the expression data supports additional experiments. Altogether this would provide clues on the potential mechanism behind the fibrotic phenotype of mice with a *Csf1r-icre* mediated depletion of *Porcn*. This study could also provide tissue to investigate the time course of fibroblast activation, proliferation and matrix deposition/removal following MI in the neonatal mouse. This would provide further insights on the specific aspects of scar free regeneration that MΦ-secreted WNTs may be involved in.

Interestingly, Palevski *et al.* (2017) showed that macrophages polarised towards an M2 phenotype were more abundant in mice unable to secrete WNTs from macrophages following MI in the adult. The Wnt signalling is indeed known to act in an autocrine manner and influence macrophage phenotype (Pereira *et al.*, 2009). Further investigation should include the influence of the Csf1r-icre mediated *Porcn* depletion on the cardiac mononuclear subsets following MI.

Clodronate MΦ depletion was shown by both Aurora *et al.* (2014) and Lavine *et al.* (2014) to diminish vascularisation of the myocardium following cardiac injury. In this chapter, MΦ-specific deletion of *Porcn* did not appear to have a notable effect on vessel density at day 21 post-MI. This suggest that MΦ-derived WNTs may not play a central role in the angiogenic response to MI in the neonatal mouse. This should however be investigated further along with the time course of scar formation and regression to confirm the absence of effect. Lavine *et al.* (2014) but not Aurora *et al.* (2014) describe a deleterious effect of MΦ depletion on cardiomyocyte proliferation following cardiac injury. Moreover, Wnt signalling activity was shown to be necessary for promotion of cardiomyocyte proliferation by the Yes-associated protein (YAP)

Chapter 5: The role of macrophage-secreted WNTs in neonatal cardiac regeneration during development and following neonatal injury (Heallen *et al.*, 2011; Xin *et al.*, 2013). The study presented here did not evaluate the effect of the genotype on proliferation due to the limited access to the mouse line in New York. This could however be investigated along with the time course of scar formation by injecting BrdU and studying its incorporation in proliferating cardiomyocytes. Cardiomyocyte cross sectional area (CMCSA) could also help determine whether MΦ-specific deletion of *Porcn* is associated with hypertrophic remodelling at day 21. This would suggest a diminished proliferative response of cardiomyocytes to MI

Further investigations of the mechanisms involved will be highly relevant. These should involve the study of earlier time points throughout the regeneration process including expression of genes involved in collagen deposition and removal. Looking at earlier time points would also allow confirmation of cell death and extent of injury at 1 day post-MI, investigation of re-vascularisation, cardiomyocytes proliferation and growth, and immune cells content and phenotype.

Altogether, these results present the first evidence of the involvement of the Wnt signalling pathway in the regulation of fibrosis following MI in the neonatal mouse. Using a *Csf1r-icre* mediated *Porcn* depletion model has pointed at a positive role of MΦ-derived WNTs in neonatal cardiac regeneration. This shed a new light on the involvement of the pathway following MI as the data thus far has mostly pointed at a detrimental role of the Wnt signalling pathway in the adult post-MI (Barandon *et al.*, 2003, 2011; Zelarayán *et al.*, 2008; He *et al.*, 2010; Laeremans *et al.*, 2010; Dawson *et al.*, 2013; Palevski *et al.*, 2017). Nevertheless, as it was described in this chapter the Wnt signalling pathway is highly complex and tightly regulated which can explain the discrepancies noted in the literature.

# Chapter 6: General discussion

Following injury such as myocardial infarction (MI) the adult mammalian heart fails to regenerate the lost tissue. Instead, a non-contractile fibrous scar forms that in the longer term can lead to the development of heart failure Neonatal mammals however retain potent regenerative capacities (Porrello *et al.*, 2011; Haubner *et al.*, 2012, 2016) which are dependent on the presence of macrophages (Aurora *et al.*, 2014). In the adult mouse, macrophage-derived WNTs have been shown to promote regeneration of the kidney (Lin *et al.*, 2010), the liver (Boulter *et al.*, 2012; Irvine *et al.*, 2015; Planas-Paz *et al.*, 2016), and the gut (Saha *et al.*, 2016). WNTs are secreted lipophilic proteins essential in development (Section 1.5.1). The primary aim of this thesis was to investigate the role of macrophages and macrophage-secreted WNTs on normal cardiac growth from neonatal to adult as well as in regeneration of the neonatal heart following injury in the mouse model.

## 6.1 Study of the neonatal myocardium

*Cardiac structure and function during postnatal growth*

The set-up of ECG-gated ultrasound methods established by research reported in this thesis has allowed measurement of cardiac systolic function using 2-D and 3-D measurements in neonates. This has provided important structural information such as cavity size, left ventricle (LV) wall thickness, and LV mass. Together with histological techniques it has allowed the identification of 3-distinct phases of myocardial growth.

A first hyperplastic phase, between postnatal day 2 (P2) and P8 characterised by increased density of $Ki67^{+ve}$, proliferative, cardiomyocytes and increasing left ventricle (LV) wall thickness on the ECG-gated ultrasound. Prior to the onset of this PhD, cardiomyocytes were known to rapidly lose their ability to proliferate during the first post-natal week in mammals (Soonpaa *et al.*, 1996; Leu *et al.*, 2001; Hirschy *et al.*, 2006); the mechanisms controlling postnatal cardiomyocyte proliferation were however less clear. Since then, several pathways have been identified including miRNAs, the transcription factors MEIS1, growth factor receptor ERB2, hypoxia, and the Hippo and Wnt signalling pathways (Heallen *et al.*, 2011; Chen *et al.*, 2013; Mahmoud *et al.*, 2013; Xin *et al.*, 2013; Puente *et al.*, 2014; H. Ma *et al.*, 2016). Interestingly, the Yes-associated protein (YAP) necessitates the nuclear localisation of β-catenin, and thereby Wnt pathway activity, in order to promote cardiomyocyte proliferation in the postnatal mouse (Heallen *et al.*, 2011; Xin *et al.*, 2013). Data from

this thesis has suggested that, in the steady state, macrophage directed depletion of the Porcupine gene (*Porcn*) does not influence the density of proliferative cardiomyocyte in the mouse neonatal heart. Macrophage-derived WNTs are therefore not likely to be the main source of Wnt activity required for YAP during this period of development. Identifying the source and identity of WNTs able to trigger pathway activation in cardiomyocytes should be envisaged as future work. Isolation and gene expression analysis of cardiomyocytes, endothelial cells, and fibroblasts, the three major cell types in the mouse heart (Pinto *et al.*, 2016), would help determine targets for manipulation of the pathway to promote cardiomyocyte proliferation in the adult.

A second hypertrophic/reorganisation phase was identified in C57BL/6Jola mice between P8 and P21 characterised by increasing cardiomyocyte size without change in LV wall thickness. The significance and mechanism behind cardiomyocyte reorganisation in normal cardiac growth is unclear and hasn't been investigated *in vivo* to the best of our knowledge. Using serial, thick, histological sections may allow investigation of tissue architecture in a 3-D manner which will be envisaged as future work.

And finally, a third, purely hypertrophic phase between P21 and P42 with increasing cardiomyocyte and LV wall thickness.

*Postnatal myocardial vascularisation*

Whilst considerable advances have been made in the understanding of coronary vasculature origin and development, the cellular pathways controlling it remain less clear (Smart, 2016). Postnatal myocardial vascularisation was originally thought to be achieved through angiogenic sprouting of blood vessels established during foetal life. Agreeing with this idea, work carried out in this thesis showed that, during the first postnatal week, vascular density increases in the outer myocardium whilst vessel size decreases. Those vessels were also shown to be expanding from those established in the foetus (Tian *et al.*, 2014). Whilst macrophages were shown to participate in the patterning of the coronary vasculature in the foetus (Leid *et al.*, 2016), data from this thesis has suggested that a constitutive depletion of macrophages does not influence postnatal vascularisation of the compact myocardium. Shortly after birth, part of the trabeculated myocardium undergoes compaction which is accompanied by *de novo*

formation of blood vessels from the endocardium (Tian *et al.*, 2014). Different myocardial compartments are thereby vascularised through different mechanisms. Since the onset of this PhD it has become clear that the mouse heart contains macrophage populations of distinct origin (Epelman *et al.*, 2014; Lavine *et al.*, 2014; Leid *et al.*, 2016). Interestingly, foetal liver/bone marrow derived macrophages expressing the C-C chemokine receptor type 2 (CCR2), indicative of their monocytic origin, were shown to preferentially localise within the trabeculated myocardium in the foetal mouse heart. Whether those $CCR2^{+ve}$ macrophages play a role in *de novo* myocardial vascularisation is unknown but could be envisaged as future work. An inducible CCR2 knock-out (KO) model would allow precise depletion of those macrophages to study their involvement in early postnatal de novo vascularisation of the compacting trabeculated myocardium.

## 6.2 Neonatal myocardial regeneration

*Models*

Several groups have now succeeded in reproducing Porrello *et al.*'s observations on both the apical resection and MI model of neonatal injury (Haubner *et al.*, 2012; Xin *et al.*, 2013; Aurora *et al.*, 2014; Han *et al.*, 2015; Konfino *et al.*, 2015). However, substantial variability in the surgical and analytical methodologies as well as the regenerative outcome can be noted. Source of variability include, the type of injury model, the surgical method, and the genetic background of the mice used.

For example, Porrello *et al.* (2013) exteriorised the heart before placing a 6-0 Prolene suture through the left ventricle on top of the LAD; Haubner *et al.* (2012) ligate the LAD without exteriorising the heart using a 10-0 Ehtilon suture. 6-0 Prolene is 3.5 times larger than 10-0 Ethilon. Using a larger suture alters the structure of the LV which may lead to more collateral damage and mechanical injury. Konfino *et al.* (2015) observed an average survival rate of 40% following MI using an 8-0 Prolene suture after exteriorising the heart. This was associated with important transmural scarring at the site of the ligation. The survival rate observed across this thesis using 9-0 Ethilon sutures without exteriorising the heart averaged around 80% with minimal scarring around the suture. This might suggest that the size of the suture may play a role in the recovery following MI.

A report by Andersen *et al.* (2014) failed to replicate Porrello *et al.* observations on regeneration following apical resection. Andersen *et al.* experiments were however carried out in C57BL/6 mice whilst Porrello *et al.* were performed on mice with a CD-1 background. This may highlight a strain dependency of neonatal cardiac regeneration, at least for the apical resection model. In this thesis, the two genetic backgrounds used were C57BL/6J and FVB and both showed functional recovery by day 21 post-MI with limited interstitial fibrosis distal of the ligation. Konfino *et al.* (2015) observed functional recovery at day 28 post-MI with mice on a CD-1 background but did not comment on fibrosis distal of the suture. Background strain therefore does not seem to influence functional recovery following MI. Survival rates may be affected, however. Konfino *et al.* (2015) observed a survival rate of 40% in CD-1 mice following MI whilst work from this thesis suggests a survival rate around 70% for C57BL/6 and 90% for FVB mice.

In a multi-author letter, Sadek *et al.* (2014), also pointed out that Andersen *et al.* had potentially resected a greater portion of the LV which could impair regeneration. The regenerative response indeed seems to be dependent on the extent and type of initial injury (Konfino *et al.*, 2015; Sen and Sadek, 2015).

*Assessment of the presence and extent of injury*

In this thesis, high-resolution *in vivo* ultrasound was used to confirm presence of injury following LAD ligation at day 1 (P2). Decreased systolic function at day 1 correlated with signs of myocardial injury on histological cardiac sections and increased plasma cardiac troponin levels (Section 2.2.2.3). Other groups have also reported myocardial damage following MI in the neonate on cardiac histological sections (Haubner *et al.*, 2012; Porrello *et al.*, 2013; Xin *et al.*, 2013; Konfino *et al.*, 2015). Ultrasound provides a valuable tool in the longitudinal study of cardiac systolic function decrease (day 1) and recovery (day 21). Currently published work assessed functional decrease at day 1 using 1-D M-mode visualisation. Following MI, part of the LV below the ligature is akinetic due to cardiomyocyte death whereas the remaining viable myocardium retains movement. Performing ECG-gated 2-D or 3-D measurements of systolic function presented in this thesis considers both parts of the myocardium following MI leading

to a more accurate reading of cardiac systolic function. Neither method of ultrasound is however able to assess the exact extent of initial myocardial damage.

In the adult mouse, the extent of initial injury is routinely measured in the Gray lab by quantifying *in vivo* plasma cardiac troponin levels 24h following permanent LAD ligation (Zhao *et al.*, 2015). This allows longitudinal follow up of animals. Whilst it was possible to obtain sufficient blood post-mortem from neonatal mice post-MI, it is unlikely that it will be possible in-vivo. A method able to accurately assess the extent of initial injury following MI in the neonatal mouse and allow longitudinal assessment of the animal is therefore lacking.

Whilst magnetic resonance imaging (MRI) and positron emission tomography (PET) have been used to evaluate the extent of cardiac injury in adult mice following MI (Stegger *et al.*, 2006; Zhao *et al.*, 2015), no currently published work describes their use in the neonate. Whilst costly, they may provide accurate measurements of extent of initial injury.

When performing neonatal coronary artery ligation, it is important to perform identical surgeries on all pups of a litter. Disparities in the recovery or behaviour of the pups can enhance maternal stress and increase the risk of cannibalisation. It is therefore preferred not to perform sham and MI surgeries on the same litter. Due to the limited access to the mouse line, it was decided to use the animals generated in the study presented in Chapter 4 as un-injured, naïve controls to the MI groups of Chapter 5. This allowed for higher numbers in the experimental groups and thereof more reliable statistical analysis. However, having another control group consisting of sham operated animals would have benefited this study. This would rule out any potential contribution of the hypothermia and thoracotomy in the fibrotic phenotype observed in Chapter 5.

A collaborative effort with the aim to investigate the differences in the surgical techniques and their influence on the regenerative response is therefore required. A thorough comparison of the influence of background strain, surgical method, and analytical protocol on the extent of initial injury and regenerative response appears critical steps that the field needs to investigate. This can provide answers on the mechanisms behind neonatal cardiac regeneration and uncover potential therapies.

*Mechanisms of neonatal myocardial regeneration*

Achieving successful cardiac regeneration necessitate three key phenomena: cardiomyocyte replenishment, removal of interstitial fibrosis, and normal vascularisation of the regenerated myocardium.

Cardiomyocyte replenishment following neonatal MI is mostly achieved through pre-existing cardiomyocytes' de-differentiation and proliferation as opposed to a stem cell based mechanism (Haubner *et al.*, 2012; Porrello *et al.*, 2013). Whilst in the kidney, liver, and gut, macrophage-derived WNTs appeared to promote proliferation of progenitor cells to replenish the lost tissue following injury (Lin *et al.*, 2010; Boulter *et al.*, 2012; Planas-Paz *et al.*, 2016; Saha *et al.*, 2016); deletion of *Porcn* from macrophages has not affected functional recovery at day 21 post-MI in the neonate, it is therefore unlikely that it will have had a significant impact on cardiomyocyte replenishment. However, formal proof of this will be required and is currently being considered as further experiment using cardiomyocyte cross sectional area and proliferation markers on cardiac sections.

Macrophages have been highlighted as having a key role in neonatal cardiac regeneration (Aurora *et al.*, 2014). Yolk-sac derived macrophages were suggested by Lavine *et al.* (2014) to be mobilised shortly after genetic ablation of cardiomyocytes in the neonate and to participate in the regenerative response. Data from this thesis however suggested that this population may be replaced later on, at day 7 post-MI, by macrophages of monocytic origin. The precise identity of these macrophages and their role is however less clear in the MI model. CCR2 is essential in the recruitment of blood derived monocytes to the site of injury (Dewald *et al.*, 2005; Nahrendorf *et al.*, 2007). Using an inducible CCR2 KO models would allow us to understand the precise role of macrophages of monocytic origin following neonatal MI. Future experiments should include a comprehensive analysis of the time line of the immune response along with the various cell types involved with the injury model used in this thesis. As described in 0, the response is likely to be dependent on the type and extent of injury and any finding should always be placed in this context. A further understanding of the mediators of the immune response following neonatal MI would help design strategies to manipulate to promote regeneration in the adult.

In both the kidney and the liver, preventing secretion of WNTs from macrophages was associated with increased fibrosis following injury (Lin *et al.*, 2010; Irvine *et al.*, 2015). Consistent with those findings, data from this thesis has suggested that macrophage-directed depletion of *Porcn* was associated with increased interstitial fibrosis at day 21 post-MI in neonatal mice. In the liver, mice unable to secrete WNTs from macrophages down-regulate the anti-fibrotic *Mmp12* and *Mmp13* (Irvine *et al.*, 2015). Investigating expression of *Mmps* in a time course experiment following MI in the Porcupine mouse would help determine if a similar mechanism is employed in the neonatal heart during regeneration. This thesis has identified *Wnt5b* and its receptor *Fzd2* as being up-regulated in the regenerating myocardium. *Wnt5b* expression was shown to reduce collagen X production in chondrocytes whilst *Fzd2* is known to be expressed on cardiac fibroblast following MI in the adult (Blankesteijn *et al.*, 1997). Whether these interact in the neonatal mouse to control fibrosis is less clear but present a potential mechanism for further investigation. Interestingly, preventing secretion of WNTs from macrophages was shown to be associated with acquisition of an M2-like phenotype following adult MI (Palevski *et al.*, 2017). M2-like macrophages are known to promote angiogenesis, which is beneficial following adult MI, but also matrix deposition to enhance scar stabilisation, (Nahrendorf *et al.*, 2007; Murray and Wynn, 2011). Whether preventing secretion of WNTs from macrophages influences their phenotype in neonatal mice is less clear but also present a potential mechanism to be investigated. It is indeed known that WNTs possess autocrine properties able to influence macrophage phenotype (Pereira *et al.*, 2008; Schaale *et al.*, 2011; Maiti *et al.*, 2012).

Re-vascularisation of the myocardium following neonatal MI was shown by Aurora et al (2014) to require macrophages. Of interest, macrophage-derived WNTs have indeed been shown to participate in patterning of the vasculature in the retina (Lobov *et al.*, 2005; James A Stefater *et al.*, 2011; Stefater *et al.*, 2013). In this thesis however, macrophage-directed depletion of *Porcn* does not seem to have influenced re-vascularisation of the myocardium at day 21 post-MI. A more thorough analysis of the re-vascularisation process is however necessary by investigating earlier time points. The 3-D structure of the vasculature could also be investigated using casts as described in (Porrello *et al.*, 2013).

The recent discovery by Tian *et al.* that the endocardium actively participates in myocardial vascularisation postnatally. It is however unclear if those different vascular beds play distinct roles following neonatal MI compared to adult MI. Using the same reporter mouse could help identify the contribution of each vascular beds to the re-vascularisation of the regenerating area in the neonate and in the peri-infarct revascularisation in the adult mouse.

## 6.3 Summary of future work

Even though considerable questions remain open, the neonatal mouse has provided the field with a strong model of postnatal mammalian cardiac regeneration. It has led to the uncovering of pathways with translational potential to achieving cardiomyocyte proliferation in the adult (Figure 6-1). Work from this thesis has investigated the role of macrophages and macrophages-derived WNTs in normal postnatal growth as well as regeneration following injury. A link between macrophage-derived WNTs and regulation of fibrosis following neonatal MI could be established. This has raised further questions which are considered for further experiments:

- *Do foetal liver/bone marrow derived macrophages play a role in postnatal vascularisation of the myocardium?* This could be investigated using an inducible CCR2 KO mouse model.

- *What is the Wnt signalling gene expression profile in cardiac macrophages during normal growth and following MI in the neonatal mouse?* This was attempted during this thesis but was unsuccessful due to low yield of cells. Further investigations should involve an mRNA amplification step.

- *What is the time course of immune response following our model of neonatal MI?* The immune response is likely to differ depending on the extent and type of injury, as well as the background of the mouse. A time course experiment would benefit interpretation of our results.

- *What is the role of macrophage-derived WNTs in fibrosis following neonatal MI?* This could be investigated using a time course experiment looking at gene expression and collagen content on cardiac section. This would give us the chance to also investigate fibroblast proliferation and differentiation into myofibroblasts.

- *What is the influence of macrophage-derived WNTs on the immune response following neonatal MI?* Using the time course established above, key time points would be identified to perform targeted experiments on macrophage polarisation.

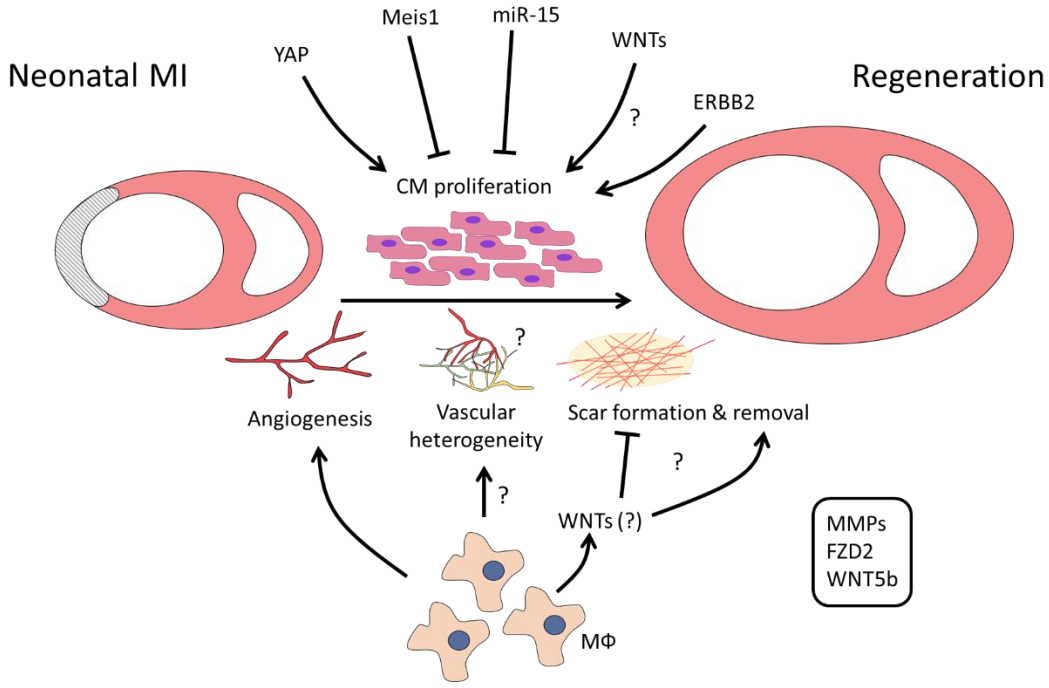


**Figure 6-1: Mechanisms of neonatal cardiac regeneration.** Cardiomyocyte (cm) proliferation is essential in replenishment of the myocardium during regeneration. Yes-associated protein (YAP) promotes cm proliferation in the neonatal mouse and in the adult which is mediated by β-catenin. ERBB2 was also shown to promote cm proliferation. Both Meis1 and miR-15 family were shown to negatively regulate cm proliferation. Macrophages (MΦ) are important in revascularisation and scar removal following neonatal MI. The role of vascular heterogeneity on neonatal cardiac regeneration is unknown, so is the role of macrophages in that process. MΦ-mediated scar removal was suggested to be dependent on secretion of WNTs. The identity of the WNTs and the mechanisms employed are however less clear. Potential mechanisms are listed in the black box. Adapted from Porrello & Olson (2014).

# Appendix

| Position | Symbol | Description |
|---|---|---|
| 1 | Aes | Amino-terminal enhancer of split |
| 2 | Apc | Adenomatosis polyposis coli |
| 3 | Axin1 | Axin 1 |
| 4 | Axin2 | Axin2 |
| 5 | Bcl9 | B-cell CLL/lymphoma 9 |
| 6 | Btrc | Beta-transducin repeat containing protein |
| 7 | Ccnd1 | Cyclin D1 |
| 8 | Ccnd2 | Cyclin D2 |
| 9 | Csnk1a1 | Casein kinase 1, alpha 1 |
| 10 | Csnk2a1 | Casein kinase 2, alpha 1 polypeptide |
| 11 | Ctbp1 | C-terminal binding protein 1 |
| 12 | Ctnnb1 | Catenin (cadherin associated protein), beta 1 |
| 13 | Ctnnbip1 | Catenin beta interacting protein 1 |
| 14 | Daam1 | Dishevelled associated activator of morphogenesis 1 |
| 15 | Dab2 | Disabled homolog 2 (Drosophila) |
| 16 | Dixdc1 | DIX domain containing 1 |
| 17 | Dkk1 | Dickkopf homolog 1 (Xenopus laevis) |
| 18 | Dkk3 | Dickkopf homolog 3 (Xenopus laevis) |
| 19 | Dvl1 | Dishevelled, dsh homolog 1 (Drosophila) |
| 20 | Dvl2 | Dishevelled 2, dsh homolog (Drosophila) |
| 21 | Ep300 | E1A binding protein p300 |
| 22 | Fbxw11 | F-box and WD-40 domain protein 11 |
| 23 | Fbxw4 | F-box and WD-40 domain protein 4 |
| 24 | Fgf4 | Fibroblast growth factor 4 |
| 25 | Fosl1 | Fos-like antigen 1 |
| 26 | Foxn1 | Forkhead box N1 |
| 27 | Frat1 | Frequently rearranged in advanced T-cell lymphomas |
| 28 | Frzb | Frizzled-related protein |
| 29 | Fzd1 | Frizzled homolog 1 (Drosophila) |
| 30 | Fzd2 | Frizzled homolog 2 (Drosophila) |
| 31 | Fzd3 | Frizzled homolog 3 (Drosophila) |
| 32 | Fzd4 | Frizzled homolog 4 (Drosophila) |
| 33 | Fzd5 | Frizzled homolog 5 (Drosophila) |
| 34 | Fzd6 | Frizzled homolog 6 (Drosophila) |
| 35 | Fzd7 | Frizzled homolog 7 (Drosophila) |
| 36 | Fzd8 | Frizzled homolog 8 (Drosophila) |
| 37 | Fzd9 | Frizzled homolog 9 (Drosophila) |

| | | |
|---|---|---|
| 38 | Gsk3b | Glycogen synthase kinase 3 beta |
| 39 | Jun | Jun oncogene |
| 40 | Kremen1 | Kringle containing transmembrane protein 1 |
| 41 | Lef1 | Lymphoid enhancer binding factor 1 |
| 42 | Lrp5 | Low density lipoprotein receptor-related protein 5 |
| 43 | Lrp6 | Low density lipoprotein receptor-related protein 6 |
| 44 | Mapk8 | Mitogen-activated protein kinase 8 |
| 45 | Mmp7 | Matrix metallopeptidase 7 |
| 46 | Myc | Myelocytomatosis oncogene |
| 47 | Nfatc1 | Nuclear factor of activated T-cells, cytoplasmic, calcineurin-dependent 1 |
| 48 | Nkd1 | Naked cuticle 1 homolog (Drosophila) |
| 49 | Nlk | Nemo like kinase |
| 50 | Pitx2 | Paired-like homeodomain transcription factor 2 |
| 51 | Porcn | Porcupine homolog (Drosophila) |
| 52 | Ppard | Peroxisome proliferator activator receptor delta |
| 53 | Prickle1 | Prickle homolog 1 (Drosophila) |
| 54 | Pygo1 | Pygopus 1 |
| 55 | Rhoa | Ras homolog gene family, member A |
| 56 | Rhou | Ras homolog gene family, member U |
| 57 | Ruvbl1 | RuvB-like protein 1 |
| 58 | Sfrp1 | Secreted frizzled-related protein 1 |
| 59 | Sfrp2 | Secreted frizzled-related protein 2 |
| 60 | Sfrp4 | Secreted frizzled-related protein 4 |
| 61 | Sox17 | SRY-box containing gene 17 |
| 62 | Tcf7 | Transcription factor 7, T-cell specific |
| 63 | Tcf7l1 | Transcription factor 7-like 1 (T-cell specific, HMG box) |
| 64 | Tle1 | Transducin-like enhancer of split 1, homolog of Drosophila E(spl) |
| 65 | Vangl2 | Vang-like 2 (van gogh, Drosophila) |
| 66 | Wif1 | Wnt inhibitory factor 1 |
| 67 | Wisp1 | WNT1 inducible signaling pathway protein 1 |
| 68 | Wnt1 | Wingless-related MMTV integration site 1 |
| 69 | Wnt10a | Wingless related MMTV integration site 10a |
| 70 | Wnt11 | Wingless-related MMTV integration site 11 |
| 71 | Wnt16 | Wingless-related MMTV integration site 16 |
| 72 | Wnt2 | Wingless-related MMTV integration site 2 |
| 73 | Wnt2b | Wingless related MMTV integration site 2b |
| 74 | Wnt3 | Wingless-related MMTV integration site 3 |
| 75 | Wnt3a | Wingless-related MMTV integration site 3A |
| 76 | Wnt4 | Wingless-related MMTV integration site 4 |
| 77 | Wnt5a | Wingless-related MMTV integration site 5A |
| 78 | Wnt5b | Wingless-related MMTV integration site 5B |

| | | |
|---|---|---|
| 79 | Wnt6 | Wingless-related MMTV integration site 6 |
| 80 | Wnt7a | Wingless-related MMTV integration site 7A |
| 81 | Wnt7b | Wingless-related MMTV integration site 7B |
| 82 | Wnt8a | Wingless-related MMTV integration site 8A |
| 83 | Wnt8b | Wingless related MMTV integration site 8b |
| 84 | Wnt9a | Wingless-type MMTV integration site 9A |
| HKG | Actb | Actin, beta |
| HKG | B2m | Beta-2 microglobulin |
| HKG | Gapdh | Glyceraldehyde-3-phosphate dehydrogenase |
| HKG | Gusb | Glucuronidase, beta |
| HKG | Hsp90ab1 | Heat shock protein 90 alpha (cytosolic), class B member |
| GDC | MGDC | Mouse Genomic DNA Contamination |
| RTC | RTC | Reverse Transcription Control |
| RTC | RTC | Reverse Transcription Control |
| RTC | RTC | Reverse Transcription Control |
| PPC | PPC | Positive PCR Control |
| PPC | PPC | Positive PCR Control |
| PPC | PPC | Positive PCR Control |

# References


Abdul-Ghani, M., Dufort, D., Stiles, R., De Repentigny, Y., Kothary, R. and Megeney, L. a (2011) 'Wnt11 promotes cardiomyocyte development by caspase-mediated suppression of canonical Wnt signals.', *Molecular and cellular biology*, 31(1), **pp. 163–178**.

Acharya, A., Baek, S. T., Huang, G., Eskiocak, B., Goetsch, S., Sung, C. Y., Banfi, S., Sauer, M. F., Olsen, G. S., Duffield, J. S., *et al.* (2012) 'The bHLH transcription factor Tcf21 is required for lineage-specific EMT of cardiac fibroblast progenitors', *Development*, 139(12), **pp. 2139–2149**.

Adams, J. E., Bodor, G. S., Davila-Roman, V. G., Delmez, J. a, Apple, F. S., Ladenson, J. H. and Jaffe, a S. (1993) 'Cardiac troponin I. A marker with high specificity for cardiac injury', *Circulation*, 88(1), **pp. 101–106**.

Ai, D., Fu, X., Wang, J., Lu, M.-F., Chen, L., Baldini, A., Klein, W. H. and Martin, J. F. (2007) 'Canonical Wnt signaling functions in second heart field to promote right ventricular growth.', *Proceedings of the National Academy of Sciences of the United States of America*, 104(22), **pp. 9319–9324**.

Alliot, F., Godin, I. and Pessac, B. (1999) 'Microglia derive from progenitors, originating from the yolk sac, and which proliferate in the brain', *Developmental Brain Research*, 117(2), **pp. 145–152**.

Andersen, D. C., Ganesalingam, S., Jensen, C. H. and Sheikh, S. P. (2014) 'Do neonatal mouse hearts regenerate following heart apex resection?', *Stem Cell Reports*. The Authors, 2(4), **pp. 406–413**.

Aurora, A. B., Porrello, E. R., Tan, W., Mahmoud, A. I., Hill, J. a., Bassel-Duby, R., Sadek, H. a. and Olson, E. N. (2014) 'Macrophages are required for neonatal heart regeneration', *Journal of Clinical Investigation*, 124(3), **pp. 1382–1392**.

Bach, L. A. (2015) 'Endothelial cells and the IGF system', *Journal of Molecular Endocrinology*, 54(1), **pp. R1–R13**.

Bain, C. C., Bravo-Blas, A., Scott, C. L., Gomez Perdiguero, E., Geissmann, F., Henri,

S., Malissen, B., Osborne, L. C., Artis, D. and Mowat, A. M. (2014) ‘Constant replenishment from circulating monocytes maintains the macrophage pool in the intestine of adult mice.’, *Nature immunology*, 15(10), **pp. 929–37**.

Bain, C. C. and Mowat, A. M. I. (2014) ‘The monocyte-macrophage axis in the intestine’, *Cellular Immunology*. Elsevier Inc., 291(1–2), **pp. 41–48**.

Banerjee, I., Fuseler, J. J. W., Price, R. L., Borg, T. K., Baudino, T. a, Jw, F., Rl, P., Tk, B. and Ta, B. (2007) ‘Determination of cell types and numbers during cardiac development in the neonatal and adult rat and mouse’, *... of Physiology-Heart ...*, 29209, **pp. 1883–1891**.

Bao, M. W., Cai, Z., Zhang, X. J., Li, L., Liu, X., Wan, N., Hu, G., Wan, F., Zhang, R., Zhu, X., *et al.* (2015) ‘Dickkopf-3 protects against cardiac dysfunction and ventricular remodelling following myocardial infarction’, *Basic Research in Cardiology*. Springer Berlin Heidelberg, 110(3).

Barandon, L., Casassus, F., Leroux, L., Moreau, C., Alli??res, C., Lamazi??re, J. M. D., Dufourcq, P., Couffinhal, T. and Dupl??a, C. (2011) ‘Secreted frizzled-related protein-1 improves postinfarction scar formation through a modulation of inflammatory response’, *Arteriosclerosis, Thrombosis, and Vascular Biology*, 31(11).

Barandon, L., Couffinhal, T., Ezan, J., Dufourcq, P., Costet, P., Alzieu, P., Leroux, L., Moreau, C., Dare, D. and Dupl??a, C. (2003) ‘Reduction of Infarct Size and Prevention of Cardiac Rupture in Transgenic Mice Overexpressing FrzA’, *Circulation*, 108(18), **pp. 2282–2289**.

Bartunek, J., Behfar, A., Dolatabadi, D., Vanderheyden, M., Ostojic, M., Dens, J., El Nakadi, B., Banovic, M., Beleslin, B., Vrolix, M., *et al.* (2013) ‘Cardiopoietic stem cell therapy in heart failure: The C-CURE (cardiopoietic stem cell therapy in heart failURE) multicenter randomized trial with lineage-specified biologics’, *Journal of the American College of Cardiology*, 61(23), **pp. 2329–2338**.

Begg, B. S. K., Radley, J. M., Pollard, J. W., Chisholm, O. T., Stanley, E. R. and Bertoncello, I. (1993) ‘Delayed Hematopoietic Development in Osteopetrotic (op/op) Mice’, *Journal of Experimental Medecine*, 177(January).

Behfar, A., Crespo-Diaz, R., Terzic, A. and Gersh, B. J. (2014) 'Cell therapy for cardiac repair--lessons from clinical trials.', *Nature reviews. Cardiology*. Nature Publishing Group, 11(4), **pp. 232–46**.

Behfar, A., Yamada, S., Crespo-Diaz, R., Nesbitt, J. J., Rowe, L. A., Perez-Terzic, C., Gaussin, V., Homsy, C., Bartunek, J. and Terzic, A. (2010) 'Guided cardiopoiesis enhances therapeutic benefit of bone marrow human mesenchymal stem cells in chronic myocardial infarction', *Journal of the American College of Cardiology*. Elsevier Inc., 56(9), **pp. 721–734**.

Beltrami, A. P., Barlucchi, L., Torella, D., Baker, M., Limana, F., Chimenti, S., Kasahara, H., Rota, M., Musso, E., Urbanek, K., *et al.* (2003) 'Adult cardiac stem cells are multipotent and support myocardial regeneration', *Cell*, 114(6), **pp. 763–776**.

Bennett, H. S. (1936) 'The development of the blood supply to the heart in the embryo pig', *American Journal of Anatomy*. Wiley Online Library, 60(1), **pp. 27–53**.

Bensley, J. G., De Matteo, R., Harding, R. and Black, M. J. (2016) 'Three-dimensional direct measurement of cardiomyocyte volume, nuclearity, and ploidy in thick histological sections.', *Scientific reports*. Nature Publishing Group, 6(April), **p. 23756**.

Bergmann, O., Bhardwaj, R. D., Bernard, S., Zdunek, S., Barnabé-Heider, F., Walsh, S., Zupicich, J., Alkass, K., Buchholz, B. a, Druid, H., *et al.* (2009) 'Evidence for cardiomyocyte renewal in humans.', *Science (New York, N.Y.)*, 324(5923), **pp. 98–102**.

van Berlo, J. H., Kanisicak, O., Maillet, M., Vagnozzi, R. J., Karch, J., Lin, S.-C. J., Middleton, R. C., Marbán, E. and Molkentin, J. D. (2014) 'C-Kit+ Cells Minimally Contribute Cardiomyocytes To the Heart', *Nature*, 509(7500), **pp. 337–341**.

Bertrand, J. Y., Jalil, A., Klaine, M., Jung, S., Cumano, A., Godin, I. and Dc, W. (2005) 'Three pathways to mature macrophages in the early mouse yolk sac Three pathways to mature macrophages in the early mouse yolk sac', *Blood*, 106(9), **pp. 3004–3011**.

Biechele, S., Cockburn, K., Lanner, F., Cox, B. J. and Rossant, J. (2013) 'Porcn-dependent Wnt signaling is not required prior to mouse gastrulation.', *Development (Cambridge, England)*, 140(14), **pp. 2961–71**.

Bielefeld, K. A., Amini-Nik, S. and Alman, B. A. (2013) 'Cutaneous wound healing: Recruiting developmental pathways for regeneration', *Cellular and Molecular Life Sciences*, 70(12), **pp. 2059–2081**.

Blankesteijn, W. M., Essers-Janssen, P. . Y., Verluyten, J. . M., Daemen, J. A. . M. and Smits, F. . J. (1997) 'A homologue of Drosophila tissue polarity gene frizzled is expressed in migrating myofibroblasts in the infarcted rat heart', *Nature Medicine*, 3, **pp. 541–544**.

Bogers, A. J., Gittenberger-de Groot, A. C., Poelmann, R. E., Péault, B. M. and Huysmans, H. A. (1989) 'Development of the origin of the coronary arteries, a matter of ingrowth or outgrowth?', *Anatomy and embryology*, 180(5), **pp. 437–41**.

Bollini, S., Smart, N. and Riley, P. R. (2011) 'Resident cardiac progenitor cells: At the heart of regeneration', *Journal of Molecular and Cellular Cardiology*. Elsevier Ltd, 50(2), **pp. 296–303**.

van den Borne, S. W. M., Diez, J., Blankesteijn, W. M., Verjans, J., Hofstra, L. and Narula, J. (2010) 'Myocardial remodeling after infarction: the role of myofibroblasts.', *Nature reviews. Cardiology*. Nature Publishing Group, 7(1), **pp. 30–37**.

Boulter, L., Govaere, O., Bird, T. G., Radulescu, S., Ramachandran, P., Pellicoro, a., Ridgway, R. a., Seo, S. S., Spee, B., Van Rooijen, N., *et al.* (2012) 'Macrophage-derived Wnt opposes Notch signaling to specify hepatic progenitor cell fate in chronic liver disease', *Nature Medicine*. Nature Publishing Group, 18(4), **pp. 572–579**.

Bradley, E. W. and Drissi, M. H. (2011) 'Wnt5b regulates mesenchymal cell aggregation and chondrocyte differentiation through the planar cell polarity pathway', *Journal of Cellular Physiology*, 226(6), **pp. 1683–1693**.

Buckingham, M., Meilhac, S. and Zaffran, S. (2005) 'Building the mammalian heart from two sources of myocardial cells', *Nature Reviews Genetics*, 6(November), **pp. 826–835**.

Cai, W. and Schaper, W. (2008) 'Mechanisms of arteriogenesis', *Acta Biochimica et Biophysica Sinica*, 40(8), **pp. 681–692**.

Camelliti, P., Borg, T. K. and Kohl, P. (2005) 'Structural and functional

characterisation of cardiac fibroblasts', *Cardiovascular Research*, 65(1), **pp. 40–51**.

Carmeliet, P. (2000) 'Mechanisms of angiogenesis and arteriogenesis.', *Nature medicine*, 6(3), **pp. 389–395**.

Carmeliet, P. (2003) 'Angiogenesis in health and disease', *Nature Medicine*, 9, **pp. 653–660**.

Caubit, X., Nicolas, S. and Le Parco, Y. (1997) 'Possible roles for Wnt genes in growth and axial patterning during regeneration of the tail in urodele amphibians', *Developmental Dynamics*, 210(1), **pp. 1–10**.

Chan, J. K., Roth, J., Oppenheim, J. J., Tracey, K. J., Vogl, T., Feldmann, M., Horwood, N., Nanchahal, J., Oppenheim, J., Yang, D., *et al.* (2012) 'Alarmins: awaiting a clinical response.', *The Journal of clinical investigation*, 122(8), **pp. 2711–9**.

Chen, B. and Frangogiannis, N. G. (2016) 'Immune cells in repair of the infarcted myocardium', *Microcirculation*, (June 2016), **pp. 1–10**.

Chen, J., Huang, Z. P., Seok, H. Y., Ding, J., Kataoka, M., Zhang, Z., Hu, X., Wang, G., Lin, Z., Wang, S., *et al.* (2013) 'Mir-17-92 cluster is required for and sufficient to induce cardiomyocyte proliferation in postnatal and adult hearts', *Circulation Research*, 112(12), **pp. 1557–1566**.

Chen, V. C., Stull, R., Joo, D., Cheng, X. and Keller, G. (2008) 'Notch signaling respecifies the hemangioblast to a cardiac fate.', *Nature biotechnology*, 26(10), **pp. 1169–1178**.

Chitu, V. and Stanley, E. R. (2006) 'Colony-stimulating factor-1 in immunity and inflammation', *Current Opinion in Immunology*, 18(1), **pp. 39–48**.

Clements, W. K., Kim, A. D., Ong, K. G., Moore, J. C., Lawson, N. D. and Traver, D. (2011) 'A somitic Wnt16/Notch pathway specifies haematopoietic stem cells.', *Nature*, 474(7350), **pp. 220–4**.

Clevers, H. and Nusse, R. (2012) 'Wnt/ β-catenin signaling and disease', *Cell*, 149(6), **pp. 1192–1205**.

Cohen, E. D., Miller, M. F., Wang, Z., Moon, R. T. and Morrisey, E. E. (2012) 'Wnt5a and Wnt11 are essential for second heart field progenitor development', *Development*, 139(11), **pp. 1931–1940**.

Cohen, E. D., Wang, Z., Lepore, J. J., Lu, M. M., Taketo, M. M., Epstein, D. J. and Morrisey, E. E. (2007) 'Wnt/β-catenin signaling promotes expansion of Isl-1–positive cardiac progenitor cells through regulation of FGF signaling', *The Journal of clinical investigation*, 117(7), **pp. 1794–804**.

Cohn, J. N., Ferrari, R. and Sharpe, N. (2000) 'Cardiac remodeling-concepts and clinical implications: A consensus paper from an International Forum on Cardiac Remodeling', *Journal of the American College of Cardiology*. Elsevier Masson SAS, 35(3), **pp. 569–582**.

Corrigan, N., Brazil, D. P. and McAuliffe, F. M. (2010) 'High-Frequency Ultrasound Assessment of the Murine Heart From Embryo Through to Juvenile', *Reproductive Sciences*, 17(2), **pp. 147–157**.

Dai, X., Ryan, G. R., Hapel, a J., Dominguez, M. G., Russell, R. G., Kapp, S., Sylvestre, V. and Stanley, E. R. (2002) 'Targeted disruption of the mouse CSF-1 receptor gene results in osteopetrosis, mononuclear phagocyte deficiency, increased primititive progenitor cell frequencies and reproductive defects.', *Blood*, 99(1), **pp. 111–120**.

Davies, L. C., Jenkins, S. J., Allen, J. E. and Taylor, P. R. (2013) 'Tissue-resident macrophages', *Nature Immunology*, 14(10), **pp. 986–995**.

Dawson, K., Aflaki, M. and Nattel, S. (2013) 'Role of the Wnt-Frizzled system in cardiac pathophysiology: a rapidly developing, poorly understood area with enormous potential.', *The Journal of physiology*, 591(Pt 6), **pp. 1409–32**.

De, A. (2011) 'Wnt / Ca 21 signaling pathway : a brief overview The Non-canonical Wnt Signaling Cascade', *Acta Biochimica et Biophysica Hungarica*, 43(10), **pp. 745–756**.

Deb, A., Wang, S., Skelding, K. A., Miller, D., Simper, D. and Caplice, N. M. (2003) 'Bone marrow-derived cardiomyocytes are present in adult human heart: A study of

gender-mismatched bone marrow transplantation patients', *Circulation*, 107(9), **pp. 1247–1249**.

Dejana, E. (2010) 'The role of wnt signaling in physiological and pathological angiogenesis', *Circulation Research*, 107(8), **pp. 943–952**.

Delewi, R., Andriessen, A., Tijssen, J. G. P., Zijlstra, F., Piek, J. J. and Hirsch, A. (2013) 'Impact of intracoronary cell therapy on left ventricular function in the setting of acute myocardial infarction: a meta-analysis of randomised controlled clinical trials.', *Heart*, 99(4), **pp. 225–32**.

Deng, L., Zhou, J.-F., Sellers, R. S., Li, J.-F., Nguyen, A. V, Wang, Y., Orlofsky, A., Liu, Q., Hume, D. A., Pollard, J. W., *et al.* (2010) 'A novel mouse model of inflammatory bowel disease links mammalian target of rapamycin-dependent hyperproliferation of colonic epithelium to inflammation-associated tumorigenesis.', *The American journal of pathology*. American Society for Investigative Pathology, 176(2), **pp. 952–67**.

Derlindati, E., Cas, A. D., Montanini, B., Spigoni, V., Curella, V., Aldigeri, R., Ardigò, D., Zavaroni, I. and Bonadonna, R. C. (2015) 'Transcriptomic analysis of human polarized macrophages: More than one role of alternative activation?', *PLoS ONE*, 10(3), **pp. 1–17**.

Descamps, B., Sewduth, R., Ferreira Tojais, N., Jaspard, B., Reynaud, A., Sohet, F., Lacolley, P., Alli??res, C., Lamazi??re, J. M. D., Moreau, C., *et al.* (2012) 'Frizzled 4 regulates arterial network organization through noncanonical Wnt/planar cell polarity signaling', *Circulation Research*, 110(1), **pp. 47–58**.

Dewald, O., Zymek, P., Winkelmann, K., Koerting, A., Ren, G., Abou-Khamis, T., Michael, L. H., Rollins, B. J., Entman, M. L. and Frangogiannis, N. G. (2005) 'CCL2/monocyte chemoattractant protein-1 regulates inflammatory responses critical to healing myocardial infarcts', *Circulation Research*, 96(8), **pp. 881–889**.

Dougall, W. C., Glaccum, M., Charrier, K., Rohrbach, K., Brasel, K., Smedt, T. De, Daro, E., Smith, J., Tometsko, M. E., Maliszewski, C. R., *et al.* (1999) 'RANK is essential for osteoclast and lymph node development', **pp. 2412–2424**.

Ellison, G. M., Vicinanza, C., Smith, A. J., Aquila, I., Leone, A., Waring, C. D., Henning, B. J., Stirparo, G. G., Papait, R., Scarfò, M., *et al.* (2013) 'Adult c-kitpos cardiac stem cells are necessary and sufficient for functional cardiac regeneration and repair', *Cell*, 154(4), **pp. 827–842**.

Epelman, S., Lavine, K. J., Beaudin, A. E., Sojka, D. K., Carrero, J. a., Calderon, B., Brija, T., Gautier, E. L., Ivanov, S., Satpathy, A. T., *et al.* (2014) 'Embryonic and adult-derived resident cardiac macrophages are maintained through distinct mechanisms at steady state and during inflammation', *Immunity*. Elsevier Inc., 40(1), **pp. 91–104**.

Erblich, B., Zhu, L., Etgen, A. M., Dobrenis, K. and Pollard, J. W. (2011) 'Absence of colony stimulation factor-1 receptor results in loss of microglia, disrupted brain development and olfactory deficits', *PLoS ONE*, 6(10).

Ezekowitz, J. A., Kaul, P., Bakal, J. A., Armstrong, P. W., Welsh, R. C. and McAlister, F. A. (2009) 'Declining In-Hospital Mortality and Increasing Heart Failure Incidence in Elderly Patients With First Myocardial Infarction', *Journal of the American College of Cardiology*. American College of Cardiology Foundation, 53(1), **pp. 13–20**.

Fantin, A., Vieira, J. M., Gestri, G., Denti, L., Schwarz, Q., Prykhozhij, S., Peri, F., Wilson, S. W. and Ruhrberg, C. (2010) 'Tissue macrophages act as cellular chaperones for vascular anastomosis downstream of VEGF-mediated endothelial tip cell induction', *Blood*, 116(5), **pp. 829–840**.

Forbes, S. J. and Newsome, P. N. (2016) 'Liver regeneration - mechanisms and models to clinical application.', *Nature reviews. Gastroenterology & hepatology*, 13(8), **pp. 473–85**.

Forbes, S. J. and Rosenthal, N. (2014) 'Preparing the ground for tissue regeneration: from mechanism to therapy.', *Nature medicine*. Nature Publishing Group, 20(8), **pp. 857–69**.

Frangogiannis, N. G. (2012) 'Regulation of the inflammatory response in cardiac repair', *Circulation Research*, 110(1), **pp. 159–173**.

Frangogiannis, N. G. (2014) 'The inflammatory response in myocardial injury, repair,

and remodelling', *Nature Reviews Cardiology*. Nature Publishing Group, 11(5), **pp. 255–265**.

Fratz, S., Hager, A., Schreiber, C., Schwaiger, M., Hess, J. and Stern, H. C. (2011) 'Long-Term Myocardial Scarring After Operation for Anomalous Left Coronary Artery From the Pulmonary Artery', *The Annals of Thoracic Surgery*. Elsevier Inc., 92(5), **pp. 1761–1765**.

van Furth, R., Cohn, Z. A., Hirsch, J. G., Humphrey, J. H., Spector, W. G. and Langevoort, H. L. (1972) 'The mononuclear phagocyte system: a new classification of macrophages, monocytes, and their precursor cells.', *Bulletin of the World Health Organization*, 46(6), **pp. 845–852**.

Geissmann, F., Jung, S. and Littman, D. R. (2003) 'Blood monocytes consist of two principal subsets with distinct migratory properties', *Immunity*, 19(1), **pp. 71–82**.

Gerdes, J., Lemke, H., Baisch, H., Wacker, H., Schwab, U. and Stein, H. (1984) 'Cell cycle analysis of a cell proliferation-associated human nuclear antigen defined by the monoclonal antibody Ki-67', *The Journal of Immunology*, 133(4), **pp. 1710–1715**.

Gessert, S. and Kühl, M. (2010) 'The multiple phases and faces of Wnt signaling during cardiac differentiation and development', *Circulation Research*, 107(2), **pp. 186–199**.

Ginhoux, F. and Guilliams, M. (2016) 'Tissue-Resident Macrophage Ontogeny and Homeostasis', *Immunity*. Elsevier Inc., 44(3), **pp. 439–449**.

Ginhoux, F., Lim, S., Hoeffel, G., Low, D. and Huber, T. (2013) 'Origin and differentiation of microglia.', *Frontiers in cellular neuroscience*, 7(April), **p. 45**.

Godfrey, M. E., Messing, B., Cohen, S. M., Valsky, D. V and Yagel, S. (2012) 'Functional assessment of the fetal heart: a review.', *Ultrasound in obstetrics & gynecology : the official journal of the International Society of Ultrasound in Obstetrics and Gynecology*, 39(January), **pp. 131–44**.

Godwin, J. W., Pinto, A. R. and Rosenthal, N. A. (2013) 'Macrophages are required for adult salamander limb regeneration', 110(23).

Goodwin, A. M., Sullivan, K. M. and D'Amore, P. A. (2006) 'Cultured endothelial cells display endogenous activation of the canonical Wnt signaling pathway and express multiple ligands, receptors, and secreted modulators of Wnt signaling', *Developmental Dynamics*, 235(11), **pp. 3110–3120**.

Gordon, S. (2003) 'Alternative activation of macrophages', in Intergovernmental Panel on Climate Change (ed.) *Nature Reviews Immunology*. Cambridge: Cambridge University Press, **pp. 23–35**.

Gordon, S. and Taylor, P. R. (2005) 'Monocyte and macrophage heterogeneity.', *Nature reviews. Immunology*, 5(12), **pp. 953–64**.

Gourdie, R. G., Dimmeler, S. and Kohl, P. (2016) 'Novel Therapeutic Strategies Targeting Fibroblasts and Fibrosis in Heart Disease', *Nature Reviews Drug Discovery*. Nature Publishing Group, In press(9), **pp. 620–638**.

Gujral, T. S., Chan, M., Peshkin, L., Sorger, P. K., Kirschner, M. W. and MacBeath, G. (2015) 'A noncanonical Frizzled2 pathway regulates epithelial- mesenchymal transition and metastasis', *Cell*, 159(4), **pp. 844–856**.

Gyongyosi, M., Wojakowski, W., Lemarchand, P., Lunde, K., Tendera, M., Bartunek, J., Marban, E., Assmus, B., Henry, T. D., Traverse, J. H., *et al.* (2015) 'Meta-analysis of cell-based CaRdiac stUdiEs (ACCRUE) in patients with acute myocardial infarction based on individual patient data', *Circulation Research*, 116(8), **pp. 1346–1360**.

Han, C., Nie, Y., Lian, H., Liu, R., He, F., Huang, H. and Hu, S. (2015) 'Acute inflammation stimulates a regenerative response in the neonatal mouse heart.', *Cell research*. Nature Publishing Group, 25(10), **pp. 1137–1151**.

Hardy, K. M., Garriock, R. J., Yatskievych, T. A., D'Agostino, S., Antin, P. B. and Krieg, P. A. (2009) 'Non-canonical Wnt signaling through Wnt5a/b and a novel Wnt11 gene, Wnt11b, regulates cell migration during avian gastrulation', *Developmental Biology*, 181(2), **pp. 391–401**.

Hare, J. M., Traverse, J. H., Henry, T. D., Dib, N., Strumpf, R. K., Schulman, S. P., Gerstenblith, G., DeMaria, A. N., Denktas, A. E., Gammon, R. S., *et al.* (2009) 'A

Randomized, Double-Blind, Placebo-Controlled, Dose-Escalation Study of Intravenous Adult Human Mesenchymal Stem Cells (Prochymal) After Acute Myocardial Infarction', *Journal of the American College of Cardiology*. Elsevier Inc., 54(24), **pp. 2277–2286**.

Haubner, B. J., Brice, M. A., Khadayate, S., Metzler, B., Aitman, T. and Penninger, J. M. (2012) 'Complete cardiac regeneration in a mouse model of myocardial infarction', 4(12), **pp. 966–977**.

Haubner, B. J., Schneider, J., Schweigmann, U., Schuetz, T., Dichtl, W., Velik-Salchner, C., Stein, J. I. and Penninger, J. M. (2016) 'Functional Recovery of a Human Neonatal Heart after Severe Myocardial Infarction', *Circulation Research*, 118(2), **pp. 216–221**.

He, W., Zhang, L., Ni, A., Zhang, Z., Mirotsou, M., Mao, L., Pratt, R. E. and Dzau, V. J. (2010) 'Exogenously administered secreted frizzled related protein 2 ( Sfrp2 ) reduces fi brosis and improves cardiac function in a rat model of myocardial infarction', *Proceedings of the National Academy of Sciences*, 107(49), **pp. 21110–21115**.

Heallen, T., Zhang, M., Wang, J., Bonilla-Claudio, M., Klysik, E., Johnson, R. L. and Martin, J. F. (2011) 'Hippo pathway inhibits Wnt signaling to restrain cardiomyocyte proliferation and heart size.', *Science (New York, N.Y.)*, 332(6028), **pp. 458–461**.

Henderson, W. R., Chi, E. Y., Ye, X., Nguyen, C., Tien, Y., Zhou, B., Borok, Z., Knight, D. A. and Kahn, M. (2010) 'Inhibition of Wnt/ β-catenin/CREB binding protein (CBP) signaling reverses pulmonary fibrosis.', *Proceedings of the National Academy of Sciences of the United States of America*, 107(32), **pp. 14309–14**.

Herr, P. and Basler, K. (2012) 'Porcupine-mediated lipidation is required for Wnt recognition by Wls', *Developmental Biology*. Elsevier Inc., 361(2), **pp. 392–402**.

Herr, P., Hausmann, G. and Basler, K. (2012) 'WNT secretion and signalling in human disease', *Trends in Molecular Medicine*. Elsevier Ltd, 18(8), **pp. 483–493**.

Hinz, B. and Gabbiani, G. (2003) 'Mechanisms of force generation and transmission by myofibroblasts', *Current Opinion in Biotechnology*, 14(5), **pp. 538–546**.

Hiratsuka, S., Nakamura, K., Iwai, S., Murakami, M., Itoh, T., Kijima, H., Shipley, J. M., Senior, R. M. and Shibuya, M. (2002) 'MMP9 induction by vascular endothelial growth factor receptor-1 is involved in lung-specific metastasis', 2(October), **pp. 289–300**.

Hirschy, A., Schatzmann, F., Ehler, E. and Perriard, J. C. (2006) 'Establishment of cardiac cytoarchitecture in the developing mouse heart', *Developmental Biology*, 289(2), **pp. 430–441**.

Holmes, J. W., Borg, T. K. and Covell, J. W. (2005) 'Structure and Mechanics of Healing Myocardial Infarcts', *Annual Review of Biomedical Engineering*, 7(1), **pp. 223–253**.

Huelsken, J., Vogel, R., Brinkmann, V., Erdmann, B., Birchmeier, C. and Birchmeier, W. (2000) 'Requirement for β-catenin in anterior-posterior axis formation in mice.', *The Journal of Cell Biology*, 148(3), **pp. 567–78**.

Ieda, M., Tsuchihashi, T., Ivey, K. N., Ross, R. S., Hong, T. T., Shaw, R. M. and Srivastava, D. (2009) 'Cardiac Fibroblasts Regulate Myocardial Proliferation through ??1 Integrin Signaling', *Developmental Cell*. Elsevier Ltd, 16(2), **pp. 233–244**.

Irvine, K. M., Clouston, A. D., Gadd, V. L., Miller, G. C., Wong, W.-Y., Melino, M., Maradana, M. R., MacDonald, K., Lang, R. A., Sweet, M. J., *et al.* (2015) 'Deletion of Wntless in myeloid cells exacerbates liver fibrosis and the ductular reaction in chronic liver injury.', *Fibrogenesis & tissue repair*. Fibrogenesis & Tissue Repair, 8, **p. 19**.

Ito, M., Yang, Z., Andl, T., Cui, C., Kim, N., Millar, S. E. and Cotsarelis, G. (2007) 'Wnt-dependent de novo hair follicle regeneration in adult mouse skin after wounding', *Nature*, 447(May), **pp. 316–320**.

Jackson, K. A., Majka, S. M., Wang, H., Pocius, J., Hartley, C. J., Majesky, M. W., Entman, M. L., Michael, L. H., Hirschi, K. K. and Goodell, M. A. (2001) 'Regeneration of ischemic cardiac muscle and vascular endothelium by adult stem cells', *Journal of Clinical Investigation*, 107(11), **pp. 1395–1402**.

Jain, R. K. (2003) ‘Molecular regulation of vessel maturation’, *Nature medicine*, 9(6), **pp. 685–693**.

Jho, E., Zhang, T., Domon, C., Joo, C.-K., Freund, J.-N. and Costantini, F. (2002) ‘Wnt/ β-catenin/Tcf signaling induces the transcription of Axin2, a negative regulator of the signaling pathway.’, *Molecular and cellular biology*, 22(4), **pp. 1172–83**.

Jopling, C., Sleep, E., Raya, M., Martí, M., Raya, A. and Izpisúa Belmonte, J. C. (2010) ‘Zebrafish heart regeneration occurs by cardiomyocyte dedifferentiation and proliferation.’, *Nature*, 464(7288), **pp. 606–9**.

Jouk, P. S., Mourad, A., Milisic, V., Michalowicz, G., Raoult, A., Caillerie, D. and Usson, Y. (2007) ‘Analysis of the fiber architecture of the heart by quantitative polarized light microscopy. Accuracy, limitations and contribution to the study of the fiber architecture of the ventricles during fetal and neonatal life.’, *European journal of cardio-thoracic surgery : official journal of the European Association for Cardio-thoracic Surgery*, 31(5), **pp. 915–921**.

Jung, K., Kim, P., Leuschner, F., Gorbatov, R., Kim, J. K., Ueno, T., Nahrendorf, M. and Yun, S. H. (2013) ‘Endoscopic time-lapse imaging of immune cells in infarcted mouse hearts’, *Circulation Research*, 112(6), **pp. 891–899**.

Jung, Y. S., Lee, H. Y., Kim, S. D., Park, J. S., Kim, J. K., Suh, P.-G. and Bae, Y.-S. (2013) ‘Wnt5a stimulates chemotactic migration and chemokine production in human neutrophils.’, *Experimental & molecular medicine*. Nature Publishing Group, 45(6), **p. e27**.

Kawakami, Y., Rodriguez, C., Raya, M., Kawakami, H., Dubova, I., Carlos, J. and Belmonte, I. (2006) ‘Wnt /b-catenin signaling regulates vertebrate limb regeneration’, *Genes & Development*, (858), **pp. 3232–3237**.

Kinnaird, T., Burnett, E. S., Shou, M., Lee, C. W., Barr, S., Fuchs, S. and Epstein, S. E. (2004) ‘Local Delivery of Marrow-Derived Stromal Cells Augments Collateral Perfusion Through Paracrine Mechanisms’, *Circulation*, 109(12), **pp. 1543–1549**.

Klaus, A., Saga, Y., Taketo, M. M., Tzahor, E. and Birchmeier, W. (2007) ‘Distinct roles of Wnt/beta-catenin and Bmp signaling during early cardiogenesis.’,

*Proceedings of the National Academy of Sciences of the United States of America*, 104(47), **pp. 18531–18536**.

Kobayashi, K., Luo, M., Zhang, Y., Wilkes, D. C., Ge, G., Grieskamp, T., Yamada, C., Liu, T.-C., Huang, G., Basson, C. T., *et al.* (2009) 'Secreted Frizzled-related protein 2 is a procollagen C proteinase enhancer with a role in fibrosis associated with myocardial infarction.', *Nature cell biology*, 11(1), **pp. 46–55**.

Komekado, H., Yamamoto, H., Chiba, T. and Kikuchi, A. (2007) 'Glycosylation and palmitoylation of Wnt-3a are coupled to produce an active form of Wnt-3a', *Genes to Cells*, 12(4), **pp. 521–534**.

Komiya, Y. and Habas, R. (2008) 'Wnt signal transduction pathways', *Organogenesis*, 4(2), **pp. 68–75**.

Konfino, T., Landa, N., Ben-Mordechai, T. and Leor, J. (2015) 'The type of injury dictates the mode of repair in neonatal and adult heart.', *Journal of the American Heart Association*, 4(1), **p. e001320**.

Kopf, M., Schneider, C. and Nobs, S. P. (2015) 'The development and function of lung-resident macrophages and dendritic cells', *Nat Immunol*, 16(1), **pp. 36–44**.

Korinek, V., Barker, N., Morin, P., van Wichen, D., de Weger, R., Kinzler, K., Vogelstein, B. and Clevers, H. (1997) 'Constitutive Transcriptional Activation by a b-Catenin–Tcf Complex in APC-/- Colon Carcinoma', *Science*, 275, **pp. 1784–1787**.

Koyanagi, M., Haendeler, J., Badorff, C., Brandes, R. P., Hoffmann, J., Pandur, P., Zeiher, A. M., Kühl, M. and Dimmeler, S. (2005) 'Non-canonical Wnt signaling enhances differentiation of human circulating progenitor cells to cardiomyogenic cells', *Journal of Biological Chemistry*, 280(17), **pp. 16838–16842**.

Kulandavelu, S., Qu, D., Sunn, N., Mu, J., Rennie, M. Y., Whiteley, K. J., Walls, J. R., Bock, N. a, Sun, J. C. H., Covelli, A., *et al.* (2006) 'Embryonic and neonatal phenotyping of genetically engineered mice.', *ILAR journal / National Research Council, Institute of Laboratory Animal Resources*, 47(2), **pp. 103–117**.

Kuswardhani, R. a T. and Soejitno, A. (2011) 'Bone marrow-derived stem cells as an adjunctive treatment for acute myocardial infarction: a systematic review and meta-

analysis.', *Acta medica Indonesiana*, 43(3), **pp. 168–77**.

Kwon, C., Arnold, J., Hsiao, E. C., Taketo, M. M., Conklin, B. R. and Srivastava, D. (2007) 'Canonical Wnt signaling is a positive regulator of mammalian cardiac progenitors', *Proc Natl Acad Sci U S A*, 104(26), **pp. 10894–10899**.

Laeremans, H., Rensen, S. S., Ottenheijm, H. C. J., Smits, J. F. M. and Blankesteijn, W. M. (2010) 'Wnt/frizzled signalling modulates the migration and differentiation of immortalized cardiac fibroblasts', *Cardiovascular Research*, 87(3), **pp. 514–523**.

Lavine, K. J., Epelman, S., Uchida, K., Weber, K. J., Nichols, C. G., Schilling, J. D., Ornitz, D. M., Randolph, G. J. and Mann, D. L. (2014) 'Distinct macrophage lineages contribute to disparate patterns of cardiac recovery and remodeling in the neonatal and adult heart', *Proceedings of the National Academy of Sciences*, 111(45), **pp. 16029–16034**.

Leid, J., Carrelha, J., Boukarabila, H., Epelman, S., Jacobsen, S. E. W. and Lavine, K. J. (2016) 'Primitive Embryonic Macrophages are Required for Coronary Development and Maturation', *Circulation Research*, 118(10), **pp. 1498–1511**.

Leu, M., Ehler, E. and Perriard, J. C. (2001) 'Characterisation of postnatal growth of the murine heart', *Anatomy and Embryology*, 204(3), **pp. 217–224**.

Li, F., Wang, X., Capasso, J. M. and Gerdes, a M. (1996) 'Rapid transition of cardiac myocytes from hyperplasia to hypertrophy during postnatal development.', *Journal of molecular and cellular cardiology*, 28(8), **pp. 1737–1746**.

Li, J., Chen, K., Zhu, L. and Pollard, J. W. (2006) 'Conditional Deletion of the Colony Stimulating Factor-1 Receptor (c-fms Proto-Oncogene) in Mice', *Genesis*, 44, **pp. 328–335**.

Li, W., Hsiao, H.-M., Higashikubo, R., Saunders, B. T., Bharat, A., Goldstein, D. R., Krupnick, A. S., Gelman, A. E., Lavine, K. J., Kreisel, D., *et al.* (2016) 'Heart-resident CCR2+ macrophages promote neutrophil extravasation through TLR9/MyD88/CXCL5 signaling', *JCI Insight*, 1(12), **pp. 1564–1568**.

Lian, X., Hsiao, C., Wilson, G., Zhu, K., Hazeltine, L. B., Azarin, S. M., Raval, K. K., Zhang, J., Kamp, T. J. and Palecek, S. P. (2012) 'Robust cardiomyocyte differentiation

from human pluripotent stem cells via temporal modulation of canonical Wnt signaling', *Proceedings of the National Academy of Sciences*, 109(27), **pp. E1848–E1857**.

Lin, H., Angeli, M., Chung, K. J., Ejimadu, C., Rivera Rosa, A. and Lee, T. (2016) 'sFRP2 activates Wnt/β-catenin signaling in cardiac fibroblasts: differential roles in cell growth, energy metabolism and extracellular matrix remodeling', *American Journal of Physiology - Cell Physiology*, (37), **p. ajpcell.00137.2016**.

Lin, H., Lee, E., Hestir, K., Leo, C., Huang, M., Bosch, E., Halenbeck, R., Wu, G., Zhou, A., Behrens, D., *et al.* (2007) 'Discovery of a Cytokine and Its Receptor by Functional Screening of the Extracellular Proteome', *Science*, 707(1996).

Lin, L., Cui, L., Zhou, W., Dufort, D., Zhang, X., Cai, C.-L., Bu, L., Yang, L., Martin, J., Kemler, R., *et al.* (2007) 'Beta-catenin directly regulates Islet1 expression in cardiovascular progenitors and is required for multiple aspects of cardiogenesis.', *Proceedings of the National Academy of Sciences of the United States of America*, 104(22), **pp. 9313–8**.

Lin, S.-L., Li, B., Rao, S., Yeo, E.-J., Hudson, T. E., Nowlin, B. T., Pei, H., Chen, L., Zheng, J. J., Carroll, T. J., *et al.* (2010) 'Macrophage Wnt7b is critical for kidney repair and regeneration.', *Proceedings of the National Academy of Sciences of the United States of America*, 107(9), **pp. 4194–4199**.

Liu, P., Wakamiya, M., Shea, M. J., Albrecht, U., Behringer, R. R. and Bradley, A. (1999) 'Requirement for Wnt3 in vertebrate axis formation.', *Nature genetics*, 22(4), **pp. 361–365**.

Lobov, I. B., Rao, S., Carroll, T. J., Vallance, J. E., Ito, M., Ondr, J. K., Kurup, S., Glass, D. a, Patel, M. S., Shu, W., *et al.* (2005) 'WNT7b mediates macrophage-induced programmed cell death in patterning of the vasculature.', *Nature*, 437(7057), **pp. 417–421**.

Loffredo, F. S., Steinhauser, M. L., Gannon, J. and Lee, R. T. (2011) 'Bone marrow-derived cell therapy stimulates endogenous cardiomyocyte progenitors and promotes cardiac repair', *Cell Stem Cell*. Elsevier Inc., 8(4), **pp. 389–398**.

Ma, H., Yin, C., Zhang, Y., Qian, L. and Liu, J. (2016) 'ErbB2 is required for cardiomyocyte proliferation in murine neonatal hearts', *Gene*. Elsevier B.V., 592(2), **pp. 325–330**.

Ma, Y., Yabluchanskiy, A., Iyer, R. P., Cannon, P. L., Flynn, E. R., Jung, M., Henry, J., Cates, C. A., Deleon-Pennell, K. Y. and Lindsey, M. L. (2016) 'Temporal neutrophil polarization following myocardial infarction', *Cardiovascular Research*, 110(1), **pp. 51–61**.

Ma, Y., Yabluchanskiy, A. and Lindsey, M. L. (2013) 'Neutrophil roles in left ventricular remodeling following myocardial infarction.', *Fibrogenesis & tissue repair*. Fibrogenesis & Tissue Repair, 6(1), **p. 11**.

Mahmoud, A. I., Kocabas, F., Muralidhar, S. A., Kimura, W., Koura, A. S., Thet, S., Porrello, E. R. and Sadek, H. A. (2013) 'Meis1 regulates postnatal cardiomyocyte cell cycle arrest.', *Nature*. Nature Publishing Group, 497(7448), **pp. 249–53**.

Mahmoud, A. I., Porrello, E. R., Kimura, W., Olson, E. N. and Sadek, H. a (2014) 'Surgical models for cardiac regeneration in neonatal mice.', *Nature protocols*. Nature Publishing Group, 9(2), **pp. 305–11**.

Maillet, M., van Berlo, J. H. and Molkentin, J. D. (2013) 'Molecular basis of physiological heart growth: fundamental concepts and new players.', *Nature reviews. Molecular cell biology*. Nature Publishing Group, 14(1), **pp. 38–48**.

Maiti, G., Naskar, D. and Sen, M. (2012) 'The Wingless homolog Wnt5a stimulates phagocytosis but not bacterial killing', *Proceedings of the National Academy of Sciences*, 109(41), **pp. 16600–16605**.

Männer, J. (1999) 'Does the subepicardial mesenchyme contribute myocardioblasts to the myocardium of the chick embryo heart? A quail-chick chimera study tracing the fate of the epicardial primordium', *Anatomical Record*, 255(2), **pp. 212–226**.

Matz, D. G., Oberpriller, J. O. and Oberpriller, J. C. (1998) 'Comparison of mitosis in binucleated and mononucleated newt cardiac myocytes', *Anatomical Record*, 251(2), **pp. 245–255**.

McSweeney, S. J., Hadoke, P. W. F., Kozak, A. M., Small, G. R., Khaled, H., Walker,

B. R. and Gray, G. A. (2010) ‘Improved heart function follows enhanced inflammatory cell recruitment and angiogenesis in 11??HSD1-deficient mice post-MI’, *Cardiovascular Research*, 88(1), **pp. 159–167**.

Meznarich, J., Malchodi, L., Helterline, D., Ramsey, S. A., Bertko, K., Plummer, T., Plawman, A., Gold, E. and Stempien-Otero, A. (2013) ‘Urokinase Plasminogen Activator Induces Pro-Fibrotic/M2 Phenotype in Murine Cardiac Macrophages’, *PLoS ONE*, 8(3), **pp. 1–10**.

Michaelson, M., Bieri, P., Mehler, M., Xu, H., Arezzo, J., Pollard, J. and Kessler, J. (1996) ‘CSF-1 deficiency in mice results in abnormal brain development’, *Development*, 122, **pp. 2661–2672**.

Mikawa, T. and Gourdie, R. G. (1996) ‘Pericardial mesoderm generates a population of coronary smooth muscle cells migrating into the heart along with ingrowth of the epicardial organ.’, *Developmental biology*, 174(2), **pp. 221–232**.

Mikels, a J. and Nusse, R. (2006) ‘Wnts as ligands: processing, secretion and reception.’, *Oncogene*, 25(57), **pp. 7461–7468**.

Mills, C. D., Kincaid, K., Alt, J. M., Heilman, M. J. and Hill, A. M. (2000) ‘M-1/M-2 Macrophages and the Th1/Th2 Paradigm’, *The Journal of Immunology*, 164(12), **pp. 6166–6173**.

Miyoshi, H., Ajima, R., Luo, C., Yamaguchi, T. and Stappenbeck, T. (2012) ‘Wnt5a Potentiates TGF- b Signaling to Promote Colonic Crypt Regeneration After Tissue Injury’, *Science*, 338(October), **pp. 108–113**.

Mizutani, M., Wu, J. C. and Nusse, R. (no date) ‘Fibrosis of the Neonatal Mouse Heart After Cryoinjury Is Accompanied by Wnt Signaling Activation and Epicardial-to-Mesenchymal Transition’.

Moldovan, N. I., Goldschmidt-clermont, P. J., Parker-thornburg, J., Shapiro, S. D. and Kolattukudy, P. E. (2000) ‘Contribution of Monocytes / Macrophages to The Drilling of Metalloelastase-Positive Tunnels in Ischemic Myocardium’, *Circulation Research*, **pp. 378–385**.

Moran, C. M., Thomson, A. J. W., Rog-Zielinska, E. and Gray, G. A. (2013) ‘High-

resolution echocardiography in the assessment of cardiac physiology and disease in preclinical models.', *Experimental physiology*, 98(3), **pp. 629–44**.

Movérare-Skrtic, S., Henning, P., Liu, X., Nagano, K., Saito, H., Börjesson, A. E., Sjögren, K., Windahl, S. H., Farman, H., Kindlund, B., *et al.* (2014) 'Osteoblast-derived WNT16 represses osteoclastogenesis and prevents cortical bone fragility fractures.', *Nature medicine*, 20(11), **pp. 1279–88**.

Mozaffarian, D., Benjamin, E. J., Go, A. S., Arnett, D. K., Blaha, M. J., Cushman, M., Das, S. R., Ferranti, S. De, Després, J. P., Fullerton, H. J., *et al.* (2016) *Heart disease and stroke statistics-2016 update a report from the American Heart Association*, *Circulation*.

Murdoch, C., Muthana, M., Coffelt, S. B. and Lewis, C. E. (2008) 'The role of myeloid cells in the promotion of tumour angiogenesis', 8(august).

Murray, P. J., Allen, J. E., Biswas, S. K., Fisher, E. A., Gilroy, D. W., Goerdt, S., Gordon, S., Hamilton, J. A., Ivashkiv, L. B., Lawrence, T., *et al.* (2014) 'Macrophage Activation and Polarization: Nomenclature and Experimental Guidelines', *Immunity*. Elsevier, 41(1), **pp. 14–20**.

Murray, P. J. and Wynn, T. a (2011) 'Obstacles and opportunities for understanding macrophage polarization.', *Journal of leukocyte biology*, 89(4), **pp. 557–563**.

Mylonas, K. J., Jenkins, S. J., Castellan, R. F. P., Ruckerl, D., McGregor, K., Phythian-Adams, A. T., Hewitson, J. P., Campbell, S. M., MacDonald, A. S., Allen, J. E., *et al.* (2015) 'The adult murine heart has a sparse, phagocytically active macrophage population that expands through monocyte recruitment and adopts an "M2" phenotype in response to Th2 immunologic challenge', *Immunobiology*. Elsevier GmbH., 220(7), **pp. 924–933**.

Nahrendorf, M. and Swirski, F. K. (2013) 'Monocyte and macrophage heterogeneity in the heart', *Circulation Research*, 112(12), **pp. 1624–1633**.

Nahrendorf, M., Swirski, F. K., Aikawa, E., Stangenberg, L., Wurdinger, T., Figueiredo, J.-L., Libby, P., Weissleder, R. and Pittet, M. J. (2007) 'The healing myocardium sequentially mobilizes two monocyte subsets with divergent and

complementary functions.', *The Journal of experimental medicine*, 204(12), **pp. 3037–47**.

Nucera, S., Biziato, D. and de Palma, M. (2011) 'The interplay between macrophages and angiogenesis in development, tissue injury and regeneration', *International Journal of Developmental Biology*, 55(4–5), **pp. 495–503**.

Nusse, R. and Varmus, H. E. (1982) 'Many tumors induced by the mouse mammary tumor virus contain a provirus integrated in the same region of the host genome.', *Cell*, 31(1), **pp. 99–109**.

Oberpriller, J. O. and Oberpriller, J. C. (1974) 'Response of the adult newt ventricle to injury', *Journal of Experimental Zoology*, 197, **p. 249**.

Oerlemans, M. I. F. J., Goumans, M.-J., van Middelaar, B., Clevers, H., Doevendans, P. a and Sluijter, J. P. G. (2010) 'Active Wnt signaling in response to cardiac injury.', *Basic research in cardiology*, 105(5), **pp. 631–641**.

Oka, T., Xu, J. and Molkentin, J. D. (2007) 'Re-employment of developmental transcription factors in adult heart disease', *Seminars in Cell and Developmental Biology*, 18(1), **pp. 117–131**.

Oparil, S., Bishop, S. P. and Clubb, F. J. (1984) 'Myocardial cell hypertrophy or hyperplasia.', *Hypertension*, 6(6 Pt 2), **p. III38**.

Orlic, D., Kajstura, J., Chimenti, S., Jakoniuk, I., Anderson, S. M., Li, B., Pickel, J., McKay, R., Nadal-Ginard, B., Bodine, D. M., *et al.* (2001) 'Bone marrow cells regenerate infarcted myocardium.', *Nature*, 410(6829), **pp. 701–705**.

Otto, A., Schmidt, C., Luke, G., Allen, S., Valasek, P., Muntoni, F., Lawrence-Watt, D. and Patel, K. (2008) 'Canonical Wnt signalling induces satellite-cell proliferation during adult skeletal muscle regeneration.', *Journal of cell science*, 121, **pp. 2939–2950**.

Palevski, D., Levin-Kotler, L., Kain, D., Naftali-Shani, N., Landa, N., Ben-Mordechai, T., Konfino, T., Holbova, R., Molotski, N., Rosin-Arbesfeld, R., *et al.* (2017) 'Loss of Macrophage Wnt Secretion Improves Remodeling and Function After Myocardial Infarction in Mice', *Journal of the American Heart Association*, 6(1), **p. e004387**.

Pan, D. (2010) ‘The hippo signaling pathway in development and cancer’, *Developmental Cell*. Elsevier Inc., 19(4), **pp. 491–505**.

Pandur, P., Lasche, M., Eisenberg, L. . and Kuhl, M. (2002) ‘Wnt-11 activation of a non-canonical Wnt signalling pathway is required for cardiogenesis’, *Nature*, 418(August), **pp. 636–641**.

Paolicelli, R. C., Bolasco, G., Pagani, F., Maggi, L., Scianni, M., Panzanelli, P., Giustetto, M., Ferreira, T. A., Guiducci, E., Dumas, L., *et al.* (2011) ‘Synaptic pruning by microglia is necessary for normal brain development.’, *Science (New York, N.Y.)*, 333(6048), **pp. 1456–8**.

Pereira, C. P., Bachli, E. B. and Schoedon, G. (2009) ‘The Wnt pathway: A macrophage effector molecule that triggers inflammation’, *Current Atherosclerosis Reports*, 11(3), **pp. 236–242**.

Pereira, C., Schaer, D. J., Bachli, E. B., Kurrer, M. O. and Schoedon, G. (2008) ‘Wnt5A/CaMKII signaling contributes to the inflammatory response of macrophages and is a target for the antiinflammatory action of activated protein C and interleukin-10’, *Arteriosclerosis, Thrombosis, and Vascular Biology*, 28(3), **pp. 504–510**.

Perez-Pomares, J. M., Carmona, R., González-Iriarte, M., Atencia, G., Wessels, A. and Muñoz-Chapuli, R. (2002) ‘Origin of coronary endothelial cells from epicardial mesothelium in avian embryos’, *International Journal of Developmental Biology*, 46(8), **pp. 1005–1013**.

Petrov, V. V, Fagard, R. H. and Lijnen, P. J. (2002) ‘Stimulation of collagen production by transforming growth factor-beta1 during differentiation of cardiac fibroblasts to myofibroblasts.’, *Hypertension*, 39(2), **pp. 258–63**.

Phoon, C. K. L. and Turnbull, D. H. (2003) ‘Ultrasound biomicroscopy-Doppler in mouse cardiovascular development.’, *Physiological Genomics*, 14(1), **pp. 3–15**.

Pinto, A. R., Godwin, J. W. and Rosenthal, N. a. (2014) ‘Macrophages in cardiac homeostasis, injury responses and progenitor cell mobilisation’, *Stem Cell Research*. Elsevier B.V.

Pinto, A. R., Ilinykh, A., Ivey, M. J., Kuwabara, J. T., D’antoni, M. L., Debuque, R.,

Chandran, A., Wang, L., Arora, K., Rosenthal, N. A., *et al.* (2016) 'Revisiting cardiac cellular composition', *Circulation Research*, 118(3), **pp. 400–409**.

Pinto, A. R., Paolicelli, R., Salimova, E., Gospocic, J., Slonimsky, E., Bilbao-cortes, D., Godwin, J. W. and Rosenthal, N. A. (2012) 'An Abundant Tissue Macrophage Population in the Adult Murine Heart with a Distinct Alternatively-Activated Macrophage Profile', 7(5).

Piquereau, J., Novotova, M., Fortin, D., Garnier, A., Ventura-Clapier, R., Veksler, V. and Joubert, F. (2010) 'Postnatal development of mouse heart: formation of energetic microdomains.', *The Journal of physiology*, 588(Pt 13), **pp. 2443–2454**.

Planas-Paz, L., Orsini, V., Boulter, L., Calabrese, D., Pikiolek, M., Nigsch, F., Xie, Y., Roma, G., Donovan, A., Marti, P., *et al.* (2016) 'The RSPO–LGR4/5–ZNRF3/RNF43 module controls liver zonation and size', *Nature Cell Biology*, (October 2015).

Pollard, J. W. (2009) 'Trophic macrophages in development and disease', *Nature Reviews Immunology*, 9(4), **pp. 259–270**.

Porrello, E. R., Mahmoud, A. I., Simpson, E., Hill, J. A., Richardson, J. A., Olson, E. N. and Sadek, H. A. (2011) 'Transient regenerative potential of the neonatal mouse heart.', *Science (New York, N.Y.)*, 331(6020), **pp. 1078–80**.

Porrello, E. R., Mahmoud, A. I., Simpson, E., Johnson, B. A., Grinsfelder, D., Canseco, D., Mammen, P. P., Rothermel, B. A., Olson, E. N. and Sadek, H. A. (2013) 'Regulation of neonatal and adult mammalian heart regeneration by the miR-15 family.', *Proceedings of the National Academy of Sciences of the United States of America*, 110(1), **pp. 187–92**.

Porrello, E. R. and Olson, E. N. (2014) 'A neonatal blueprint for cardiac regeneration', *Stem Cell Research*, 13(3), **pp. 556–570**.

Port, F., Kuster, M., Herr, P., Furger, E., Bänziger, C., Hausmann, G. and Basler, K. (2008) 'Wingless secretion promotes and requires retromer-dependent cycling of Wntless.', *Nature cell biology*, 10(2), **pp. 178–185**.

Porter, K. E. and Turner, N. A. (2009) 'Cardiac fibroblasts: At the heart of myocardial

remodeling', *Pharmacology and Therapeutics*, 123(2), **pp. 255–278**.

Poss, K. D. (2010) 'Advances in understanding tissue regenerative capacity and mechanisms in animals', *Nature Reviews Genetics*, 11(10), **pp. 710–722**.

Poss, K. D., Shen, J. and Keating, M. T. (2000) 'Induction of lef1 during zebrafish fin regeneration', *Developmental Dynamics*, 219(2), **pp. 282–286**.

Poss, K. D., Wilson, L. G. and Keating, M. T. (2002) 'Heart regeneration in zebrafish', *Science*, 298(5601), **pp. 2188–2190**.

Pow, D. V, Perry, V. H., Morris, J. F. and Gordon, S. (1989) 'Microglia in the Neurohypophysis Associate with and Endocytose Terminal Portions of Neurosecretory Neurons', *Neuroscience*, 33(3), **pp. 567–578**.

Puente, B. N., Kimura, W., Muralidhar, S. A., Moon, J., Amatruda, J. F., Phelps, K. L., Grinsfelder, D., Rothermel, B. A., Chen, R., Garcia, J. A., *et al.* (2014) 'The oxygen-rich postnatal environment induces cardiomyocyte cell-cycle arrest through DNA damage response', *Cell*. Elsevier, 157(3), **pp. 565–579**.

Rao, T. P. and Kühl, M. (2010) 'An updated overview on wnt signaling pathways: A prelude for more', *Circulation Research*, 106(12), **pp. 1798–1806**.

Red-Horse, K., Ueno, H., Weissman, I. L. and Krasnow, M. a (2010) 'Coronary arteries form by developmental reprogramming of venous cells.', *Nature*. Nature Publishing Group, 464(7288), **pp. 549–553**.

Resh, M. D. (2012) 'Targeting protein lipidation in disease', *Trends in Molecular Medicine*. Elsevier Ltd, 18(4), **pp. 206–214**.

Rijsewijk, F., Schuermann, M., Wagenaar, E., Parren, P., Weigel, D. and Nusse, R. (1987) 'The Drosophila homology of the mouse mammary oncogene int-1 is identical to the segment polarity gene wingless', *Cell*, 50(4), **pp. 649–657**.

Rohini, A., Agrawal, N., Koyani, C. N. and Singh, R. (2010) 'Molecular targets and regulators of cardiac hypertrophy', *Pharmacological Research*. Elsevier Ltd, 61(4), **pp. 269–280**.

Rumyantsev, P. . (1966) 'Autoradiographic study on the synthesis of DNA, RNA, and

proteins in normal cardiac muscle cells and those changed by experimental injury', *Folia Histochem. Cytochem*, 4, **p. 397**.

Rymo, S. F., Gerhardt, H., Sand, F. W., Lang, R. and Uv, A. (2011) 'A Two-Way Communication between Microglial Cells and Angiogenic Sprouts Regulates Angiogenesis in Aortic Ring Cultures', 6(1).

Sadek, H. A., Martin, J. F., Takeuchi, J. K., Leor, J., Nie, Y., Giacca, M. and Lee, R. T. (2014) 'Multi-Investigator Letter on Reproducibility of Neonatal Heart Regeneration following Apical Resection', *Stem Cell Reports*. Elsevier, 3(1), **p. 1**.

Saha, S., Aranda, E., Hayakawa, Y., Bhanja, P., Atay, S., Brodin, N. P., Li, J., Asfaha, S., Liu, L., Tailor, Y., *et al.* (2016) 'Macrophage-derived extracellular vesicle-packaged WNTs rescue intestinal stem cells and enhance survival after radiation injury', *Nature Communications*. Nature Publishing Group, 7, **p. 13096**.

Salegio, E. a A., Pollard, A. N., Smith, M. and Zhou, X.-F. (2011) 'Macrophage presence is essential for the regeneration of ascending afferent fibres following a conditioning sciatic nerve lesion in adult rats.', *BMC neuroscience*. BioMed Central Ltd, 12(1), **p. 11**.

Santini, M. P., Forte, E., Harvey, R. P. and Kovacic, J. C. (2016) 'Developmental origin and lineage plasticity of endogenous cardiac stem cells', *Development*, 143, **pp. 1242–1258**.

Sasmono, R. T., Ehrnsperger, A., Cronau, S. L., Ravasi, T., Kandane, R., Hickey, M. J., Cook, A. D., Himes, S. R., Hamilton, J. a and Hume, D. a (2007) 'Mouse neutrophilic granulocytes express mRNA encoding the macrophage colony-stimulating factor receptor (CSF-1R) as well as many other macrophage-specific transcripts and can transdifferentiate into macrophages in vitro in response to CSF-1.', *Journal of leukocyte biology*, 82(1), **pp. 111–23**.

Sasmono, R. T., Oceandy, D., Pollard, J. W., Tong, W., Pavli, P., Wainwright, B. J., Ostrowski, M. C., Himes, S. R. and Hume, D. A. (2003) 'A macrophage colony-stimulating factor receptor-green fluorescent protein transgene is expressed throughout the mononuclear phagocyte system of the mouse', *Blood*, 101(3), **pp. 1155–1163**.

Schaale, K., Neumann, J., Schneider, D., Ehlers, S. and Reiling, N. (2011) 'Wnt signaling in macrophages: Augmenting and inhibiting mycobacteria-induced inflammatory responses', *European Journal of Cell Biology*. Elsevier GmbH., 90(6–7), **pp. 553–559**.

Schulz, C., Perdiguero, E. G., Chorro, L., Szabo-rogers, H., Cagnard, N., Kierdorf, K., Prinz, M., Wu, B., Jacobsen, S. E. W., Pollard, J. W., *et al.* (2012) 'A Lineage of Myeloid Cells', *Science*, 336(86), **pp. 2–7**.

Schulz, R. a. and Yutzey, K. E. (2004) 'Calcineurin signaling and NFAT activation in cardiovascular and skeletal muscle development', *Developmental Biology*, 266(1), **pp. 1–16**.

Sedmera, D., Pexieder, T., Vuillemin, M., Thompson, R. and Henderson, R. (2000) 'Developmental Patterning of the Myocardium', *The anatomical record*, 337(258), **pp. 319–337**.

Sen, S. and Sadek, H. a. (2015) 'Neonatal Heart Regeneration: Mounting Support and Need for Technical Standards', *Journal of the American Heart Association*, 4, **pp. e001727–e001727**.

Shake, J. G., Gruber, P. J., Baumgartner, W. A., Senechal, G., Meyers, J., Redmond, J. M., Pittenger, M. F. and Martin, B. J. (2002) 'Mesenchymal stem cell implantation in a swine myocardial infarct model: Engraftment and functional effects', *Annals of Thoracic Surgery*, 73(6), **pp. 1919–1926**.

Smart, N. (2016) 'Prospects for Improving Neovascularisation of the Ischaemic Heart: Lessons from Development', *Microcirculation*, (November 2016), **pp. 1–15**.

Smith, S. J. and Mohun, T. J. (2011) 'Early cardiac morphogenesis defects caused by loss of embryonic macrophage function in Xenopus', *Mechanisms of Development*. Elsevier Ireland Ltd, 128(5–6), **pp. 303–315**.

Soonpaa, M. H. and Field, L. J. (1998) 'Point / Counterpoint Survey of Studies Examining Mammalian Cardiomyocyte DNA Synthesis', **pp. 15–26**.

Soonpaa, M. H., Kim, K. K., Pajak, L., Franklin, M. and Field, L. J. (1996) 'Cardiomyocyte DNA synthesis and binucleation during murine development.', *The*

*American journal of physiology*, 271(5 Pt 2), **pp. H2183–H2189**.

Stamos, J. L. and Weis, W. I. (2013) 'The b-catenin destruction complex', *Cold Spring Harbor Perspectives in Biology*, 5(1), **pp. 1–16**.

Stefater, J. A., Lewkowich, I., Rao, S., Mariggi, G., Carpenter, A. C., Burr, A. R., Fan, J., Ajima, R., Molkentin, J. D., Williams, B. O., *et al.* (2011) 'Regulation of angiogenesis by a non-canonical Wnt-Flt1 pathway in myeloid cells.', *Nature*. Nature Publishing Group, 474(7352), **pp. 511–5**.

Stefater, J. a., Rao, S., Bezold, K., Aplin, A. C., Nicosia, R. F., Pollard, J. W., Ferrara, N. and Lang, R. a. (2013) 'Macrophage Wnt-Calcineurin-Flt1 signaling regulates mouse wound angiogenesis and repair.', *Blood*, 121(13), **pp. 2574–2578**.

Stefater, J. A., Ren, S., Lang, R. A. and Duffield, J. S. (2011) 'Metchnikoff's policemen: Macrophages in development, homeostasis and regeneration', *Trends in Molecular Medicine*. Elsevier Ltd, 17(12), **pp. 743–752**.

Stegger, L., Hoffmeier, A.-N., Schäfers, K. P., Hermann, S., Schober, O., Schäfers, M. a and Theilmeier, G. (2006) 'Accurate noninvasive measurement of infarct size in mice with high-resolution PET.', *Journal of nuclear medicine : official publication, Society of Nuclear Medicine*, 47(11), **pp. 1837–1844**.

Stein, M., Keshav, S., Harris, N. and Gordon, S. (1992) 'Interleukin 4 potently enhances murine macrophage mannose receptor activity: a marker of alternative immunologic macrophage activation.', *The Journal of experimental medicine*, 176(1), **pp. 287–92**.

Stephenson, R. S., Agger, P., Lunkenheimer, P. P., Zhao, J., Smerup, M., Niederer, P., Anderson, R. H. and Jarvis, J. C. (2016) 'The functional architecture of skeletal compared to cardiac musculature: Myocyte orientation, lamellar unit morphology, and the helical ventricular myocardial band', *Clinical Anatomy*, 29(3), **pp. 316–332**.

Sunderkötter, C., Steinbrink, K., Goebeler, M., Bhardwaj, R. and Sorg, C. (1994) 'Macrophages and angiogenesis.', *Journal of leukocyte biology*, 55(3), **pp. 410–422**.

Takada, R., Satomi, Y., Kurata, T., Ueno, N., Norioka, S., Kondoh, H., Takao, T. and Takada, S. (2006) 'Monounsaturated Fatty Acid Modification of Wnt Protein: Its Role

in Wnt Secretion', *Developmental Cell*, 11(6), **pp. 791–801**.

Takeda, N., Manabe, I. and Uchino, Y. (2010) 'Cardiac fibroblasts are essential for the adaptve response of the murine heart to pressure overload', *The Journal of clinical*, 120(1), **pp. 254–265**.

Thygesen, K., Alpert, J., Jaffe, A., Simoons, M., Chaitman, B. and White, H. (2013) 'Third Universal Definition of Myocardial Infarction', *Clinical Biochemistry*, 46(1–2), **pp. 1–4**.

Tian, X., Hu, T., Zhang, H., He, L., Huang, X., Liu, Q., Yu, W., He, L., Yang, Z., Yan, Y., *et al.* (2014) 'De novo formation of a distinct coronary vascular population in neonatal heart', *Science*, 345(6192), **pp. 90–94**.

Timmers, L., Pasterkamp, G., De Hoog, V. C., Arslan, F., Appelman, Y. and De Kleijn, D. P. V (2012) 'The innate immune response in reperfused myocardium', *Cardiovascular Research*, 94(2), **pp. 276–283**.

Toma, C., Pittenger, M. F., Cahill, K. S., Byrne, B. J. and Kessler, P. D. (2002) 'Human mesenchymal stem cells differentiate to a cardiomyocyte phenotype in the adult murine heart.', *Circulation*, 105(1), **pp. 93–8**.

Tomasek, J. J., Gabbiani, G., Hinz, B., Chaponnier, C. and Brown, R. a (2002) 'Myofibroblasts and mechano-regulation of connective tissue remodelling.', *Nature reviews. Molecular cell biology*, 3(5), **pp. 349–63**.

Turner, N. a and Porter, K. E. (2013) 'Function and fate of myofibroblasts after myocardial infarction.', *Fibrogenesis & tissue repair*. Fibrogenesis & Tissue Repair, 6(1), **p. 5**.

Ueno, S., Weidinger, G., Osugi, T., Kohn, A. D., Golob, J. L., Pabon, L., Reinecke, H., Moon, R. T. and Murry, C. E. (2007) 'Biphasic role for Wnt/beta-catenin signaling in cardiac specification in zebrafish and embryonic stem cells.', *Proceedings of the National Academy of Sciences of the United States of America*, 104(23), **pp. 9685–9690**.

Vanhoutte, D., Schellings, M., Pinto, Y. and Heymans, S. (2006) 'Relevance of matrix metalloproteinases and their inhibitors after myocardial infarction: A temporal and

spatial window', *Cardiovascular Research*, 69(3), **pp. 604–613**.

Vincent, S. D. and Buckingham, M. E. (2010) 'How to make a heart. The origin and regulation of cardiac progenitor cells', *Current Topics in Developmental Biology*, 90(C), **pp. 1–41**.

Walsh, S., Pontén, A., Fleischmann, B. K. and Jovinge, S. (2010) 'Cardiomyocyte cell cycle control and growth estimation in vivo-An analysis based on cardiomyocyte nuclei', *Cardiovascular Research*, 86(3), **pp. 365–373**.

Wiktor-Jedrzejczak, W., Bartocci, A., Ferrante, A. W., Ahmed-Ansari, A., Sell, K. W., Pollard, J. W. and Stanley, E. R. (1990) 'Total absence of colony-stimulating factor 1 in the macrophage-deficient osteopetrotic (op/op) mouse.', *Proceedings of the National Academy of Sciences of the United States of America*, 87(12), **pp. 4828–32**.

Willert, K., Brown, J. D., Danenberg, E., Duncan, A. W., Weissman, I. L., Reya, T., Yates, J. R. and Nusse, R. (2003) 'Wnt proteins are lipid-modified and can act as stem cell growth factors.', *Nature*, 423(6938), **pp. 448–452**.

Williams, A. R. and Hare, J. M. (2011) 'Mesenchymal stem cells: Biology, pathophysiology, translational findings, and therapeutic implications for cardiac disease', *Circulation Research*, 109(8), **pp. 923–940**.

Wilm, B., Ipenberg, A., Hastie, N. D., Burch, J. B. E. and Bader, D. M. (2005) 'The serosal mesothelium is a major source of smooth muscle cells of the gut vasculature.', *Development (Cambridge, England)*, 132(23), **pp. 5317–5328**.

Wu, S. M., Chien, K. R. and Mummery, C. (2008) 'Origins and Fates of Cardiovascular Progenitor Cells', *Cell*, 132(4), **pp. 537–543**.

Wynn, T. a, Chawla, A. and Pollard, J. W. (2013) 'Macrophage biology in development, homeostasis and disease.', *Nature*. Nature Publishing Group, 496(7446), **pp. 445–55**.

Xin, M., Kim, Y., Sutherland, L. B., Murakami, M., Qi, X., McAnally, J., Porrello, E. R., Mahmoud, A. I., Tan, W., Shelton, J. M., *et al.* (2013) 'Hippo pathway effector Yap promotes cardiac regeneration.', *Proceedings of the National Academy of Sciences of the United States of America*, 110(34), **pp. 13839–44**.

Xu, W., Zhang, X., Qian, H., Zhu, W., Sun, X., Hu, J., Zhou, H. and Chen, Y. (2004) 'Mesenchymal stem cells from adult human bone marrow differentiate into a cardiomyocyte phenotype in vitro.', *Experimental biology and medicine (Maywood, N.J.)*, 229(7), **pp. 623–631**.

Yan, X., Anzai, A., Katsumata, Y., Matsuhashi, T., Ito, K., Endo, J., Yamamoto, T., Takeshima, A., Shinmura, K., Shen, W., *et al.* (2013) 'Temporal dynamics of cardiac immune cell accumulation following acute myocardial infarction', *Journal of Molecular and Cellular Cardiology*. Elsevier Ltd, 62, **pp. 24–35**.

Yang, L., Jung, Y., Omenetti, A., Witek, R. P., Choi, S., Vandongen, H. M., Huang, J., Alpini, G. D. and Diehl, A. M. (2008) 'Fate-mapping evidence that hepatic stellate cells are epithelial progenitors in adult mouse livers.', *Stem cells*, 26(8), **pp. 2104–2113**.

Yoshida, H., Hayashi, S., Kunisada, T., Ogawa, M., Nishikawa, S., Okamura, H., Sudo, T. and Shultz, L. D. (1990) 'The murine mutation osteopetrosis is in the coding region of the macrophage colony stimulating factor gene.', *Nature*, **pp. 442–4**.

Yu, Q., Leatherbury, L., Tian, X. and Lo, C. W. (2008) 'Cardiovascular Assessment of Fetal Mice by In Utero Echocardiography', *Ultrasound in Medicine and Biology*, 34(5), **pp. 741–752**.

Zamilpa, R. and Lindsey, M. L. (2010) 'Extracellular matrix turnover and signaling during cardiac remodeling following MI: Causes and consequences', *Journal of Molecular and Cellular Cardiology*. Elsevier Ltd, 48(3), **pp. 558–563**.

Zelarayán, L. C., Noack, C., Sekkali, B., Kmecova, J., Gehrke, C., Renger, A., Zafiriou, M.-P., van Der Nagel, R., Dietz, R., de Windt, L. J., *et al.* (2008) 'Beta-Catenin downregulation attenuates ischemic cardiac remodeling through enhanced resident precursor cell differentiation.', *Proceedings of the National Academy of Sciences of the United States of America*, 105(50), **pp. 19762–7**.

Zhao, B., Tumaneng, K. and Guan, K. L. (2011) 'The Hippo pathway in organ size control, tissue regeneration and stem cell self-renewal', *Nature Cell Biology*. Nature Publishing Group, 13(8), **pp. 877–883**.

Zhao, X., Wu, J., Gray, C. D., McGregor, K., Rossi, A. G., Morrison, H., Jansen, M. a and Gray, G. a (2015) 'Optical projection tomography permits efficient assessment of infarct volume in the murine heart postmyocardial infarction', *American Journal of Physiology - Heart and Circulatory Physiology*, 309(4), **pp. H702–H710**.

Zhou, Y.-Q., Foster, F. S., Parkes, R. and Adamson, S. L. (2003a) 'Developmental changes in left and right ventricular diastolic filling patterns in mice', *American Journal of Physiology - Heart and Circulatory Physiology*, 285(4), **pp. H1563–H1575**.

Zhou, Y.-Q., Foster, F. S., Parkes, R. and Adamson, S. L. (2003b) 'Developmental changes in left and right ventricular diastolic filling patterns in mice.', *American journal of physiology. Heart and circulatory physiology*, 285(4), **pp. H1563–H1575**.